Recombinant Human Indoleamine 2,3-Dioxygenase

A thesis submitted in partial fulfilment of
the requirements for the degree
Doctor of Philosophy

from
Macquarie University

by
Priambudi Kosim-Satyaputra

Supervisors
Associate Professor Joanne Faith Jamie
Associate Professor Robert Drant Willows

Department of Chemistry and Biomolecular Sciences
Faculty of Science
December 2009

Dedicated to my mother
Siti Zuraida,

my family
Qaris, Qamal and **Ika-Wiani**,

my sisters
Listiana and **Widyastuti,**

and the memory of my father
Mohammad Kosim-Satyaputra.

***... "the wise talk because they have something to say ... fools, because they have to say something"*---Plato ...**

Acknowledgements

I thank my supervisors A. Prof. Joanne F. Jamie and A. Prof. Robert D. Willows for their supervision, advice, guidance and help. To my thesis examiners I express my gratitude.

I extend my gratitude to the staff of the Department of Chemistry and Biomolecular Sciences and the Department of Biological Sciences, Faculty of Science, Macquarie University, for their kind and helpful support as well as for the Macquarie University, Environmental and Life Sciences Higher Degree Research Tuition Fee Scholarship. Also to Staff of the Research Office, Higher Degree Research Unit and the Biotechnology Research Institute, Macquarie University, for the International Macquarie University Research Scholarship. Especially to Prof. Jim Piper, Prof. Elizabeth Deane, A. Prof. Peter H. Karuso, Prof. Hatch W. Stokes, Prof. Helena Nevalainen, Prof. Roger Hiller, A. Prof. Bridget C. Mabbutt, Dr Christopher McRae, Dr Paul Worden, Dr Angela Conolly, Dr Moreland Gibbs, Dr Ian Jamie, Dr Danny K.Y. Wong, Dr Tom Roberts, Dr Andrew C. Try, Maria Hyland, Catherine Wong, Keith Tonkin, Mark Tran, Thulasy Jeyendra, Elsa Mardones, Keiran Morgan, Hong Nguyen, Ron Claassens, Frank P. Sharples, Monika King, Jenny Minard, Lanna Leung, Jane Kim and Anne Thoeming.

To all my friends in the Department of Chemistry and Biomolecular Sciences as well as the Department of Biological Sciences, Faculty of Science, Macquarie University, I thank you for being there and being what you are, friends. Especially to Artur Sawicki, Simone Ciampi, Qian Liu, Unnikrishnan Kuzhiumparambil and Sudhir R. Shengule, also to Jasminka Mizdrak, Michelle Camenzuli, Soo Jean Park and Thomas M. Dzeha. My appreciation also goes to Anil Gautam, Stephen White, Nicholas Gad, Yen Li Lee, Tom Joss, Danuta Kalinowski, Luise Jensen, Margaret Whitelaw, Rama D. Nimmagadda, Gareth Watkins, Stephanus T. Wanandy, Isla Streete, Nienke Brouwer, Christopher J.D. Austin, Azadeh Matin, Jeremy Fowler, Robert Laich, Meyanungsang, Amy Guilfoyle,

Andrew Robinson, May Xu, Jean-Marc Garnier, Ben Stephens, Andrew Piggott, Alison Kriegel, Michael Gotsbacher, Chandrika Deshpande, Visaahini Sureshan, Andrew Mahon, Xiaoqiang Liu, Blair Nield, Jody Allen, Mohammed Bhuiyan, Subbiah Alwarappan, Yanyan Mulyana, Tony Jerkovic, George Wilson, Wei Fan, Fiona Scarff, Alamgir Khan, Hong Yu, Ning Xu, Ping Yin, Yabai He, as well as to A. Prof. Roger W. Read, Prof. David StC. Black, A. Prof. Jim Kohen, Prof. Shurook Saadedin, Prof. Ben Staskun, Dr Helen Tweedale and Dr Alexander Charlson.

Thank you to my mother Siti Zuraida (Ibu), my family Qaris (Ade), Qamal (Aa) and Ika-Wiani (Bubu) as well as her parents and family, my sisters Listiana (Tita) and Widyastuti (Tatuk) and all my extended families, especially Dedi Rahadian (Kang Dedi) and family, Faika A. Rahadian (Teteh), Bustanul A. Nawas (Om Nul) and family, Muhamad A. Nawas (Om Pin) and family, Elicia Wong and family, Henry T. Gibby (Uncle Harry), Maria Retnanestri and family, Heru A.S. Pribadi, Dachyar Saleh, Arief K. Sunardjono, Yana M. Syah, Unang Supratman and Tien Soesaktihadi and family. To all the others, I could not list personally one by one in this limited space, but the memories will stay forever with me. I do appreciate all the support, help and encouragement that have been given to me, to which I am indebted. Thank you.

Contents

Figures

Tables

Thesis declaration

This thesis contains no material that has been accepted for the award of any higher degree or diploma at any university or institution and to the best of my knowledge contains no material previously published or written by another person, except where due references is made in the text of the thesis.

Research goals

A multi-disciplinary approach to the research on indoleamine 2,3-dioxygenase and IDO related studies is essential as IDO is involved in a variety of biological functions. The increasing focus and research on IDO demands large quantities of good quality IDO. The expression of recombinant human IDO (rhIDO) in *Escherichia coli* (*E. coli*) is therefore crucial. The expression of rhIDO in *E. coli* (pQE-9-IDO, pREP4) has been investigated but inadequacies still prevailed upon commencement of this study. Therefore the aims of this study were to i) optimise the expression of rhIDO in *E. coli* (pQE-9-IDO, pREP4) in order to obtain high quality enzyme, ii) evaluate the characteristics and stability of rhIDO in order to understand its behaviour as a support towards further studies, iii) study the re-incorporation of the heme *b* co-factor of rhIDO as an approach to optimise the availability of the enzyme for further studies and iv) evaluate the contribution of individual cysteines towards the overall catalytic properties and stability of the rhIDO through mutagenesis studies.

Abstract

Indoleamine 2,3-dioxygenase (IDO) is a heme-containing dioxygenase that catalyses the first and rate-limiting step in the kynurenine (Kyn) pathway of L-tryptophan (L-Trp) catabolism. Attention has been focused on IDO because the Kyn metabolic pathway is involved in a variety of physiological functions and diseases. In this study the expression and purification of recombinant human indoleamine 2,3-dioxygenase (rhIDO) in *E. coli* (pQE-9-IDO, pREP4) was investigated in order to obtain high quality enzyme in high yields. This study concluded that optimisation could still be achieved by lowering the growth temperature from 37 °C to 30 °C and reduction of IPTG induction from 100 μM to 10 μM. Better yields of rhIDO were obtained when the expression was carried out under dark conditions without the addition of PMSF, addition of hemin prior to lysis of the cells, increasing the NaCl concentration from 150 mM to 500 mM and lowering the imidazole variation from 10, 30, 40, 65, 80, 90, 190 to 10, 30, 60, 300 mM in the purification through Ni-NTA.

Evaluation of the characteristics and stability of rhIDO in order to understand its behaviour as a support towards further studies showed that rhIDO activity and yield under certain conditions of purification were significantly decreased. Further studies concluded that the loss of rhIDO activity was most probably due to the loss of the heme prosthetic group of the enzyme or the non effectiveness of the heme-protein complex. A study with hemin to examine the possibility of re-incorporation of heme showed

moderate re-incorporation. It was concluded, however, that keeping the heme intact through the supplementation of hemin prior to lysis is a much better alternative for preserving the activity of the enzyme. Comparison studies between rhIDO and rmIDO showed that the relative catalytic efficiency of rhIDO towards L-Trp (3.73) was higher compared to rmIDO (1.40) whereas the relative catalytic efficiency of rhIDO towards D-Trp (0.02) was lower compared to rmIDO (0.03). CD and thermal melt studies established that rhIDO is less helical (61% helix) than rmIDO (71% helix). The studies also showed that rhIDO has a lower melt temperature (50 ºC) than rmIDO (65 ºC) indicating that rmIDO is more thermostable than rhIDO.

The contribution of individual cysteines towards the overall catalytic properties and stability of the rhIDO was evaluated through mutagenesis studies. This was done by comparing the resulting outcomes from the C126A, C286A, C322A and C349A rhIDO mutations towards that of the non-mutated rhIDO. All the mutants exhibited a decrease in specificity towards L-Trp with C322A showing the highest decrease of 78% loss. However, with D-Trp, mutants C126A and C322A showed increased specificity where C126A showed the highest increase (280%). Mutants C286A and C349A showed decreased activity with C349A having the most (67% loss). This study confirms that the Cys to Ala site-directed mutagenesis contributes to the changes in the kinetics of the mutated rhIDO, and that the cysteine moieties of rhIDO are involved in the normal catalytic function of the enzyme. It is highly likely that the change from Cys to Ala in the mutants changed the conformation of the enzyme, which was a determining factor to the accessibility of the specific substrates to the active site. This change in conformation resulted in diverse kinetics observed.

Abbreviations

6xHis-tag	hexahistidyl-tag
ALA	δ-aminolevulinic acid
CAS	Chemical Abstracts Service
CD	circular dichroism
cDNA	copy deoxyribonucleic acid
CHES	2-(*N*-cyclohexylamino)ethane sulfonic acid
DMSO	dimethyl sulfoxide
DNA	deoxyribonucleic acid
DNase	deoxyribonuclease
dsDNA	double-stranded deoxyribonucleic acid
EC	Enzyme Commission
EDTA	ethylenediaminetetraacetic acid
ESI-MS	electrospray ionisation mass spectrometry
FMNH2	tetrahydrobiopterin dihydroriboflavin mononucleotide
FPLC	fast protein liquid chromatography
HEL	human erythroleukemic
heme	iron protoporphyrin IX; heme *b*
hIDO	human indoleamine 2,3-dioxygenase
hIFN-γ	human interferon-gamma
IDO	indoleamine 2,3-dioxygenase
IFN	interferon
IFN-γ	IFNG, gamma-interferon
IL-1	interleukin-1
INDO	indoleamine 2,3-dioxygenase gene
IPTG	isopropyl-β-D-thiogalactopyranoside
IRF1	interferon-regulatory factor 1

Kyn	kynurenine
LB	Luria-Bertani
MALDI	matrix assisted laser desorption ionisation
mRNA	messenger ribonucleic acid
NAD	nicotinamide adenine dinucleotide
Ni-NTA	nickel-nitrilotriacetic acid
OD	optical density
PBS	phosphate-buffered saline
PCR	polymerase chain reaction
PI	4-phenylimidazole
pI	isoelectric point
PMSF	phenylmethylsulfonylfluoride
QA	quinolinic acid
rhIDO	recombinant human indoleamine 2,3-dioxygenase
rmIDO	recombinant mouse indoleamine 2,3-dioxygenase
RNA	ribonucleic acid
SDS-PAGE	sodium dodecyl sulfate polyacrylamide gel electrophoresis
ssDNA	single-stranded deoxyribonucleic acid
STAT1	signal transducer and activator of transcription 1
$t_{1/2}$	half-life
TFA	trifluoroacetic acid; trifluoroacetate
TOF	time of flight
Tris	tris(hydroxymethyl)methylamine
tRNA	transfer ribonucleic acid
UV	ultraviolet
UV-Vis	ultraviolet-visible

Chapter 1

Introduction

Chapter 1

Introduction

The overall aim of this chapter is to give background information on the history, properties and importance of indoleamine 2,3-dioxygenase. This is an enzyme that is involved in various physiological functions and diseases in humans.

1.1. Indoleamine 2,3-dioxygenase

Indoleamine 2,3-dioxygenase (IDO, EC 1.13.11.52; previously EC 1.13.11.42 indoleamine-pyrrole 2,3-dioxygenase) is a heme-containing dioxygenase that catalyses the first and rate-limiting step in the kynurenine (Kyn) pathway of L-tryptophan (L-Trp) catabolism.[7,163,302] Human IDO is a product of the INDO gene (*Homo sapiens,* 8p12-p11).[122] Its expression is induced by interferon-gamma (IFNG) and enhanced synergistically by proinflammatory cytokines.[2,71,175,256,295,313] Human IDO has a molecular weight of 45.326 kDa[50,318] and a sequence consisting of 403 amino acids (**Figure 1.1**):

```
  1 MAHAMENSWT ISKEYHIDEE VGFALPNPQE NLPDFYNDWM FIAKHLPDLI ESGQLRERVE  60
 61 KLNMLSIDHL TDHKSQRLAR LVLGCITMAY VWGKGHGDVR KVLPRNIAVP YCQLSKKLEL 120
121 PPILVYADCV LANWKKKDPN KPLTYENMDV LFSFRDGDCS KGFFLVSLLV EIAAASAIKV 180
181 IPTVFKAMQM QERDTLLKAL LEIASCLEKA LQVFHQIHDH VNPKAFFSVL RIYLSGWKGN 240
241 PQLSDGLVYE GFWEDPKEFA GGSAGQSSVF QCFDVLLGIQ QTAGGGHAAQ FLQDMRRYMP 300
301 PAHRNFLCSL ESNPSVREFV LSKGDAGLRE AYDACVKALV SLRSYHLQIV TKYILIPASQ 360
361 QPKENKTSED PSKLEAKGTG GTDLMNFLKT VRSTTEKSLL KEG.....  .......... 420
```

Figure 1.1 The human IDO protein sequence containing 403 amino acids and a molecular weight of 45.326 kDa (Primary accession number: P14902). Conserved regions of IDO as signatures for the IDO family of proteins are depicted in **red**.

1.2. Characteristics and catalytic properties of IDO

IDO as a cytosolic heme protein is one of the few heme-containing dioxygenases known to exist.[154] Two conserved regions of IDO are signatures for the IDO family of proteins.[287] These include ([261]**GGSAGQSSVFQ**[271]) in the central section of the protein, which is rich in glycine and serine residues, and ([291]**FLQDMRRYMPPAHR**[304]) in the second third section of the sequence, which is rich in arginine residues. IDO contains a conserved histidine (**His346**) that serves as a proximal ligand to the heme *b* co-factor iron. The His346 is potentially a base that can differentiate human (*Homo sapiens*) IDO (hIDO) from that of other species.[154]

IDO catalyses the addition of oxygen (O_2) across the C2-C3 double bond of the indole-pyrrole ring in L-Trp to form *N*-formyl-L-kynurenine (*N*-formylKyn)[17] (**Figure 1.2**).

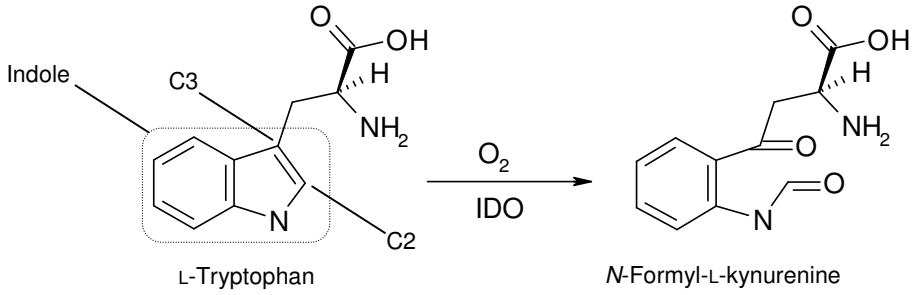

Figure 1.2 IDO catalyses the addition of oxygen (O_2) across the C2-C3 bond of the indole pyrrole ring in L-Trp to form *N*-formylKyn.

Additionally, it uses heme (iron protoporphyrin IX, heme *b*, **Figure 1.3**) as a co-factor. The co-factor serves as the prosthetic group that maintains the catalytic activity of the enzyme. Reduced flavin mononucleotide (FMNH2),[216,218] NADPH-cytochrome b5 reductase/cytochrome b5[167] (**Figure 1.4**) or other reductive activators are believed to

serve the role of maintaining the heme *b* co-factor iron in its active ferrous (Fe^{2+}) state *in vivo*. *In vitro*, an artificial reducing system consisting of ascorbic acid and methylene blue are typically used to maintain maximum catalytic activity by ensuring the ferrous state of the heme *b* iron (**Figure 1.5**).[152,211,277,278,279,304] This process involves a co-substrate of O_2, oxygen radicals or superoxide ($O_2^{\bullet -}$).[52,58,128,170,171]

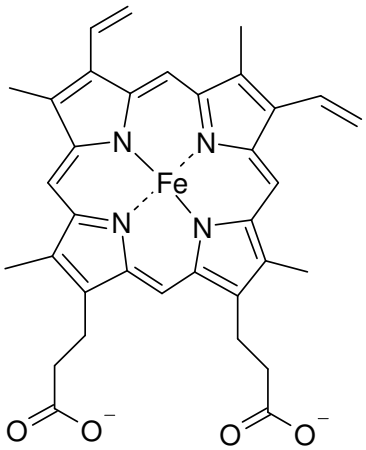

Figure 1.3 Heme (iron protoporphyrin IX, heme *b*).

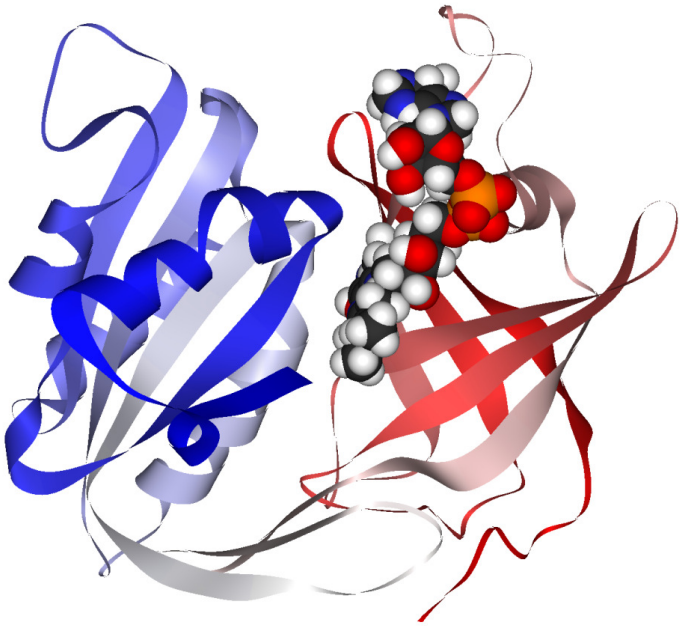

Figure 1.4 NADPH-cytochrome b5 reductase/cytochrome b5 (GNU General Public Licence).

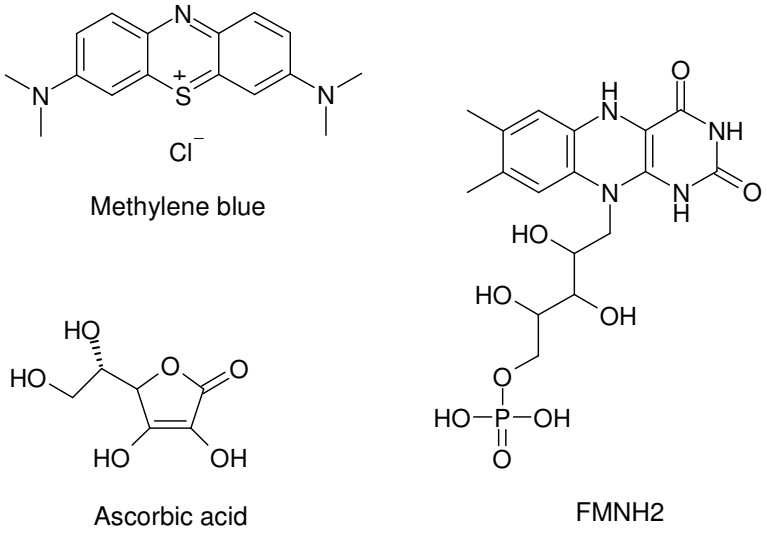

Figure 1.5 *In vivo* a flavin (reduced flavin mononucleotide, FMNH2) or cytochrome b5 (**Figure 1.4**) is believed to be the reducing system needed to maintain maximum catalytic activity of IDO, ensuring that the heme *b* iron is in its ferrous (Fe^{2+}) state. *In vitro*, methylene blue and ascorbic acid are used to serve this role.

1.3. Discovery of IDO and the IDO gene

IDO was discovered in rabbit intestine by Hayaishi and co-workers in 1963.[96] In 1967, IDO was determined to be an enzyme capable of catalysing the conversion of L-Trp to *N*-formylKyn in the rabbit intestine.[347] It was purified from rabbit intestine in 1978 and was identified as a heme-containing dioxygenase. It was named indoleamine 2,3-dioxygenase because it exhibited a broad substrate specificity.[97,107,232,286] It oxidised not only L-Trp [**1**] but also D-Trp [**2**], D-5-hydroxykynurenine and L-5-hydroxykynurenine [**3**, **4**], serotonin [**5**] and tryptamine [**6**][18,65,73,96,314] (**Figure 1.6**). Human IDO was purified in 1988 from the placenta and was found to be inactive for serotonin.[295]

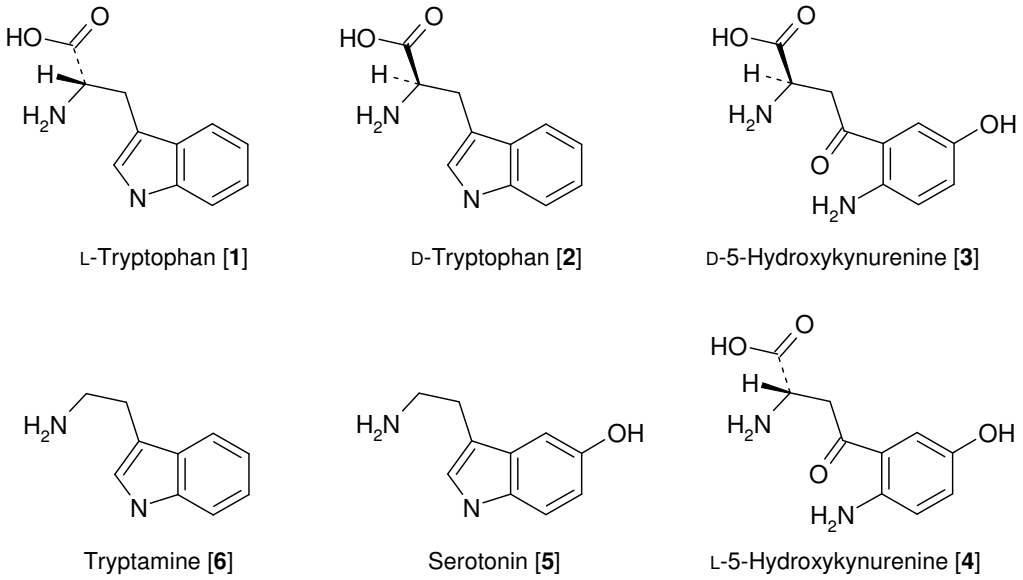

Figure 1.6 IDO exhibits broad substrate specificity. Rabbit IDO oxidises L-Trp [**1**], D-Trp [**2**], D-5-hydroxykynurenine [**3**], L-5-hydroxykynurenine [**4**], serotonin [**5**] and tryptamine [**6**]. Human IDO is inactive for serotonin.

A genomic DNA clone containing part of the transcribed region of the IDO gene (INDO) and approximately 13 kilobases (kb) of the 5'-upstream DNA sequence was isolated and analysed in 1990.[49] The nucleotide sequence and its protein product was identified as IDO. The cDNA clone was isolated from an Xgtl 1 cDNA library that was prepared from the mRNA of IFNG-treated human erythroleukemic (HEL) fibroblasts with a monoclonal antibody against IDO. This gene was named INDO. Its open reading frame was 1209 nucleotides in length and encodes the protein with a molecular weight of 45.326 kDa containing 403 amino acid residues (**Figure 1.7**).[318]

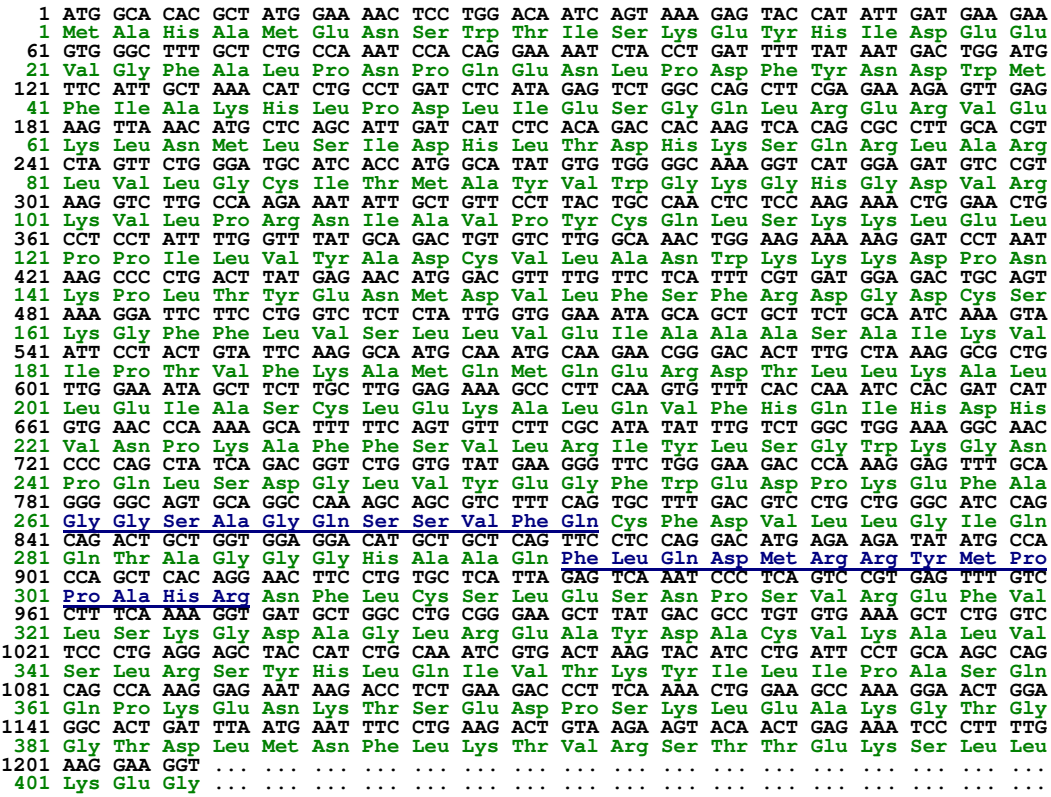

Figure 1.7 The human IDO cDNA, with an open reading frame of 1209 nucleotides in length, encoding the protein with a molecular weight of 45.326 kDa and containing 403 amino acid residues. Regions conserved in IDO family members are depicted in blue.

No homology with any known gene in the gene database (National Center for Biotechnology Information, NCBI) was found for INDO and the cDNA codes for IDO.[50] The primary structure of human indoleamine 2,3-dioxygenase (hIDO),[317,318] as deduced from the nucleotide sequences of the cDNA clones, was published by Tone and co-workers in 1994.[317]

1.4. Localisation of IDO

IDO is expressed in many cells and tissues including astrocytes,[1,3,86,87,227] astrocytoma cells,[2,3,54] carcinoma cells,[2,32] glioblastoma cells,[54,165] peripheral blood mononuclear

cells,[21,34,35,71,119] natural killer cells,[124,292] lymphocytes, monocytes, fibroblasts, syncytiotrophoblasts, macrophages, mononuclear phagocytes, endometrium, decidua, brain, liver, lung, small and large intestine, colon, spleen, kidney, stomach, fallopian tube, cervical mucus, placenta, chorion, lens, retina and ciliary body.[3,87,93,94,156,159,185,204,250,260]

IDO is expressed by microglia and its levels are up-regulated by IFNG.[6,249] Although the INDO gene is IFNG-induced,[37,88,272] its expression is enhanced synergistically by proinflammatory cytokines including tumor necrosis factor α and interleukin-1 (IL-1) in macrophages,[100,102] monocytes and epithelial cells.[2,26,54,109,110,320,326] High levels of IDO are expressed in the lung,[324,348,349,350,351] intestines,[45,73,89,271] and in term placenta,[135,139] the latter of which has the highest expression of IDO so far known.[150,268]

1.5. Expression of IDO

IDO expression is highly responsive to signals from the immune system[112,118,126,134,159] and can be induced in various cell types. The factors that regulate the expression of IDO are highly cell-type specific. IDO is encoded by a single gene (2 kbp) spreading over 15 kbp of DNA. It is located in a syntenic region of human chromosome 8 (*Homo sapiens,* 8p12-p11).[41,122] The human IDO gene (INDO) promoters contain multiple sequence elements that confer potent responsiveness to type II interferons such as IFNG.[306] Various cell types including monocyte-derived macrophages, dendritic cells, fibroblasts, endothelial cells and some tumor-cell lines, express IDO after exposure to IFNG.[13] Signal transducer and activator of transcription 1 (STAT1) and IFN-regulatory

factor 1 (IRF1) function cooperatively to mediate the induction of IDO expression[13,41,71,137,191,281] by IFNG.[165,178,354]

In women, IDO expression is stimulated by immune factors and increases with placenta development in healthy pregnancy.[103] This causes a decrease in blood Trp concentration and the elevation of Kyn. The expression of IDO does not play an essential role in men but it can be activated by immune factors. In pregnant women, changes in Trp metabolism are observed from the first weeks of pregnancy.[103,289] The expression occurs in the trophoblast and then in the placenta. IDO expression is correlated with placenta development. During pregnancy, IDO activation plays an essential role in the immunological tolerance between the mother and the fetus.[103,231] The induction of IDO expression in the trophoblast suppresses T-cell activity against the fetus. IDO induction in the trophoblast and placenta is sufficient to inhibit the immune system of the mother and to prevent expulsion of the fetus. Administration of the IDO inhibitor 1-methyltryptophan causes allogeneic foetal rejection.[289] IDO-initiated Trp degradation in the placenta has been implicated in the prevention of the allogeneic fetal rejection.[289,311]

1.6. IDO and L-tryptophan

L-Tryptophan (L-Trp) is an essential amino acid for many organisms including humans. It cannot be synthesised by humans and therefore must be part of the diet. L-Trp is a building block in protein biosynthesis and is a biochemical precursor for many biological compounds.[22,51,55,59] In addition to its utilisation for protein synthesis, L-Trp is also used for the synthesis of the neurotransmitter serotonin [**5**], which is further converted into

melatonin [**7**] in the pineal body in the brain.[72,96,234,251] Whereas a small amount (about 1%) of L-Trp from dietary intake is converted to serotonin, more than 95% is metabolised along the kynurenine (Kyn) pathway[1,176] (**Figure 1.8**) to form *N*-formylkynurenine (*N*-formylKyn) [**8**], kynurenine (Kyn) [**9**], kynurenic acid [**10**], 3-hydroxykynurenine (3-hydroxyKyn) [**11**], xanthurenic acid [**12**], quinolinic acid [**13**] and nicotinamide adenine dinucleotide (NAD) [**14**] (**Figure 1.9**).

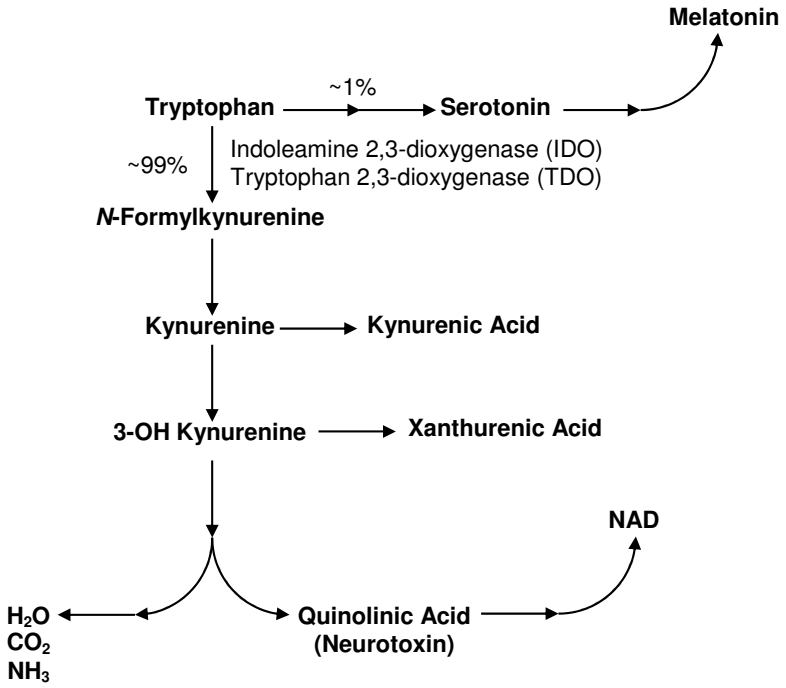

Figure 1.8 The kynurenine pathway, the major metabolic pathway of L-Trp in humans involving IDO. TDO is highly specific to L-Trp and is therefore called L-tryptophan 2,3-dioxygenase (EC 1.13.1.12) and is abundantly expressed in the liver.

Although the metabolites in the Kyn pathway are pharmacologically active, unbalancing in their local concentrations could lead to pathological situations.[56,61,68,314,341] In the immune system, a reduction in Trp and an increase in Kyn by IDO suppresses T-cell

function.[21,254,309,330] In the nervous system, Kyn can be further metabolised to the neurotoxic quinolinic acid.[44,83,196] The enzymes tryptophan 2,3-dioxygenase (TDO) and IDO catalyse L-Trp to form *N*-formyl-L-kynurenine. As already described, this transformation by IDO, but not TDO, is activated by immune factors such as IFNG and in pregnancy.

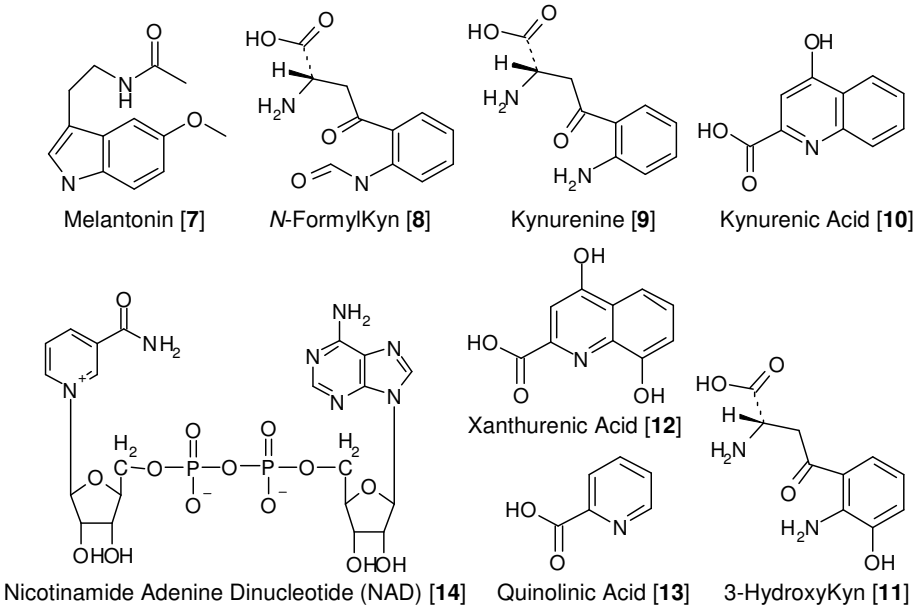

Figure 1.9 The major metabolic pathway of L-Trp leads to the formation of melatonin [7], *N*-formylkynurenine [8], Kyn [9], kynurenic acid [10], 3-hydroxykynurenine [11], xanthurenic acid [12], quinolinic acid [13] and nicotinamide adenine dinucleotide (NAD) [14].

1.7. Degradative action of IDO on L-Trp

The degradative action of IDO on the essential and relatively scarce amino acid L-Trp leads to a number of significant consequences. The activity depletes pools of L-Trp available for protein synthesis, thereby restricting the growth of L-Trp dependent cell system.[64,314] The catabolism of the essential amino acid L-Trp halts reproduction of pathogens in infected cells and stops malignant growth.[158,187,302.303] Bacterial, parasitic or

viral action and infections activate T-cells and NK-cells to produce IFNG. IFNG induces the expression of IDO leading to the decrease[297,327,342] of localised or systemic L-Trp levels, a mechanism by which INFG inhibits the production and growth of certain bacteria, intercellular parasites and viruses.[204,206,215,225,238,239,246] Consequently, induction of IDO[250,262,291,299,353] is considered as one of several anti-proliferative[49,50,51,88] pathways that are induced by the Th1-type cytokine IFNG established during immune response.[48,320,321,345] The L-Trp depletion also renders a significant reduction in T-lymphocyte proliferation.[124,143,144,173]

Studies have established that the resultant inhibition of T-lymphocyte replication leads to immunosuppression[203,220,229] and tolerogenicity.[142,157,161,198,201] This finding has implications in the science of fetal rejection[166,282] and organ transplant survival.[7,221,241,290,296] The expression of IDO and L-Trp depletion also leads to the elevation of Kyn pathway metabolites and decreased levels of serotonin, which produce a wide range of effects. Studies have described the excitatory and toxic effects of quinolinic acid, which affects neuronal activity.[86] IDO studies have expanded the understanding of the role of L-Trp in immunology, AIDS, organ transplant, autoimmune diseases, immune response,[188,141,200,260,261] immunosuppression,[12,66,177] cancer and mental functions.[82,259] IDO is now accepted as an important therapeutic target for many diseases.[16,222,345] This includes Alzheimer's disease which is caused by the aberrant production of the neurotoxin quinolinic acid,[105,140,328] and age-related cataract which is caused by a post-translational modification of lens proteins with L-Trp-derived ultraviolet (UV) filters.[298,301,302,303,334]

1.8. Heme *b* and IDO binding pocket

Sono,[274,275,276] Terentis,[308] Littlejohn,[154] Aitken[5] and co-workers showed that the iron protoporphyrin IX (heme *b*), the sole prosthetic group that is essential for enzymatic activity in hIDO, is strongly bound at the proximal ligand (Fe^{2+}-His346, **Figure 1.10**).

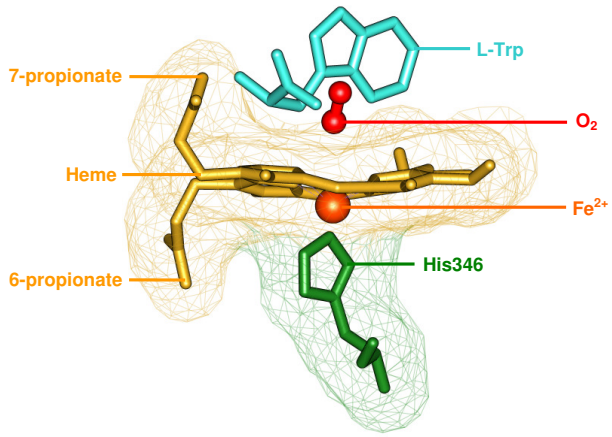

Figure 1.10 Iron protoporphyrin IX (heme *b*), the sole prosthetic group that is essential for enzymatic activity in hIDO, is strongly bound at the proximal ligand (Fe^{2+}-His346). The strength of the proximal Fe-His346 bond is stronger when iron of the heme *b* in at its Fe^{2+} state (in comparison to its Fe^{3+} state).[154,284]

The strength of the proximal Fe-His346 bond is greater with the iron of the heme *b* in its Fe^{2+} state and not its Fe^{3+} state.[151,280] Binding of the heme *b* with L-Trp in the distal pocket followed by interaction with dioxygen bound to the heme *b* iron (Fe^{2+}), is crucial for the enzymatic activity of IDO. The binding of L-Trp in the distal pocket does not seem to affect the proximal Fe-His346 bond strength. A water molecule probably occupies the distal binding site at physiological pH and it is plausible that the heme-bound water is not stabilised by any His distal ligand. IDO is highly autoxidisable to its inactive ferric form (Fe^{3+} state).[96,97,107,108] None of the polar amino acid residues in

the distal heme pocket are essential for activity, suggesting that no amino acid group of IDO is essential in dioxygen (O_2) activation or proton (H) abstraction.[162,163,208,284,285]

Hirata, Ohnishi and co-workers[107,108,211] suggested that reductants are required not only to initiate but also to maintain the apparent maximal catalytic activity. Ozaki[216,218] and co-workers suggested that tetrahydrobiopterin dihydroriboflavin mononucleotide (FMNH2) is the natural reductant for IDO *in* vivo, while Maghzal[167] and co-workers suggested cytochrome b5. Evidence supports that *in vivo* the reaction mechanism for IDO catalysis precedes where the ferrous (Fe^{2+} state) enzyme binds with molecular oxygen (O_2) and L-Trp. *In vitro* the ferric (Fe^{3+} state) enzyme, on the other hand, binds first with the superoxide anion ($O_2^{\bullet -}$) and the resulting oxygenated enzyme reacts with L-Trp through the ferrous (Fe^{2+} state) enzyme to form the ternary complex.[107,208,218,274,280] IDO has a large substrate binding pocket that can accommodate a variety of relatively large substrates and inhibitors.[284,308]

1.9. Structure of IDO

In 2006 Sugimoto and co-workers successfully crystallised rhIDO (**Figure 1.11**) and resolved its crystal structures.[208,284,285] The recombinant human IDO (rhIDO) was crystallised as a dimer linked with a disulfide bridge (SS-bond) at Cys308 (Cys308-Cys308) by the vapour-diffusion technique. It was complexed with the ligand inhibitor 4-phenylimidazole (PI) and cyanide (CN^-). The addition of 4-phenylimidazole as a heme ligand was essential for crystallisation. 2-(*N*-cyclohexylamino)ethane sulfonic acid (CHES) was reported to be an important component of the crystallisation buffer that

interacted within the active site. Diffraction data were collected at resolutions of 2.3 and 3.4 Å, respectively. The crystals belong to space group P212121, with unit-cell parameters a=86.1, b=98.0, c=131.0 Å.[208,284]

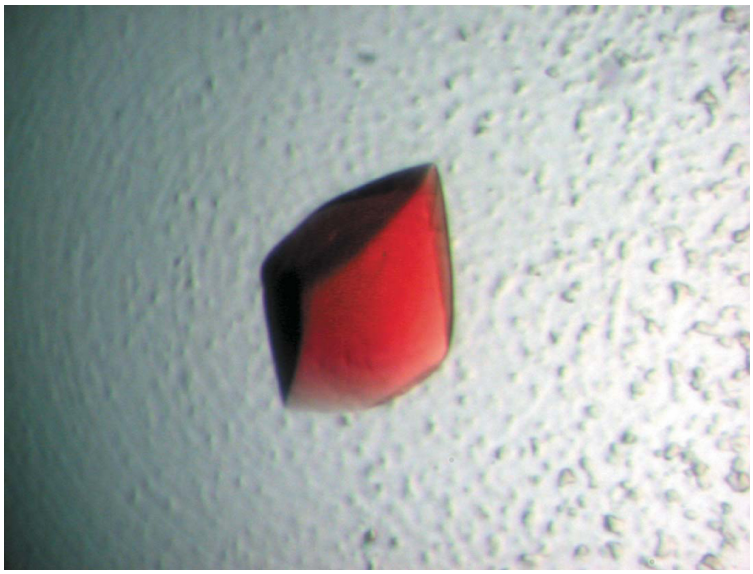

Figure 1.11 Crystals of IDO as photographed by Oda, Sugimoto and co-workers.[208,284]

1.9.1. Three dimensional structure of IDO

The structure of IDO (**Figure 1.12**) is folded into two distinct domains, small and large. The helices are named in order of appearance in the primary sequence, A to S. The small domain (helices A to F) comprises of six α-helices, two short β-sheets and three 3_{10} helices. The large domain (helices G to S) is all-helical and comprises of 13 α-helices with two 3_{10} helices. Helices G, I, Q and S of the large domain run parallel to the heme *b* co-factor plane. These helices interact with neighbouring helices by hydrophobic interactions. Helix Q provides the proximal ligand (His346 imidazole) for the heme *b* iron at the fifth coordination position.

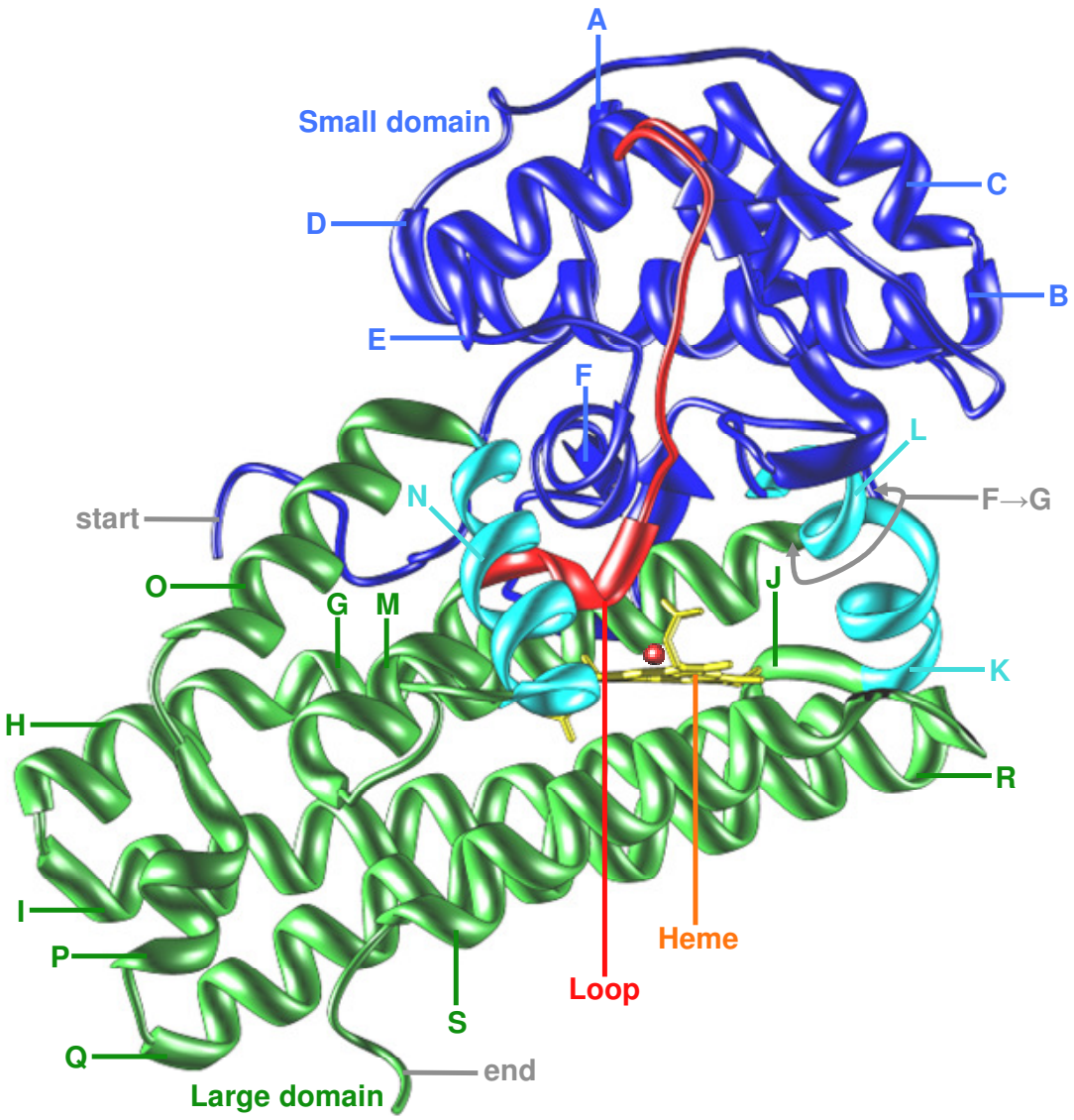

Figure 1.12 Ribbon presentation of the structure of human IDO. The small and large domains are presented as blue and green ribbons, respectively. The helices A to S are named in order of appearance in the primary sequence. The connecting helices (K-L and N) of the two domains are in cyan. The long loop connecting the two domains (between helices L and M) is in red. The helices of the large domain (green) create the cavity for the heme *b* co-factor. The connecting loop (red) and a small domain above the sixth-coordination site (heme distal side) cover the top of cavity on the heme *b* (yellow). Four proximal helices I, G, Q and S (green) run in parallel.

Interfaces between the two domains are formed by combinations of hydrophobic interactions, salt bridge and hydrogen bonds mediated by side chains of the amino acid

residues. Sugimoto and co-workers reported that the particular folding of each domain in IDO was not identical to any other known protein structures in the similarity-searching database.[284] In their study they were not able to construct a model for the region outside the heme pocket between helices R and S (residues Gln360 to Gly380) due to disordered electron density. This region was presumed to be a flexible loop.[162,208,284,285]

The heme-binding pocket in IDO is created by helices G, I, Q and S and helices K-L and N. The side chains of helices K (Phe226), L (Arg231, Leu234, Ser235, Gly236) and N (His287, Phe261) connect the two existing domains (helices A to F and helices G to S) and contribute to the heme-protein-substrate interactions.

A small domain before the start of the M helix and a long loop (residues Glu250 to Ser267) between L and M connects the two domains above the sixth-coordination site of the heme *b* (distal side), covering the top of the heme pocket.[162,208,284,285] Contacts between the two domains are very extensive with a buried surface area of 3,100 Å.[208]

1.9.2. Surface electrostatic potential and surface hydrophobicity of IDO

IDO has a symmetric charge distribution on its molecular surface and therefore no suitable region can be identified in the proximal surface for the interaction with possible reductases.[284] The molecular surface representation (**Figure 1.13**) shows the surface electrostatic potential of IDO and the entrance for ligands towards the heme pocket.

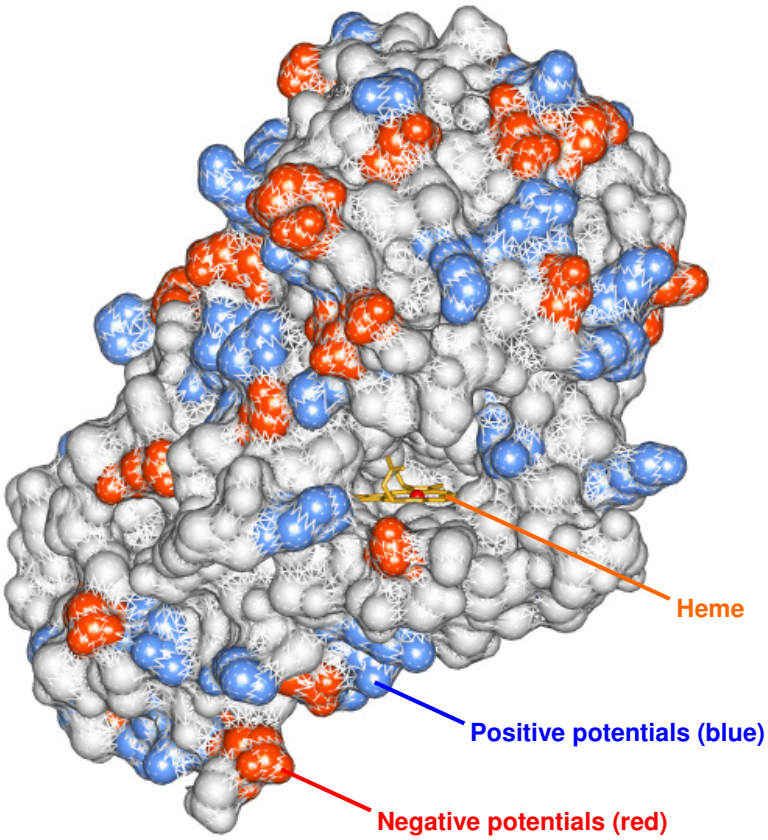

Figure 1.13 The surface electrostatic potential of IDO. Positive potentials are in blue and negative potentials are in red. The heme *b* is shown as a stick model (yellow) with its 7-propionate partially exposed to the solvent. Asymmetric distribution of positively and negatively charged areas is not observed in IDO. [184]

These electrostatic potentials, which are caused by charged side chains and bound ions, play a significant role in protein folding, stability, catalysis and in specific protein-protein recognition. The positive (blue) and negative (red) potentials of the surface represent the charge distribution on IDO. This distribution forms the characteristic anisotropic electric field of the enzyme. The heme *b*, which is shown as a stick model (yellow) has its 7-propionate partially exposed.[162,208,284,285] Significant polar amino acids and water molecules are absent from the active site of IDO, suggesting that the hydrogen-bonding network that connects the active site to the solvent region is lacking in the distal pocket of

the IDO structure. These structural characteristics around the heme pocket of IDO are in good agreement with the proposed catalytic reaction, in which IDO in the active site does not require the supply of either protons or electrons for its catalytic purposes.[162,208,284,285]

Surface hydrophobicity can be used to identify regions of the protein surface that are most likely to interact with binding ligands. Changes in protein conformations are often associated with changes in surface hydrophobicity. The heme pocket of IDO is lined with a flexible loop (residues Ala260 to Gly265) by which the indole ring of the substrate L-Trp is believed to interact. This interaction is hydrophobic in nature, a key element that affects the conformational equilibrium between the active and inactive forms of IDO.[284] The amino-acidic moiety of L-Trp faces the entrance of the enzyme where the α-amino group interacts with the 7-propionate moiety of the heme *b*. The α-carboxylic acid group points toward Arg231 whereupon conformational rearrangement may promote the formation of a salt bridge interaction.[163] The hydrophobic solvent-accessible surface and overall hydrophobicity of IDO derived from the its 3D structure as reported by Sugimoto and co-workers is given in **Figure 1.14**, showing the distribution of hydrophobic, polar and solvent-accessible surface areas.

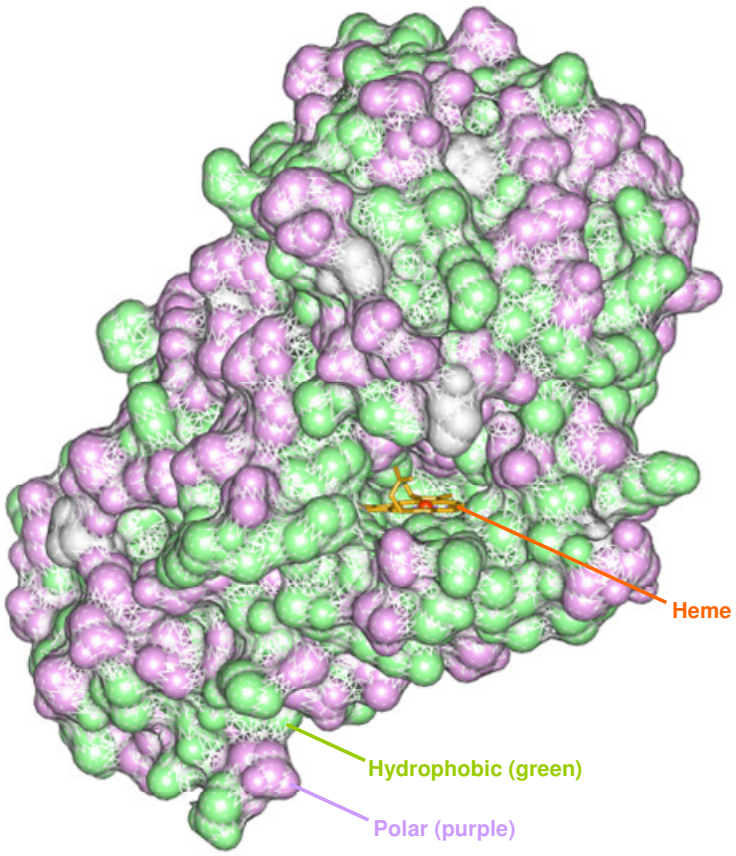

Figure 1.14 The surface hydrophobicity of IDO. Hydrophobic residues are drawn in green and polar residues are in purple. The heme *b* is shown as a stick model (yellow) with the 7-propionate partially exposed.

1.10. IDO inhibitors

IDO weakens a vigorous antitumor immune response[76,169,182,193] by promoting peripheral tolerance and shaping the host environment to be more hospitable to tumor survival and growth. The study of IDO inhibitors[39,123,136,174,189] and the development of potent IDO inhibitors that compromise tolerogenic mechanism is an important therapeutic goal. The phenomenon of immune escape is central to tumor cell survival, the basis of which is still poorly understood.[8,242] An appropriate activated immune system can eradicate cancer,

even when it is aggressive and disseminated. However, spontaneous occurrences are rare, prompting the development of numerous anticancer therapies[119,149] such as the use of IDO inhibitors aimed at supporting the immune system.[30,193,195,226]

Literature studies highlight that the rational design and development of IDO inhibitors requires an understanding of Trp catabolism,[163,180,214,228] enzyme structure and mechanism.[162,208,284,285] Unique structures have been discovered to have IDO-inhibitory activity.[30,77,169,226,279] The majority of active structures contain the indole core or resemble L-Trp.[192] An important goal in the development of IDO inhibitors for therapy is to discover potent inhibitors on the basis of the catalytic reaction mechanism and active site environment of IDO. IDO inhibition produces antitumor efficacy in certain tumor models when combined with certain cytotoxic chemotherapeutic agents.[30,193,195,226]

1.11. Conclusion

IDO catabolises Trp to Kyn.[33,117,209] In recent years there has been a lot of attention on IDO because of its role in human diseases.[172,181,183,186] The structure, occurrence and catalytic properties of IDO have become a major area of research.[47,111,138,146,155,179,184] Metabolism and catabolism of L-Trp in organisms[84,145,147,307,331] and the deprivation[143,219] and depletion of L-Trp[115,164,267,269] are equally important areas of research. IDO catalysed degradation of L-Trp[294] has been intensively studied *in vitro* and *in vivo* conditions in human and non-human cells.[199,223,319,338,339] Studies have shown that the degradative action of IDO on L-Trp leads to cell death.[57,106,205,292] IDO is involved in various important biological processes and expressed in various tissues and

microbes.[190,197,202,207,212,300,301] Other major areas of research include IDO and IDO induction[210,213,217,244,245] and studies on IDO-like proteins.[287,288]

As IDO is involved in various aspects of biological systems and functions,[247,252,253] a multi-disciplinary approach to the research on IDO and IDO related studies is essential. With the ever increasing studies on IDO, large quantities of good quality and well studied IDO is therefore crucial. The expression of recombinant human IDO (rhIDO) in *Escherichia coli* (*E. coli*) serves this purpose. The expression of rhIDO in *E. coli* (pQE-9-IDO, pREP4) has been investigated but inadequacies still prevail from earlier studies. This current study, therefore aimed to i) optimise the expression of rhIDO in *E. coli* (pQE-9-IDO, pREP4) in order to obtain high quality enzyme, ii) evaluate the characteristics and stability of rhIDO in order to understand its behaviour as a support towards further studies, iii) study the re-incorporation of the heme *b* co-factor of rhIDO as an approach to optimising the availability of the enzyme for further studies and iv) evaluate the contribution of individual cysteines towards the overall catalytic properties and stability of rhIDO through mutagenesis studies.

Chapter 2

Expression and purification of indoleamine 2,3-dioxygenase

Chapter 2

Expression and purification of indoleamine 2,3-dioxygenase

The overall aim of this study was to optimise the conditions for growth of E. coli EC538 (pQ-E-9-IDO, pREP4) suitable for the expression of quality rhIDO and improved yields of the enzyme.

2.1. Recombinant human indoleamine 2,3-dioxygenase

Since the late 1970s, there has been a major expansion in the research conducted on indoleamine 2,3-dioxygenase (IDO) and IDO initiated L-tryptophan (L-Trp) metabolism. These studies have aimed at understanding the role of IDO and the expression of IDO in humans.[16,42,46,79,101] IDO in humans is associated with many diseases and therefore the therapeutic inhibition of IDO as an effort to prevent or treat IDO induced diseases is a major research avenue.[30,193,195,226] Native human IDO has been isolated and purified from the human placenta using sequential cation exchange chromatography, hydroxyapatite chromatography, gel filtration and isoelectric focusing.[98,131] The study of IDO and design of IDO related therapeutics requires significant amounts of protein. Recombinant human IDO (rhIDO) therefore provides a more viable source of protein compared with native IDO from human placenta.[9,10,11,152]

Recombinant human IDO with a hexahistidyl-tag (6xHis-tag) at the *N*-terminus has been expressed in *Escherichia coli (E. coli)* EC538 strain.[9,10,11,152] 6xHis-tagged rhIDO has a

molecular weight of 46,960 Da and consists of 417 amino acids, with a 1634 Da 6xHis-tag (**Figure 2.1**). The 6xHis-tag enables the purification of the rhIDO by affinity chromatography.[9,10,11,152,337]

```
                                                    [Hexahistidyl-tag]
                                                      MRGS HHHHHHGSVD    0
  1 MAHAMENSWT ISKEYHIDEE VGFALPNPQE NLPDFYNDWM FIAKHLPDLI ESGQLRERVE   60
 61 KLNMLSIDHL TDHKSQRLAR LVLGCITMAY VWGKGHGDVR KVLPRNIAVP YCQLSKKLEL  120
121 PPILVYADCV LANWKKKDPN KPLTYENMDV LFSFRDGDCS KGFFLVSLLV EIAAASAIKV  180
181 IPTVFKAMQM QERDTLLKAL LEIASCLEKA LQVFHQIHDH VNPKAFFSVL RIYLSGWKGN  240
241 PQLSDGLVYE GFWEDPKEFA GGSAGQSSVF QCFDVLLGIQ QTAGGGHAAQ FLQDMRRYMP  300
301 PAHRNFLCSL ESNPSVREFV LSKGDAGLRE AYDACVKALV SLRSYHLQIV TKYILIPASQ  360
361 QPKENKTSED PSKLEAKGTG GTDLMNFLKT VRSTTEKSLL KEG.....  .........  420
```

Figure 2.1 rhIDO sequence of 417 amino acids with the 6xHis-tag at the *N*-terminus depicted in **blue**.

Expression of rhIDO in *E. coli* EC538 was first reported by Littlejohn and co-workers in 2000.[152] The *E. coli* EC538 contains the pQE-9-IDO plasmid (Qiagen pQE-9 with a 6xHis-tag, ampicillin resistance vectors and the human IDO cDNA) and the pREP4 plasmid (Qiagen pREP4 with kanamycin resistance and *lac* repressor protein vectors) (**Figure 2.2**).[236] Littlejohn and co-workers[152] cultured the *E. coli* EC538 (pQE-9-IDO, pREP4) at 37 ^{o}C in Luria-Bertani (LB) media that incorporated 10 µM isopropyl-β-D-thiogalactopyranoside (IPTG) and the protease inhibitor phenylmethylsulfonyl-fluoride (PMSF). The inhibitor was added to the media to prevent formation of truncated rhIDO.[153] The growth media was supplemented with 7 µM hemin as an exogenous heme source.[152] Subsequent purification of the rhIDO using a combination of phosphocellulose and nickel-agarose affinity chromatography provided rhIDO with a specific activity of 149 µmoles of kynurenine/h/mg of protein, 0.8 moles of heme/mole of rhIDO and a yield of 1.4 mg per litre of *E. coli* EC538 (pQE-9-IDO, pREP4) culture.[152]

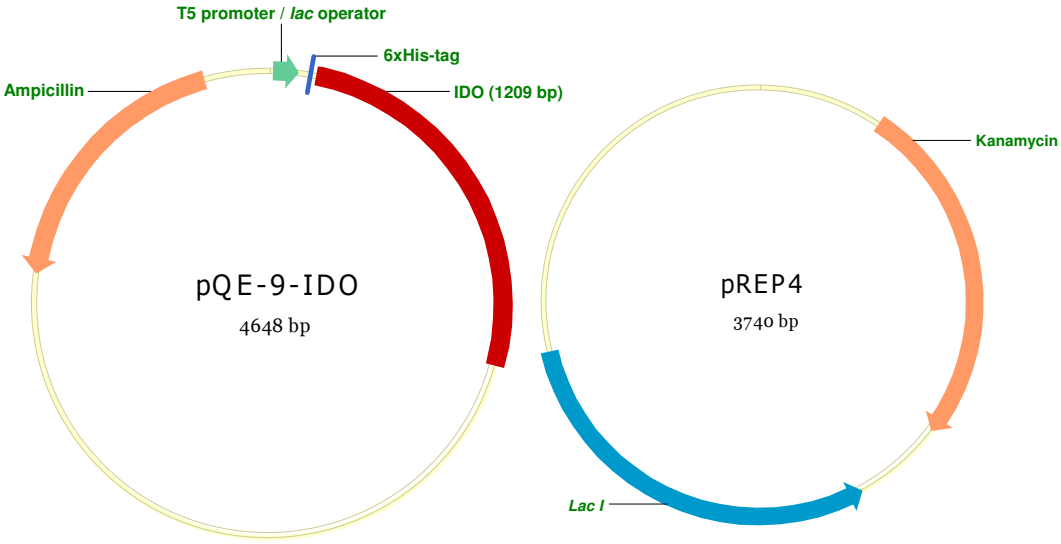

Figure 2.2 pQE-9-IDO (Qiagen pQE-9 with a T5/*lac* operator, 6xHis-tag, ampicillin resistance vectors and the human IDO cDNA) plasmid and pREP4 (Qiagen pREP4 with kanamycin resistance and *lac* repressor protein vector, *lac I*) plasmid. rhIDO expression through QE-9-IDO is under the transcriptional control of the T5 promoter/*lac* operator and repressed by the *lac* repressor protein (*lac I*) expressed through pREP4.

2.1.1. The expression method of Littlejohn and co-workers[152]

Whereas the *E. coli* EC538 (pQE-9-IDO and pREP4) expression method of Littlejohn and co-workers[152] provided higher yields of rhIDO compared with the isolation from placenta (1.4 mg rhIDO per litre of culture), the yields of soluble (active) protein were low and the heme incorporation was variable. The maximum yield of the holoenzyme (heme-incorporated enzyme) rhIDO using this method was 80%.[10] The failure of the expression method to fully incorporate heme into the recombinant protein and of the purification method to separate apoenzyme (enzyme free of heme) from holoenzyme was considered as a possible limiting factor in the studies of rhIDO.[10]

In order to optimise yields of rhIDO, Littlejohn and co-workers examined the effect of the incorporation of the inducing agent isopropyl-β-D-thiogalactopyranoside (IPTG) to the expression system. This incorporation provided a maximum yield of soluble rhIDO at approximately 10 μM IPTG (**Figure 2.3**). These trends were confirmed by Austin and co-workers.[10] Qiagen, the manufacturers of the expression vector used in these studies, recommend 1 mM IPTG induction for optimal yields of recombinant proteins.[236] The low rhIDO specific activity at high IPTG concentrations was hypothesised to arise from the formation of insoluble (and inactive) rhIDO inclusion bodies.[9]

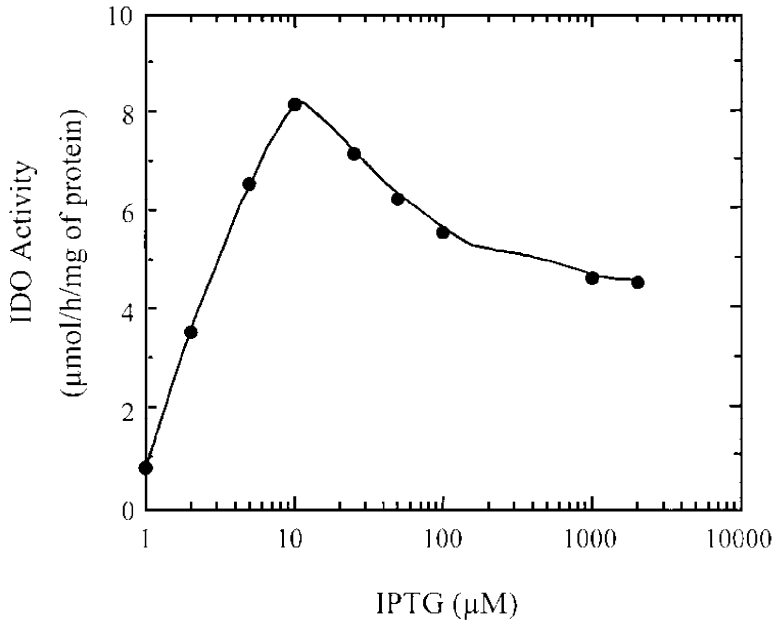

Figure 2.3 IPTG dependency on expression of soluble active rhIDO from *E. coli* EC538 (pQE-9-IDO, pREP4). Reproduced from Littlejohn *et al.*[152]

Inclusion bodies are dense aggregates of misfolded protein.[14] They are often formed when large evolutionary distances are crossed, as in the case for recombinant human proteins, where a cDNA isolated from eukarya (humans) is expressed as a recombinant

gene in a prokaryote (*E. coli*, bacteria).[14,24,264] While the cDNA may properly code for a translatable mRNA, the resulting protein emerges in a foreign microenvironment different from that of the original source of the gene. In this foreign microenvironment, mechanisms for a proper folding of the protein may also be absent. Additionally, hydrophobic residues that would otherwise be buried may be exposed and rendered available for interaction with similarly exposed sites on other xenogenic proteins.[264,265] The lack of mechanism for maintaining low concentrations of protein and the filling of the prokaryotic cell with xenogenic protein (even if it were properly folded) are further limitations to expressing recombinant protein in a prokaryotic system.[14,24,264,265] A number of approaches have been used to limit the formation of inclusion bodies and to increase the formation of soluble active protein.[255] These include lowering the concentrations of the inducing agent (IPTG), lowering the growth temperature, inducing for a shorter period of time, inducing at a higher cell density for a shorter period of time and increasing aeration.[255,257]

2.1.2. The expression method of Austin and co-workers[9,10]

In order to increase heme availability in the expression of rhIDO in *E. coli* EC538 (pQE-9-IDO and pREP4), Austin and co-workers[9,10] incorporated δ-aminolevulinic acid (ALA) during the growth of the *E. coli*. ALA is the natural biosynthetic precursor to heme *b* (**Figure 2.4**). It is more soluble and less toxic to bacteria than the exogenous heme source hemin and has been used to increase heme content of other hemoproteins.[9,10] Austin and co-workers[9,10] established that the addition of 0.5 mM ALA during the growth increased the specific activity of the resulting rhIDO from 5.1 μmoles of kynurenine/h/mg of protein to 12.4 μmoles of kynurenine/h/mg of protein.[9,10]

Additionally, they modified the method to include initial purification with nickel-agarose affinity chromatography prior to size exclusion chromatography,[9] which made this a faster method than that of Littlejohn and co-workers.[152] It gave a Soret/protein ratio (406:280 nm) of 2.2:1.0 and a specific activity of 160 μmoles of kynurenine/h/mg of protein. The specific Soret/protein ratio and specific activity were the same as those reported for the native enzyme.[10]

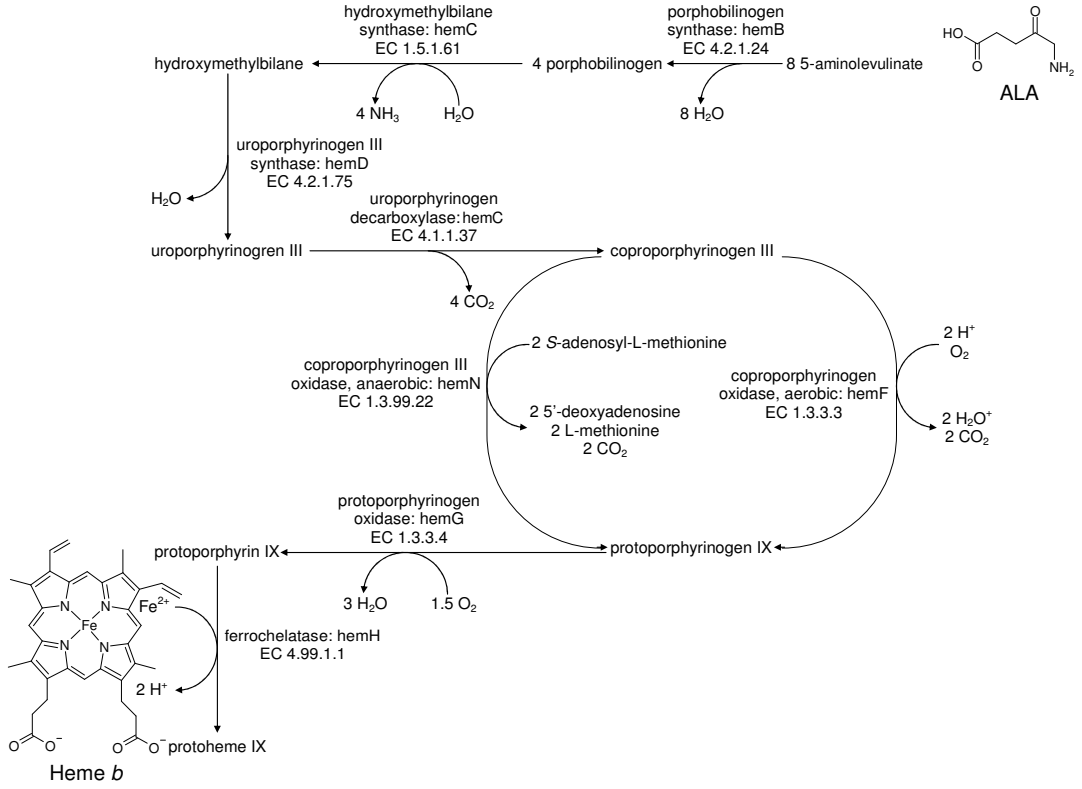

Figure 2.4 Biosyntheses of heme (iron protoporphyrin IX, heme *b*) from ALA in *E. coli*.

2.1.3. Optimisation of the expression method

The limitation of both Littlejohn[152] and co-workers and of the initial attempt by Austin[9,10] and co-workers to enhance yields and quality of rhIDO, prompted further investigations

into the expression of rhIDO in *E. coli* EC538 (pQE-9-IDO, pREP4). The overall aim of this study was therefore to i) express and purify rhIDO produced from *E. coli* EC538 (pQE-9-IDO, pREP4), ii) enhance the yield and quality of the soluble active rhIDO, iii) establish the relationship between inclusion bodies and the low yields of soluble rhIDO by examining the effect of temperature on the levels of soluble rhIDO produced and iv) explore other factors that may enhance the expression and purification of soluble active rhIDO. The expression and subsequent purifications initially employed the method developed by Austin and co-workers[9,10] with modification. This is summarised in **Figure 2.5**.

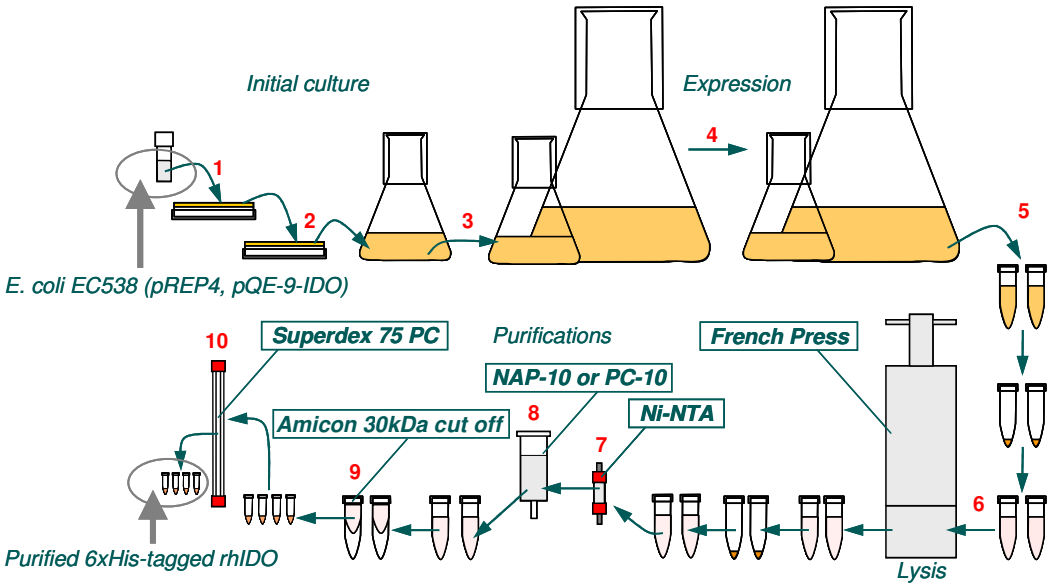

Figure 2.5 Expression and purification of rhIDO. [1] Stock *E. coli* EC538 (pQE-9-IDO, pREP4) was streaked on LB agar plates and grown. [2] A single colony from the plate was regrown and was inoculated for a starter culture. [3] Inoculation of the starter culture into the main growth liquid media. [4] Induction of growth media with addition of IPTG. ALA (0.5 mM) was added unless stated otherwise. [5] The cells produced were pelleted. [6] The pellet was resuspended, lysed using the French Press and centrifuged. [7] rhIDO purification with Ni-NTA affinity chromatography. [8] Desalting with Sephadex G-25. [9] Concentration by centrifugal filtration (30 kDa cut off). [10] Purified by Superdex FPLC size exclusion chromatography.[9,10]

2.1.4. Growth of *E. coli* at 37 ºC

Initially, *E. coli* EC538 (pQE-9-IDO, pREP4) in LB media was cultured at 37 °C with 10 μM IPTG induction using the general protocol (**Figure 2.5**). The growth profile of the bacteria was determined from aliquots of the growth media every 0.5 hours over a period of 10 hours. The optical density (OD_{600}) over time was plotted as the growth profile (**Figure 2.6**).

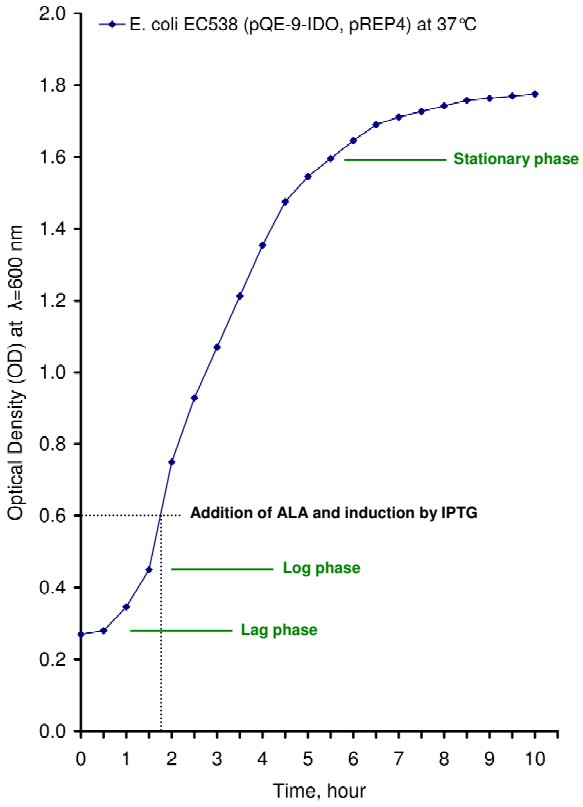

Figure 2.6 Growth profile of *E. coli* EC538 (pQE-9-IDO, pREP4) plotted as cell density (OD_{600}) against time at 37°C.

The growth media aliquots were lysed. The supernatant from the lysis was visualised for protein using sodium dodecyl sulfate polyacrylamide gel electrophoresis (**Figure 2.7**).

Time, hour	OD_{600}
0.00	0.270
0.50	0.280
1.00	0.346
1.50	0.450
1.75	0.600
2.00	0.750
2.50	0.929
3.00	1.070
3.50	1.212
4.00	1.354
4.50	1.475
5.00	1.545
5.50	1.596
6.00	1.646
6.50	1.690
7.00	1.711
7.50	1.727
8.00	1.742
8.50	1.758
9.00	1.764
9.50	1.770
10.00	1.776

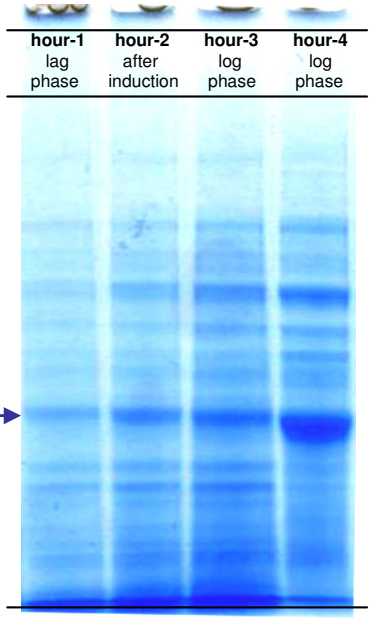

Figure 2.7 SDS-PAGE of supernatant from lysed *E. coli* EC538 (pQE-9-IDO, pREP4), following electrophoresis (100V) and visualisation with Coomassie Brilliant Blue.

The growth profile consisted of the lag, log and stationary phase expected for the *E. coli*. The lag phase is the period occurring directly after inoculation, in which the cells undergo a change in chemical composition before they grow. The log phase is the duration for which the cells undergo binary fission at an exponential rate.[236,237] This is the time during which the pQE-9-IDO is induced to produce the rhIDO. The stationary phase is the period where the cells cease to actively grow. Cells were collected by centrifugation, resuspended in Tris-HCl re-suspension buffer and lysed. The lysis utilised two passes through a French Press. The French Press forces the cells through a narrow hole under high pressure to release the pressure in order to rupture the cells. Two passes are considered sufficient for efficient lysis of the cells. During the lysis the samples were kept on ice and the French Press piston was pre-chilled to prevent protein denaturation

and aggregation arising from localised heating. SDS-PAGE of the supernatants provided levels of protein and bands consistent with those of rhIDO, as expected. The SDS-PAGE also showed fast growth and high rhIDO expression at the log phase after IPTG induction. Following lysis, severe cloudiness of the lysed cell homogenate was observed. Centrifugation of the lysed cells afforded an abundance of a residual pellet, indicating the formation of inclusion bodies.[10]

2.1.5. Presence of inclusion bodies

In joint experiments with Austin to determine if the formation of rhIDO as inclusion bodies had occurred, *E. coli* EC538 (pQE-9-IDO, pREP4) was grown at 37 ºC for 3 hours and induced with varying concentrations of IPTG (0 - 1000 μM). High concentrations of IPTG, as suggested by the manufacturer, were also evaluated. To allow for direct comparison with the experiments conducted by Littlejohn and co-workers,[152] the cultures did not include ALA. Low IPTG induction concentrations (5 - 10 μM) were used because they typically increase the proportion of protein expressed in a soluble active form.[255] This is because the low IPTG leads to slower production of recombinant protein, which in turn decreases the opportunity for aggregation and misfolding of the protein.

The residual pellets collected after centrifugation of the lysed cells were resuspended twice in Milli-Q water and centrifuged. Thereafter, the cells were treated with lysozyme and washed with Triton X-100 and Milli-Q water. This treatment ensured the complete lysis of the *E. coli* EC538 (pQE-9-IDO, pREP4) cells and the removal of soluble rhIDO from the pelleted cellular material. SDS-PAGE of the insoluble residual material (**Figure 2.8**) showed rhIDO bands at all IPTG concentrations above 1 μM. This

observation was consistent with the presence of rhIDO inclusion bodies formation at 37 ºC.

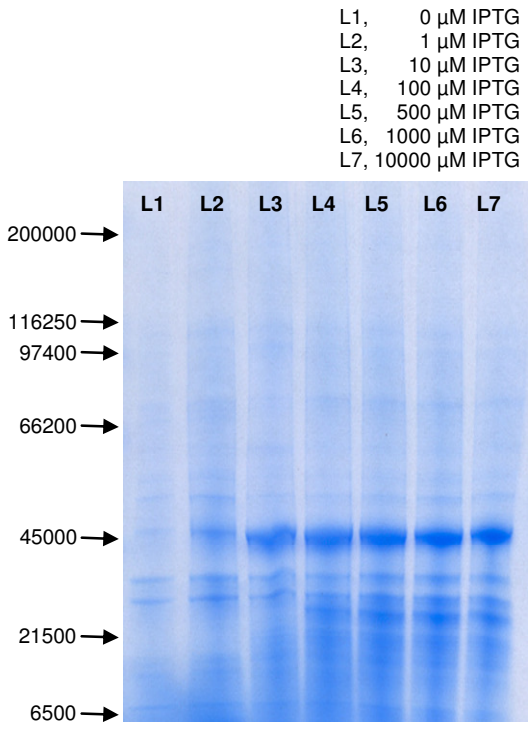

Figure 2.8 SDS-PAGE analysis of the inclusion bodies formed by *E. coli* EC538 (pQE-9-IDO, pREP4) at growth temperatures of 37 ºC with different levels of IPTG concentrations. The numbers on the left indicate molecular mass of markers in Daltons.[10]

The SDS-PAGE band at approximately 45 kDa (consistent with the molecular weight of rhIDO) was cut out and analysed for peptide sequencing at the Australian Proteome Analysis Facility, APAF, Macquarie University. The band was subjected to tryptic digest and Matrix Assisted Laser Desorption/Ionisation-Time of Flight-Mass Spectrometry (MALDI-TOF-MS) analysis. When the spectral data of the peptides from the tryptic digest were submitted to the database search program Mascot (Matrix Science Ltd,

London, UK) it confirmed the presence of rhIDO and of *E. coli* specific proteins (**Figure 2.9**).

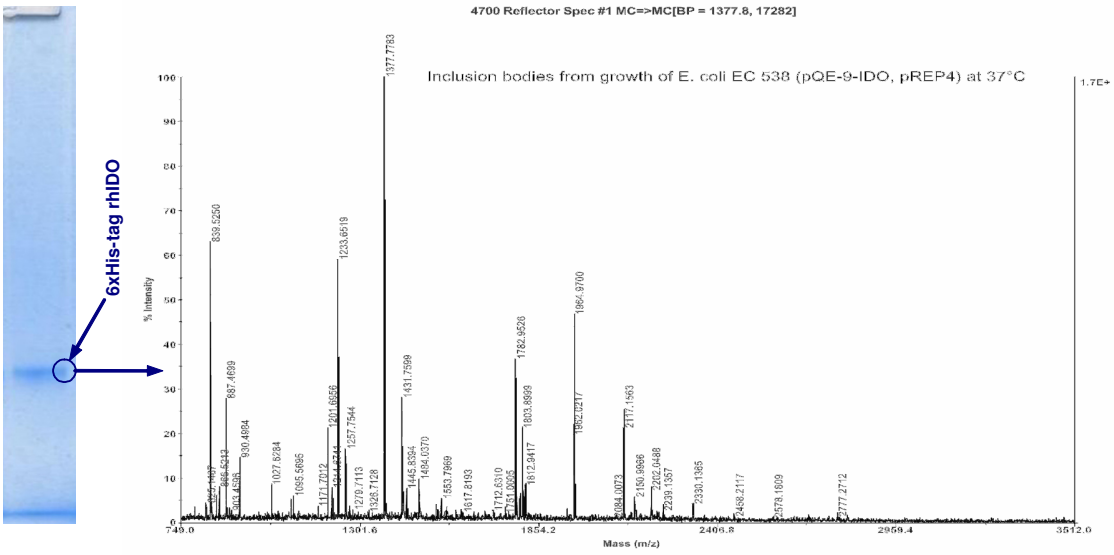

Matched peptides shown in **Bold Red**

```
  1 MAHAMENSWT ISKEYHIDEE VGFALPNPQE NLPDFYNDWM FIAKHLPDLI
 51 ESGQLRERVE KLNMLSIDHL TDHKSQRLAR LVLGCITMAY VWGKGHGDVR
101 KVLPRNIAVP YCQLSKKLEL PPILVYADCV LANWKKKDPN KPLTYENMDV
151 LFSFRDGDCS KGFFLVSLLV EIAAASAIKV IPTVFKAMQM QERDTLLKAL
201 LEIASCLEKA LQVFHQIHDH VNPKAFFSVL RIYLSGWKGN PQLSDGLVYE
251 GFWEDPKEFA GGSAGQSSVF QCFDVLLGIQ QTAGGGHAAQ FLQDMRRYMP
301 PAHRNFLCSL ESNPSVREFV LSKGDAGLRE AYDACVKALV SLRSYHLQIV
351 TKYILIPASQ QPKENKTSED PSKLEAKGTG GTDLMNFLKT VRSTTEKSLL
401 KEG
```

Figure 2.9 Peptide sequence match to IDO [*Homo sapiens*] *via* MALDI-TOF-MS. Nominal mass (MW): 45297; Sequence Coverage: 34%; Matched peptides shown in **Bold Red.**

2.1.6. Growth of *E. coli* at 30 ºC in comparison to 37 ºC

Chaperone proteins aid in the proper folding of proteins. It has been postulated that misfolding of recombinant proteins in *E. coli* is due in part to chaperone proteins not being able to cope with the large concentrations of expressed recombinant protein, or being not ideally suited to folding the foreign protein.[14,24,264] Lowering growth

temperature from 37 °C has successfully reduced inclusion bodies for *E. coli* recombinant human expression systems.[255,264] A lowering of the temperature decreases the rate of protein production in the system, thereby decreasing the burden on the chaperones.[255,263] In order to examine the effect of lowering of the temperature on the formation of rhIDO inclusion bodies, *E. coli* EC538 (pQE-9-IDO, pREP4) was cultured in tandem at both 30 °C and 37 °C with the incorporation of IPTG (0 – 1000 µM). The insoluble residual material obtained following lysis and washing of the lysed cells (**Section 2.1.5**) was investigated for rhIDO inclusion bodies using SDS-PAGE. The SDS PAGE showed that fewer inclusion bodies were formed at 30 ºC compared to 37 ºC at the same IPTG levels (**Figure 2.10**).

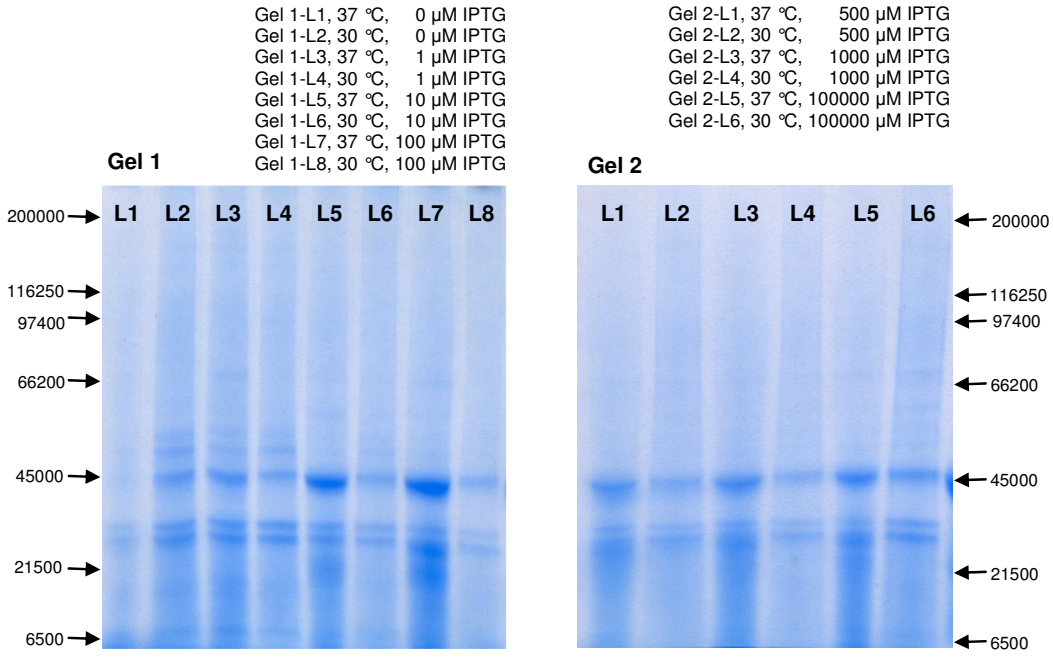

Figure 2.10 SDS-PAGE analysis of the inclusion bodies formed by *E. coli* EC538 (pQE-9-IDO, pREP4) at growth temperatures of 37 ºC and 30 ºC and with different levels of IPTG. The numbers on the left and right indicate molecular mass of markers in Daltons.[10]

Densitometric analysis of the SDS-PAGE gels showed that inclusion bodies were significantly reduced (up to 50 – 75%) at the lower temperature of 30 °C (**Figure 2.11**).

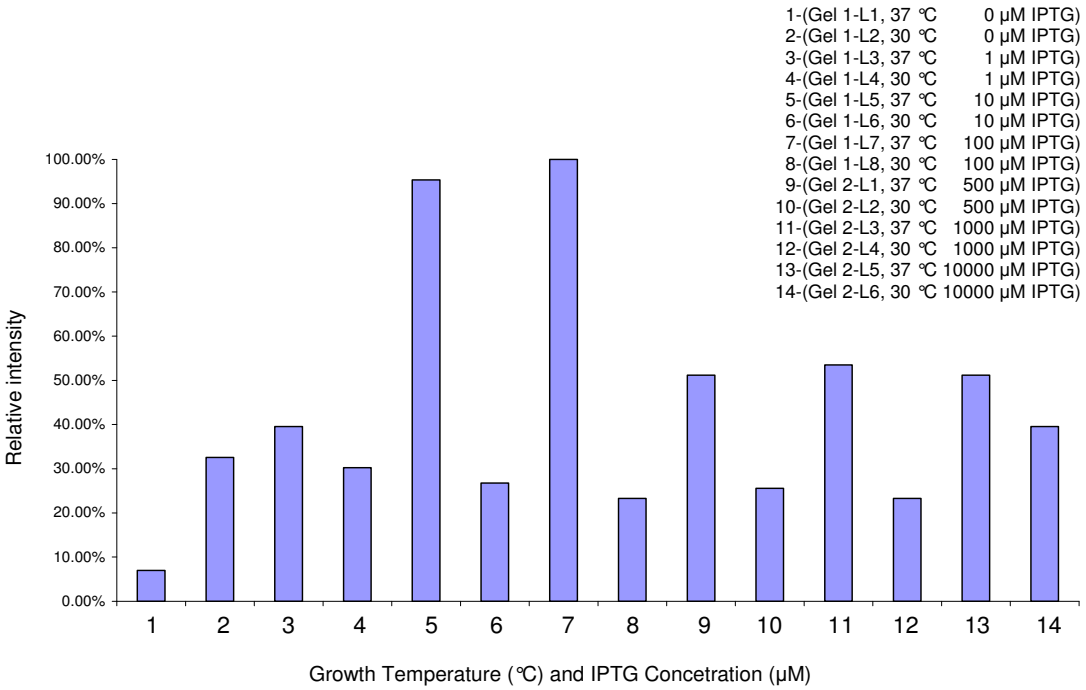

Figure 2.11 SDS-PAGE densitometric analysis of *E. coli* EC538 (pQE-9-IDO, pREP4) for various IPTG concentration in µM at growth temperatures of 37 ℃ and 30 ℃. All inclusion bodies levels are expressed as a relative percentage of the maximum density observed.[10]

This study established that the culturing of *E. coli* EC538 (pQE-9-IDO, pREP4) at 30 °C significantly reduced the presence of rhIDO inclusion bodies in the expression system. Specific activity determinations also confirmed that the activity for the expressed rhIDO at the concentration of IPTG of 10 µM was only 70% that of 100 µM. Concerns on optimising the specific activity of the rhIDO led to the incorporation of 0.5 mM ALA along with 100 µM IPTG to the expression system. Culturing was carried out at 30 °C and 37°C. Details on these investigations are outlined below.

The growth profile at 30 °C and 37 °C of *E. coli* EC538 (pQE-9-IDO, pREP4) at OD_{600} over time was determined from aliquots of the growth media with IPTG induction of 100 μM and the incorporation of 0.5 mM of ALA (**Figure 2.12**).

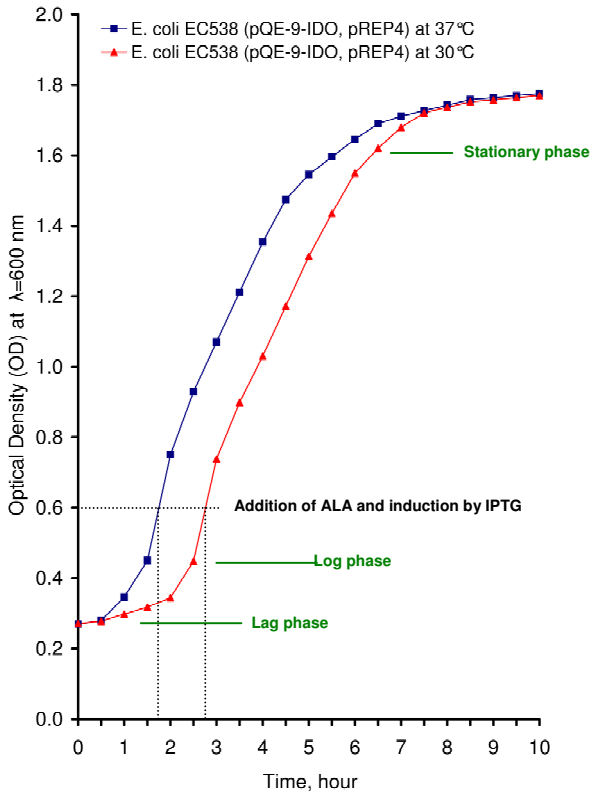

Figure 2.12 Growth profile of *E. coli* EC538 (pQE-9-IDO, pREP4) plotted as the optical density (OD_{600}) against time at 30 °C and 37 °C with IPTG induction of 100 μM and incorporation of 0.5 mM ALA.

As in the previous experiments (**Section 2.14** and **Section 2.16**), the aliquots of growth media were lysed and the rhIDO supernatant examined by SDS-PAGE (**Figure 2.13**). As expected, the growth of *E. coli* EC538 (pQE-9-IDO, pREP4) at 30 ºC was slower compared to 37 ºC. The SDS-PAGE analysis of rhIDO containing supernatants after lysis showed increased levels of soluble rhIDO at 30 ºC compared to 37 ºC. These

comparisons were for samples with the same levels of cell densities (OD_{600}). The optimisation of the growth condition for the expression of rhIDO in *E. coli* EC538 (pQE-9-IDO, pREP4) was followed by purification of the rhIDO by affinity chromatography.

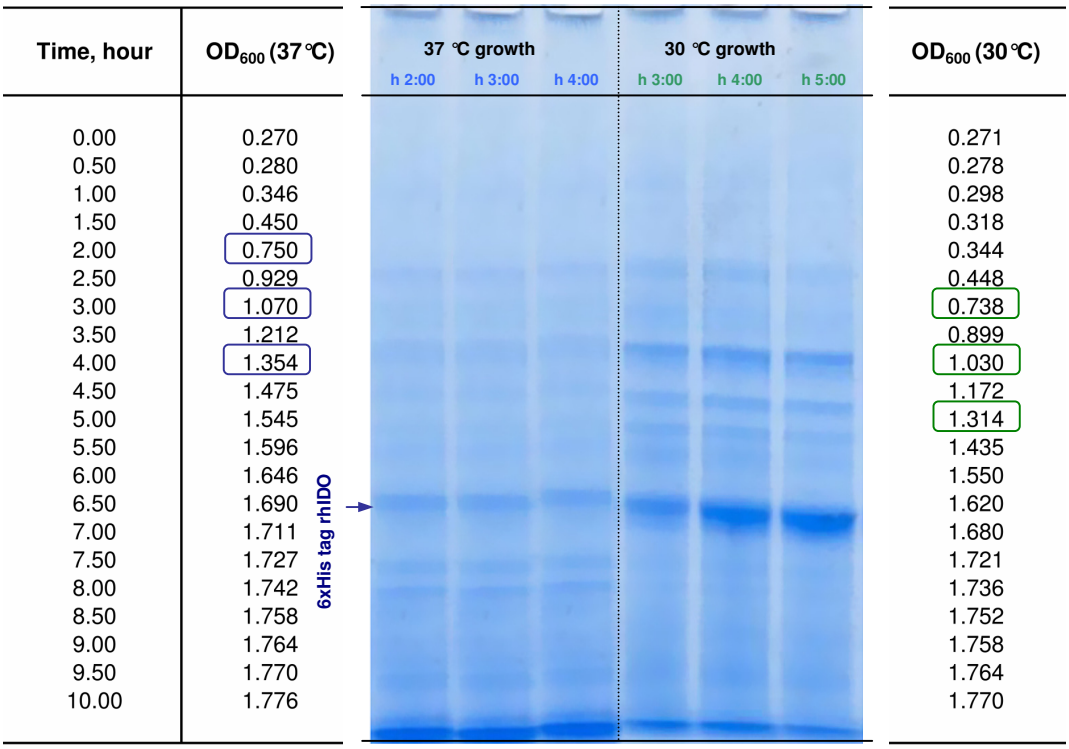

Figure 2.13 SDS-PAGE of sampled cells of *E. coli* EC538 (pQE-9-IDO, pREP4) grown at 30 ℃ and 37 ℃ following electrophoresis (100V) and visualisation with Coomassie Brilliant Blue.

2.2. Purification of rhIDO using Ni-NTA metal affinity chromatography

Purification of rhIDO utilised Ni-NTA metal affinity chromatography. This was followed by size exclusion chromatography, as outlined by Austin and co-workers,[9,10] with modifications. A tag of six histidines (6xHis-tag) is commonly engineered into the *N*-terminus of recombinant proteins to aid purification.[236] It is a small tag and therefore it

does not typically affect the folding of the recombinant proteins within the cell or their activity and function.[236] rhIDO has been shown to have similar properties to the native protein and is therefore a good model. Such a tag is considered good for biological screening and structural studies.[236] The 6xHis-tagged protein purification system utilises nickel-nitrilotriacetic acid (Ni-NTA) immobilised on a resin (**Figure 2.14**). The system relies on Ni-NTA's remarkable selectivity and affinity for imidazole groups.

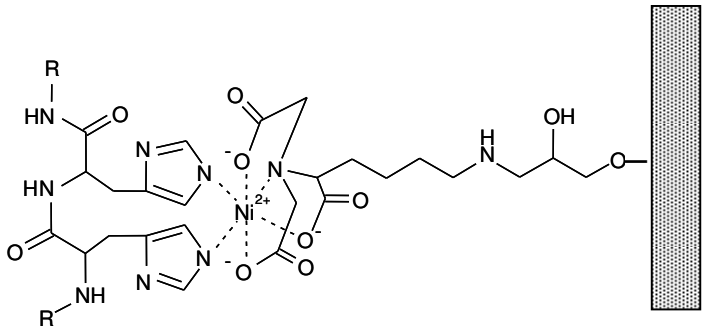

Figure 2.14 Nickel-nitrilotriacetic acid (Ni-NTA).

6xHis-tagged proteins, which are imidazole rich due to the histidines, bind strongly to the nickel ions on the resin. 6xHis-untagged proteins elute through the column. In this study, large scale preparative purification of 6xHis-tagged rhIDO by immobilised metal ion affinity chromatography (IMAC) utilised a HisTrap FF from Amersham Biosciences. HisTrap FF columns are packed with Ni Sepharose 6 Fast Flow that consists of 90 μm highly cross-linked agarose-beads with an immobilised chelating group. The tagged protein can then be eluted with increasing concentrations of imidazole, which competes with the polyhistidine tag[236] bound to the resin (**Figure 2.15**).

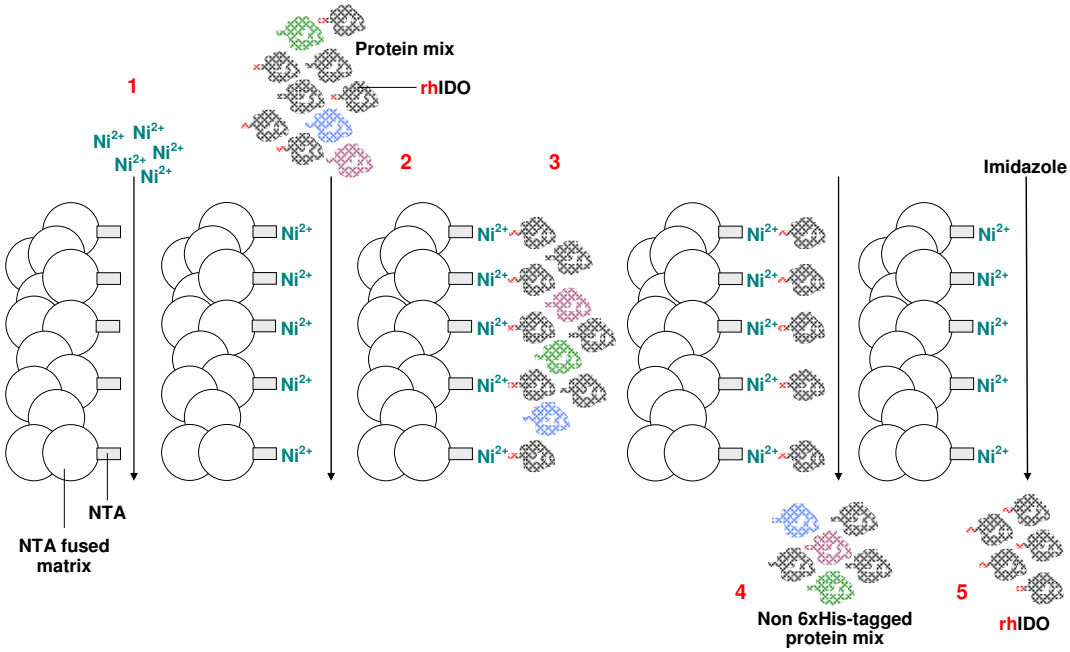

Figure 2.15 Purification of 6xHis-tagged recombinant proteins using Ni-NTA affinity chromatography. [1] Nickel ions are immobilised in a resin matrix, which is packed in a column. [2] Protein mix is passed through the resin. [3] The tagged protein binds to the resin, while untagged proteins pass through the column [4]. [5] The tagged protein is then eluted with imidazole, which competes with the polyhistidine tag.

In this study, lysis of *E. coli* EC538 (pQE-9-IDO, pREP4) cells cultured at 30 °C provided a clear red supernatant. The supernatant was applied to a Ni-NTA sepharose column (Hi-Trap chelating column, GE/Pharmacia-Amersham Biosciences) charged with nickel ions and equilibrated with the basal buffer (25 mM Tris-HCl pH 7.4, 500 mM NaCl and 1 mM PMSF) containing 10 mM imidazole. The sequential elution of the supernatant using the basal buffer containing 30 mM and 60 mM imidazole allowed removal of 6xHis-untagged proteins. rhIDO was eluted with 300 mM imidazole. In this procedure, as opposed to that by Austin and co-workers,[10] the NaCl concentration was

increased from 150 mM to 500 mM to avoid ion exchange effects and non-specific binding.[236] The sequential use of 10, 30, 40, 50, 65, 80 and 190 mM imidazole in the basal buffer as reported earlier[10] was changed to 10, 30, 60 and 300 mM, to avoid excessive dilution of the rhIDO. These modifications were made after evaluation of their respective SDS-PAGE.

The eluted rhIDO was subsequently desalted with 50 mM Tris-HCl pH 7.4 using a Sephadex G25 column (GE NAP-10/Amersham PD-10 desalting column, or PC-10). This step was considered essential because rhIDO is unstable in the presence of imidazole.[9,10,152] The desalted fractions were pooled and concentrated with an Amicon 30 kDa molecular weight cut-off centrifugal device (Millipore, Australia). The resulting rhIDO in Eppendorf tubes and the respective SDS-PAGE are shown in **Figure 2.16** and **Figure 2.17**.

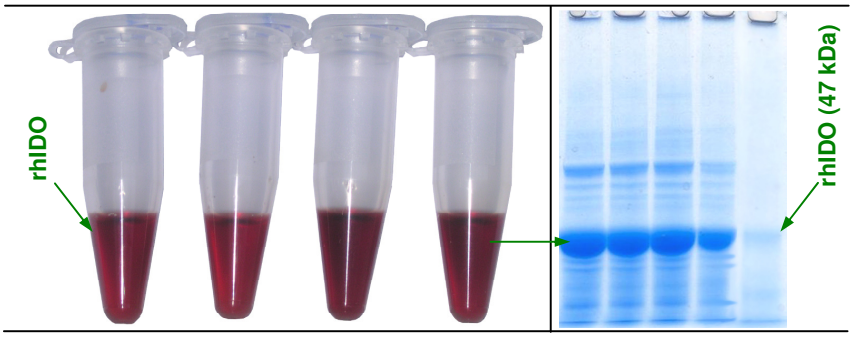

Figure 2.16 Purified rhIDO and their SDS-PAGE from *E. coli* EC538 (pQE-9-IDO, pREP4) grown at 30 ºC showing consistency of results from 4 batches of culture.

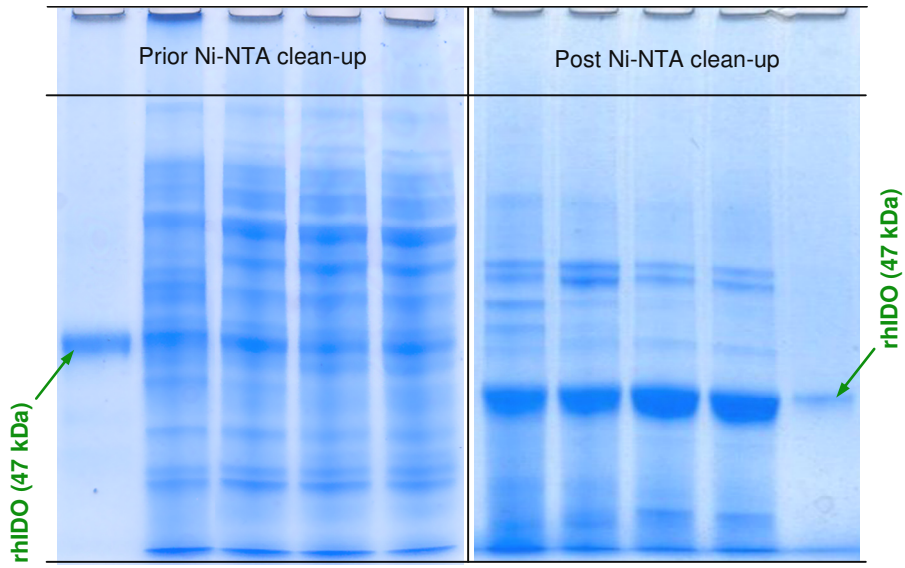

Figure 2.17 SDS-PAGE of rhIDO from *E. coli* EC538 (pQE-9-IDO, pREP4) as visualised with Coomassie Brilliant Blue for pre (prior) and post Ni-NTA clean-up. Electrophoresis was run at 100 V.

SDS-PAGE of rhIDO from pre and post Ni-NTA clean-up samples showed impurities. This was not surprising because polyhistidine-tag affinity columns are known to retain several protein impurities.[10] In the pursuit to obtain high quality rhIDO, the resulting rhIDO was purified further using size exclusion chromatography.

2.3. Purification of rhIDO through size-exclusion chromatography

Post Ni-NTA purification of rhIDO utilised size exclusion chromatography. Size exclusion chromatography is a method in which molecules are separated based on their size or more precisely, their hydrodynamic volume.[10] It uses porous particles. Molecules smaller than the pore size can enter the particles and are therefore retained because they have a longer path and transit time compared with larger molecules that cannot enter the particles (**Figure 2.18**). Most biochemical work typically uses polyacrylamide, dextran or

agarose.[10] In this study a Superdex column consisting of cross-linked agarose and dextran was used. Superdex columns have been used previously to purify rhIDO[9,10]

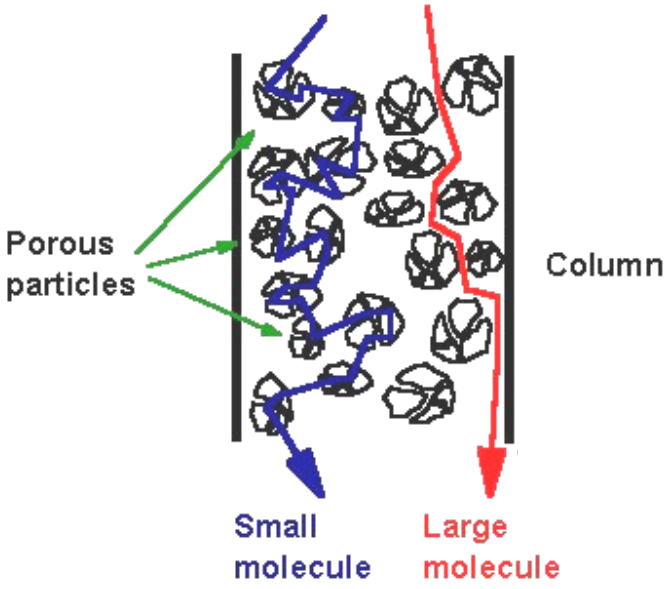

Figure 2.18 Schematic representation of a size-exclusion chromatography.[312]

Following Ni-NTA purification and desalting, the rhIDO was concentrated (**Section 2.2**) and equilibrated with 50 mM Tris-HCl pH 7.4 prior to eluting through a Superdex 75 PC 3.2/30 (GE/Pharmacia) column. Peaks were monitored on a fast protein liquid chromatography (FPLC) System (SMART-Pharmacia LKB Biotechnology) at λ_{280} nm and λ_{406} nm for protein and heme content, respectively. Fractions with the same Soret/protein ratios were pooled and evaluated by SDS-PAGE (**Figure 2.19**). The yield of the best rhIDO characteristic fraction was 3.5 mg soluble rhIDO per litre of *E. coli* EC538 (pQE-9-IDO, pREP4) culture. The rhIDO major peaks were pooled together and concentrated. Re-chromatography of the major rhIDO peak on Superdex 75 PC 3.2/30 column afforded a soluble and active rhIDO as one band in the SDS-PAGE (**Figure 2.20**).

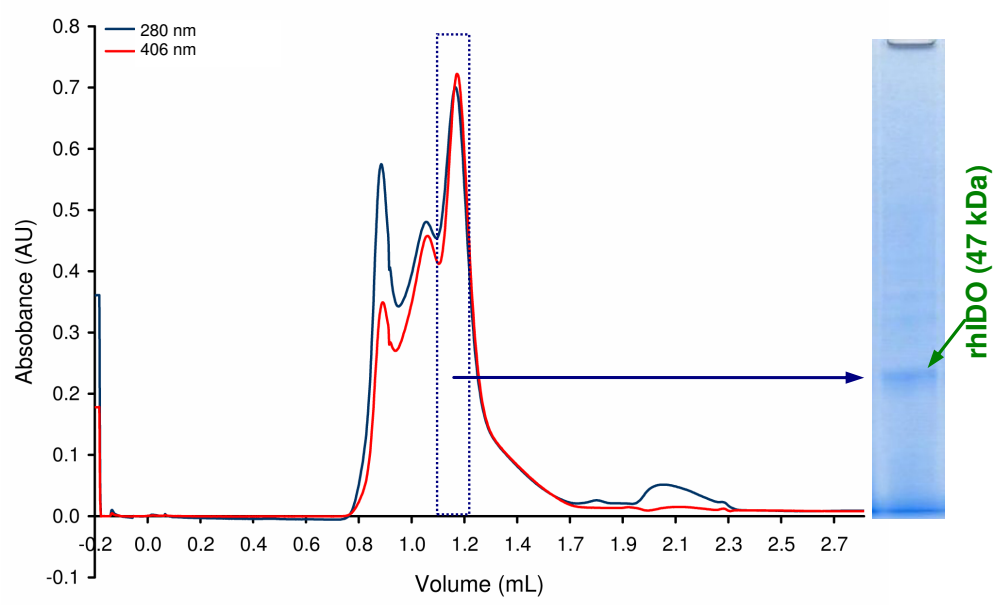

Figure 2.19 Chromatogram (FPLC) and SDS-PAGE of post Ni-NTA purified rhIDO, eluted with 50 mM Tris-HCl pH 7.4 using Superdex 75 PC 3.2/30 (λ_{280}, λ_{406} nm, 100 µL min^{-1}).

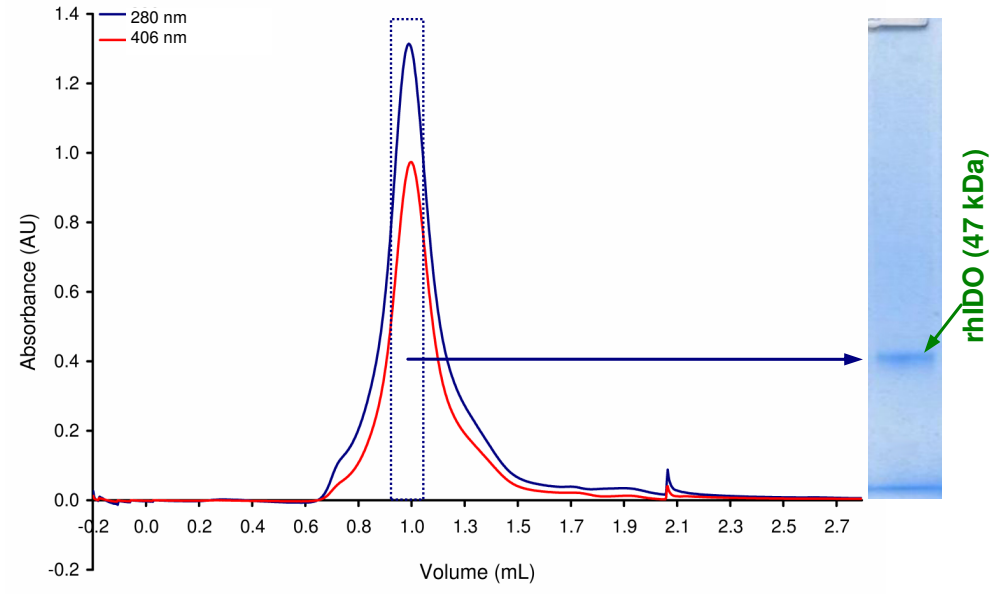

Figure 2.20 Chromatogram (FPLC) and SDS-PAGE of purified rhIDO, re-chromatographed and eluted with 50 mM Tris-HCl pH 7.4 using Superdex 75 PC 3.2/30 (λ_{280}, λ_{406} nm, 100 µL min^{-1}).

The yield of the re-chromatographed rhIDO was 1.5 mg soluble rhIDO per litre of *E. coli* EC538 (pQE-9-IDO, pREP4) culture. After the Superdex 75 PC 3.2/30 purification, the Soret/protein ratio (406:280 nm) of the rhIDO increased from 1.42:1.00 to 1.62:1.00 (14%) and its relative activity increased by 28% from 86 to 120 μmol kynurenine/h/mg protein (μmol/h/mg). The circular dichroism (CD) spectrum of the rhIDO was consistent with that of previously isolated rhIDO.[9,10,152] Details on CD studies of the rhIDO are provided elsewhere in this thesis (**Section 3.6**).

2.4. Experiments to increase the yield and quality of rhIDO

Despite the findings of Austin and co-workers,[10] in this study, the yields of rhIDO were low and the Soret/protein ratios obtained, especially after re-chromatography of the post Ni-NTA rhIDO through Superdex 75 PC 3.2/30, were inconsistent. In our continued interest to optimise further the yield and the quality of rhIDO from *E. coli* EC538 (pQE-9-IDO, pREP4), approaches were pursued to evaluate the influence of i) 10 μM and 100 μM IPTG induction on rhIDO production, ii) absence of light during growth on rhIDO production, iii) semi-anaerobic growth conditions on rhIDO production, iv) presence of PMSF during growth on rhIDO production, and v) addition of hemin prior to lysis through the French Press. In these approaches, the *E. coli* EC538 (pQE-9-IDO, pREP4) was cultured at 30 °C with addition of ALA (0.5 mM). Soluble rhIDO from lysis of the *E. coli* EC538 (pQE-9-IDO, pREP4) cells was semi-purified by Ni-NTA affinity chromatography, continued with desalting through NAP-10 (or PC-10) and filtered with the Amicon Ultra-15 filters. The rhIDO yield (Bio-Rad dye), Soret/protein ratio (406:280 nm) and specific activity (μmol/h/mg, μmol kynurenine/h/mg protein) were determined for each study.

2.4.1. Effect of 10 μM and 100 μM IPTG induction

Qiagen, the manufacturers of the expression plasmids pQE-9 and pREP4 used in these studies, recommend 1 mM IPTG induction for optimal yields of recombinant proteins.[236] Littlejohn, Austin and their co-workers[9,10,152] had examined the effect of the incorporation of the inducing agent IPTG on the expression of rhIDO in *E. coli* EC538 (pQE-9-IDO, pREP4).

Austin and co-workers established that induction in the absence of ALA with 100 μM IPTG gave optimum rhIDO production (**Section 2.1.5**). In our current investigations, induction of the cultures with both 10 μM and 100 μM IPTG were done in the presence of ALA (0.5 mM) at 30 °C. Ten μM IPTG increased significantly ($p < 0.05$, **Table 2.1**) the protein yield from 10.3 to 10.6 mg/L (3%), the Soret/protein ratio from 1.3:1.0 to 1.5:1.0 (15%) and specific activity from 86 to 98 μmol/h/mg (14%).

These observations on the suitability of 10 μM IPTG induction for rhIDO expression in *E. coli* EC538 (pQE-9-IDO, pREP4) cultured with 0.5 mM ALA at 30 °C, were confirmed when cultures induced with IPTG (0 – 1000 μM) showed the highest values for Soret/protein ratio and specific activity at 10 μM IPTG (**Figure 2.21** and **Figure 2.22**).

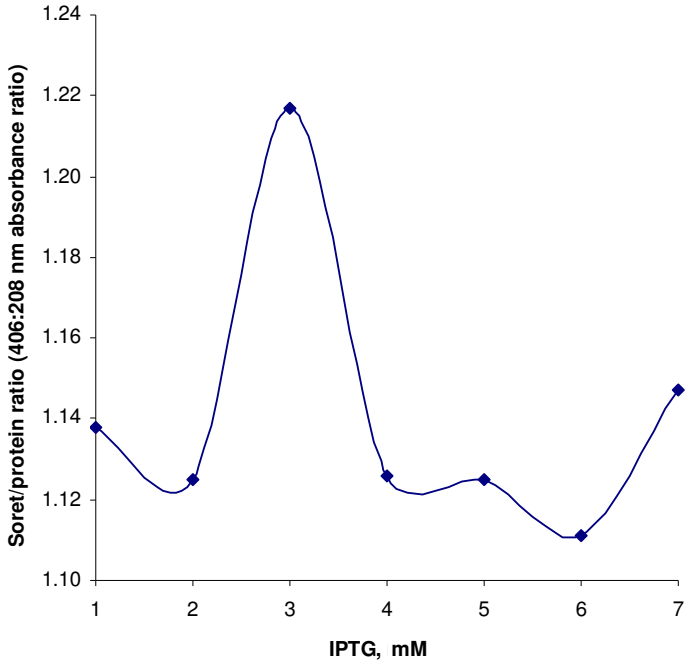

Figure 2.21 Effect of IPTG concentration on Soret/protein ratio of rhIDO expressed in *E. coli* EC538 (pQE-9-IDO, pREP4) grown at 30 °C in LB media.

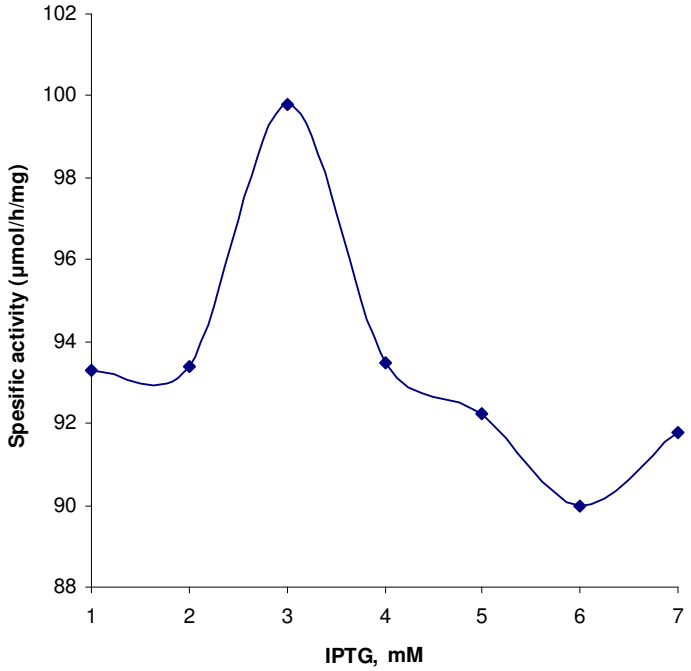

Figure 2.22 Effect of IPTG concentration on specific activity of rhIDO expressed in *E. coli* EC538 (pQE-9-IDO, pREP4) grown at 30 °C in LB media.

2.4.2. Effect of absence of light

δ-Aminolevulinic acid (ALA) is the natural biosynthetic precursor of iron protoporphyrin IX (heme *b*). It was added to *E. coli* EC538 (pQE-9-IDO, pREP4) cultures to increase heme *b* incorporation in rhIDO (**Section 2.1.2**). Protoporphyrin IX (heme *b*) is photoactive and can therefore react with oxygen to produce reactive oxygen species, including harmful singlet oxygen and hydrogen peroxide (H_2O_2). rhIDO is highly sensitive to reactive oxygen species including H_2O_2.[233] There were concerns in this study that the protoporphyrin IX (heme *b*), produced in the aerobic media, could lead to the production of reactive oxygen species and therefore damage the rhIDO. Culturing of *E. coli* EC538 (pQE-9-IDO, pREP4) in the dark as opposed to normal light conditions (exposure to fluorescent light) significantly increased ($p<0.05$, **Table 2.1**) the rhIDO yield from 10.3 to 10.7 mg/L (4%), the Soret/protein ratio from 1.3:1.0 to 1.6:1.0 (23%) and the specific activity from 83 to 103 μmol/h/mg (24%).

2.4.3. Effect of semi-anaerobic growth condition

The result of culturing *E. coli* EC538 (pQE-9-IDO, pREP4) in the dark and the known instability of rhIDO upon addition of H_2O_2,[233] led to the investigation of the use of minimal oxygen during growths. The LB media used for the growth of the *E. coli* throughout this work is not supportive of anaerobic growth. Subsequently, complete removal of oxygen was not considered. Instead, growths were conducted under semi-anaerobic conditions with a tightly covered flask and gentle shaking of 100 rpm, while the standard shaking conditions were 250 rpm (**Section 7.1.2**) in a lightly stoppered flask. Results from the semi-anaerobic conditions were not consistent but increases

($p<0.05$, **Table 2.1**) of rhIDO yield from 10.4 to 11.8 mg/L (14%), Soret/protein ratio from 1.2:1.0 to 1.5:1.0 (25%) and specific activity from 79 to 98 μmol/h/mg (24%) were noted.

2.4.4. Effect of presence of PMSF during growth of *E. coli*

In the studies of Littlejohn and co-workers,[152] and those conducted by Austin and co-workers,[9,10] the protease inhibitor phenylmethylsulfonylfluoride (PMSF, 1 mM) was added to the growth media and during purification to prevent the formation of truncated rhIDO.[153] *E. coli* EC538 is a protease deficient strain of *E. coli* and PMSF is a general serine protease inhibitor. PMSF is the most commonly used inhibitor in protein purification. However, *in vivo* PMSF interferes with cellular energy production.[85] It is also rapidly degraded in water and proteolytic inhibition occurs when a concentration between 0.1 - 1 mM PMSF is used. The half-life of PMSF in aqueous solutions is 110 min at pH 7 and 35 min at pH 8.[168] Truncation would only occur upon lysis and therefore was not necessary or beneficial to add during growth.[85,168]

Incorporation of PMSF in the cultures was investigated to study its effect on the expression of rhIDO in *E. coli* EC538 (pQE-9-IDO, pREP4). A negative control in which no PMSF was added to the cultures was also done. In both cases PMSF was added to a final concentration of 1 mM prior to lysis of the cells.[9,10,152] The negative control in which no PMSF was added increased ($p<0.05$, **Table 2.1**) the rhIDO yield from 10.5 to 11.5 mg/L (10%), Soret/protein ratio from 1.3:1.0 to 1.5:1.0 (15%) and specific activity from 85 to 99 μmol/h/mg (17%).

2.4.5. Effect of addition of hemin prior to lysis

The addition of ALA during the culturing of *E. coli* EC538 (pQE-9-IDO, pREP4) in these studies increased the incorporation of heme levels in rhIDO. Whereas a Soret/protein ratio consistent with the native enzyme (2.2:1.0) had been achieved by Austin and co-workers,[10] losses of the heme were observed during purification in this study (**Section 2.3**). Consequently, it was difficult to achieve full heme incorporation. Details on heme incorporation into rhIDO are provided elsewhere in this thesis (**Chapter 4**).

Hemin as hemin chloride has been incorporated into heme proteins during purification.[315] It was not regarded as necessary to be incorporated in the growth phase in these studies because it exhibits antibacterial activity.[10] However, it was hypothesised that its incorporation during the lysis of the cells may be beneficial in maintaining or increasing heme levels. In this study, hemin was added to the resuspension buffer (**Section 7.1.7**) prior to lysis of the *E. coli* EC538 (pQE-9-IDO, pREP4) cells in the French Press. The addition of hemin during the lysis (**Section 4.8**) was found to increase ($p<0.05$, **Table 2.1**) protein yield from 10.4 to 10.5 mg/L (1%), Soret/protein ratio from 1.4:1.0 to 1.7:1.0 (21%) and specific activity from 81 to 102 μmol/h/mg (26%). This was compared to cells lysed with the buffer without hemin.

2.4.6. Results of experiments to increase the yield and quality of rhIDO

From the preceding experiments (**Section 2.4.1** to **Section 2.4.5**) where *E. coli* EC538 (pQE-9-IDO, pREP4) were cultured with 0.5 mM ALA at 30 °C, it was observed that lowering of IPTG from 100 μM to 10 μM, absence of light, absence of PMSF during the

growth and addition of 10 μM hemin prior to lysis increased the yield and improved the quality of rhIDO expressed in *E. coli* EC538 (pQE-9-IDO, pREP4). Semi-anaerobic growths gave inconsistent results. The overall results of the experiments are given in **Table 2.1**.

Table 2.1 The results of the influence of the lowering of IPTG from 100 μM to 10 μM, absence of light, semi-anaerobic conditions and absence of PMSF during the growth and addition of hemin prior to lysis of *E. coli* EC538 (pQE-9-IDO, pREP4) cells. The protein yield, the Soret/protein ratio and the specific activity of the purified protein (post Ni-NTA work-up) are shown.

	Protein yield *(mg/L)*		**Soret/protein ratio** *(406 : 280 nm)*		**Specific activity** *(μmol/h/mg)*	
***E. coli* EC538 (pQE-9-IDO, pREP4) recombinant human IDO**	**normal**	**changed**	**normal**	**changed**	**normal**	**changed**
IPTG from 100 μM to 10 μM	10.3	10.6	1.3 : 1.0	1.5 : 1.0	86.0	98.0
Absence of light	10.3	10.7	1.3 : 1.0	1.6 : 1.0	83.0	103.0
Semi-anaerobic	10.4	11.8	1.2 : 1.0	1.5 : 1.0	79.0	98.0
Absence of PMSF	10.5	11.5	1.3 : 1.0	1.5 : 1.0	85.0	99.0
Hemin addition prior to lysis	10.4	10.5	1.4 : 1.0	1.7 : 1.0	81.0	102.0
average	10.380±0.084	11.020±0.589	1.300±0.071	1.560±0.089	82.800±2.864	100.000±2.345
t		-2.41		-5.10		-10.40
P		95.700 (0.043)		99.900 (0.001)		100.000 (0.000)
paired-t		-2.640		-10.600		-9.710
P		94.300 (0.057)		100.000 (0.000)		99.900 (0.001)

Subsequent growths and purifications were therefore conducted using these modifications and the optimised procedure of purification (**Section 2.2**). The following scheme (**Figure 2.23**) summarises the modified conditions for the optimisation of rhIDO expression in *E. coli* EC538 (pQE-9-IDO, pREP4) and the purification of the rhIDO. The results of the optimised conditions are given in **Chapter 3.**

Figure 2.23 Flow chart summarising the overall process and conditions for the optimisation of rhIDO expression in *E. coli* EC538 (pQE-9-IDO, pREP4) and the purification of the rhIDO.

2.5. Conclusion

The study of IDO expression and design of IDO related therapeutics requires a viable source of IDO compared with that from human placenta. Recombinant human indoleamine 2,3-dioxygenase (rhIDO) expressed in *E. coli* EC538 (pQE-9-IDO, pREP4) has a potential to offer a viable supply of IDO. In order to obtain substantial quantities of high quality rhIDO, the methods for the expression of rhIDO in *E. coli* EC538

(pQE-9-IDO, pREP4) by Littlejohn,[152] Austin[9,10] and their co-workers were optimised. The incorporation of ALA and the optimal concentration of IPTG for induction for the expression of rhIDO were considered. Induction with high concentration of IPTG (100 μM or higher) was associated with the formation of rhIDO as inclusion bodies. Lowering the growth temperature of *E. coli* EC538 (pQE-9-IDO, pREP4) from 37 °C to 30 °C was shown to significantly reduce the formation of rhIDO as inclusion bodies and to enhance the yield of soluble rhIDO. High Soret/protein ratios and specific activity values that are characteristics of high quality rhIDO were achieved by inducing the expression of rhIDO in *E. coli* EC538 (pQE-9-IDO, pREP4) with 10 μM IPTG. Better yields of rhIDO were obtained when the expression was carried out under dark conditions, without the addition of PMSF, and with the addition of hemin prior to lysis of the cells. Semi-anaerobic conditions did not have a significant effect on the yield and quality of the rhIDO.

In the quest to further increase the yield and quality of rhIDO, the above optimised conditions for the expression of rhIDO in *E. coli* EC538 (pQE-9-IDO, pREP4) were used. The next chapter (**Chapter 3**) therefore highlights the result of the optimised expression system with the modified conditions and the use of the afforded rhIDO for the characterisation of rhIDO.

Chapter 3

Characterisation of indoleamine 2,3-dioxygenase

Chapter 3

Characterisation of indoleamine 2,3-dioxygenase

*The overall aim of this chapter is to present the characterisation of recombinant human indoleamine 2,3-dioxygenase (rhIDO) afforded from the optimised expression and purification conditions given in the previous chapter (**Figure 2.23**) and the comparison of rhIDO to recombinant mouse IDO (rmIDO).*

3.1. Mass spectra of rhIDO

rhIDO obtained from the optimised expression and purification protocol (**Figure 2.23**) was identified by electrospray ionisation mass spectrometry (ESI-MS). The raw mass spectral data from a direct injection ESI-MS of rhIDO was deconvoluted with Micromass MaxEnt1 processing to give the final mass spectra with a parent peak at 47,758 kDa (rhIDO). The mass spectra and the sodium dodecyl sulfate polyacrylamide gel electrophoresis (SDS-PAGE) confirmed that its molecular weight was as expected for rhIDO[152] (**Figure 3.1**). The calculated mass of rhIDO without hemin is 46,938 kDa and 47,590 kDa with hemin. Due to adduct ion species of multiply charge rhIDO in the ESI-MS spectra, the value of 47,758 kDa for a direct injection ESI-MS of rhIDO is consistent with this mass.

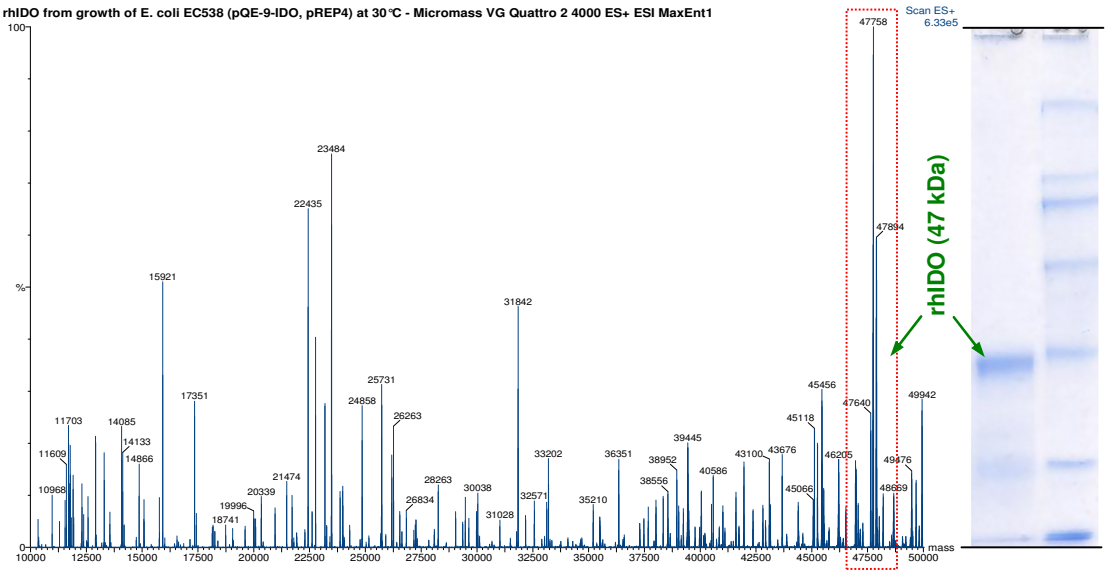

Figure 3.1 Direct injection ESI mass spectrum deconvoluted with the Micromass MaxEnt1 processing and SDS-PAGE of rhIDO expressed in *E. coli* EC538 (pQE-9-IDO, pREP4). The rhIDO was obtained from the optimised expression and purification protocol (**Figure 2.23**).

3.2. Soret band and Soret/protein ratio of rhIDO

Ultraviolet-Visible (UV-Vis) absorption spectroscopy is an invaluable tool for studying protein-ligand interactions of heme proteins.[276] The heme *b* prosthetic group, which is the co-factor in IDO, has a strong electronic absorbance band, known as the Soret band, that depends on the oxidation, ligation and conformational states of the chromophores.[276,322] It is sensitive to conformational changes of the polypeptide chain into which it is embedded. The Soret band of rhIDO in Tris-HCl pH 7.4 is due to ferric (Fe^{3+}) rhIDO.[276] The UV-Vis spectra of rhIDO in Tris-HCl (pH 7.4) showed distinct maxima at $\lambda_{280\ nm}$ and $\lambda_{406\ nm}$. The 280 nm maxima is due to the tyrosine and tryptophan in the protein and the 406 nm maxima (Soret band) to the heme *b* moiety (Fe^{3+} state). The Soret/protein ratio of rhIDO samples obtained from the optimised expression and purification protocol (**Figure 2.23**) varied from 1.42:1.00 to 1.70:1.00. The typical UV-Vis spectrum showing

a Soret/protein ratio of 1.42:1.00 is given in **Figure 3.2**. The reported value for wild-type IDO from placenta is 2.2:1.0.[152]

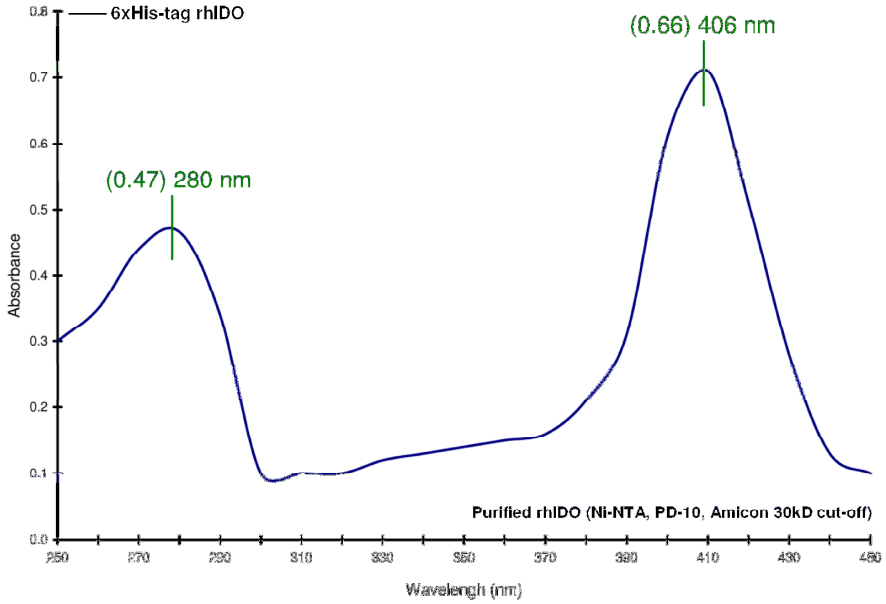

Figure 3.2 UV-Vis spectrum of rhIDO showing the Soret band maxima at $\lambda_{406\ nm}$ and a Soret/protein ratio of 1.42:1.00.

3.3. UV-Vis spectra of rhIDO upon dithionite reduction

The purpose of this study was to gain a better understanding of the processes that took place during the dithionite reduction of rhIDO. In its native Fe^{3+} state, the heme *b* moiety of IDO is inactive.[108,277,305] For it to be active, it requires reduction to its ferrous form (Fe^{2+} state).[30,224,322] In the *in vitro* assay for IDO activity, ascorbate-reduced methylene blue (leuco-methylene blue) reduces the heme *b* co-factor iron from Fe^{3+} to Fe^{2+}.[107,277,278,313]

In this study reduction experiments of rhIDO heme *b* iron were conducted using sodium dithionite without the presence of the substrate L-Trp. Sodium dithionite (sodium hydrosulfite, $Na_2S_2O_4$) is a reducing agent capable of reducing the heme *b* co-factor ferric iron (Fe^{3+}) to its ferrous state (Fe^{2+}). Time-wise spectral observations (t = 0, 1, 10 min) of sodium dithionite treatment of rhIDO using 5 mM $Na_2S_2O_4$ showed significant spectral changes (**Figure 3.3**) that were attributed to the reduction of the heme *b* co-factor iron from Fe^{3+} to Fe^{2+}. From the study, at one minute upon reaction, an additional peak of dithionite at 314 nm[60] and a shift of the peak at 406 nm to 421 nm were observed. After ten minutes, the peaks returned to their original positions (prior to the reduction) with a lower absorption at 406 nm. The experiment was not done in the absence of air and the occurrence of an additional peak at 314 nm (dithionite) upon sodium dithionite reduction was not reported in an earlier study by Littlejohn,[152] Terentis[308] and their co-workers.

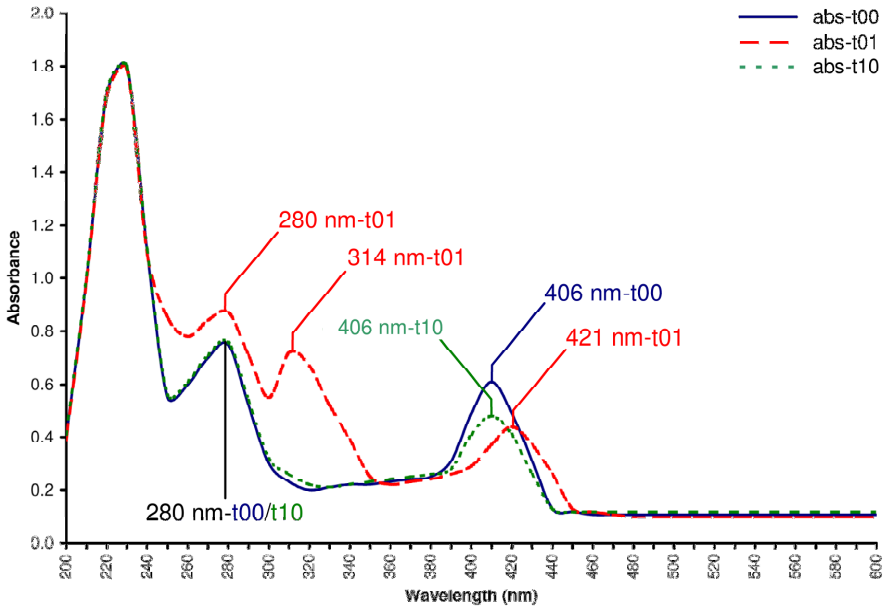

Figure 3.3 UV-Vis spectra of rhIDO reaction with sodium dithionite using 5 mM $Na_2S_2O_4$ and time-wise observations showing significant spectral changes at t = 0, 1, 10 min.

3.4. CD spectra of rhIDO upon dithionite reduction

Circular dichroism (CD) spectra of the sodium dithionite treated rhIDO were determined (t = 0, 1, 10 min). The spectra were analysed using the CDPro software (**Table 3.1**). These investigations were carried out to establish whether or not the changes observed from the UV-Vis absorption spectroscopy (**Section 3.3**) affected the conformation of the rhIDO. Similar to the UV-Vis experiment, one minute upon reaction a high α-helix conformation (73% from 67%), a lowered β-strand (2% from 4%) and random-coil (24% from 29%) conformations were observed. The conformations changed after ten minutes with a lowered α-helix (58%) and higher β-strand (8%) and random-coil (34%) as shown in **Figure 3.4**.

Table 3.1 Analysis of the CD data between 190 to 240 nm using CDPro Software from Colorado State University with three programs for CD analysis (SELCON3, CDSSTR and CONTINLL) of sodium dithionite (5 mM) treatment of rhIDO (1 mg/mL) determined at t = 0, 1, 10 minutes in 10 mM Tris-HCl pH 7.4 and 0.2 cm cell length using a Jasco J-810 Circular Dichroism Spectropolarimeter.

Purified recombinant human IDO *(dithionite reduction experiment)*	α-Helix (%)	β-Strand (%)	Random-Coil (%)
t00 (t = 0 minute)	67	4	29
t01 (t = 1 minute)	73	2	24
t10 (t = 10 minutes)	58	8	34

The UV-Vis and CD spectra suggested that dithionite treatment has an effect on the nature of the heme *b* co-factor and the conformation of the rhIDO. The transformation of IDO from its inactive native (Fe^{3+}) state to its active (Fe^{2+}) state was not in the presence of L-Trp. It may be argued that the transformation facilitates the reaction of IDO in its

active site. This preliminary finding was not pursued further as it was not the immediate focus of this study, but this study does recommend that the rational design and development of potential IDO inhibitors need to take account of this transformation state.

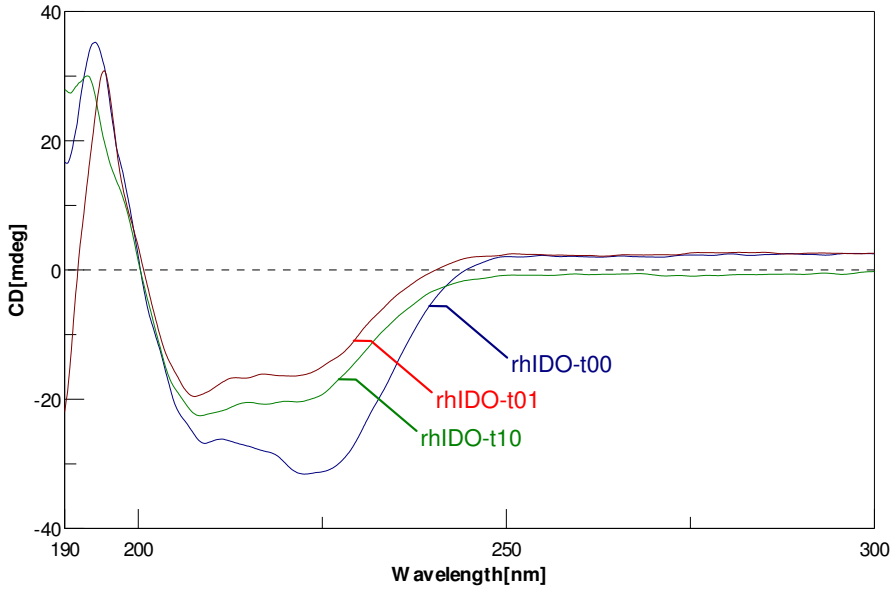

Figure 3.4 CD Spectra of sodium dithionite (5 mM) treatment of rhIDO (1 mg/mL) determined at t = 0 (blue), 1 (green), 10 (red) minutes in 10 mM Tris-HCl pH 7.4 and 0.2 cm cell length using a Jasco J-810 Circular Dichroism Spectropolarimeter (190 - 300 nm shown).

3.5. Stability and minimising loss of rhIDO activity

Most enzymes are stable for months if refrigerated (0 – 4 °C).[236] Cooling below 0 °C, in the presence of additives such as DMSO or glycerol, can generally increase storage stability further. Freezing enzyme solutions is often avoided because it causes denaturation of the enzyme and leads to pH variations.[236,237] The former is attributed to stress and the latter to ice-crystal formation. The effect of temperature on the storage of rhIDO are described here.

3.5.1. Effect of temperature on rhIDO

The influence of temperature on rhIDO was investigated following storage of rhIDO in 25 mM Tris-HCl pH 7.4 at 4, 10 and 20 ºC for 2, 4 and 6 hours respectively. After storage, the rhIDO was eluted through a Fast Desalting PC3.2/10 column and analysed to evaluate the Soret/protein ratios, specific activities and protein conformations (circular dichroism, CD analysed using CDPro Software from Colorado State University with three programs SELCON3, CDSSTR and CONTINLL for CD analysis). All samples did not show any significant change in their Soret/protein ratio, specific activity and CD (**Table 3.2**).

Table 3.2 The influence of temperature on rhIDO. Samples were incubated at 4, 10 and 20 ºC at 2, 4 and 6 hours prior to elution through a Fast Desalting PC3.2/10 column. Results of the Soret/protein ratio, specific activity and CD (190 to 240 nm) are shown.

Purified recombinant human IDO *(temperature experiment)*		Temperature 4 ºC Incubation (h)			Temperature 10 ºC Incubation (h)			Temperature 20 ºC Incubation (h)		
		2	4	6	2	4	6	2	4	6
Soret/protein ratio* (406 : 280 nm)		1.35	1.42	1.36	1.38	1.33	1.42	1.37	1.39	1.34
Specific activity** (µmol/h/mg)		74±5	76±7	72±5	77±6	70±5	73±6	76±7	71±5	78±8
CD analysis***	α-helix (%)	63	60	61	63	63	61	63	60	64
	β-strand (%)	6	7	7	6	5	6	5	7	5
	random-coil (%)	31	33	32	31	32	33	32	33	31

*Initial ratio=1.44; **(Triplicate) Initial specific activity=80±5; ***Initial CD=62 (α-helix), 6 (β-sheet) and 32 (random-coil).

The observations showed no significant difference in the Soret/protein ratios, specific activities or conformation of the rhIDO, despite the findings of Littlejohn, Austin and their co-workers[10,152] on rhIDO instability upon storage at room temperature. This study shows that temperature fluctuations between 4 to 20 °C within a period of 2 to 6 hours does not reduce the quality of rhIDO.

3.5.2. Effect of cryoprotectants on rhIDO

In order to understand the effect of freeze denaturation on rhIDO, the protein in 25 mM Tris-HCl pH 7.4 was investigated in the absence of cryoprotectants (without preservation) and with the common cryoprotectants glycerol, sucrose and DMSO at final concentrations of 40%, 0.5 M and 10%, respectively. In this investigation, rhIDO was frozen in liquid nitrogen and kept at -80 ºC for 48 hours. It was then thawed on ice and purified through Ni-NTA and NAP-10 columns prior to the evaluation of protein recovery, Soret/protein ratio, specific activity and protein conformation. The results are given in **Table 3.3**.

Table 3.3 The influence of freezing on rhIDO in 25 mM Tris-HCl pH 7.4, investigated in the absence of cryoprotectants (without preservation) and with 40% glycerol, 0.5 M sucrose and 10% DMSO as protectants. Freezing with liquid nitrogen and storage at -80 ºC for 48 hours followed by re-purification through Ni-NTA and NAP-10 columns were done.

Purified rhIDO *(freezing-thawing experiment)*		Untreated prior to freezing	Frozen without cryoprotectant	Frozen with 40% Glycerol	Frozen with 10% DMSO	Frozen with 0.5 M Sucrose
Protein recovery (%)		100	75	80	70	30
Soret/protein ratio (406 : 280 nm)		1.40	0.80	0.90	0.75	0.60
Specific activity (µmol/h/mg)		75±6	43±7	48±5	40±7	32±8
CD analysis	α-helix (%)	62	63	62	61	64
	β-strand (%)	6	6	6	7	5
	random-coil (%)	32	31	32	32	31
Protein aggregation*		non (-)	slight (+)	slight (+)	slight (+)	severe (+++)

*Protein aggregation, non (-), slight (+), significant (++), severe (+++)

The results showed that in terms of protein recovery, Soret/protein ratio, protein conformation and protein aggregation, the freeze-thawing process was destructive in all

cases, with the use of 0.5 M sucrose being the most damaging. The use of 40% glycerol gave the most protection towards rhIDO.

3.5.3. Effect of storage and protectants on rhIDO

In an effort to further understand the influence of storage temperature and protectants over time on rhIDO, the protein was stored in 25 mM Tris-HCl pH 7.4 at 20 ºC, 0 - 4 °C and -20 ºC for 0, 1, 2 and 3 months, respectively, in the absence of protectants as well as using 40% glycerol and 10% DMSO as protectants. In this study, the Soret/protein ratios, specific activities and protein conformations were analysed (**Table 3.4**).

The results showed that storage of rhIDO in 40% glycerol at -20 ºC gave the smallest decrease in Soret/protein ratio, specific activity and protein concentration. The rhIDO stored at 20 ºC at the prolonged period of 3 months showed significant deterioration in all cases, giving protein aggregates and a severe decrease in the Soret/protein ratio and specific activity. The rhIDO stored at 0 - 4 ºC showed a relatively small decrease in Soret/protein ratio, specific activity and protein concentration upon the short storage period of a month.

Table 3.4 The influence of temperature on storage of rhIDO. rhIDO in 25 mM Tris-HCl pH 7.4 was stored at 20 ºC, 0 - 4 °C and -20 ºC in the absence of protectants (without preservation) as well as using 40% glycerol and 10% DMSO as protectants. Samples at 0, 1, 2 and 3 months were taken for analysis. Results of the Soret/protein ratio and specific activity are shown.

Purified recombinant human IDO* *(storage experiment) -20 °C*	40% Glycerol			10% DMSO			Protectant (none)		
	1 mo	2 mo	3 mo	1 mo	2 mo	3 mo	1 mo	2 mo	3 mo
Soret/protein ratio** (406 : 280 nm)	1.42	1.40	1.40	1.40	1.37	1.36	1.39	1.37	1.33
Specific activity*** (µmol/h/mg)	76±7	75±6	73±4	75±6	73±7	73±6	74±6	73±5	71±6
Protein concentration**** (% after centrifugation)	no (84)	no (83)	no (82)	no (83)	no (81)	slight (81)	no (82)	no (81)	slight (79)

Purified recombinant human IDO* *(storage experiment) 0 - 4 °C*	40% Glycerol			10% DMSO			Protectant (none)		
	1 mo	2 mo	3 mo	1 mo	2 mo	3 mo	1 mo	2 mo	3 mo
Soret/protein ratio** (406 : 280 nm)	1.42	1.40	1.40	1.40	1.37	1.36	1.39	1.37	1.33
Specific activity*** (µmol/h/mg)	76±7	75±6	73±4	75±6	73±7	73±6	74±6	73±5	71±6
Protein concentration**** (% after centrifugation)	no (83)	no (77)	no (68)	no (79)	no (71)	slight (60)	no (75)	no (64)	slight (57)

Purified recombinant human IDO* *(storage experiment) 20 °C*	40% Glycerol			10% DMSO			Protectant (none)		
	1 mo	2 mo	3 mo	1 mo	2 mo	3 mo	1 mo	2 mo	3 mo
Soret/protein ratio** (406 : 280 nm)	0.91	0.75	0.52	0.81	0.63	0.32	0.71	0.43	0.27
Specific activity*** (µmol/h/mg)	48±6	40±7	29±6	44±6	34±5	18±6	38±7	23±4	15±6
Protein concentration**** (% after centrifugation)	slight (54)	slight (44)	severe (31)	slight (48)	severe (38)	severe (19)	severe (42)	severe (26)	severe (16)

*mo = month; **Initial ratio = 1.44; ***Initial specific activity = 80±5; ****no, slight, severe=aggregation

3.6. Comparison of rhIDO and rmIDO

Murine models are commonly used to represent human IDO for the study of human conditions relevant to over-expression of IDO.[91,262,299,350] It is therefore important to understand the similarities and differences between hIDO and mIDO.[11] Unlike rhIDO, for

which the crystal structure has been reported,[284.285] the 3D structure of native or rmIDO is not available.

Database analysis of the rhIDO (human, *Homo sapiens*) compared to that of the rmIDO (mouse, *Mus musculus*) is shown in **Table 3.5** and their homology in **Figure 3.5**.

Table 3.5 Comparison of protein analysis of rhIDO (human, *Homo sapiens*) and rmIDO (mouse, *Mus musculus*) from various databases.[266]

rhIDO, human, *Homo sapiens*		rmIDO, mouse, *Mus musculus*	
Analysis	Entire Protein	Analysis	Entire Protein
Length	417 aa	Length	421 aa
Molecular Weight	46936.08 m.w.	Molecular Weight	47251.21 m.w.
1 microgram =	21.306 pMoles	1 microgram =	21.163 pMoles
Molar Extinction coefficient	50460	Molar Extinction coefficient	48820
1 A[280] corr. to	0.93 mg/ml	1 A[280] corr. to	0.97 mg/ml
A[280] of 1 mg/ml	1.08 AU	A[280] of 1 mg/ml	1.03 AU
Isoelectric Point	7.08	Isoelectric Point	6.21
Charge at pH 7	0.30	Charge at pH 7	-5.73

The amino acid sequence of rmIDO is longer than that of rhIDO and its pI and charge at pH 7 are significantly lower that that of rhIDO. In the protein homology analysis, although rmIDO shows sections in which the amino acid sequence differs with those of rhIDO (highlighted green in **Figure 3.5**), there is a 60% identity (highlighted yellow in **Figure 3.5**). Homology and protein analysis data has been compiled on human IDO, mouse IDO as well as IDO-like enzymes from other organisms (**Appendix 1** and **Appendix 2**).

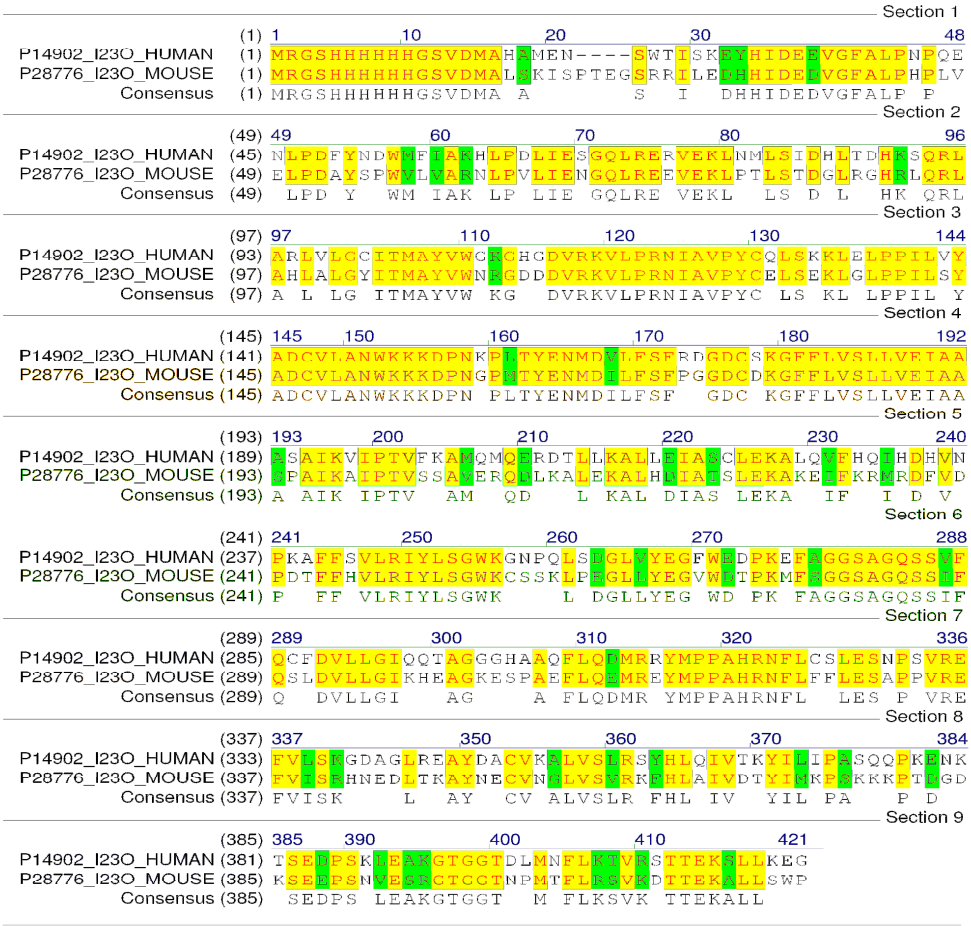

Figure 3.5 Protein homology analysis of 6xHis-tagged-rhIDO (human, *Homo sapiens*) and 6xHis-tagged rmIDO (mouse, *Mus musculus*) showing the 60% identity of rmIDO towards rhIDO.

3.6.1. Specific activity of rhIDO and rmIDO and their kinetics

The specific activity of rhIDO from the optimised expression and purification (**Chapter 2**) was measured using the procedure described by Takikawa and co-workers (**Chapter 7**, **Section 7.2.2**).[9] The protein concentration was determined using the Bradford[25] protein assay using a standard curve of bovine serum albumin and determined on a UV-Vis spectrophotometer at 595 nm (**Chapter 7**, **Section 7.2.2**). In this study, 6xHis-tagged recombinant human and mouse IDO were used. The rmIDO used in this study was kindly provided by Austin and co-workers (University of Sydney). The

specific activity of rhIDO was observed to reach 120 μmol kynurenine/h/mg protein while the rmIDO was observed to reach 150 μmol kynurenine/h/mg protein. The kinetics of rhIDO and rmIDO were studied with L-Trp and D-Trp as substrates[11] using the standard assay system of Takikawa and co-workers.[9] Varying concentrations of substrates were used (0, 10, 25, 50, 100, 200 μM for L-Trp and 0, 100, 250, 750, 1500, 3000 μM for D-Trp). IDO needs higher concentration of D-Trp compared to L-Trp for it to become saturated with the substrate as IDO has a preference for L-Trp as a substrate.

The study of enzyme kinetics is important because it helps to explain how enzymes work and to predict the nature of the enzymes in their environment. The Michaelis-Menten constant (K_m) is the basis for most single-substrate enzyme kinetics. It describes how the reaction rate depends on the position of the substrate-binding equilibrium and the rate constant. The Michaelis-Menten hyperbolic function relates the initial reaction rate to the substrate concentration of the enzyme where the maximum rate is described as V_{max}. K_m is an intrinsic property of an enzyme related to the binding constant for the forming of its enzyme-substrate complex and defined as the rate constants for the formation and breakdown of the complex. The ratio V_{max}/K_m measures the efficiency of the enzyme towards a substrate. The Lineweaver-Burk plot or double reciprocal plot is commonly used to illustrate and evaluate kinetic data from the Michaelis-Menten equation and is derived from the reciprocal of both sides of the equation. In this study, the Michaelis-Menten and Lineweaver-Burk kinetic plots and calculations of V_{max}, K_m and V_{max}/K_m were done using Prism 4 for Windows Version 4.02 (GraphPad Software Inc.).

The Michaelis-Menten and Lineweaver-Burk kinetic plots for rhIDO with L-Trp as substrate are shown in **Figure 3.6** and **Figure 3.7**.

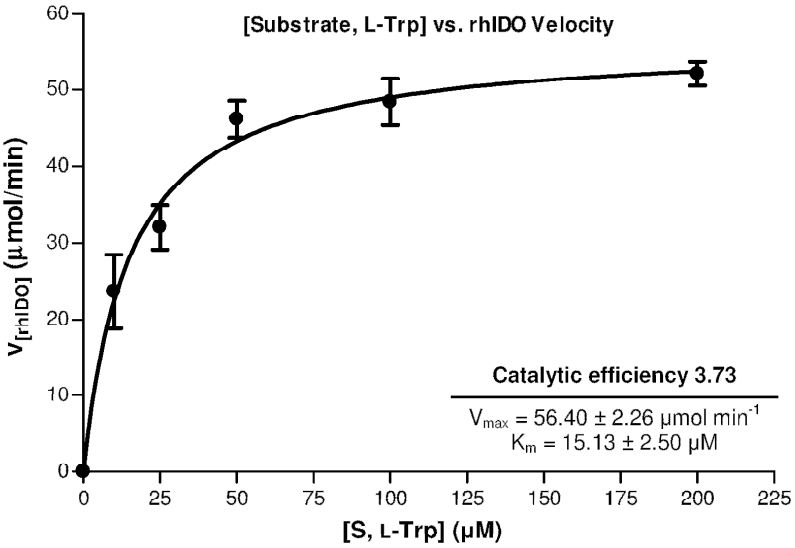

Figure 3.6 Michaelis-Menten plot of rhIDO kinetics with L-Trp as substrate showing a V_{max} of 56.40 ± 2.26 µmol min^{-1} and K_m of 15.13 ± 2.50 µM with catalytic efficiency (V_{max}/K_m) of 3.73.

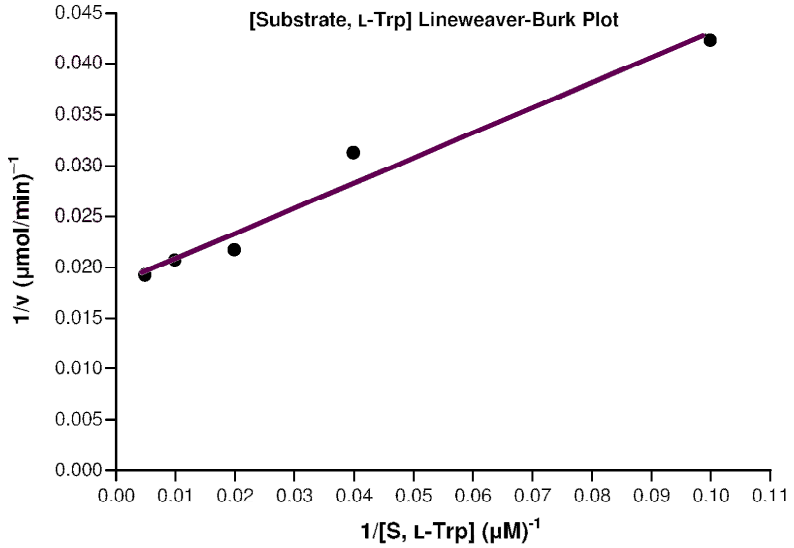

Figure 3.7 Lineweaver-Burk plot of rhIDO kinetics with L-Trp as substrate and derived from the Michaelis-Menten plot (**Figure 3.6**).

The Michaelis-Menten and Lineweaver-Burk kinetic plots for rhIDO with D-Trp as substrate are shown in **Figure 3.8** and **Figure 3.9**.

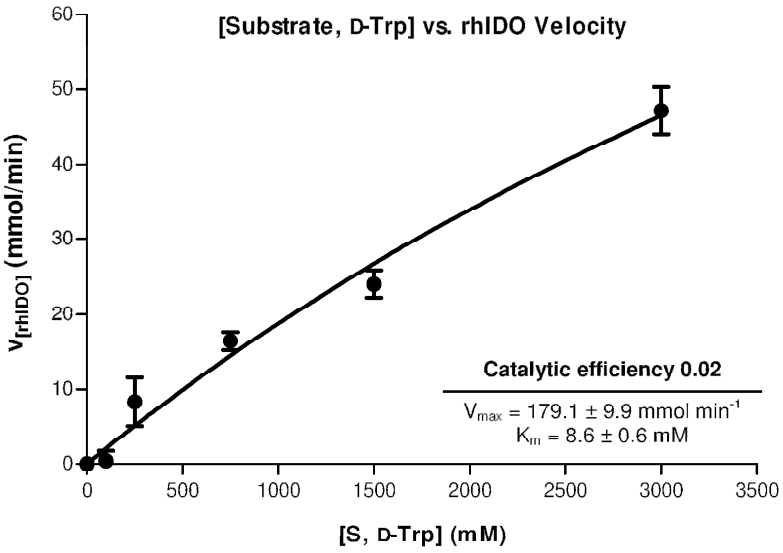

Figure 3.8 Michaelis-Menten plot of rhIDO with D-Trp as substrate showing a V_{max} of 179.1 ± 9.9 mmol min^{-1} and K_m of 8.6 ± 0.6 mM with catalytic efficiency (V_{max}/K_m) of 0.02.

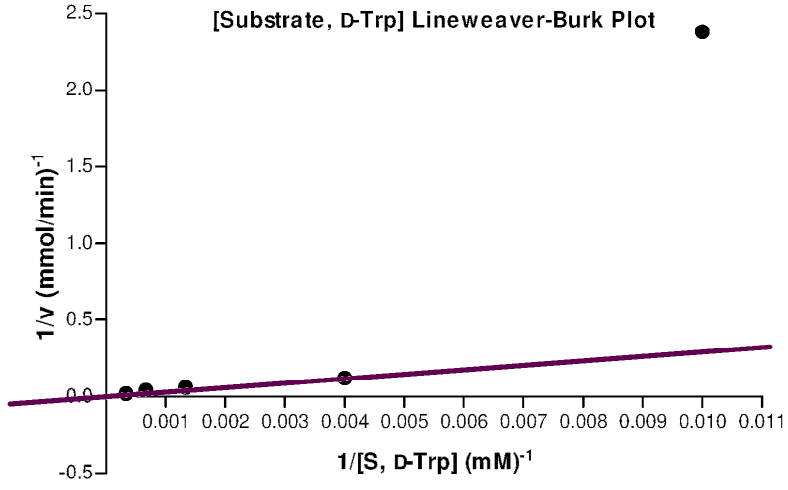

Figure 3.9 Lineweaver-Burk plot of rhIDO with D-Trp as substrate and derived from the Michaelis-Menten plot (**Figure 3.8**).

The Michaelis-Menten and Lineweaver-Burk kinetic plots for rmIDO with L-Trp as substrate are shown in **Figure 3.10** and **Figure 3.11** whereas rmIDO with D-Trp as substrate are shown in **Figure 3.12** and **Figure 3.13**.

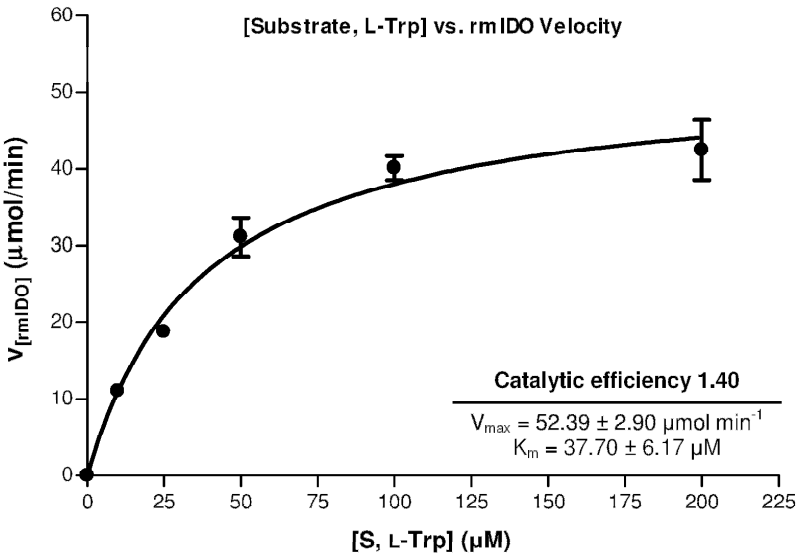

Figure 3.10 Michaelis-Menten plot of rmIDO with L-Trp as substrate showing a V_{max} of 52.39 ± 2.90 µmol min^{-1} and K_m of 37.70 ± 6.17 µM with catalytic efficiency (V_{max}/K_m) of 1.40.

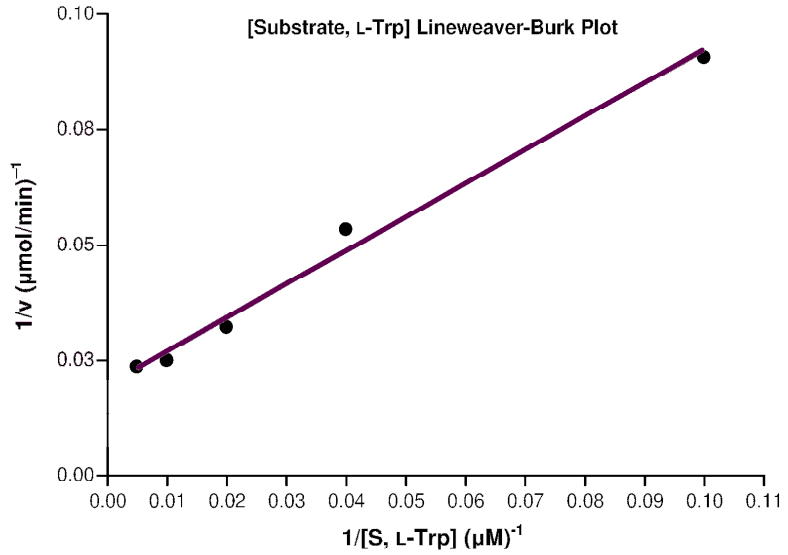

Figure 3.11 Lineweaver-Burk plot of rmIDO with L-Trp as substrate and derived from the Michaelis-Menten plot (**Figure 3.10**).

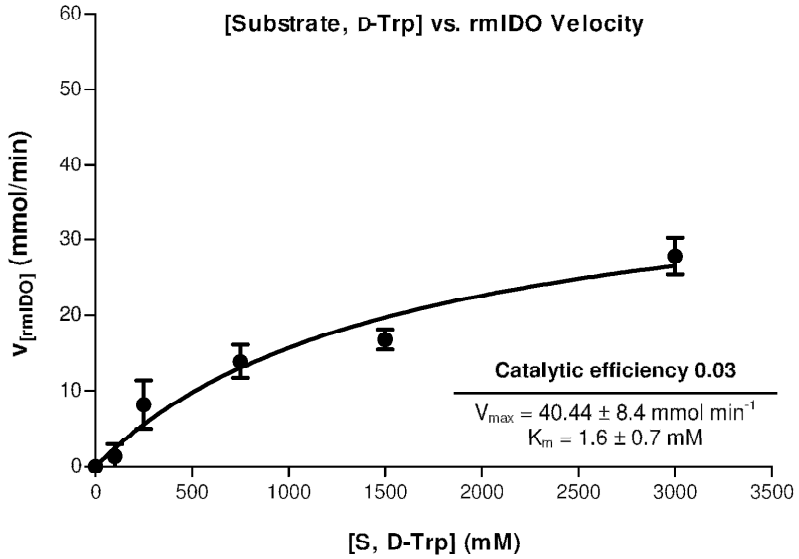

Figure 3.12 Michaelis-Menten plot of rmIDO with D-Trp as substrate showing a V_{max} of 40.44 ± 8.4 mmol min^{-1} and K_m of 1.6 ± 0.7 mM with catalytic efficiency (V_{max}/K_m) of 0.03.

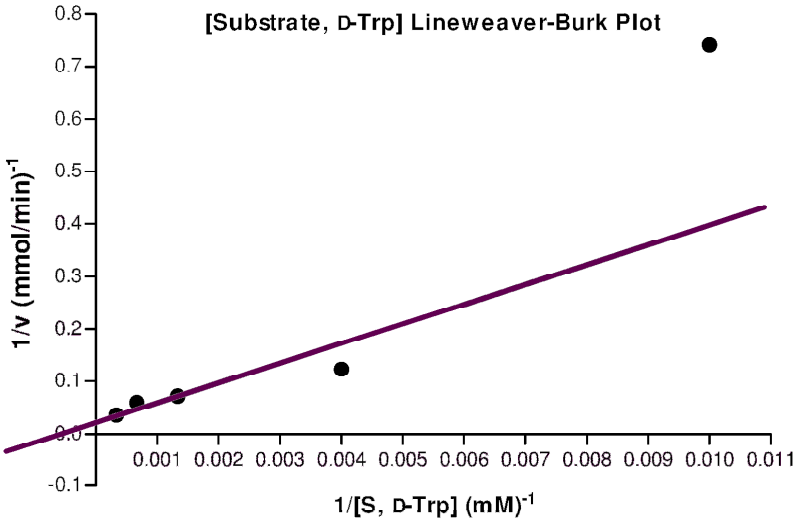

Figure 3.13 Lineweaver-Burk plot of rmIDO with D-Trp as substrate and derived from the Michaelis-Menten plot (**Figure 3.12**).

The V_{max}/K_m values showed similar substrate preferences for rhIDO and rmIDO, with a marked preference for L-Trp (μM range) over D-Trp (mM range). The relative catalytic efficiency of rmIDO towards L-Trp compared to D-Trp is slightly greater than that of rhIDO (**Table 3.6**).

Table 3.6 A summary of the kinetic studies of rhIDO and rmIDO using L-Trp and D-Trp as substrates.

Purified recombinant IDO	Substrate (L-Trp, μM)	Substrate (D-Trp, mM)
rhIDO recombinant human IDO Activity 62.82±2.62 μmol/h/mg	V_{max} = 56.40 ± 2.26 μmol min^{-1} K_m = 15.13 ± 2.50 μM V_{max}/K_m = 3.73	V_{max} = 179.1 ± 9.9 mmol min^{-1} K_m = 8.6 ± 0.6 mM V_{max}/K_m = 0.02
rmIDO recombinant mouse IDO Activity 50.35±2.91 μmol/h/mg *(as a comparison to rhIDO)*	V_{max} = 52.39 ± 2.90 μmol min^{-1} K_m = 37.70 ± 6.17 μM V_{max}/K_m = 1.40	V_{max} = 40.44 ± 8.4 mmol min^{-1} K_m = 1.6 ± 0.7 mM V_{max}/K_m = 0.03

K_m is an expression of the amount of substrate needed to reach half of the maximal velocity V_{max}. It describes the enzyme-substrate interaction. A lower K_m is associated with a tighter fit between the enzyme and the substrate and a low K_m and high V_{max} is associated with a more effective enzyme-substrate system. From this study it was observed that the K_m of both rhIDO and rmIDO is much higher when the substrate is D-Trp (mM level) compared to when the substrate is L-Trp (μM level). This showed that both rhIDO and rmIDO have a preference towards L-Trp as their substrate. From the K_m values it could also be observed that the preference of rhIDO towards L-Trp (15.13 μM) as substrate is higher than that of rmIDO (37.70 μM). On the other hand the preference of rmIDO towards D-Trp (1.6 mM) as substrate is higher than that of rhIDO (8.6 mM). In terms of relative catalytic efficiency (V_{max}/K_m), it was observed that the order of efficiency was rhIDO-L-Trp (3.73) > rmIDO-L-Trp (1.40) > rmIDO-D-Trp (0.03) > rhIDO-D-Trp (0.02). These results clearly show the significant kinetic differences of rmIDO to rhIDO in the catalysis towards the dioxygenation of L-Trp and D-Trp.

3.6.2. Conformational studies and thermal melts of rhIDO and rmIDO

Circular dichroism (CD) studies were also done to determine conformation of the secondary structure of rhIDO and rmIDO. The ultraviolet CD spectrum of proteins can predict important conformational characteristics of their secondary structure including the fraction of the protein that is in the α-helix, the β-sheet, or random-coil conformation. CD is an invaluable tool for showing changes in conformation.[275,278] In this study the rhIDO and rmIDO (in 10 mM Tris-HCl pH 7.4) were analysed by CD for their conformational characteristics (190 - 300 nm) and the results is shown in **Figure 3.14**.

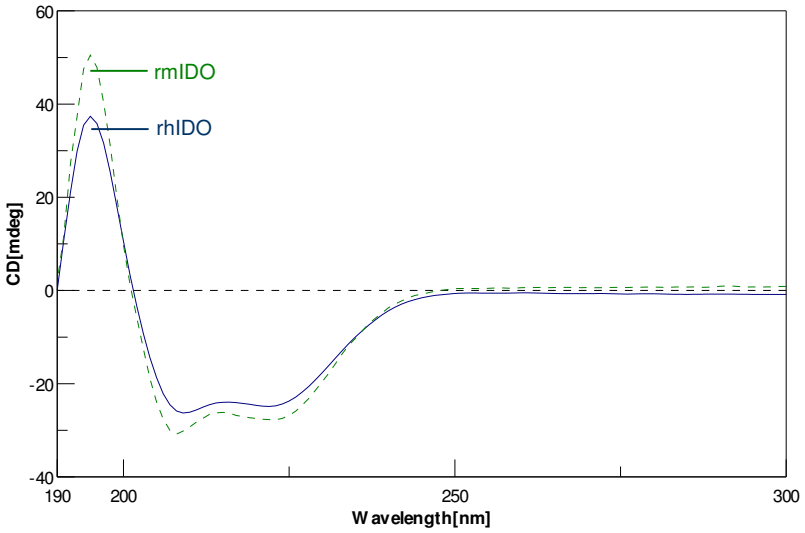

Figure 3.14 CD Spectra (190 - 300 nm) of rhIDO (blue) and rmIDO (green) in 10 mM Tris-HCl pH 7.4. A 0.2 cm cell was used in a Jasco J-810 Circular Dichroism Spectropolarimeter.

The results showed that the CD spectra (190 - 300 nm) of rhIDO were relatively similar to that of rmIDO. Analysis of the CD data between 190 to 240 nm using CDPro Software (Colorado State University) with SELCON3, CDSSTR and CONTINLL for CD analysis confirmed that the rhIDO was less helical (61% helix) compared to rmIDO (71% helix), as shown in **Table 3.7**.

Table 3.7 Analysis of the CD data between 190 to 240 nm using CDPro Software (Colorado State University) with SELCON3, CDSSTR and CONTINLL for CD analysis of rhIDO and rmIDO in 10 mM Tris-HCl pH 7.4. A 0.2 cm cell was used in a Jasco J-810 Circular Dichroism Spectropolarimeter.

Purified recombinant IDO	α-Helix (%)	β-Strand (%)	Random-Coil (%)
rhIDO recombinant human IDO	61	7	32
rmIDO recombinant mouse IDO *(as a comparison to rhIDO)*	71	4	25

CD can be used to study the effects of temperature and concentration of denaturing agents on the conformation of the secondary structure of a molecule. In this way it can reveal important thermodynamic information about the protein that cannot otherwise be easily obtained.[321,322] In this study the rhIDO and rmIDO (in 10 mM Tris-HCl pH 7.4) were analysed by CD for their thermal melts (221 nm, 20 - 99 ºC). The results are shown in **Figure 3.15**.

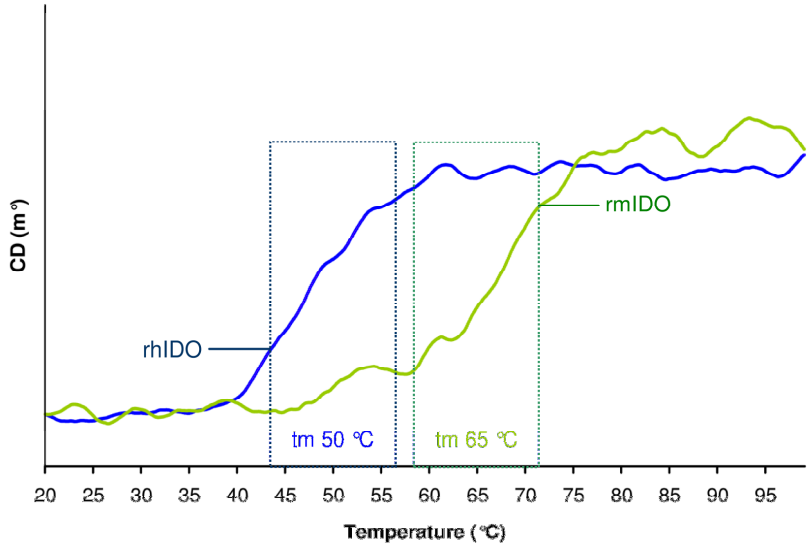

Figure 3.15 Thermal melt experiment (20 - 99 ºC) superimposed CD spectra of rhIDO (tm 50 ºC, blue) and rmIDO (tm 65 ºC, green) in 10 mM Tris-HCl pH 7.4. A 0.2 cm cell was used a Jasco J-810 Circular Dichroism Spectropolarimeter.

In thermal melt experiments, rhIDO was shown to have a lower melt temperature (tm 50 ºC) compared to rmIDO (tm 65 ºC), suggesting that the rmIDO is more thermostable than rhIDO.

The conformational and thermal melts studies of rhIDO and rmIDO suggest that the 60% identity in the protein sequence of rmIDO towards rhIDO contributes to the difference in their conformations. This difference in conformations where rmIDO is more helical than rhIDO could be the reason for rmIDO being more thermostable than rhIDO and the existing differences in their catalytic nature. To further clarify this findings, the 3D structure of rmIDO is required.

3.7. Modelling of rhIDO active site

Using the data from the findings of Sugimoto,[284,285] Oda,[208] Marcchiarulo[162,163] and their co-workers with data from Research Collaboratory for Structural Bioinformatics (RCSB) Protein Data Bank™ database, ChemDraw™, ArgusLab™ and University of California San Francisco (UCSF) Chimera™ software, the 3D modelling was done to study the active site of IDO. The ArgusDock docking engine has an efficient grid-based docking method that approximates an exhaustive search. ArgusLab employs a simple geometric fit of a ligand in the binding site at carefully-chosen search points within the free volume of the binding site cavity. This fit is corroborated with incremental construction of the ligand's torsions in a breadth-first order that maximises the early rejection of unproductive pose fragments, enhancing the efficiency of the conformational search. ArgusLab can obtain 80% agreement of the lowest scoring pose being within 2.5 Å root

mean square deviation (RMSD) of the X-Ray structure. Using ArgusLab, the heme *b* co-factor environment and the active site of IDO was docked with L-Trp as a ligand and mapped in this study (**Figure 3.16**).

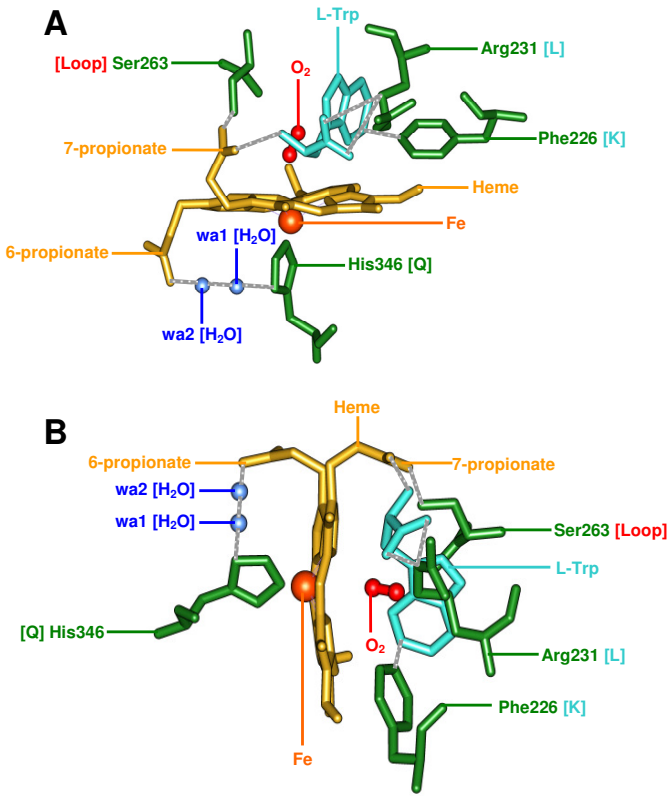

Figure 3.16 L-Trp docked complex in the active site of IDO. (A) View of the residues around the heme *b* of IDO viewed from the side of the heme *b* plane. The 6-propionate of the heme *b* is in contact with wa2 and wa1 (water) and wa1 is hydrogen-bonded to the proximal ligand His346. L-Trp is bound in the distal pocket. The aromatic ring of L-Trp (cyan) is in contact with Phe226. The 7-propionate of the heme *b* interacts with the amino group of L-Trp and the side chain of Ser263. (B) Top view of (A) by a rotation of 90°.

The figure shows the heme *b* co-factor (yellow) with the surrounding residues of the L-Trp-bound form (blue) in the active site of IDO. The heme *b* 6-propionate is in contact in the proximal side to the water molecule (wa2), which also interacts with wa1 and the

hydrogen bonded proximal ligand His346. The environment of the heme *b* proximal side of IDO suggests that the His346 imidazole is rendered partially anionic by the 6-propionate through the mediation of the two waters (wa1 and wa2). In the modelling of the active site it can be seen that the 7-propionate of the heme *b* points upward from the heme *b* plane and interacts with the hydroxyl group of Ser263. The proximal side of the heme *b* co-factor is occupied only by side chains from the large domain Q (His346), S (Leu384, Phe387) and N (His287), as shown in **Figure 3.17**.

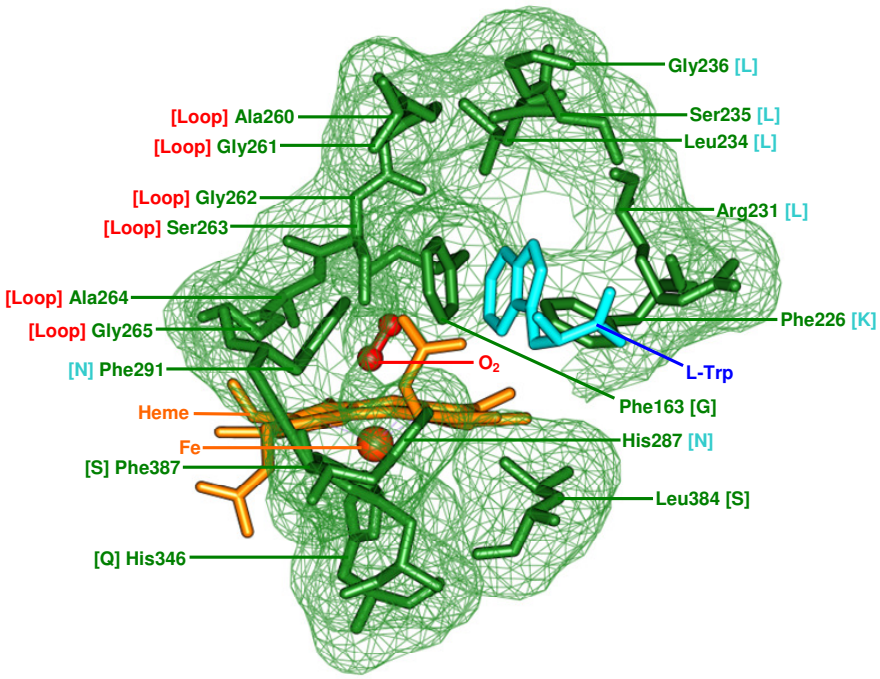

Figure 3.17 The surface representation of the active site of IDO docked with L-Trp (cyan) as a ligand (substrate). The proximal helices G, Q and S run in parallel. The helices N and K-L are the helices connecting the two (small and large) domains. The connecting loop (Ala260 to Gly265) between helices L and M is above the sixth-coordination site of the heme *b* co-factor covering the top of the heme cavity. All the important binding residues and domains are in green.

3.7.1. Modelling of docked L-Trp complex in IDO

The distal heme pocket, which is the coordination site of the heme *b* iron for the sixth external ligand (docked L-Trp and O_2), is a combination of the small domain, the large domain and the loop connecting the two domains of IDO[284] (**Figure 3.18**).

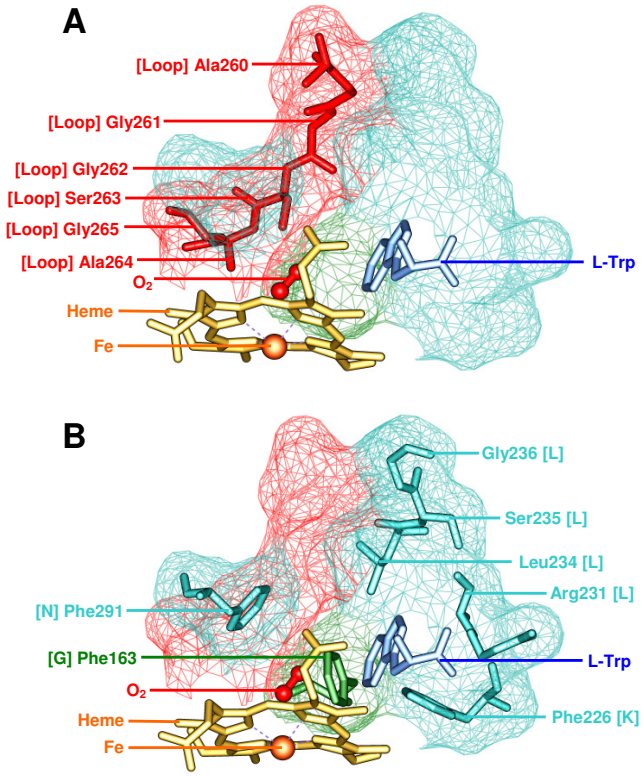

Figure 3.18 Active site of the docked L-Trp bound IDO as viewed from the distal side. L-Trp (blue) bound structures are shown as a stick model in blue. (A) The L to M connecting loop (red) facilitates the conformational change needed for flexibility especially in the main chain of the connecting loop. Sugimoto and co-workers reported that the largest movement is observed in the Ala264 and Gly265 region with a 1.3 Å shift toward the center of the heme *b* (yellow). (B) The L, K and N connecting loop (cyan) along with Phe163 of helix G (green) facilitates the binding of the substrate.

Molecular oxygen (O_2) binds at the distal side of the active site and therefore it could be argued that the structural properties of the distal heme pocket are responsible for the IDO catalysed dioxygenase reaction. From the findings of Sugimoto[284] and co-workers, which were supported by Macchiarulo[162,163] and co-workers and from the mapped structures of the docked L-Trp complex that were done in this study, it can be concluded that His is not present in the heme distal side and that neither polar residues nor water molecules are available to interact with the iron-bound ligand, in this case, the docked L-Trp. Sugimoto[284] and co-workers showed that the connecting loop exhibits a large conformational change in the main chain with a displacement of 1.3 Å, whereas the values for all common atoms is 0.2 Å. The highly conserved sequences (Ala260-Gly261-Gly262-Ser263-Ala264-Gly265 residues) in the loop appear to provide flexibility. The binding of the ligand (substrate) induces a conformational change in the connecting loop (Ala260 to Gly265), as shown in the L-Trp docked complex of IDO (**Figure 3.18**).

In the docked L-Trp-bound form (**Figure 3.17** and **Figure 3.18**) Phe163 interacts with the phenyl group of L-Trp by π-π stacking. The side chain of Phe226 in the heme distal pocket is in contact with the docked L-Trp. Gly261 and Gly262 of the connecting loop also interacts with L-Trp, where the amino group of the L-Trp interacts with the 7-propionate of the heme *b*. In the L-Trp docked IDO complexes, Ala260, Gly261, Gly262, Ser263, Ala264 and Gly265 residues in the connecting loop interact with the docked substrates. This study supported the significance of the interaction of Phe226 of the K helix with the phenyl group of the substrate in a π-π stacking, the interaction of the 7-propionate of the heme *b* with the amino group (of the substrates) and the interaction of

the side chain Arg231 of the L helix with the carboxylate (of the substrates). These findings were consistent with the mutational studies done by Sugimoto[284] and co-workers (**Table 3.8**).

3.8. IDO catalysed reaction mechanism

Based on the present crystal structure and mutational analysis, Sugimoto[284] and co-workers demonstrated that no polar or charged protein side chains act as a catalytic base. They proposed that proton abstraction by iron-bound dioxygen (**Figure 3.19**) was the most probable event occurring in the IDO catalysed conversion of L-Trp to *N*-formylKyn.[162,208,284,285] The orientation of the binding of O_2 and the substrate L-Trp was proposed to be restricted by Phe226 and Arg231, enabling an interaction between the NH group of indole and the dioxygen.

It has been previously proposed that the rearrangement of the electronic structure of the indole ring induces an electrophilic reaction, which involves the formation of a bond between the terminal oxygen atom of dioxygen and the C3 atom. Subsequent cleavage of the Fe-O bond results in the formation of the 3-hydroperoxyindolenine intermediate. A dioxetane has been proposed as the intermediate formed during the incorporation of dioxygen. The product *N*-formylKyn is then converted to Kyn non-enzymatically or by Kyn formamidase (**Figure 3.19**).

The mutations of Phe226A, Phe227A and Arg231A (**Table 3.8**), as demonstrated by Sugimoto[284] and co-workers, did not affect the *K*d values of IDO but reduced the activity

dramatically. These mutation studies suggest that a necessary condition for the reaction is the orientation of the substrate with respect to the dioxygen for proton abstraction.

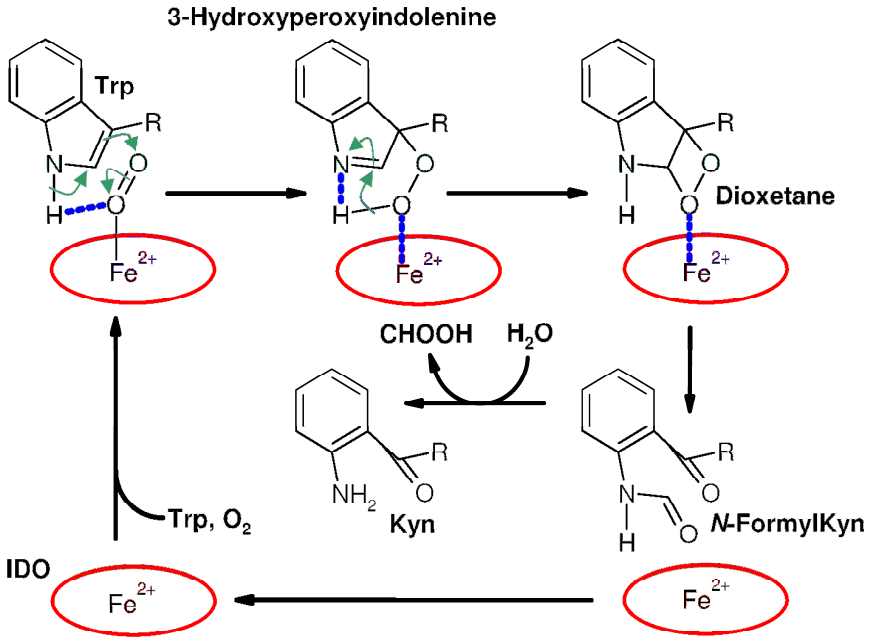

Figure 3.19 Proposed reaction mechanisms for IDO catalysing the cleavage of the bond between C_2 and C_3 of L-Trp (substrate). The trigger for the reaction is the abstraction of a proton from 1-*N* of L-Trp.[284]

Table 3.8 Comparison of activity and dissociation constants (*K*d) for L-Trp of non-mutated and mutants rhIDO.[284]

Mutation	Activity*	Kd, mM		
		Fe^{3+}	Fe^{2+}	Fe^{2+}-CO
Wild type	126±12	0.32±0.03	0.53±0.05	0.43±0.01
Cys129A	134±6	0.40±0.04	0.46±0.06	0.33±0.03
Phe163A	148±9	1.08±0.10	0.87±0.05	0.63±0.05
Ser167A	117±5	1.37±0.15	1.01±0.12	0.53±0.04
Phe226A	1.3±0.3	0.80±0.12	0.93±0.10	0.41±0.02
Phe227A	1.2±0.5	0.65±0.07	0.53±0.09	NA‡
Arg231A	2.3±1.0	0.77±0.11	ND†	NA‡
Ser263A	19±7	42±5	ND†	NA‡

* Mol of product/mol of holoenzyme per min.
† ND, spectrum change was not detectable.
‡ NA, Kd was not deduced from flash photolysis experiment because of unusual behaviour.

This orientation is believed to be accomplished through the strict interactions between the indole ring of the substrate and a hydrophobic moiety of the protein. It is evident that strict interactions are not required for L-Trp binding, which may reflect the broad substrate specificity of IDO. The structural differences between indoleamine derivatives may be accommodated by the flexibility of the long connecting loop between helices L and M and this is a very important aspect to be taken account of for the docking of various indoleamine derived compounds in terms of drug discovery.

The mechanism proposed by Sugimoto[284] and co-workers, which is further supported by Chung,[43] Macchiarulo[162,163] and co-workers, for the enzymatic catalysis reaction at the active site of IDO was based on the surface and structural characteristics around the heme pocket as no significant electropositive surface around the dioxygen was apparent. In the distal side, hydroxyl or carboxyl groups in the conserved and acidic residues (**Figure 3.20**) play a crucial role in the formation of a specific hydrogen-bonding network to deliver the protons from the solvent media (water) to the active site during the catalytic reaction.[162,208,284,285] The structure of human IDO as resolved by Sugimoto[284] and co-workers provided evidence that the reaction mechanism in IDO catalysis involves the proton abstraction by iron-bound dioxygen. Analysis of site-directed mutants of IDO strongly suggests that substrate binding and geometry between the substrate and iron-bound dioxygen is required for the reaction. Recognition of the substrate is likely to involve strict complementary interactions between the indole ring of the substrate and protein groups. The O-O bond of the dioxygen co-substrate is precisely controlled by the heme proximal and distal environment and is not likely to be cleaved before the incorporation of the dioxygen atoms into the substrate.

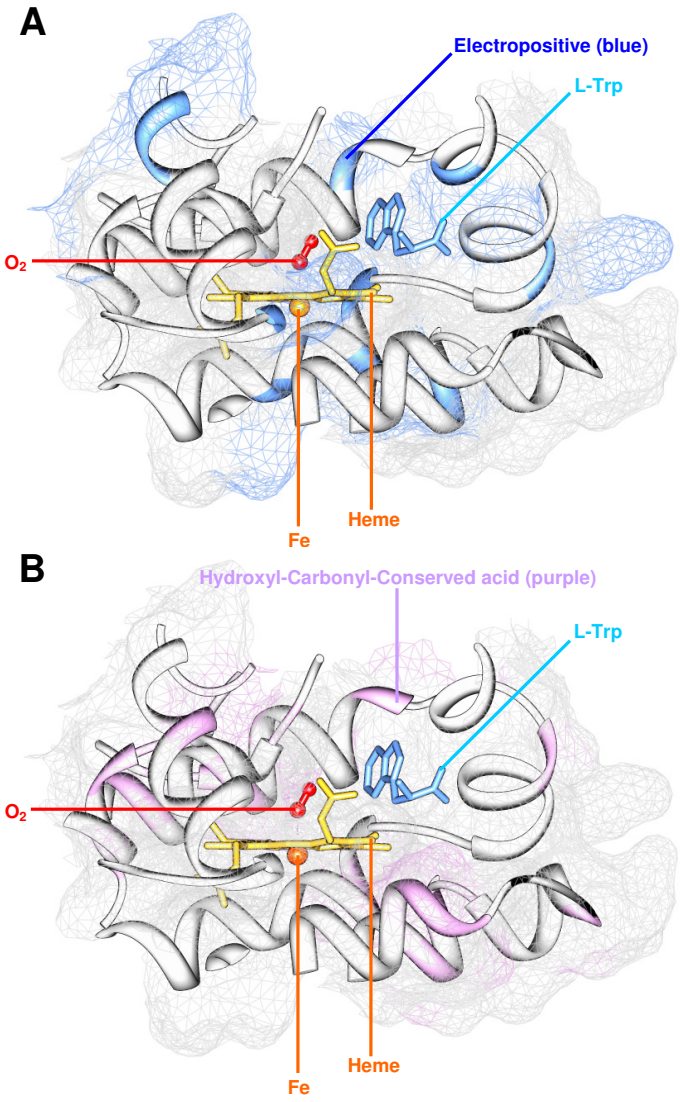

Figure 3.20 Surfaces of the active site in IDO. (A) No significant electropositive surface around O_2. (B) In the distal side, hydroxyl or carboxyl groups in the conserved and acidic residues (purple) play a crucial role in the formation of a specific hydrogen-bonding network to deliver the protons from the solvent media (water) to the active site during the catalytic reaction.

3.9. Conclusion

rhIDO expressed and purified using the protocol described in **Chapter 2** (**Figure 2.23**) was characterised. The mass spectrum from a direct injection ESI-MS of rhIDO was

deconvoluted with Micromass MaxEnt1 processing giving a mass of 47,758 kDa for the rhIDO and due to adduct ion species of multiply charge rhIDO in the ESI-MS spectra, the value of 47,758 kDa for a direct injection ESI-MS of rhIDO is consistent with this mass. The SDS-PAGE of the rhIDO was consistent to the ESI-MS result. In this study, the Soret/protein ratio of rhIDO was observed to reach a maximum of 1.70:1.00. However, it was established that the ratios fluctuated from sample to sample depending upon the treatment of the samples.

Reduction of the rhIDO heme *b* co-factor iron from its ferric (Fe^{3+}) to its ferrous (Fe^{2+}) state with sodium dithionite was done. One minute after the initial reaction, the UV-Vis spectra showed an additional peak at 314 nm for dithionite and a shift of the peak at 406 nm to 421 nm. After ten minutes the peaks returned to their original position with a lower absorption at 406 nm. CD studies of the reduction suggested that one minute after the initial reaction, an increased α-helix but a lowered β-strand and random-coil conformations occurred. A conformational change may be expected between the Fe^{2+}/Fe^{3+} state as Fe^{2+} heme is usually 5 coordinate while Fe^{3+} is six coordinate and also requires a neutralising charge. This shift in state may cause changes in the conformation to accommodate the additional coordination bond possibly to a negatively charged species. This result suggested that changes in conformations occurred to facilitate the reaction of rhIDO in its active site and perhaps it is important to take account this conformational changes in order to support the efficacy of IDO as a novel target in therapy and drug discovery.[113,119,126,163,169,192] Further studies on this are required.

Discrepancies between the previous findings[10,174] and the findings in this study were observed in the Soret/protein ratios, specific activities and CD spectral studies when rhIDO was incubated at a temperature range of 4 to 20 °C in a period of 2 to 6 hours. In this study it was found that under those conditions rhIDO was highly stable and retained its activity. In the study of the effect of cryoprotectants it was found that the use of 0.5 M sucrose as a cyroprotectant severely degraded rhIDO. The preservative effects of cyroprotectants in the freezing of rhIDO was in the order of 40% glycerol > 10% DMSO > absence of cryoprotectants > 0.5 M sucrose. From the study it could be seen that the process of freezing and thawing can result in severe damage to rhIDO. This could perhaps be ascribed to surface-induced denaturation during the freezing and thawing process.[236] It can be assumed that upon fast freezing, small ice crystals and a relatively large surface area of ice-liquid interface are formed, which increases the exposure of the rhIDO molecules to the damaging ice-liquid interface.[237] During thawing, damage could be attributed due to recrystallisation which exerts additional interfacial tension on entrapped rhIDO. The patterns of the dependency on cryoprotectants showed that damage of rhIDO in aqueous solutions could be reduced by preserving rhIDO in 40% glycerol at -20°C as this resulted in only a small decrease in Soret/protein ratio (6%), specific activity (24%) and protein concentration (17%).

Homology and database analysis of rhIDO and rmIDO showed some similarities in both physical and kinetic properties. Kinetic studies of rhIDO and rmIDO using L-Trp and D-Trp as substrates showed similar substrate preferences where the preference towards L-Trp (μM range) was greater than towards D-Trp (mM range). The relative catalytic

efficiency of rhIDO towards L-Trp (3.73) was higher compared to rmIDO (1.40) whereas the relative catalytic efficiency of rhIDO towards D-Trp (0.02) was lower compared to rmIDO (0.03). From the study it could be concluded that rhIDO utilises L-Trp more efficiently than rmIDO but the reverse is true for D-Trp. CD and thermal melt studies established that rhIDO is less helical (61% helix) than rmIDO (71% helix). The studies also showed that rhIDO has a lower melt temperature (50 ºC) than rmIDO (65 ºC), indicating that rmIDO is more thermostable than rhIDO. From these observations, it could be concluded that there are significant differences between rhIDO and rmIDO despite their 60% similarities. These differences must be recognised and accounted for, before the interpretation of experimental findings from one system to another is applied, especially as murine models are commonly used to study human conditions relevant to the expression of IDO.

In the 3D modelling of IDO, the ArgusDock docking engine was used to dock L-Trp into the active site of IDO. The docking experiments supported that the proximal side of the heme *b* co-factor is occupied only by side chains from the large domain Q (His346), S (Leu384, Phe387) and N (His287). The modelling and docking experiments were able to map IDO's active site and its complex with L-Trp.

Chapter 4

Re-incorporation of heme into indoleamine 2,3-dioxygenase

Chapter 4

Re-incorporation of heme into indoleamine 2,3-dioxygenase

The overall aim of this chapter is to give an account of the studies that were done to evaluate the phenomenon of heme loss in recombinant human IDO (rhIDO) and the efforts to optimise the availability of active rhIDO through the re-incorporation of heme.

4.1. IDO as a hemoprotein

Hemoproteins are heme containing proteins that are important components of living organisms. A diversity of hemoproteins participate in many functions including electron transfer reactions, heme metabolism, regulatory functions based on nitric oxide and activation, insertion, transport, storage and sensing of oxygen.[293,352] Despite the wide range of chemical and physiological functions displayed by hemoproteins, they all share the same prosthetic group, heme. Heme is an essential molecule with various biological functions.[280] It is widely distributed in all eukaryotic cells. The most common heme prosthetic group is protoheme IX, also known as heme *b* (**Chapter 1, Figure 1.3**). The role of heme in dioxygenases depends on the nature of the heme as a proximal ligand, the heme environment and the substrate. Indoleamine 2,3-dioxygenase (IDO) is a hemoprotein.[293,352] In common with many of the heme-containing dioxygenases, IDO goes through a key ferrous-dioxygen complex intermediate in its catalytic reaction cycle. In IDO the heme *b* co-factor comprises an iron atom coordinated to four nitrogen atoms of a tetrapyrrole macrocyclic porphyrin ring.[280] This heme is held within the confines of

the protein by a combination of hydrophobic interactions and a metal-protein coordinate bond at one axial position of the iron (**Chapter 1, Figure 1.10** and **Chapter 3, Figure 3.16**). Oxygen binds to the Fe^{2+} (reduced) active form of IDO and the Fe^{3+} (oxidised) inactive form of the native IDO binds to a variety of exogenous ligands.[280] The heme *b* co-factor of IDO has a strong absorbance (Soret band) at 406 nm, which provides a convenient probe of the heme site in IDO.

4.2. Heme release by hemoproteins and heme re-incorporation

The phenomenon of heme release by hemoproteins has been well studied.[273,248] The reaction is best described as heme release into water where the energetics of the activated process are large and interpreted as connected to both polypeptide motions during release and the ordering of water around the heme during solvation.[151,248, 273] Side chain positions on the proximal side[280,355] of the heme pocket strongly influence heme affinity.[151] The roles of the amino acids in preventing heme loss have been examined.[151] Important surface amino acids that interact either sterically or electrostatically with the edges of the porphyrin ring (heme *b*) which influence heme loss has also studied.[151] Apolar amino acids can waterproof the heme pocket by forming a barrier to solvent penetration, thereby minimising the size of the proximal cavity, and maintaining a hydrophobic environment. Smaller or polar side chains in the proximity of the proximal pocket result in exposure of the heme to solvent and water molecules, leading to large increases in the rate of hemin loss.[151] Heme release in rhIDO is observed as a lowering of its Soret/protein ratio. These findings were observed during storage and purification in this study and in previous work on rhIDO by Austin.[10]

The heme moiety in hemoproteins has been reported to dissociate from the proteins in aqueous solution at neutral pH and room temperature.[248] Slow heme release from hemoproteins such as horseradish peroxidases, cytochrome peroxidase, chloroperoxidase, and leghemoglobins has been reported.[273] Heme re-constitution into heme deficient hemoproteins has been extensively studied.[355] Myoglobin is a heme containing protein and re-constitution of apo-myoglobin is well documented.[67] Heme re-constitution of other heme containing proteins such as horseradish peroxidase, cytochrome P-450 has also been done.[273,335]

4.3. Re-purification of rhIDO with Amicon Ultra-15 filter

To confirm that purification of rhIDO leads to lowering of the Soret/protein ratio, samples of size-exclusion chromatography purified rhIDO were re-purified by filtering with an Amicon Ultra-15 filter prior to desalting and concentration. After each pass 80% glycerol (1:1 v/v) was added to the rhIDO samples, which were stored in the freezer (-20 ºC, 2 hours) prior to the next re-purification cycle. Up to 10 consecutive passes of cycle were done. The results (**Figure 4.1**) showed a direct correlation between the number of consecutive passes and the lowering of the Soret/protein ratio, protein content and enzyme activity of the rhIDO.

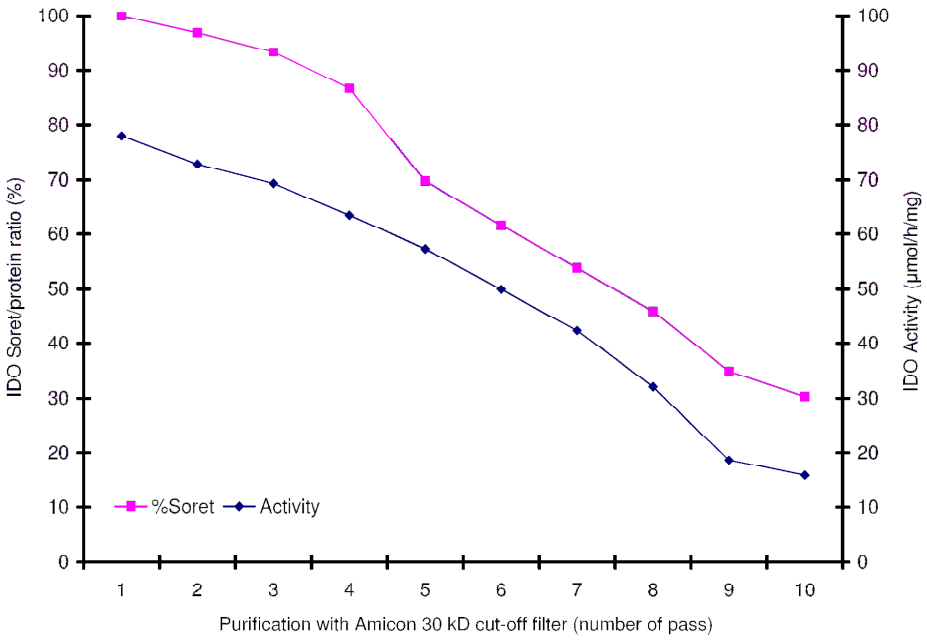

Figure 4.1 Re-purification of rhIDO from 25 mM Tris-HCl pH 7.4 (desalting) with a Millipore Amicon Ultra-15 30 kD cut-off filter (2.5 mL to 250 µL), from 1 to 10 consecutive pass respectively.

The study showed that the re-purification of rhIDO by filtering with the Amicon Ultra-15 filter lowered the intense maxima at 406 nm (Soret band), suggesting lowering of heme content of the treated rhIDO.[276] Decrease in the Soret/protein ratio after 10 consecutive passes reached 70% from the initial pass, while the decrease in activity reached 93% from the initial pass. A superimposed UV-Vis spectrum of the rhIDO that underwent re-purification of up to 10 consecutive passes with the Amicon Ultra-15 filter is given in **Figure 4.2** showing decrease in the Soret/protein ratio.

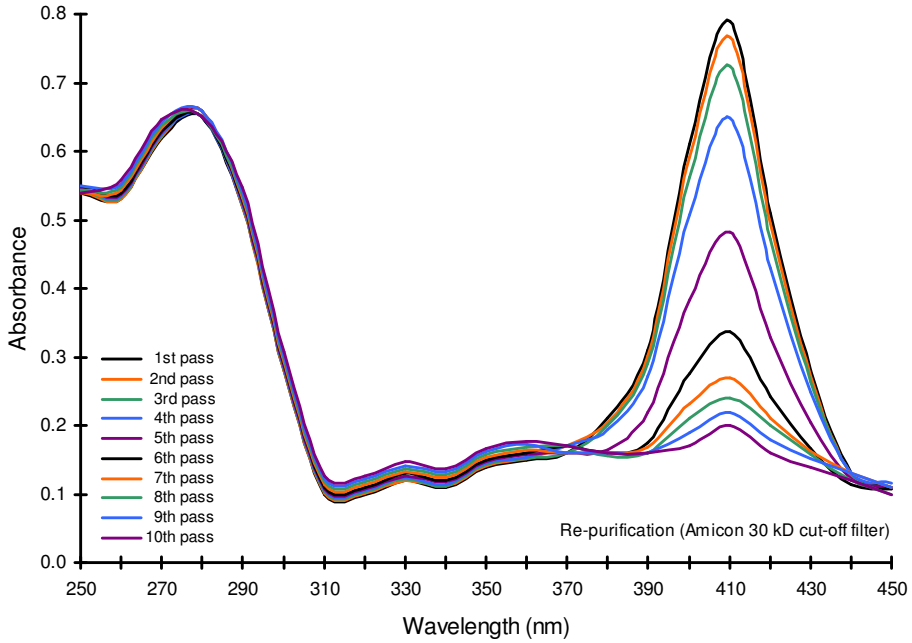

Figure 4.2 Superimposed spectra of rhIDO supernatant (2.5 mL) which underwent re-purification of 1 to 10 passes with a Millipore Amicon Utra-15 30 kD cut-off filter (desalting from 25 mM Tris-HCl pH 7.4) concentrating 2.5 mL to 250 µL protein.

The effect of the intensive re-purification treatment of the rhIDO on the protein content and enzyme activity were also evaluated. The degree of loss in protein content and enzyme activity from the re-purification upon re-freezing, re-thawing, re-dissolving and re-filtering rhIDO with the Amicon Ultra-15 filter is given in **Figure 4.3**.

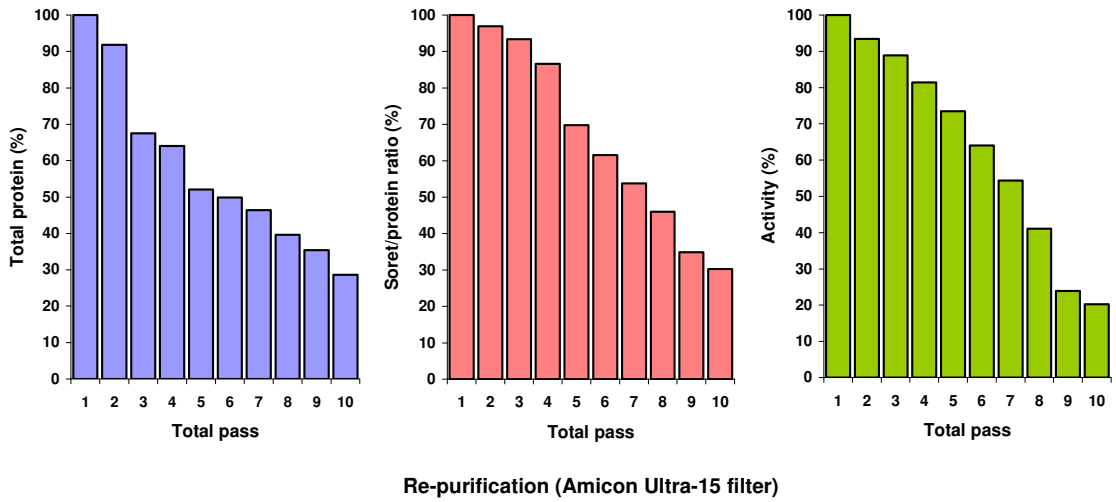

Figure 4.3 Percentage of total protein yields (in 2.5 ml) of individual passes (1 to 10) for the re-purification of rhIDO from 25 mM Tris-HCl pH 7.4 (desalting) with a Millipore Amicon Ultra-15 30 kD cut-off filter (2.5 mL to 250 µL) from 1 to 10 consecutive pass respectively. All values (% total protein, % Soret/protein ratio and % activity) were compared to the 1st-pass which was arbitrarily set at 100%.

The overall results of the study showed that re-purification of rhIDO involving freezing, thawing, dissolving and filtering with the Amicon Ultra-15 filter has a severe impact on the yield and quality of the rhIDO. The decrease in Soret/protein ratio, protein content and enzyme activity reached up to 71, 70 and 80% respectively after 10 consecutive passes. To study this further a desalting step using a PD-10 column prior to the concentration with an Amicon Ultra-15 filter was done. This was considered to see whether the loss of heme was salt dependent as the re-dissolving cycles of concentrated rhIDO prior to the concentration with Amicon Ultra-15 filter might have contributed to the loss.

4.4. Re-purification of rhIDO with PD-10 and Amicon Ultra-15 filter

Because of the detrimental effects observed for the re-purification of rhIDO with Amicon Ultra-15 filter, a desalting step using an Amersham Biosciences PD-10 Sephadex G-25M

(PD-10) desalting column prior to the concentrating step was incorporated. Re-purification of rhIDO (2.5 mL) by elution through a PD-10 desalting column, followed by filtration with an Amicon Ultra-15 filter for up to 10 consecutive passes was done. After each pass, sample preparation and treatment followed the guidelines given in **Section 4.3**. The results showed that the desalting step changed the trend of the decrease of the Soret/protein ratio of rhIDO and its activity, as given in **Figure 4.4**. The decrease in the Soret/protein ratio after 10 consecutive passes reached 82% from the initial pass, while the decrease in activity reached 62% from the initial pass.

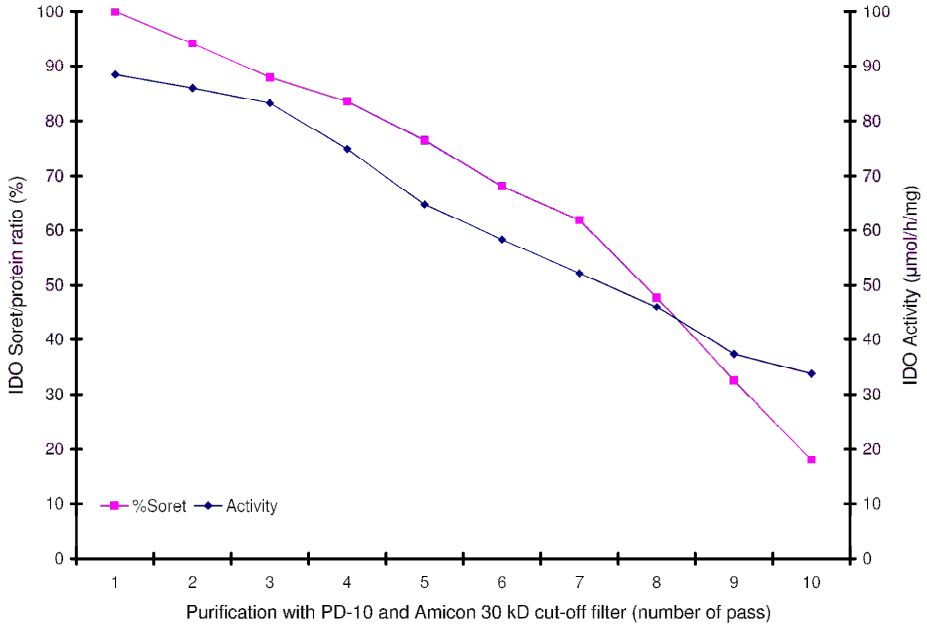

Figure 4.4 Re-purification of rhIDO (2.5 mL) from 25 mM Tris-HCl pH 7.4 (desalting) through an Amersham Biosciences PD-10 (Sephadex G-25M) column and filtering with a Millipore Amicon Ultra-15 30 kD cut-off filter (2.5 mL to 250 µL) from 1 to 10 consecutive passes respectively.

As observed previously with the re-purification of rhIDO with the Amicon Ultra-15 filter, re-purification by elution through a PD-10 desalting column, followed by filtering with an Amicon Ultra-15 filter, did not defer the decrease of the intense maxima at 406 nm (Soret band) of the rhIDO. This suggested that the salt concentration was not a factor in heme loss. All spectra were superimposed to the spectrum of the initial supernatant (the first pass), as perfect concentration of the supernatant cannot be made. The superimposed spectra of the rhIDO that were subjected to this re-purification are shown in **Figure 4.5**. The degree of loss in protein content and enzyme activity are shown in **Figure 4.6**.

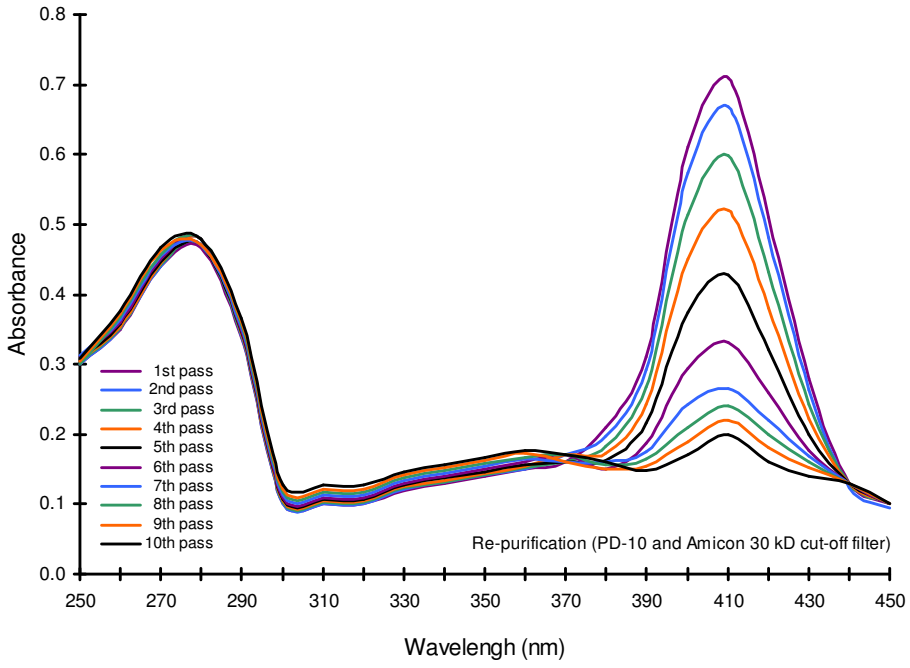

Figure 4.5 Superimposed spectra of rhIDO supernatant (2.5 mL) which underwent re-purification of 1 to 10 passes through an Amersham Biosciences PD-10 (Sephadex G-25M) desalting column followed by concentration (and further desalting) with a Millipore Amicon Ultra-15 30 kD cut-off filter (desalting from 25 mM Tris-HCl pH 7.4) concentrating 2.5 mL to 250 µL protein.

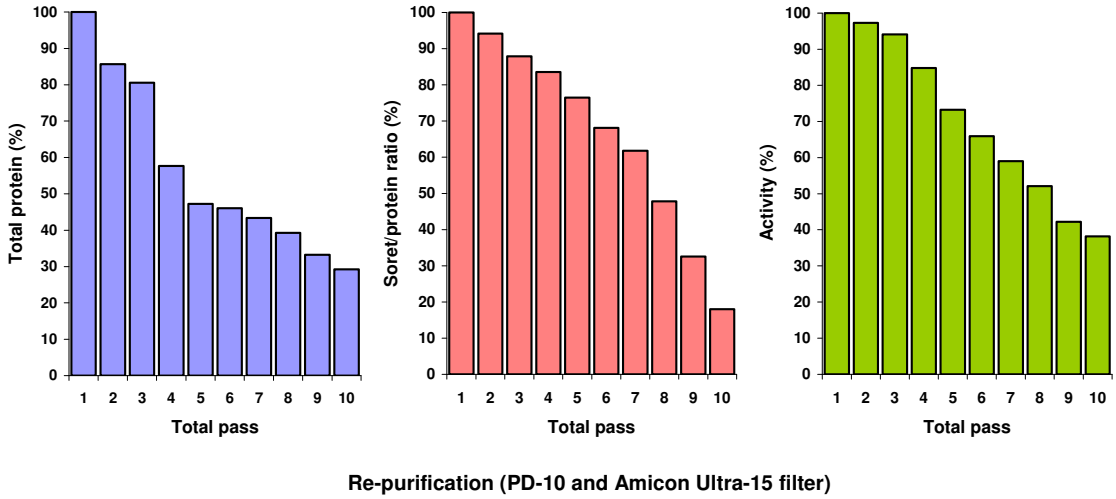

Figure 4.6 Percentage of total protein yields (in 2.5 ml) of individual passes (1 to 10) for the re-purification of rhIDO from 25 mM Tris-HCl pH 7.4 (desalting) through an Amersham Biosciences PD-10 column and continued with a Millipore Amicon Ultra-15 filter (2.5 mL 250 µL) from 1 to 10 consecutive pass respectively. All values (% total protein, % Soret/protein ratio and % activity) were compared to the 1st-pass which was arbitrarily set at 100%.

The overall results of the study showed that the process of re-purifying of rhIDO with Amicon Ultra-15 filter showed decrease in Soret/protein ratio, protein content and enzyme activity. Desalting through PD-10 prior to re-purification with an Amicon Ultra-15 filter had no detrimental effect. The differences in the results of the two processes concluded that the quality and yield of rhIDO is dependent on the manner in which the rhIDO is treated. The lowering of the Soret/protein ratio prompted the optimisation of the availability of active rhIDO, through the re-incorporation of heme.

4.5. Heme re-incorporation of rhIDO

Hemin chloride has been used for re-incorporation of heme into proteins.[67,273,355] This approach was therefore decided upon for rhIDO. In this study rhIDO re-purified with Ni-NTA, PD-10, Amicon Ultra-15 filter and Superdex 75 PC 3.2/30 columns were used

(**Section 2.2** and **Section 2.3**). To evaluate the extend of efficiency of the heme re-incorporation, two samples were used for the heme re-incorporation study with hemin chloride, representing a low Soret/protein ratio of 1.1:1.0 and a high ratio of 1.4:1.0 respectively.

The experiments showed that concentrations of 0.0, 1.5, 3.0, 4.5, 6.0 and 7.5 µM of hemin chloride (in 20 mM NaOH) towards 600 µL rhIDO samples (1 mg/L in 25 mM Tris-HCl pH 7.4) gave satisfactory results for rhIDO with a Soret/protein ratio of 1.1:1.0 as shown in **Figure 4.7**.

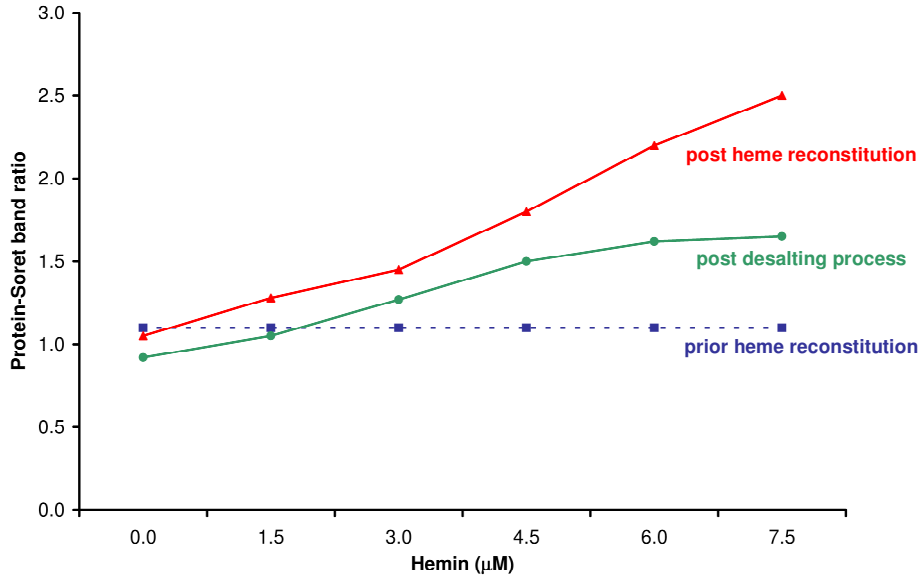

Figure 4.7 Results of rhIDO Soret/protein ratio of heme re-incorporation on low Soret/protein ratio of 1.1:1.0 fraction of rhIDO with 0.0, 1.5, 3.0, 4.5, 6.0 and 7.5 µM of hemin chloride (in 20 mM NaOH). Soret/protein ratio of the initial preparation (prior to heme re-incorporation), post heme re-incorporation and post fast desalting process are shown.

The result of heme re-incorporation showed an increased Soret/protein ratio of 127% (from the initial 1.1:1.0 to 2.5:1.0) prior to desalting. Upon desalting the ratio was

reduced 77% (from 2.5:1.0 to 1.7:1.0), an increase of 50% from the initial ratio. This suggested that high concentration of hemin chloride did not effectively re-incorporate the heme into rhIDO. The resulting enzyme activity of the rhIDO is given in **Figure 4.8**. The result of heme re-incorporation showed an increased enzyme activity of 36% (from the initial 60.5 to 82.4 µmol/h/mg) prior to desalting. Upon desalting the activity was increased 35% (from 82.4 to 103.6 µmol/h/mg), an increase of 71% from the initial activity. This supported that high concentration of hemin lowered the efficiency of the heme re-incorporation.

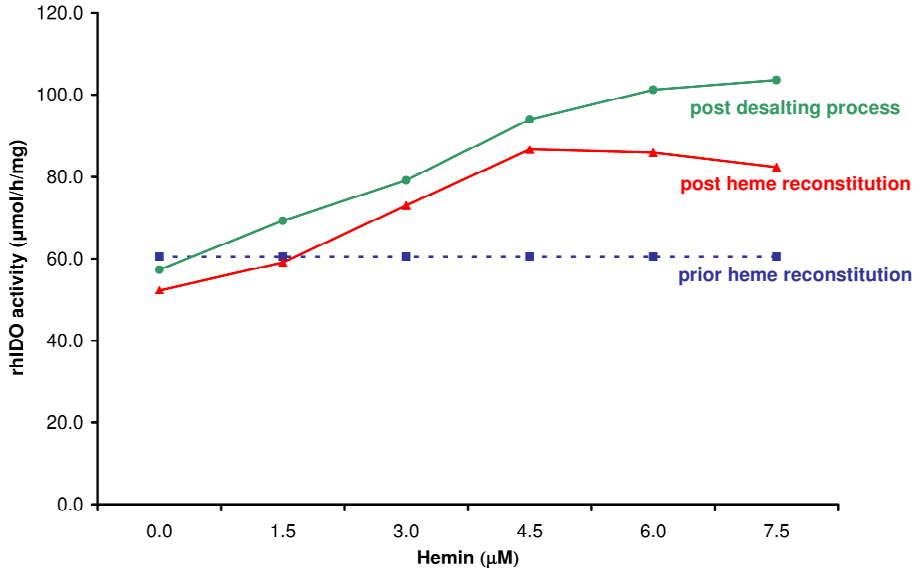

Figure 4.8 Results of rhIDO activity of heme re-incorporation on low Soret/protein ratio of 1.1:1.0 fraction of rhIDO with 0.0, 1.5, 3.0, 4.5, 6.0 and 7.5 µM of hemin chloride (in 20 mM NaOH). Soret/protein ratio of the initial preparation (prior to heme re-incorporation), post heme re-incorporation and post fast desalting process are shown.

The experiments also showed that concentrations of 0.0, 1.7, 3.3, 5.0, 6.7 and 8.3 µM of hemin chloride towards 600 µL rhIDO samples (1 mg/L in 25 mM Tris-HCl pH 7.4) gave satisfactory results for rhIDO with a Soret/protein ratio of 1.4:1.0 (**Figure 4.9**). The result

of heme re-incorporation showed an increased Soret/protein ratio of 93% (from the initial 1.4:1.0 to 2.7:1.0) prior to desalting. Upon desalting the ratio was reduced 65% (from 2.7:1.0 to 1.8:1.0), an increase of 28% from the initial ratio. The result also suggested that high concentration of hemin chloride did not effectively re-incorporate the heme into rhIDO.

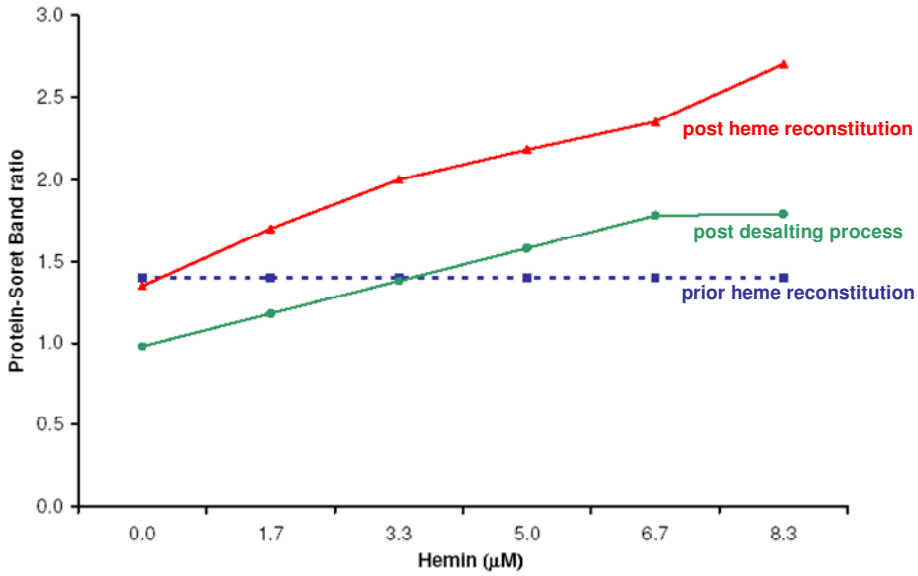

Figure 4.9 Results of rhIDO Soret/protein ratio of heme re-incorporation on high Soret/protein ratio of 1.4:1.0 fraction of rhIDO with 0.0, 1.7, 3.3, 5.0, 6.7 and 8.3 µM of hemin chloride (in 20 mM NaOH). Soret/protein ratio of the initial preparation (prior to heme re-incorporation), post heme re-incorporation and post fast desalting process are shown.

The resulting enzyme activity of the rhIDO is given in **Figure 4.10**. The result of heme re-incorporation showed an increased enzyme activity of 24% (from the initial 76.1 to 94.1 µmol/h/mg) prior to desalting. Upon desalting the activity was increased 14% (from 94.1 to 105.0 µmol/h/mg), an increase of 38% from the initial activity. The result also supported that high concentration of hemin lowered the efficiency of the heme

re-incorporation. From the experiments it is observed that the desalting process lowers the Soret/protein ratios and increase the activity of the hemin re-incorporated rhIDO, suggesting that there is a limit to the specific capacity for the accommodation of the inactive rhIDO which are brought about by heme deficiency.

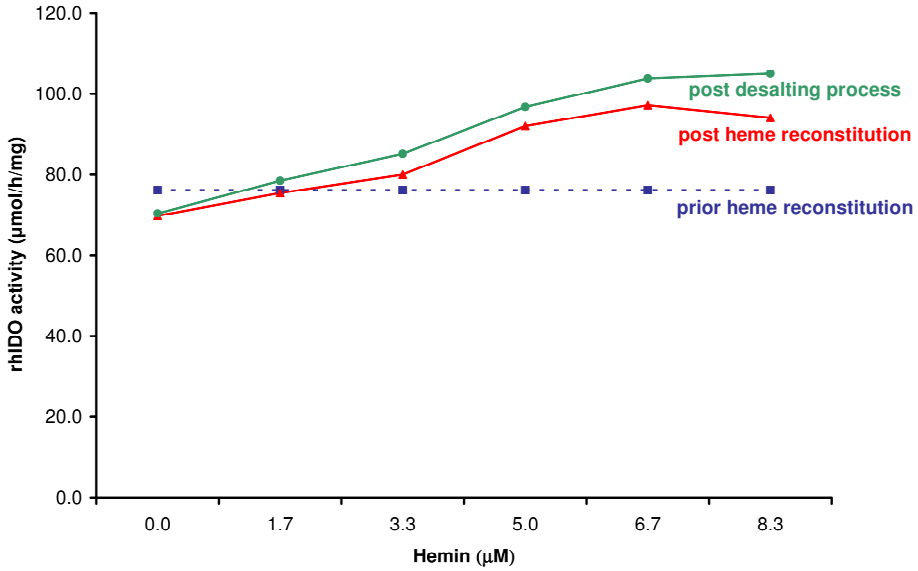

Figure 4.10 Results of rhIDO activity of heme re-incorporation on high Soret/protein ratio of 1.4:1.0 fraction of rhIDO with 0.0, 1.7, 3.3, 5.0, 6.7 and 8.3 µM of hemin chloride (in 20 mM NaOH). Soret/protein ratio of the initial preparation (prior to heme re-incorporation), post heme re-incorporation and post fast desalting process are shown.

Results of the heme re-incorporation experiments were evaluated before and after elution through the Fast Desalting column (GE/Pharmacia), which was equilibrated with 50 mM Tris-HCl pH 7.4 prior to use. The desalting was monitored at 280 and 406 nm on a fast protein liquid chromatography (FPLC) System (SMART-Pharmacia LKB Biotechnology) with sample injections of 200 µL, which afforded 600 µL (3x) of combined desalted samples. rhIDO activities and respective Soret/protein ratio were evaluated. The outcome of the trials showed a consistent increase in rhIDO activity with increased hemin chloride

availability during heme incorporation, both before and after the desalting. An increase of Soret/protein ratio and activity after heme re-incorporation was observed. The heme re-incorporation profile for the rhIDO with an initial Soret/protein ratio of 1.1:1.0, which was titrated with low concentrations of hemin chloride and desalted through the Fast Desalting column, is shown in **Figure 4.11**.

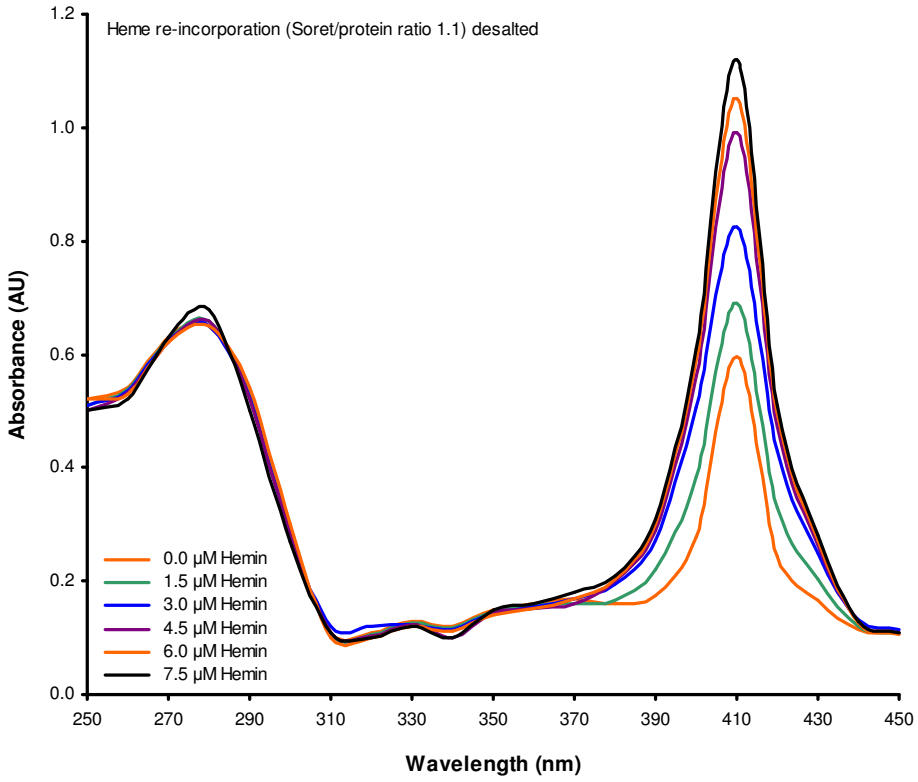

Figure 4.11 Superimposed heme re-incorporation profile of rhIDO of low Soret/protein ratio of 1.1:1.0 fraction with 0.0, 1.5, 3.0, 4.5, 6.0 and 7.5 µM of hemin chloride (in 20 mM NaOH) after desalting through the Fast Desalting column PC 3.2/10 (Pharmacia LKB Biotechnology) on a FPLC System (SMART-Pharmacia LKB Biotechnology) with 50 mM Tris-HCl pH 7.4.

The profile for the rhIDO with an initial Soret/protein ratio of 1:4:1.0 titrated with high concentration of hemin chloride is given in **Figure 4.12**. Both profiles show an increase

in the intense maxima at 406 nm (Soret band) of the rhIDO and consistent maxima at 280 nm, suggesting that the heme re-incorporation did achieve its purpose.

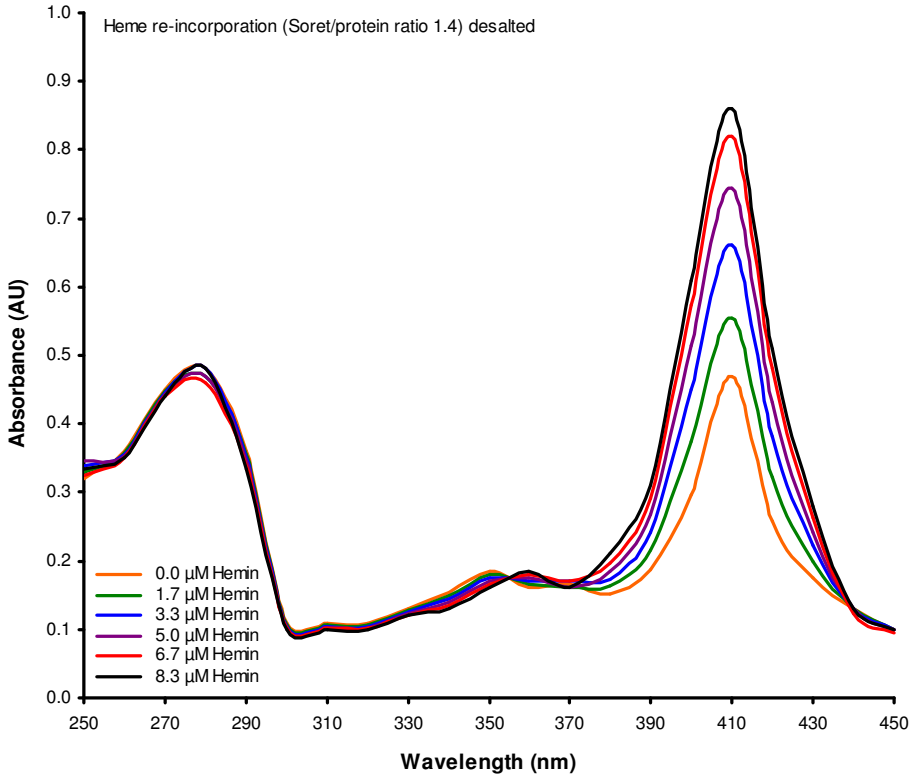

Figure 4.12 Superimposed heme re-incorporation profile of rhIDO of high Soret/protein ratio of 1.4:1.0 fraction with 0.0, 1.7, 3.3, 5.0, 6.7 and 8.3 µM of hemin chloride (in 20 mM NaOH) after desalting through the Fast Desalting column PC 3.2/10 (Pharmacia LKB Biotechnology) on a FPLC System (SMART-Pharmacia LKB Biotechnology) with 50 mM Tris-HCl pH 7.4.

The overall investigation of hemin chloride titration into heme-deficient rhIDO showed that there was a consistent increase of rhIDO activity with increased hemin availability. This was observed for rhIDO having a low initial Soret/protein ratio of 1.1:1.0 as well as those having a high initial ratio of 1.4:1.0. Heme re-incorporation using low concentration of hemin chloride to rhIDO of low Soret/protein ratio, showed an increase of 50% in Soret/protein ratio (from 1.1:1.0 to 1.7:1.0), with an increase of enzyme

activity of 71% (from 60.5 to 103.6 μmol/h/mg). Heme re-incorporation using a high concentration hemin chloride towards high Soret/protein ratio rhIDO showed an increase of 28% in Soret/protein ratio (from 1.4:1.0 to 1.8:1.0) with an increase of enzyme activity of 38% (from 76.1 to 105.0 μmol/h/mg). High initial Soret/protein ratio rhIDO showed a higher lowering of enzyme activity and Soret/protein ratio with increased hemin concentration after desalting than low initial Soret/protein ratio rhIDO. The study verified that burdening the availability of hemin chloride was not the best option in heme re-incorporation of heme-deficient rhIDO. As low Soret/protein ratio is related to heme availability and protein concentration, the studies suggested that burdening the heme deficient rhIDO with high concentration of hemin chloride did not effectively re-incorporate the heme and determining the variations of the hemin chloride concentrations needed were necessary to ensure the best availability of hemin during the heme re-incorporation titrations. The highest possible Soret/protein ratio achieved through the re-incorporation of heme using hemin chloride was in the range of 1.7:1.0 to 1.8:1.0 with rhIDO activity of 104 - 105.0 μmol/h/mg. The studies and outcomes of the heme re-incorporation experiments prompted investigations into the supplementation of hemin chloride prior to lysis of the *E. coli* EC538 (pQE-9-IDO, pREP4) cells (**Chapter 2**, **Section 2.4.5** and **Section 2.4.6**).

4.6. Anion exchange of rhIDO

The findings of heme loss upon re-purification of rhIDO and the results of heme re-incorporation into heme deficient rhIDO prompted the study of anion exchange chromatography experiments. This was done to evaluate the posibility of totally stripping

the heme *b* co-factor from purified rhIDO for the purpose of separating different forms of rhIDO without the heme *b* co-factor intact (apo-rhIDO) and the subsequent re-incorporation of heme. In this study rhIDO re-purified with Ni-NTA, PD-10, Amicon Ultra-15 filter and Superdex 75 PC 3.2/30 columns were used (**Section 2.2** and **Section 2.3**). These investigations utilised resin based anion chromatography where polyethyleneimine (PI) and quaternary amine polyethyleneimine (QE and HQ) resins were used as the anion exchange resins. The anion exchange chromatographies were performed using buffers at pH 7.4 and 8.0 with a gradient buffer solution containing KCN, KCl or NaCl respectively. The salt in the solution competes in the binding towards the immobilised matrix, thereby releasing the rhIDO from its bound state at a given concentration with the heme bound to the immobilised matrix. The amount of salt required to compete varies with the external charge of the rhIDO. Since rhIDO is a charged molecule, it will interact with the column resin depending on the distribution of charged molecules on the surface of the rhIDO, displacing mobile counter ions and the heme that are bound to the resin. The net charge on rhIDO depends on the composition of its amino acids, charge distribution and on the pH of the buffering solution. The isoelectric point (pI) of rhIDO is the pH at which rhIDO is neutral. To study the strength of the heme *b* binding in rhIDO using anion chromatography, the surface charge of the rhIDO should be above its theoritical pI of 6.2.

In this study PI-20 (PEI Ligand/Binding capacity 35 mg/mL), QE-20 (QPEI Ligand/Binding capacity 40 mg/mL), and HQ-20 (QPEI Ligand/Binding capacity 60 mg/mL) POROS columns were used. A gradient elution from 0 to 1 M NaCl, KCl and

KCN (flow rate 2 mL/min) in 50 mM Tris-HCl pH 7.4 and 8.0 on a fast protein liquid chromatography (FPLC) system were done. The processes were monitored at 280 and 406 nm. The studies showed that elution through the HQ-20 column with NaCl (0 to 1 M, gradient) at pH 8.0 provided the best result in stripping the heme *b* from rhIDO and not causing retention of the rhIDO in the column (**Figure 4.13**), nevertheless the resulting fraction gave agregated proteins.

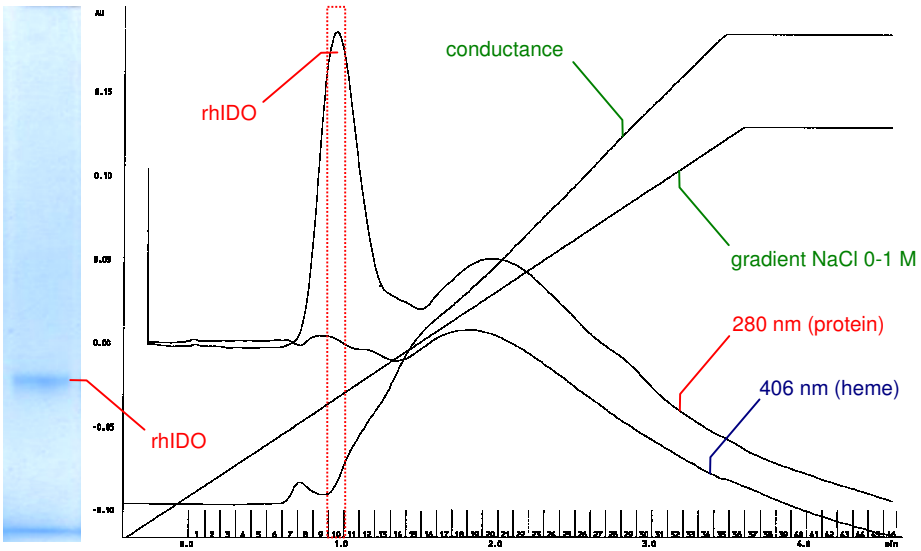

Figure 4.13 Chromatogram of rhIDO eluted through HQ-20 (POROS) column with NaCl (0 to 1 M, gradient, 2 mL/min) in 50 mM Tris-HCl pH 8.0 (0 to 1 M, gradient) on a FPLC (fast protein liquid chromatography system (SMART-Pharmacia) monitored at 280 and 406 nm with the heme *b* co-factor stripped from the protein. SDS-PAGE of the peak fraction (aggregated protein) is shown.

The anion exchange chromatography of rhIDO using HQ-20 with gradient KCl and KCN, PI-20 and QE-20 with gradient NaCl, KCl and KCN did not strip the heme *b* from rhIDO and caused retention of the rhIDO in the column (**Figure 4.14**).

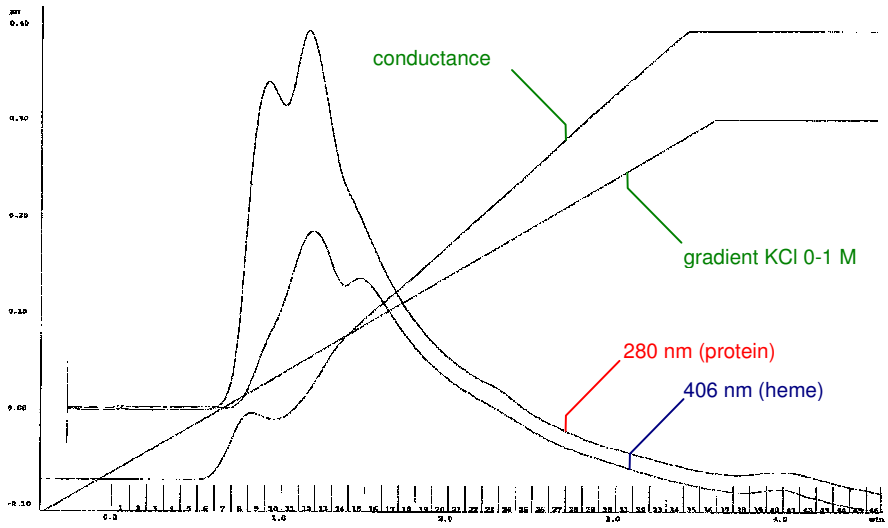

Figure 4.14 Chromatogram of rhIDO eluted through QE-20 (POROS) column with KCl (0 to 1M, gradient, 2 mL/min) in 50 mM Tris-HCl pH 8.0 (0 to 1 M, gradient) on a FPLC (fast protein liquid chromatography system (SMART-Pharmacia) monitored at 280 and 406 nm with the heme *b* co-factor unstripped from the protein.

Of these observations, it could be argued that the POROS columns used did have an effect on the stripping of the heme *b* from rhIDO, yet the performances of the systems suggests that it may not be appropriate for use in these studies. The ionic composition used had an influence on the stripping of the heme *b* and retention of the rhIDO, with KCN and KCl performing poorly compared to NaCl at pH 8.0 (**Table 4.1**). These qualitative studies suggest that within the specific limits of the anion exchange experiments that was done, it could be considered that the total stripping the heme *b* co-factor from purified rhIDO for the purpose of separating different forms of rhIDO without the heme *b* co-factor intact (apo-rhIDO) and the subsequent re-incorporation of heme cannot be done in this respect.

Table 4.1 Anion exchange experiment to strip the heme *b* co-factor from rhIDO using PI-20 (PEI Ligand/Binding capacity 35 mg/mL), QE-20 (QPEI Ligand/Binding capacity 40 mg/mL), and HQ-20 (QPEI Ligand/Binding capacity 60 mg/mL) POROS columns. These were done using gradient NaCl, KCl and KCN (0 to 1M, gradient, 2 mL/min) in 50 mM Tris-HCl pH 7.4 and 8.0 on a fast protein liquid chromatography (FPLC) System (SMART-Pharmacia LKB Biotechnology) monitored at 280 and 406 nm.

Purified recombinant human IDO *(anion exchange experiment)*	**KCN (0-1 M, gradient)**		**KCl (0-1 M, gradient)**		**NaCl (0-1 M, gradient)**	
	pH 7.4	**pH 8.0**	**pH 7.4**	**pH 8.0**	**pH 7.4**	**pH 8.0**
PI-20 POROS (Binding capacity 35 mg/mL)	retained not good	retained not good	retained not good	unretained not good	Unretained not good	unretained not good
QE-20 POROS (Binding capacity 40 mg/mL)	unretained not good	unretained not good	unretained not good	unretained not good	unretained not good	unretained fair
HQ-20 POROS (Binding capacity 60 mg/mL)	unretained fair	unretained fair	unretained fair	unretained fair	unretained good	unretained very good

4.7. Supplementation of hemin prior to lysis

Due to the findings of heme loss upon re-purification of rhIDO and the results of heme re-incorporation into heme deficient rhIDO, investigations of supplementing hemin chloride prior to lysis of *E. coli* EC538 (pQE-9-IDO, pREP4) cells in the French Press were done (**Chapter 2, Section 2.4.5**). This was considered conducive in sustaining the availability of the heme. Purification of rhIDO from lysed cells containing hemin chloride resulted in a higher rhIDO enzyme activity and Soret/protein ratio (**Table 4.2**).

Table 4.2 The influence of the addition of hemin prior to lysis through the French Press of *E. coli* EC538 (pQE-9-IDO, pREP4) cells in the over-expression of rhIDO. Results of the Soret/protein ratio and the specific activity of the protein (post Ni-NA work-up) are shown.

Purified recombinant human IDO *(hemin addition prior to lysis)*	**Normal**	**Hemin addition**
Protein-Soret band ratio *(ratio towards 1)*	1.4	1.7
Specific activity *(µmol/h/mg)*	81±3	102±5

The UV-Vis absorption spectrum of the resulting rhIDO with a Soret/protein ratio of 1.7:1.0 is given in **Figure 4.15**. The native enzyme from placenta was reported to have a Soret/protein ratio of 2.2:1.0.[152] Further analysis of rhIDO by CD analysis and kinetic studies showed that the results were as expected of rhIDO, as given elsewhere in this thesis (**Chapter 3**, **Section 3.6**).

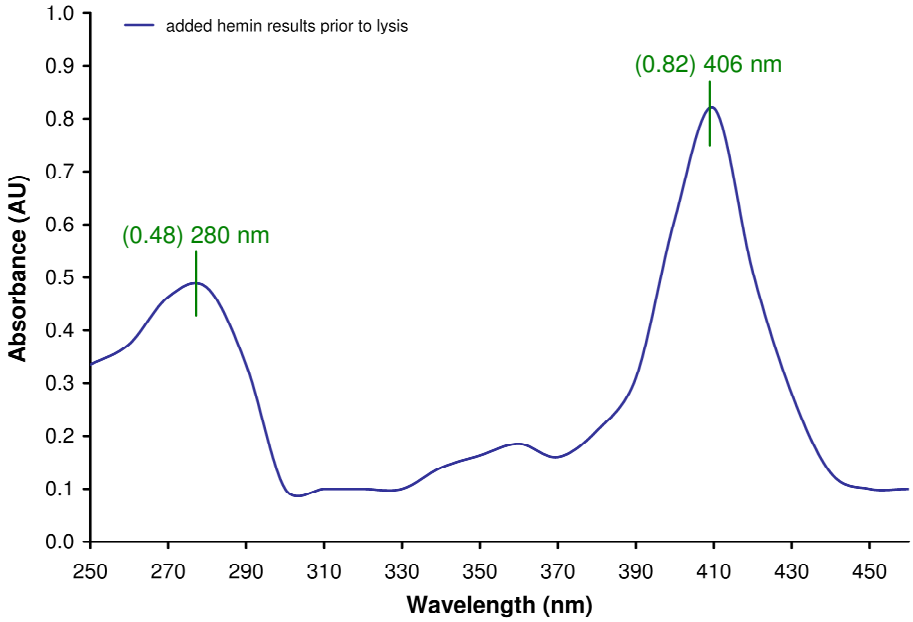

Figure 4.15 Absorption profile of rhIDO as an influence of the addition of hemin prior to lysis through the French Press of *E. coli* EC538 (pQE-9-IDO, pREP4) cells in the over-expression of rhIDO, showing a Soret/protein ratio of 1.7:1.0 after purification.

4.8. Conclusion

Heme release in rhIDO was observed during purification. This was consistent with fluctuations and decreases in the rhIDO Soret/protein ratio observed in previous studies on rhIDO by Austin.[10] Studies of re-purification of rhIDO over ten cycles of consecutive re-freezing, re-thawing, re-dissolving and re-filtering with the Amicon Ultra-15 filter

concluded that the degree of loss in Soret/protein ratio, protein content and enzyme activity could reach up to 71, 70 and 80% respectively. A desalting step using a PD-10 column prior to re-filtering with the Amicon Ultra-15 filter showed that the decrease in Soret/protein ratio, protein content and enzyme activity could reach 71, 82 and 62% respectively. This outcome concluded that elution through a PD-10 desalting column did not hinder the severe loss of heme during the re-purification with the Amicon Ultra-15 filter suggesting that the process of heme loss from rhIDO upon re-purifications is not salt dependent.

In this study, it was established that a gradual heme re-incorporation with hemin chloride showed a consistent gradual increase in Soret/protein ratio and enzyme activities. This increase was observed before and after the desalting process. Heme re-incorporation using low concentration of hemin chloride to rhIDO of low Soret/protein ratio, showed an increase in Soret/protein ratio and enzyme activity of 50% (from 1.1:1.0 to 1.7:1.0) and 71% (from 60.5 to 103.6 μmol/h/mg), respectively. Heme re-incorporation using a high concentration hemin chloride towards high Soret/protein ratio rhIDO showed an increase of Soret/protein ratio and enzyme activity of 28% (from 1.4:1.0 to 1.8:1.0) and 38% (from 76.1 to 105.0 μmol/h/mg), respectively. High initial Soret/protein ratio rhIDO showed a higher lowering of enzyme activity and Soret/protein ratio with increased hemin concentration after desalting than low initial Soret/protein ratio rhIDO. From this study, the observed lowering of rhIDO enzyme activity and Soret/protein ratio after desalting during the heme re-incorporation titration verified that burdening the availability of heme occurred.

It can be concluded that the loss of rhIDO activity is caused by the loss of the heme prosthetic group of the enzyme. The re-incorporation of the heme was considered to reverse the process. It was observed that the re-incorporation of heme to the apo-protein through heme re-incorporation was a possibility. However, supplementing hemin chloride prior to lysis of *E. coli* EC538 (pQE-9-IDO, pREP4) cells in the French Press was considered conducive in sustaining the availability of the heme. Investigations in this study also established that the stripping of the heme *b* co-factor of rhIDO through anion exchange chromatography resulted towards aggregated proteins. The matrices and elution conditions of the anion exchange chromatography used in this study did not result in the efficient stripping of the heme *b* co-factor from the rhIDO. However, this needs to be investigated further in light of the possibility of using anion exchange for the purification of rhIDO.

Chapter 5

Mutagenesis of indoleamine 2,3-dioxygenase

Chapter 5

Mutagenesis of indoleamine 2,3-dioxygenase

The overall aim of this chapter is to give an account of mutagenic studies on rhIDO that were done to establish the contribution of individual cysteines towards the overall characteristics of rhIDO.

5.1. Cysteine residues of IDO

Structurally, cysteine belongs to the sulphur amino acids. It contains the sulfhydryl (-SH) group, which is very reactive.[233] The sulfhydryl group of cysteine is important for many proteins. It can readily act as a nucleophile and form thiol radicals, making it possible to form a covalent bond with other molecules. The ease of formation of such a covalent bond depends on the overall redox potential, the spatial environment as well as pH. Cysteines that are not involved in disulfide bridge formation, such as that in IDO, can stabilise the α-helix conformation in a protein. However, the high reactivity of the -SH group can possibly distort the regular structure by interactions with reactive oxygen species or other reactive groups.[240]

The cysteines in IDO are well distributed, mostly in its helices. Three of the cysteines are found in the small domain and five in the large domain. Those found in the small domain include Cys99 at helix D, Cys126 at helix E and Cys143 at helix F. Cys173 at helix G, Cys220 at helix I, Cys286 at helix M, Cys322 at helix O and Cys349 at helix Q are

located in the large domain. Cys143 at helix F of the small domain and Cys173 at helix G of the large domain are close to the heme cavity. None of the cysteines are deeply buried inside the structure of IDO (**Figure 5.1**). To understand the role of these cysteines, this study aimed to replace them individually with alanine in the rhIDO and then examine the change in conformation and kinetics of the mutant enzymes against the non-mutated rhIDO.

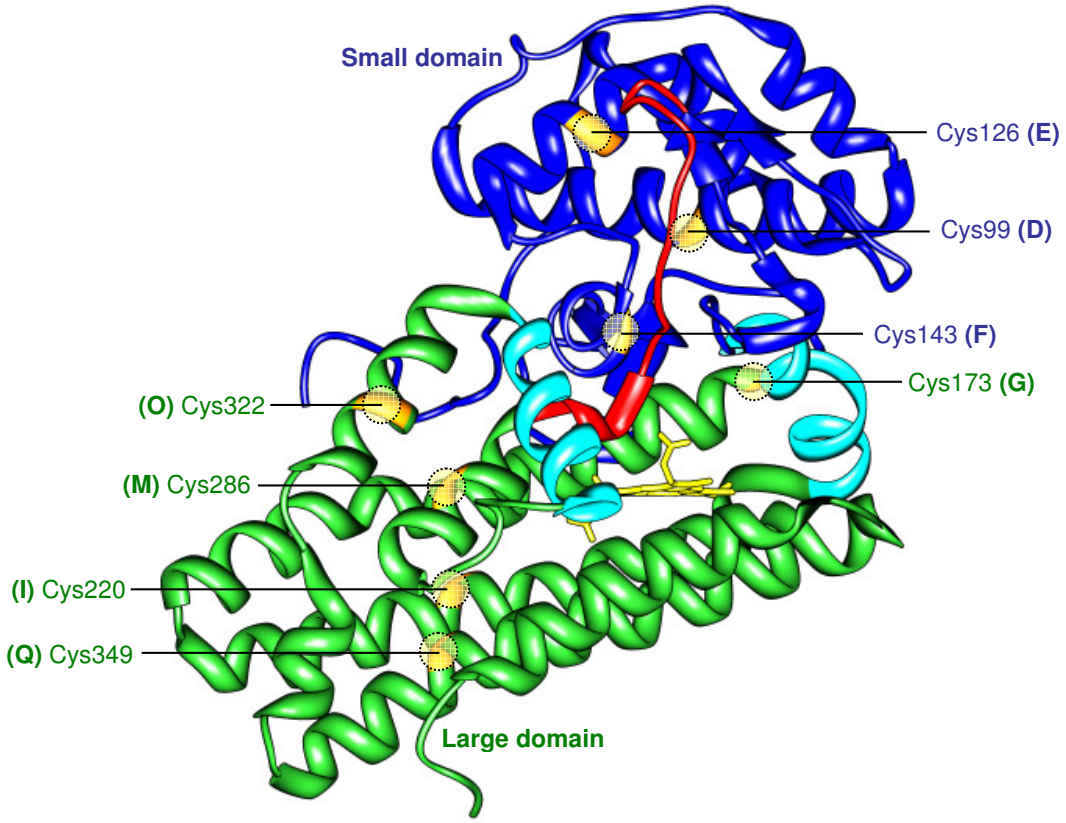

Figure 5.1 Structure of IDO showing the distribution of cysteines in the small and large domains. Cys99 at helix D, Cys126 at helix E and Cys143 at helix F are located in the small domain. Cys173 at helix G, Cys220 at helix I, Cys286 at helix M, Cys322 at helix O and Cys349 at helix Q are located in the large domain. Cys143 at helix F of the small domain and Cys173 at helix G of the large domain are close to the heme cavity.

5.2. Site-directed mutagenesis of rhIDO

Site-directed mutagenesis is a molecular biology technique in which a mutation is created at a defined site in a DNA molecule. Site-directed mutagenesis is an invaluable technique for studying protein structure-function relationships and gene expression.[153,154,162] Several approaches to this technique are known.[10,236] All the methods generally require single-stranded DNA (ssDNA) as the template.[236] Site-directed mutagenesis of recombinant human indoleamine 2,3-dioxygenase cDNA (hIDO cDNA) was focused on the plasmid templates of hIDO cDNA using the polymerase chain reaction (PCR) method. This method involves the use of oligonucleotide primers containing the desired mutation.

Site-directed mutagenesis of hIDO cDNA to express mutated 6xHis-tagged rhIDO in *E. coli* EC538 (pQE-9-IDO-mutant, pREP4) has been done by Littlejohn[152] (His16Ala, His303Ala, His346Ala, Val109Ala, Asp247Ala, Lys352Ala, a cut of Leu389), Austin[10] (Cys99Ala, Cys143Ala, Cys173Ala and Cys220Ala) and their co-workers. Site-directed mutations of rhIDO by Littlejohn and co-workers[152] were aimed at identifying amino acid residues involved in either heme or substrate binding and to investigate the functional properties of a truncated rhIDO. The study by Austin[10] and co-workers investigated selected cysteine residues for the influence on their vulnerability towards hydrogen peroxide. In this study, site-directed mutagenesis was done to make Cys126Ala, Cys286Ala, Cys322Ala and Cys349Ala mutants of rhIDO. This was to investigate whether or not selected cysteines contribute to the conformation, function and stability of

rhIDO. The site of mutagenesis of hIDO cDNA for the expression of the mutants in *E. coli* EC538 (pQE-9-IDO-mutant, pREP4) is shown in **Figure 5.2**.

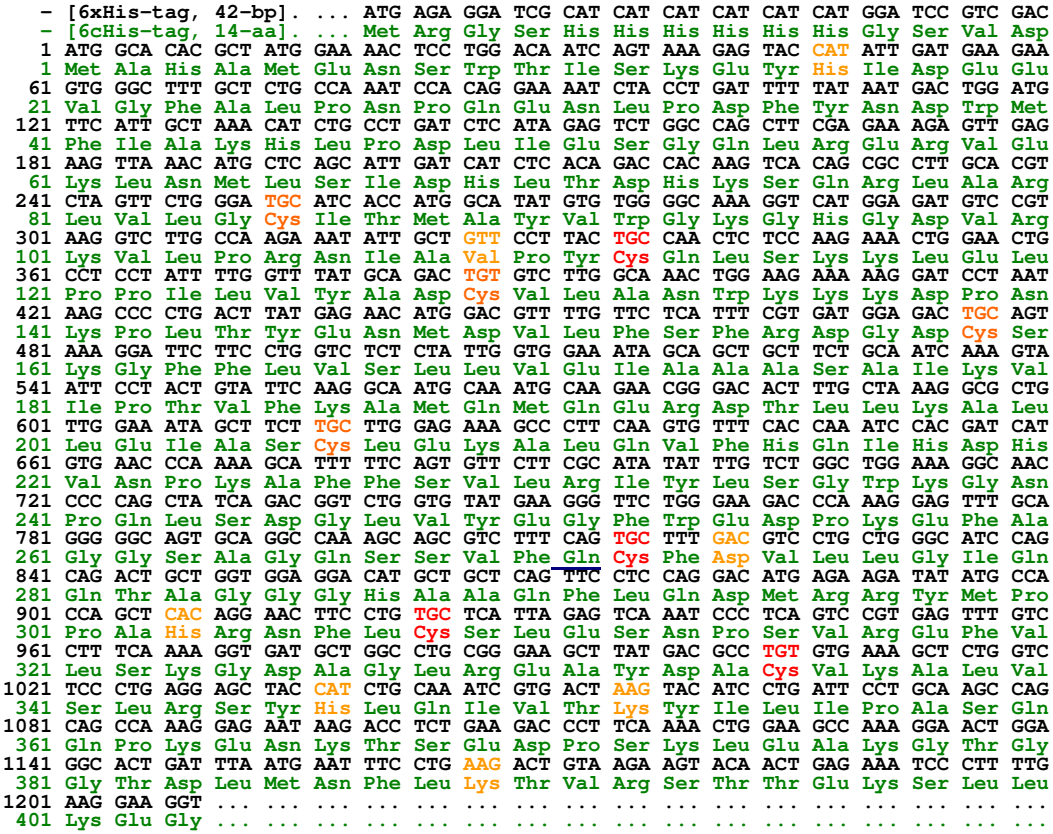

Figure 5.2 Map of the site of mutagenesis of recombinant human indoleamine 2,3-dioxygenase cDNA (hIDO cDNA) to express mutated rhIDO in *E. coli* strain EC538 (pQE-9-IDO-mutant, pREP4) done by Littlejohn, Austin and co-workers (orange). Mutagenesis proposed in this study is included (red).

In this study, the mutagenic oligonucleotide primers (Sigma Genosys) for use in the mutation of Cys126Ala, Cys286Ala, Cys322Ala and Cys349Ala in rhIDO are shown in **Table 5.1**. The oligonucleotide primers were designed to be used with the QuikChange II Site-Directed Mutagenesis Kit from Stratagene.

Table 5.1 Mutagenic oligonucleotide primers designed to facilitate the mutation of hIDO cDNA (Sigma Genosys). The mutation of Cys126Ala, Cys286Ala, Cys349Ala and Cys322Ala used the QuikChange II Site-Directed Mutagenesis Kit from Stratagene.

C126A	+KpnI Ala primer(1)-3′..ATTGCGGTACCTTACGCCCAACTCTCCAAGAAA..5′ 3′..ATTGCTGTTCCTTACTGCCAACTCTCCAAGAAA..5′ Cys 5′..TAACGACAAGGAATGACGGTTGAGAGGTTCTTT..3′ primer(2)-5′..TAACGCCATGGAATGCGGGTTGAGAGGTTCTTT..3′ Ala +KpnI
C286A	+HindIII Ala primer(1)-3′..AGCAGCGTCTTTCAAGCTTTTGACGTCCTGCTG..5′ 3′..AGCAGCGTCTTTCAGTGCTTTGACGTCCTGCTG..5′ Cys 5′..TCGTCGCAGAAAGTCACGAAACTGCAGGACGAC..3′ primer(2)-5′..TCGTCGCAGAAAGTTCGAAAACTGCAGGACGAC..3′ Ala +HindIII
C349A	-HindIII Ala primer(1)-3′..GAAGCCTATGACGCCGCTGTGAAAGCTCTGGTC..5′ 3′..GAAGCTTATGACGCCTGTGTGAAAGCTCTGGTC..5′ Cys 5′..CTTCGAATACTGCGGACACACTTTCGAGACCAG..3′ primer(2)-5′..CTTCGGATACTGCGGCGACACTTTCGAGACCAG..3′ Ala -HindIII
C322A	+XbaI Ala primer(1)-3′..CACAGGAACTTCCTGGCCTCTCTAGAGTCAAAT..5′ 3′..CACAGGAACTTCCTGTGCTCATTAGAGTCAAAT..5′ Cys 5′..GTGTCCTTGAAGGACACGAGTAATCTCAGTTTA..3′ primer(2)-5′..GTGTCCTTGAAGGACCGGAGAGATCTCAGTTTA..3′ Ala +XbaI

The mutation of Cys126Ala, Cys286Ala, Cys322Ala and Cys349Ala were initially attempted by site-specific mutation of the double-stranded (dsDNA) plasmid of hIDO cDNA using the Stratagene's QuikChange® II Site-Directed Mutagenesis Kit system. The method did not require the need for sub-cloning, specialised vectors, unique restriction sites or multiple transformations. The rapid three-step procedure system typically generates mutants with greater than 80% efficiency in a single reaction (**Figure 5.3**).[283] The QuikChange® II site-directed mutagenesis method is performed using PfuUltra® high-fidelity (HF) DNA polymerase for mutagenic primer-directed replication of both plasmid strands with the highest fidelity.

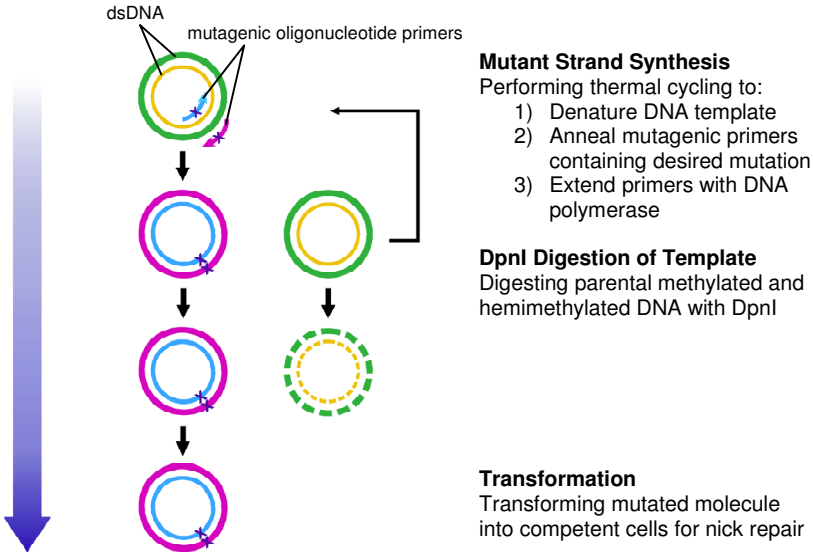

Figure 5.3 Overview of the proposed strategy using the Stratagene's QuikChange® II Site-Directed Mutagenesis for the mutations of hIDO cDNA. The three steps are mutant strand synthesis, DpnI digestion of template and transformation.

5.2.1. Site-directed mutagenesis of C126A, C286A, C349A and C322A

Site-directed mutagenesis of Cys126 to Ala126 (C126A) was done using plasmid primer (1) 3'..ATTGCGGTACCTTACGCCCAACTCTCCAAGAAA..5'and plasmid primer (2) 5'..TAACGCCATGGAATGCGGGTTGAGAGGTTCTTT..3', with lengths of 33 base-pairs (bp). They were from Sigma-Genosys and had an inserted silent mutation site for the DNA restriction enzyme digestion, KpnI, 3'..GGTACC..5' and 5'..CCATGG..3' replacing 3'..TGTTCC..5' and 5'..ACAAGG..3' (**Table 5.1**).

Mutation of Cys286 to Ala286 (C286A) was achieved using the same approach and technique as given above for the mutation of C126A. The mutation utilised plasmid primer (1) 3'..AGCAGCGTCTTTCAAGCTTTTGACGTCCTGCTG..5', primer (2) 5'..TCGTCGCAGAAAGTTCGAAAACTGCAGGACGAC..3' and an inserted silent

mutation site for a DNA restriction enzyme digestion HindIII, replacing 3'..AAGCTT..5' and 5'..TTCGAA..3' with 3'..AGTGCT..5' and 5'..TCACGA..3' (**Table 5.1**). The length of the primers was 33 bp.

As above, mutagenesis of Cys349 to Ala349 (C349A) was done using the plasmid primer (1) 3'..GAAGCCTATGACGCCGCTGTGAAAGCTCTGGTC..5' and primer (2) 5'..CTTCGGATACTGCGGCGACACTTTCGAGACCAG..3' (33 bp) with an inserted silent mutation site taking away a DNA restriction enzyme digestion for HindIII, replacing 3'..AAGCTT ..5' and 5'..TTCGAA..3' with the existing 3'..AAGCCCT..5' and 5'..TTCGGA..3' (**Table 5.1**).

Initially the site-directed mutagenesis for the mutation of Cys322 to Ala322 (C322A) was done using the same approach and procedure as for C126A, C286A and C349A. Plasmid primer (1) 3'..CACAGGAACTTCCTGGCCTCTCTAGAGTCAAAT..5' and plasmid primer (2) 5'..GTGTCCTTGAAGGACCGGAGAGATCTCAGTTTA..3' (33 bp) with an inserted silent mutation site for a DNA restriction enzyme digestion, XbaI 3'..TCTAGA..5' and 5'..AGATCT..3' in place of 3'..ATTAGA..5' and 5'..TAATCT..5' were used (**Table 5.1**). Using the approach, the mutation C322A was not successful.

The mutations of C126A, C286A, and C349A were successful as indicated by their agarose gel electrophoresis of the restriction enzyme digested DNA (KpnI for C126A and HindIII for both C286A and C349A) compared to the undigested DNA, the non-mutated (non-mutant) DNA and the digested non-mutated DNA. DNA sequence analysis of the

mutated pQE-9-IDO-C126A, pQE-9-IDO-C286A and pQE-9-IDO-C349A afforded the electropherograms of the DNA with the desired mutations conferring to the change of Cys126 to Ala126, Cys286 to Ala286 and Cys349 to Ala349 respectively (**Figure 5.4**).

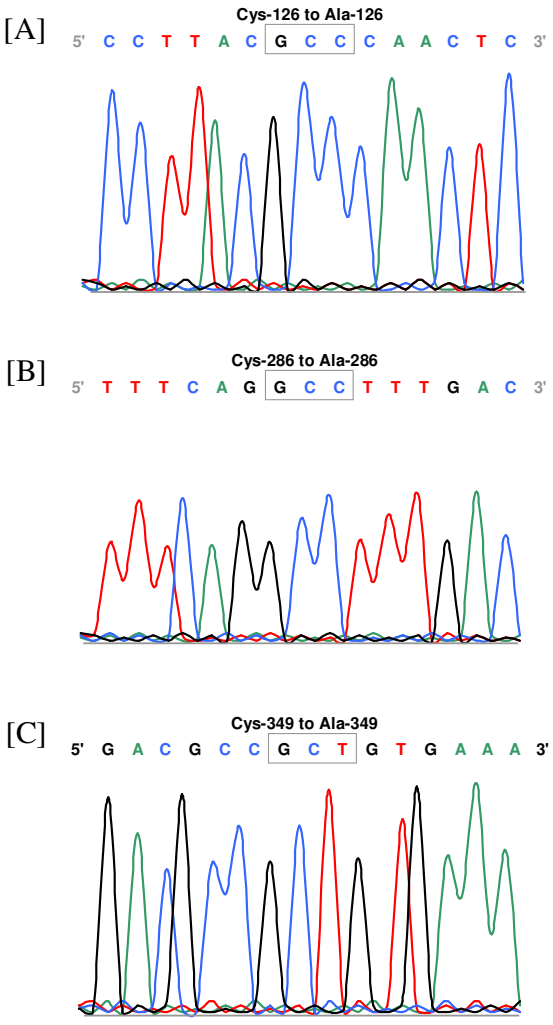

Figure 5.4 Electropherograms of the DNA sequence analysis of mutated pQE-9-IDO-C126A [A], pQE-9-IDO-C286A [B] and pQE-9-IDO-C349A [C] showing the desired mutations conferring to the change of Cys126 to Ala126, Cys286 to Ala286 and Cys349 to Ala349 respectively.

The mutation of C322A was shown to be not successful, as indicated by its agarose gel electrophoresis of the restriction enzyme XbaI digested DNA compared to the undigested DNA, non-mutated DNA and digested non-mutated DNA. The digestion of the mutation result by XbaI did not show incision of the DNA and DNA sequence analysis did not show an electropherogram of the desired mutation.

5.2.2. Troubleshooting the C322A site-directed mutagenesis

As the standard thermal cycling parameters suggested by the manufacturer (Stratagene, **Table 5.2**) did not bring about the desired C322A mutation, modifications were made. The thermal cycling parameters were changed to those given in **Table 5.2** (Change-1) by increasing the cycle in the second segment from 18 to 25 bases in length and lowering the annealing temperature from 79 °C to 55°C. This was to increase the efficiency of the PCR process. The C322A mutation did not occur as indicated from the agarose gel electrophoresis. As a result of this outcome, the cycle in the second segment was increased from 18 to 24 bases in length. The annealing temperature of the cycles were reduced from 79 °C to 76°C and the duration changed from 60 seconds (1 min) to 45 seconds (**Table 5.2**, Change-2). This approach also did not give the desired mutations, suggesting that difficulties in the mutation were probably not due to the inefficiency of the thermal cycle. As mutation did not occur by using standard thermal cycling parameters given by the manufacturer (Stratagene) and through modifications, mutation experiments were done by processing the plasmids separately using the parameters to optimise the PCR process, as given in **Table 5.2** (Change-3)**.**

Table 5.2 Standard thermal cycling parameters for the QuikChange II site-directed mutagenesis method (Stratagene) for rhIDO (pQE-9-IDO=4.7 kb) and changes (Change-1, Change-2, Change-3).

Segment	Cycle	Temperature	Duration
1	1	95 °C	30 sec
2	18	95 °C	30 sec
		79 °C	1 min
		68 °C	5 min
Change-1, segment-2 to 40 cycle, annealing temperature to 55 °C			
1	1	95 °C	30 sec
2	40	95 °C	30 sec
		55 °C	1 min
		68 °C	5 min
Change-2, segment-2 to 25 cycle, annealing temperature to 76 °C (45 sec)			
1	1	95 °C	30 sec
2	25	95 °C	30 sec
		76 °C	45 sec
		68 °C	5 min
Change-3, segment-2 to 40, annealing temperature to 65 °C (1 min)			
Individual			
1	1	95 °C	30 sec
2	40	95 °C	30 sec
		65 °C	1 min
		68 °C	5 min
Mixed			
3	1	95 °C	10 min

At the first change, in the second segment the thermal cycles was increased from 18 to 40 cycles and the annealing temperature lowered from 79 °C to 55 °C. At the third change, a third segment (95 °C for 10 minutes) was introduced for the mixed plasmids and this method was also unsuccessful to bring about the mutation of C322A.

It is commonly believed that the guanine-cytosine (GC) content, as the nitrogenous bases of the plasmid, plays a part in the adaptation to higher melting temperatures during PCR.[283] Therefore, in this study the length of the plasmid was increased from 33 to 39 bases to increase the GC content from 48% to 54%. In this experiment, primer (1)

3’..GCTCACAGGAACTTCCTGTGCTCATTAGAGTCAAATCCC..5’ and primer (2) 5’..CGAGTGTCCTTGAAGGACACGAGTAATCTCAGTTTAGGG..3’ were used with an inserted silent mutation site for an XbaI DNA restriction enzyme digestion (**Table 5.3**) for the mutation of C322A.

Table 5.3 Mutagenic oligonucleotide primers designed to facilitate the mutation of C322A at hIDO cDNA (Sigma Genosys). The mutation of Cys322Ala was done using the QuikChange II Site-Directed Mutagenesis Kit from Stratagene.

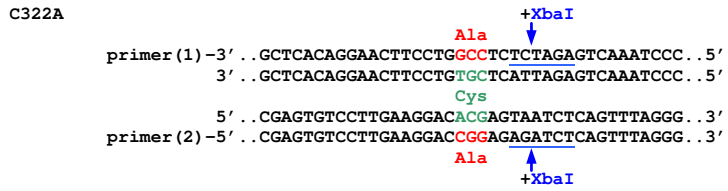

The mutation was tried again with the new primers using the thermal cycling parameters given in **Table 5.2**. The mutation of Cys322 to Ala322 (C322A) was still unsuccessful. Subsequently, the mutation of C322A using the 5’-phosphate ends of the oligonucleotide primers to facilitate the mutation was examined. In this approach, plasmid (21 bases in length) primer (1) 3’..GCCTCATTAGAGTCAAATCCC..5’ and plasmid (21 bases in length) primer (2) 5’..GGTCGAGTGTCCTTGAAGGAC..3’ were used for the mutation of C322A (**Table 5.4**).

Table 5.4 Mutagenic oligonucleotide primers designed to facilitate the mutation of C322A at hIDO cDNA (Sigma Genosys). The mutation of Cys322Ala was done using the TripleMaster PCR System from Eppendorf.

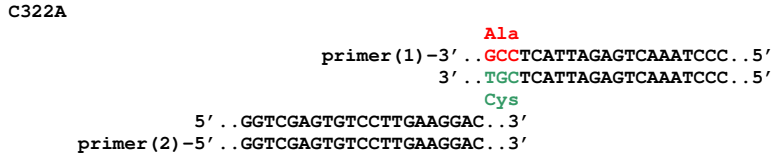

The mutation was done using the TripleMaster PCR System (Eppendorf), where the 5'-phosphate ends of the non-mutagenic and mutagenic oligonucleotide primers were used with ligation at the final step (**Figure 5.5**) and the cycling parameters as given in **Table 5.5**.

Table 5.5 Cycling parameters for the TripleMaster PCR System mutagenesis method (Eppendorf) for rhIDO (pQE-9-IDO=4.7 kb).

Cycle	Temperature	Duration	Step	Discription
1	94 ℃	2 min	1	Initial template denaturation
35	94 ℃	20 sec	2	Template denaturation
	65 ℃	20 sec	3	Primer annealing
	72 ℃	3 min	4	Primer extension/elongation
	4 ℃	(++) min	5	Stop

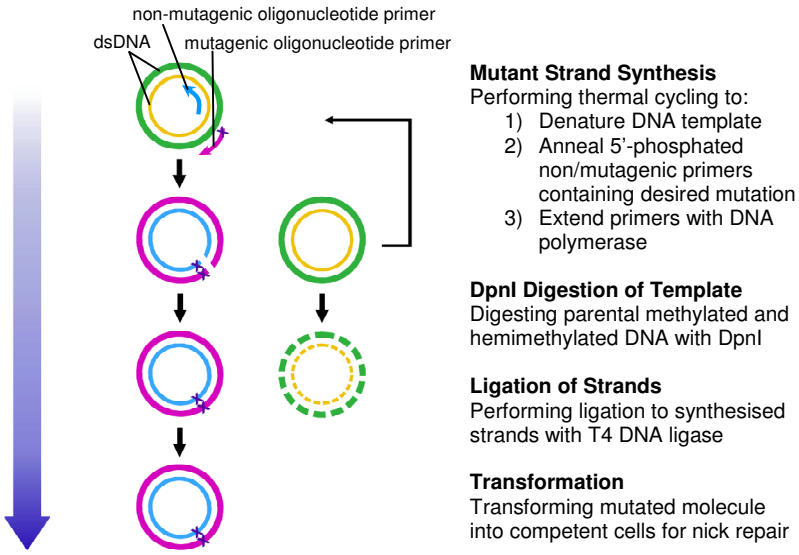

Figure 5.5 Overview of the mutation of hIDO cDNA to change Cys to Ala Cys322Ala in the rhIDO using the TripleMaster PCR System from Eppendorf and ligation with T4 DNA ligase. The four steps are mutant strand synthesis, DpnI digestion of template, ligation of strands and transformation.

The mutation was successful as indicated by its DNA sequence analysis of the mutant C322A of the pQE-9-IDO. **Figure 5.6** shows the electropherogram of the DNA with the desired mutations.

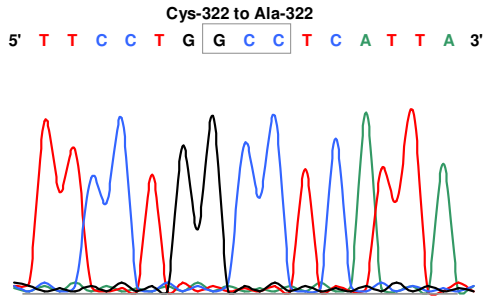

Figure 5.6 Electropherograms of the DNA sequence analysis of mutated pQE-9-IDO-C322A [D] showing the desired mutations conferring to the change of Cys322 to Ala322.

The mutated hIDO cDNA plasmids C126A, C286A, C322A and C349A were then transformed to competent cells of *E. coli* 538 (pREP4) with a view to expressing the mutated rhIDO. The mutated rhIDOs were then expressed and purified using the protocols given in **Chapter 2**. The mutated rhIDOs were then compared to the non-mutated rhIDO using the protocols given in **Chapter 3**.

5.3. CD of the non-mutated and mutated rhIDOs

Circular dichroism (CD) studies of the non-mutated and mutated rhIDO (C126A, C286A, C322A and C349A) were done to observe the effect of the cysteines on the overall secondary structure of rhIDO. The secondary structure can be determined by CD spectroscopy in the far-UV spectral region (190 - 250 nm). At these wavelengths the

chromophore is the peptide bond. The signal arises when it is located in a regular folded environment. CD signals for α-helix, β-sheet and random-coil structures each give rise to a characteristic shape and magnitude. The approximate fraction of each secondary structure type that is present in any protein can thus be determined by analysing its far-UV CD spectrum.[30,275,278,321,322] The far UV circular dichroism (CD) spectra of the non-mutated and mutated rhIDO are shown in **Figure 5.7**.

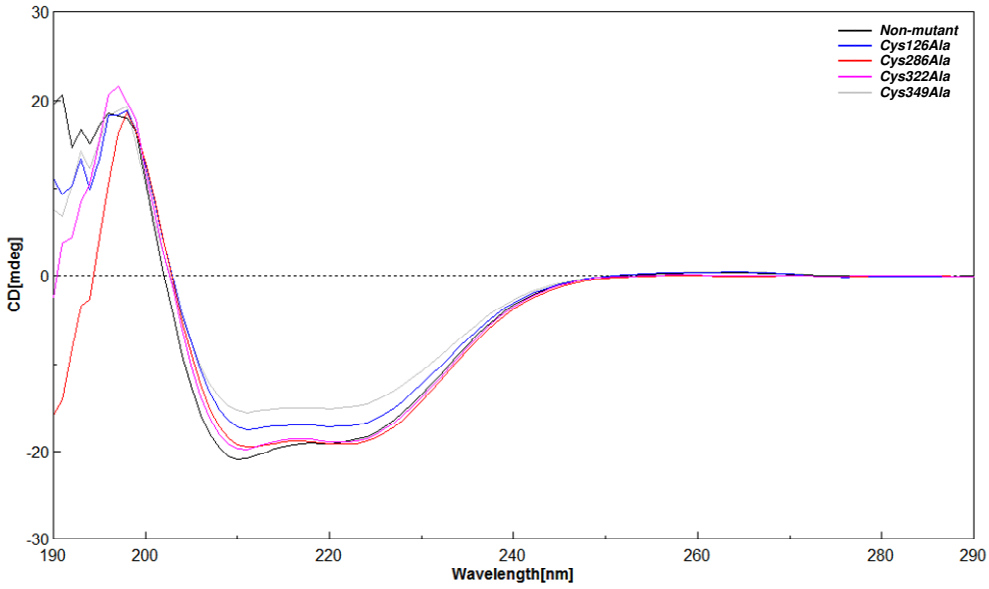

Figure 5.7 Circular dichroism (CD) spectra of non-mutated and mutated C126A, C286A, C322A and C349A rhIDO. The CD spectra (190 - 290 nm) were taken with 25 mM Tris-HCl pH 7.4 in 2 mm pathlength cuvettes at 20 ℃. The protein concentrations were approximately 1 mg/mL.

Analysis of the CD spectra of the non-mutated and mutated rhIDO using comparisons to proteins of known proportion of α-helix and β-strand content showed structural characteristics of the mutated rhIDO. The K2D and K2D2 programs (EMBL, Heidelberg, Germany) and CDPro Software consisting of three programs SELCON3, CDSSTR and

CONTINLL for CD analysis (Colorado State University) were used for the determinations. The determined conformational characteristics of the non-mutated and mutated rhIDO are given in **Table 5.6**.

Table 5.6 Secondary structure analysis of circular dichroism (CD) spectra of non-mutated and mutated C126A, C286A, C322A and C349A rhIDO. The CD spectral data (200 - 240 nm) were analysed using the K2D and K2D2 programs and confirmed by the CDPro program.

	α-Helix (%)	β-Strand (%)	random-Coil (%)
non-mutant	68	4	28
C126A	61	7	32
C286A	59	15	26
C322A	62	11	27
C349A	57	10	33

Non-mutated rhIDO had 68% α-helix, 4% β-strand and 28% random-coil. The mutated rhIDO showed similar structural characteristics of 57 - 62% α-helix, 7 - 15% β-strand and 27 - 33% random-coil. The results indicated that the site-directed mutagenesis of the Cys to Ala at positions Cys126, Cys286, Cys322 and Cys349 did not affect the secondary structure of the rhIDO.[322] Both the non mutated and the mutated rhIDO had the order of conformational characteristics of α-helix (57 - 68%) > random-coil (26 - 33%) > β-strand (4 - 11%). However, it was evident that the site-directed mutagenesis brought about changes in the overall conformation of the rhIDO. The smallest difference in the CD spectra was observed between the mutant C286A and C322A of the rhIDO, which may be attributed to the spatial proximity of Cys286 to Cys322 in the 3D structure of IDO. Other observed changes included the β-strand conformational contribution of C286A, C322A and C349A mutated rhIDO compared to that of C126A mutant. This contribution

may possibly be due to the location of Cys126, which is at the small domain whereas the other cysteines (Cys286, Cys322 and Cys349) are at the large domain of the rhIDO (**Figure 5.1**). These CD studies of the non-mutated and mutated rhIDO suggest that there are significant effects of the cysteines, in particularly their localisation in regard to the overall secondary structure of rhIDO.

5.4. Soret region CD of the non-mutated and mutated rhIDOs

In heme containing proteins, the dipole-dipole coupling involving heme transitions and allowed $\pi \rightarrow \pi^*$ transitions of nearby aromatic side chains, gives rise to circular dichroism (CD) at the wavelength ($\lambda_{350 - 450\ nm}$) of the Soret band region (Soret region). Residues as far as 12 Å away, depending on the relative orientation, can affect the CD of heme groups at the Soret region. Simple alterations of the polarisation direction or orientation of a distal aromatic chromophore can result in significant alterations of both the complexity and magnitude of the CD spectra without implying any major conformational change in the protein structure or the heme group.[276,322] The heme *b* co-factor (heme) of the rhIDO is a non-chiral molecule therefore it does not exhibit a CD signal in solution. However, when heme is incorporated into the highly asymmetric environment of rhIDO, a pronounced dichroism signal in the Soret region of the CD is observed. Heme CD has been attributed to coupled oscillator interactions between heme transitions and allowed π-π^* transitions on nearby aromatic residues.[114] In addition, inherent heme chirality arising from non-planar distortions can contribute to the Soret region of the CD.[114,276,322] CD spectroscopy of the Soret region of heme containing proteins has been recognised for its utility and simplicity in operations for conformational studies, even though interpreting the data has not been simple and there have been major controversies

concerning the technique.[276,322] In this study, the CD Soret region spectra of non-mutated and mutated rhIDO were done. From the spectra, it was observed that changes from Cys to Ala in rhIDO gave rise to changes in the Soret region CD, suggesting environmental changes in the heme pocket[275] (**Figure 5.8**).

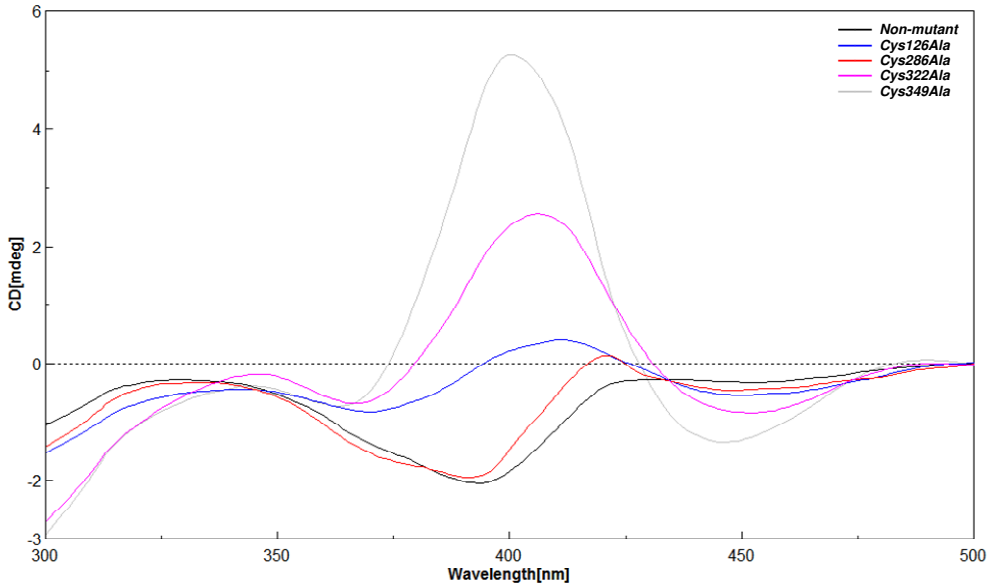

Figure 5.8 Circular dichroism (CD) Soret region spectra of non-mutated and the mutated C126A, C286A, C322A and C349A rhIDO. The CD spectra (300-500 nm) were taken with 25 mM Tris-HCl pH 7.4 in 2 mm pathlength cuvettes at 20 ℃. The protein concentrations were approximately 5 mg/mL.

It was also observed that the Soret region CD spectrum for the rhIDO C126A mutant was almost identical to that of the non-mutated rhIDO. This suggested that Cys286 was not directly associated with the heme *b* co-factor binding. By contrast, the mutagenesis of C126A, C322A and C349A showed a shift from the non-mutated rhIDO, suggesting associations of these cysteines with the heme *b* co-factor binding.

The degree of the complexity and magnitude of the CD spectral change was in the order of C349A > C322A > C126A. This is possibly attributed to the fact that Cys349 is in close proximity to the proximal His346 (**Figure 5.1**). His346 is directly bound to the heme *b* co-factor iron (**Chapter 3**, **Figure 3.16**).[284] Both His346 and Cys349 are located in the same helix Q (**Figure 5.1**). From the study it was conceivable that the Cys to Ala site-directed mutagenesis of C349A, C322A and C126A of rhIDO induces changes in the protein secondary structure. These changes are associated with the binding of the heme *b* co-factor. This was not the case for C286A. Studies to understand the significance of the cysteines towards the nature of the heme *b* binding in rhIDO were not done as they were not the immediate focus of these investigations.

5.5. Thermal stabilities of the non-mutated and mutated rhIDOs

Thermal stabilities and conformational transitions of mutated rhIDO were assessed using CD. This was achieved by investigating changes in the spectra with increasing temperature (20 - 99 °C) and comparing them to that of the non-mutated rhIDO (**Figure 5.9**). A single wavelength of 222 nm that monitors the specific feature of the protein α-helix structure as the major conformation of IDO was chosen. To determine the thermal melt, a first order peak derivate of the CD thermal melt spectra of non-mutated and mutated rhIDO were plotted (**Figure 5.10**). The thermal melt values from the first order peak derivate of the CD thermal melt spectra are shown in **Table 5.7**.

Results of the thermal melt experiments did not show any significant change in the thermal melt of the mutated rhIDO in comparison to the non-mutated rhIDO.

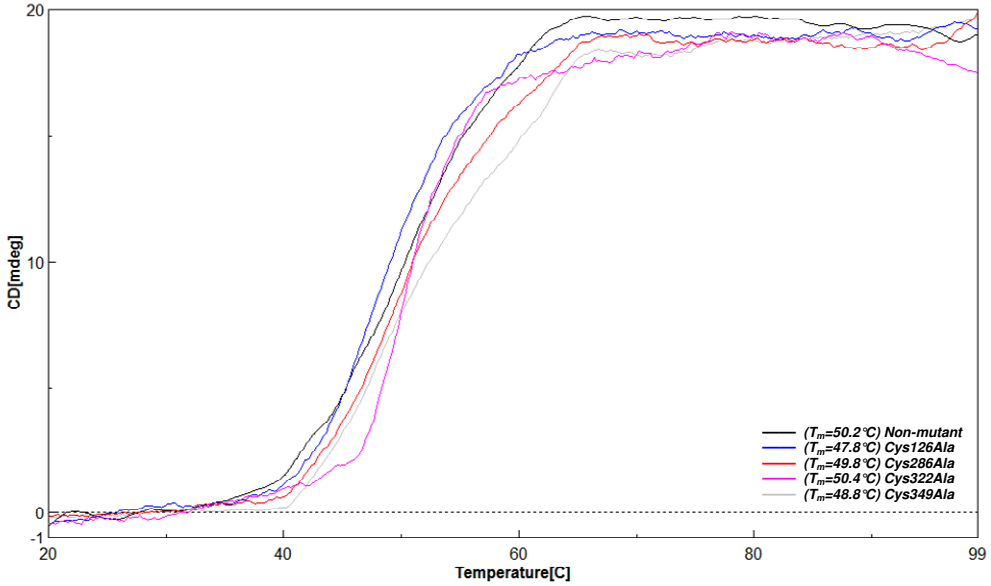

Figure 5.9 Circular dichroism (CD) thermal melt spectra of non-mutated and mutated C126A, C286A, C322A, and C349A rhIDO. The CD spectra (222 nm) were taken with 25 mM Tris-HCl pH 7.4 in 2 mm pathlength cuvettes at 20 - 99 ℃. The protein concentrations were approximately 1 mg/mL.

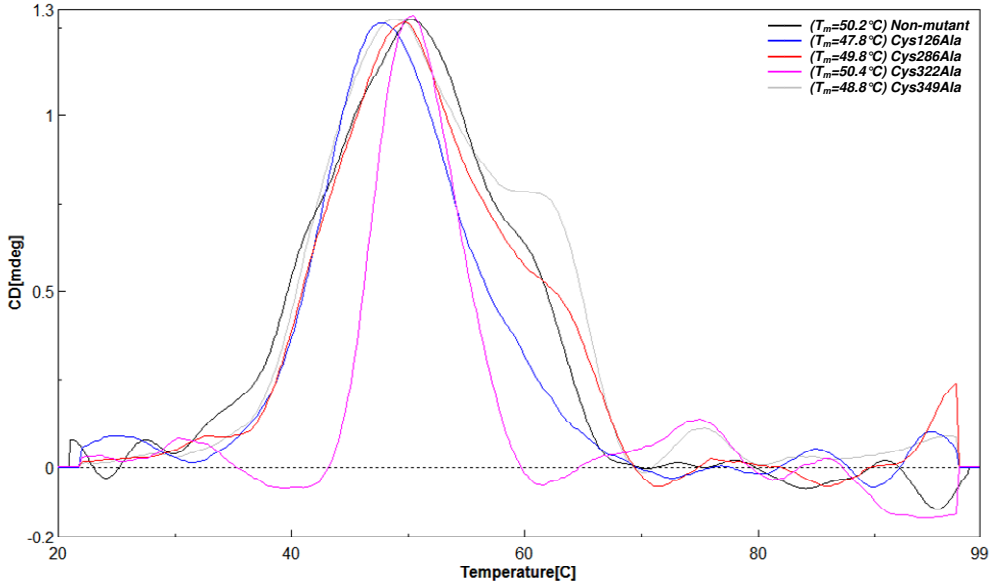

Figure 5.10 First order peak derivate of circular dichroism (CD) thermal melt spectra of non-mutated and mutated C126A, C286A, C322A, and C349A rhIDO. The CD spectra (222 nm) were taken with 25 mM Tris-HCl pH 7.4 in 2 mm pathlength cuvettes at 20 - 99 ℃. The protein concentrations were approximately 1 mg/mL.

Table 5.7 Thermal melt values from first order peak derivate of circular dichroism (CD) thermal melt spectra of non-mutated and mutated C126A, C286A, C322A, and C349A rhIDO.

rhIDO	T_m (°C)
non-mutant	50.2
mutant C126A	47.8
mutant C286A	49.8
mutant C322A	50.4
mutant C349A	48.8

The melt temperatures were in the range of 47.8 - 50.4 °C. The rhIDO C322A resides in the upper range of 50.4 °C and the mutant C126 resides in the lower end of 47.8 °C.

5.6. UV-Vis spectroscopy of non-mutated and mutated rhIDOs

UV-Vis spectroscopy was done on the non-mutated and mutated rhIDO. The mutants gave the same spectroscopic profile as the non mutants with maxima at 280 nm and 406 nm (**Figure 5.11**).

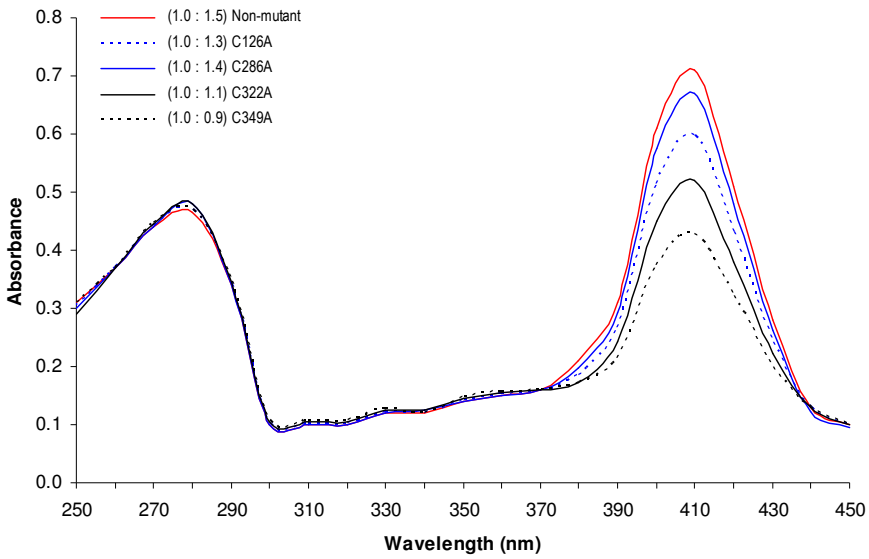

Figure 5.11 UV-Vis spectra of non-mutated and mutated C126A, C286A, C322A, and C349A rhIDO. The spectra (250 - 450 nm) were taken with 25 mM Tris-HCl pH 7.4 in 2 mm pathlength cuvettes at room temperature. The protein concentrations were approximately 1 mg/mL.

This suggested that the site-directed mutagenesis towards the cysteines did not affect the UV-Vis characteristics of rhIDO. The Soret/protein ratios were also deduced (**Table 5.8**). It should be noted that batch to batch variations of the Soret/protein ratio was observed for rhIDO and the magnitude of the Soret band maximum at 406 nm depends on the oxidation, ligation, and conformation states of the chromophores of the rhIDO.[322] (**Chapter 4**).

Table 5.8 The Soret/protein ratio (406:280 nm) calculated from spectra (250 - 450 nm) taken with 25 mM Tris-HCl pH 7.4 in 2 mm pathlength cuvettes at room temperature. The protein concentrations were approximately 1 mg/mL.

rhIDO	Soret/protein ratio (406:280 nm)
non-mutant	1.5 : 1.0
C126A	1.3 : 1.0
C286A	1.4 : 1.0
C322A	1.1 : 1.0
C349A	0.9 : 1.0

5.7. Kinetics of non-mutated and mutated rhIDOs

The enzyme kinetics of non-mutated and mutated rhIDO were analysed and compared using L-Trp and D-Trp as substrates. As the enzyme pool might contain inactive enzyme, the kinetics were determined as a function of the active enzyme. To determine the concentration of the active enzymes, the extinction coefficient at 280 nm, $\varepsilon = 51380\ M^{-1}\ cm^{-1}$ in 6.0 M guanidium hydrochloride (pH 6.5) was used. The kinetics of the non-mutated as well as the mutated rhIDO as plots of the substrate concentrations (S) against velocity (v) were constructed. Six substrate concentrations for L-Trp and D-Trp were used to construct the Michaelis-Menten, Lineweaver-Burk and Eadie-Hofstee plots.

The Michaelis-Menten kinetics is relevant to situations where simple kinetics can be assumed (**Chapter 3**, **Section 3.6.1**). The standard analyses of enzyme kinetics were used in this study, where it is assumed that the production of product is linear with time. It is assumed that the concentration of substrate vastly exceeds the concentration of enzyme and no cooperativity and neither substrate nor product acts as an allosteric modulator to alter the enzyme velocity (**Chapter 3**, **Section 3.6.1**).

In order to determine the maximum rate of rhIDO mediated reaction, the initial rate (v) of product formation (20 minutes) for various substrate concentrations was measured. The measurements were then plotted in a Lineweaver-Burk plot (**Chapter 3**, **Section 3.6.1**). As the double reciprocal plot can distort the error structure of the data, the Eadie-Hofstee plots were also constructed. The Eadie-Hofstee plot is a graphical representation of enzyme kinetics, in which reaction velocity is plotted as a function of the velocity versus substrate concentration ratio to linearise the Michaelis-Menten equation. It is more robust against error-prone data than the Lineweaver-Burk plot, particularly because it gives equal weight to data points in any range of substrate concentration or reaction velocity. Both plots remain useful as a means of presenting the data graphically to accompany the Michaelis-Menten plot.

The Michaelis-Menten, Lineweaver-Burk and Eadie-Hofstee plots for L-Trp as substrate are shown in **Figure 5.12**, **Figure 5.13** and **Figure 5.14** respectively. Similar plots for D-Trp as substrate are shown in **Figure 5.15**, **Figure 5.16** and **Figure 5.17** respectively.

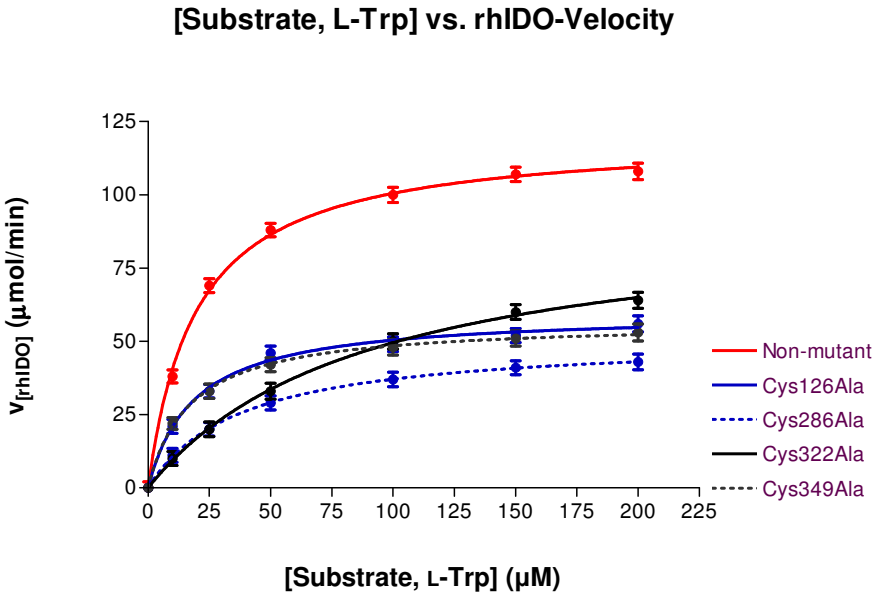

Figure 5.12 Michaelis-Menten plot of the kinetic study of non-mutated rhIDO and mutated C126A, C286A, C322A, and C349A rhIDO with L-Trp as substrate, showing the substrate concentration versus the turnover rate in µmoles of kynurenine produced per mg of protein.

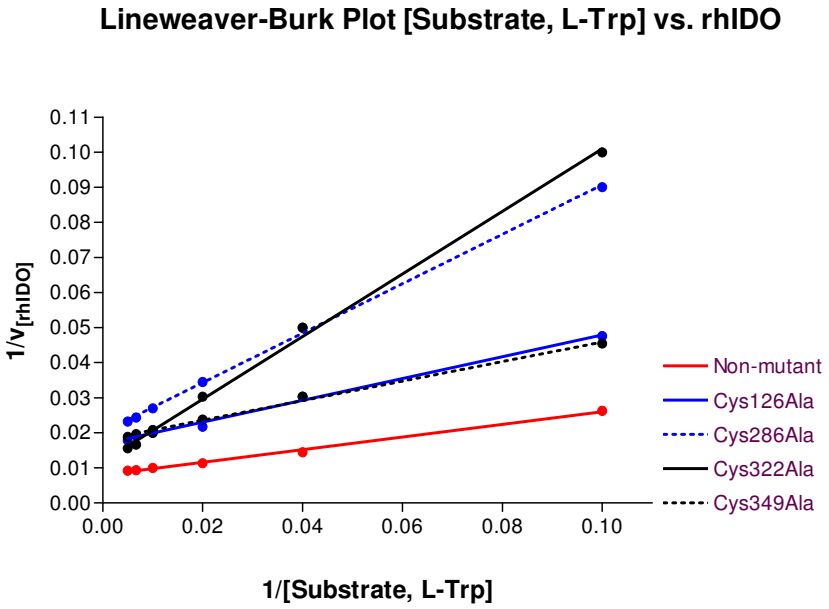

Figure 5.13 Lineweaver-Burk plot of the kinetic study of non-mutated and mutated C126A, C286A, C322A, and C349A rhIDO with L-Trp substrate, showing the substrate concentration versus the turnover rate in µmoles of kynurenine produced per mg of protein.

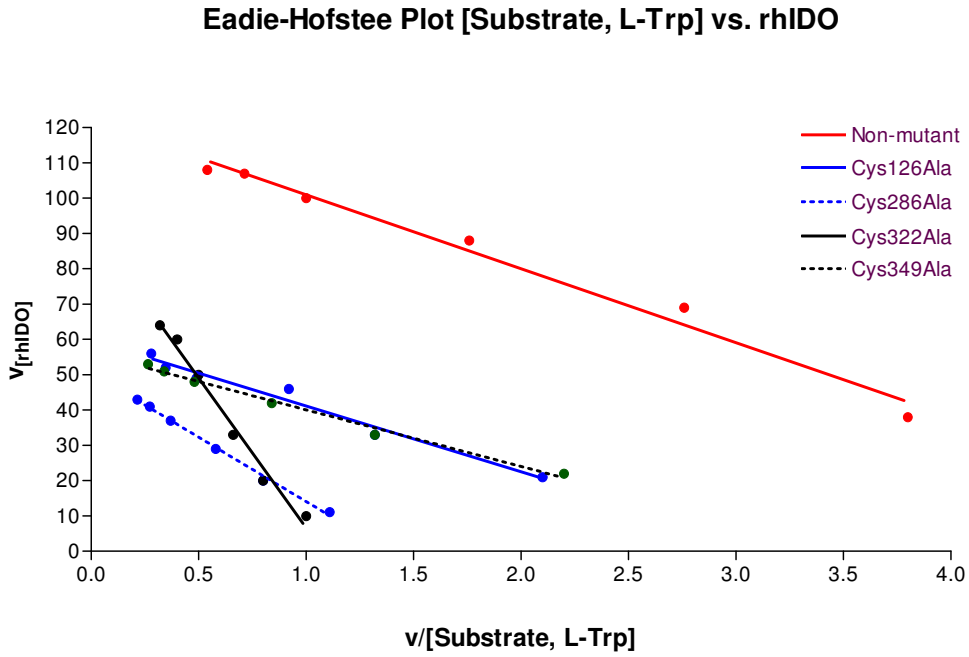

Figure 5.14 Eadie-Hofstee plot of the kinetic study of non-mutated and the mutated 126A, C286A, C322A, and C349A rhIDO with L-Trp substrate, showing the substrate concentration versus the turnover rate in µmoles of kynurenine produced per mg of protein.

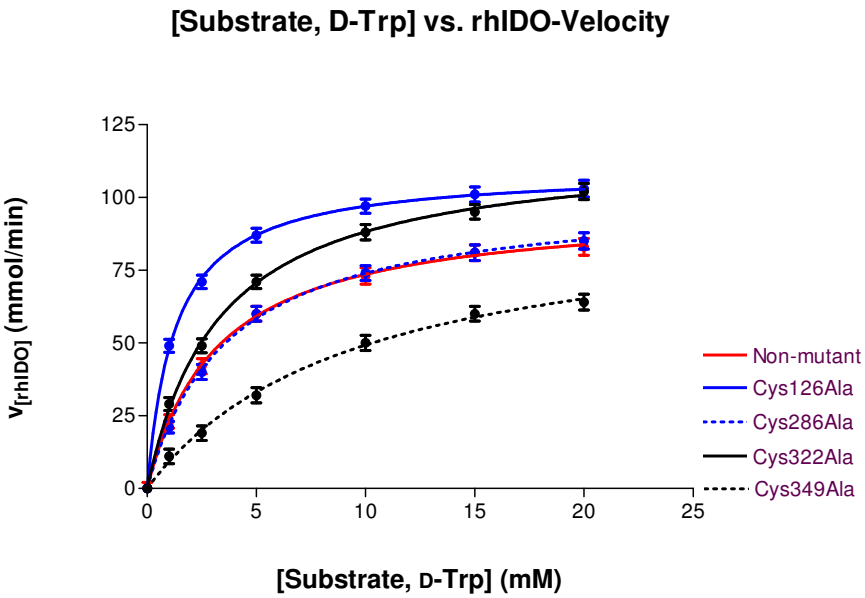

Figure 5.15 Michaelis-Menten plot of the kinetic study of non-mutated and mutated C126A, C286A, C322A, and C349A rhIDO with D-Trp as substrate, showing the substrate concentration versus the turnover rate in µmoles of kynurenine produced per mg of protein.

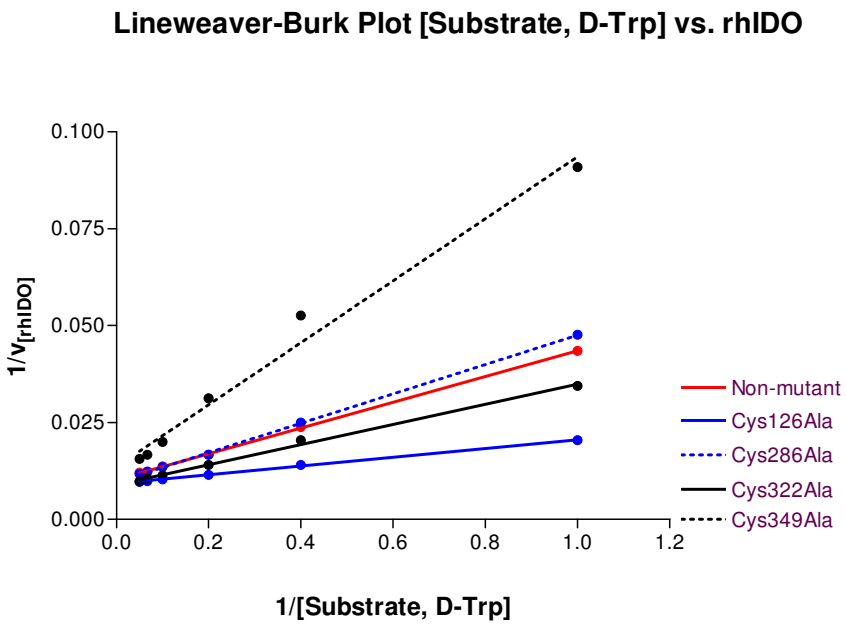

Figure 5.16 Lineweaver-Burk plots of the kinetic study of non-mutated and the mutated C126A, C286A, C322A, and C349A rhIDO with D-Trp as substrate, showing the substrate concentration versus the turnover rate in µmoles of kynurenine produced per mg of protein.

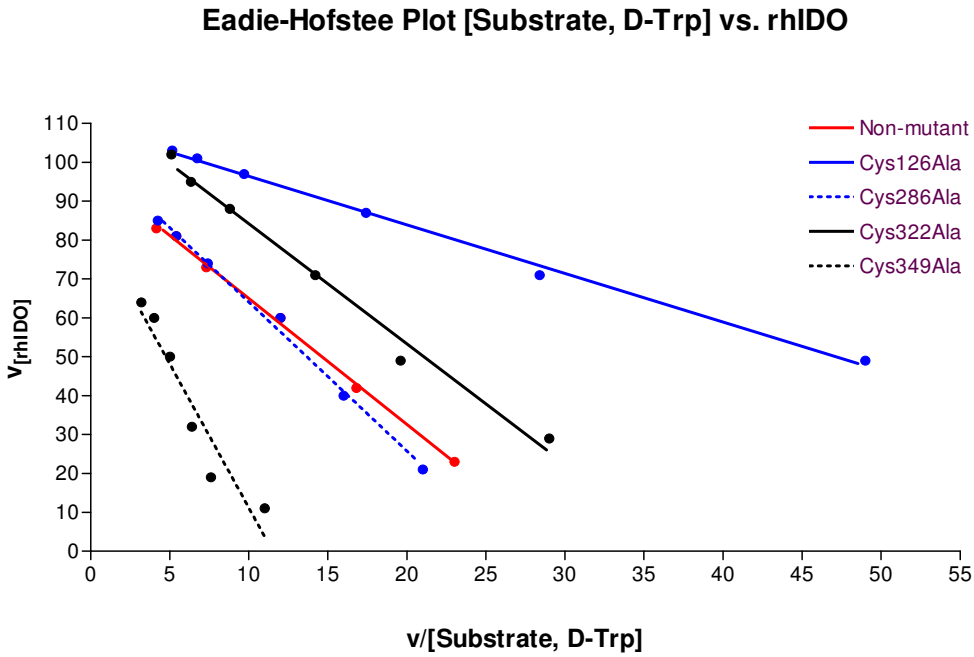

Figure 5.17 Eadie-Hofstee plot of the kinetic study of non-mutated and mutated C126A, C286A, C322A, and C349A rhIDO with L-Trp as substrate, showing the substrate concentration versus the turnover rate in µmoles of kynurenine produced per mg of protein.

The resulting values for K_m and V_{max} of the mutated rhIDO were compared to those of the non-mutated rhIDO. Comparison of the values of the V_{max} / K_m gives an idea of the effect of the site-directed mutagenesis towards the catalytic efficiency of the enzyme for a specific substrate. The kinetic parameters of the non-mutated and C126A, C286A, C322A and C349A mutated rhIDO from the plots were analysed and are given in **Table 5.9**.

Table 5.9 Kinetic parameters of the kinetic study of non-mutated and mutated C126A, C286A, C322A, and C349A rhIDO with L-Trp and with D-Trp as substrate for the substrate concentration versus the turnover rate in µmoles of kynurenine produced per mg of protein.

	L-Tryptophan			D-Tryptophan		
rhIDO	V_{max} (min^{-1})	K_m (µM)	V_{max}/K_m (μM^{-1} min^{-1})	V_{max} (min^{-1})	K_m (mM)	V_{max}/K_m (mM^{-1} min^{-1})
non-mutant	120.2±1.7	19.6±1.1	6.1±0.4	97.2±0.9	3.2±0.1	30.3±1.0
C126A	59.8±1.5	18.7±2.0	3.2±0.3	109.4±0.6	1.3±0.0	85.3±2.4
C286A	51.2±0.4	38.1±0.9	1.3±0.0	101.0±1.3	3.7±0.2	27.6±1.2
C322A	94.3±2.4	90.3±5.3	1.0±0.1	117.5±1.7	3.3±0.2	35.4±1.8
C349A	56.8±0.6	17.1±0.8	3.3±0.2	96.1±4.2	9.5±0.9	10.1±1.1

From the study, it was observed that the specificity of mutant C126A towards L-Trp was approximately half that of the non-mutant rhIDO (48% loss). The specificity towards D-Trp was nearly 2.8 fold to that of the non-mutant rhIDO (182% gain). Mutant C286A specificity towards L-Trp was 0.2 times that of the non-mutant (78% loss), whereas the specificity towards D-Trp was 0.9 fold to that of the non-mutant (9% loss). The specificity of mutant C322A towards L-Trp was 0.2 times that of the non-mutant (83% loss), whereas the specificity towards D-Trp was 1.2 times that of the non-mutant (17% gain). Mutant C349A specificity towards L-Trp was 0.5 times that of the non-mutant (46% loss) and the specificity towards D-Trp was 0.3 times that of the

non-mutant (67% loss). All the mutants, C126A, C286A, C322A and C349A showed a decrease in specificity towards L-Trp with C322A showing the highest decrease (78% loss). However, mutants C126A and C322A showed increased specificity towards D-Trp, with C126A showing the highest increase (2.8 fold, 280%). Mutants C286A and C349A showed decreases with C349A having the highest decrease (67% loss).

This study confirmed that the Cys to Ala site-directed mutagenesis contributed to the changes in the kinetics of the mutated rhIDO, as compared to the non-mutated rhIDO. From the results, it can be concluded that the cysteine residue of rhIDO, is to a certain extent involved in the normal catalytic function of the enzyme. It is also highly likely that the change from Cys to Ala in the mutants changed the conformation of the enzyme. This change of conformation may have been responsible for the accessibility of the specific substrates to the active site, resulting in the diverse kinetics observed.

5.8. Conclusion

Cysteines are well distributed in the helices of IDO, with Cys99 at helix D, Cys126 at helix E, Cys143 at helix F, Cys173 at helix G, Cys220 at helix I, Cys286 at helix M, Cys322 at helix O and Cys349 at helix Q. Site-directed mutagenesis of Cys126, Cys286, Cys322 and Cys347 to their corresponding alanines were done to investigate the influence of the selected cysteine residues on the overall characteristics and stability of rhIDO. The mutation of Cys126Ala, Cys286Ala and Cys349Ala utilised the QuikChange II Site-Directed Mutagenesis Kit (Stratagene) using the direct mutation of the double-stranded plasmid of pQE-9-IDO. The system could not be used for the mutation of Cys322Ala. Modifications in the oligonucleotide primers, procedures and conditions

for the mutations, including steps in the PCR were unsuccessful. Mutation of Cys322Ala was accomplished by using the TripleMaster PCR System (Eppendorf). The significant difference between the mutation of Cys126Ala, Cys286Ala and Cys349Ala and that of Cys322Ala is that whereas the mutation of Cys322Ala did not use the direct mutation of the double-stranded plasmid of pQE-9-IDO, the mutation of Cys322Ala used the 5'-phosphate ends of the oligonucleotide primers that were ligated at the final step. The mutagenic oligonucleotide used is given in **Table 5.10**.

Table 5.10 Mutagenic oligonucleotide primers for the site-directed mutagenesis at hIDO cDNA. The mutation of Cys126Ala, Cys286Ala and Cys349Ala were done using the QuikChange II Site-Directed Mutagenesis Kit from Stratagene with the approach as suggested, and the mutation of Cys322Ala was accomplished by using the TripleMaster PCR System from Eppendorf with the approach as suggested.

```
Cys126Ala                                                +KpnI
                                                          Ala
                                    primer(1)-3'..ATTGCGGTACCTTACGCCCAACTCTCCAAGAAA..5'
 321  3'..CAAAGGTCATGGAGATGTCCGTAAGGTCTTGCCAAGAAATATTGCTGTTCCTTACTGCCAACTCTCCAAGAAACTGGAAC..5'  400
                                                          Cys
 321  5'..GTTTCCAGTACCTCTACAGGCATTCCAGAACGGTTCTTTATAACGACAAGGAATGACGTTGAGAGGTTCTTTGACCTTG..3'  400
                                    primer(2)-5'..TAACGCCATGGAATGCGGGTTGAGAGGTTCTTT..3'
                                                          Ala
                                              +KpnI

Cys286Ala                                                    +HindIII
                                                              Ala
                                    primer(1)-3'..AGCAGCGTCTTTCAAGCTTTGACGTCCTGCTG..5'
 801  3'..GGAAGACCCAAAGGAGTTTGCAGGGGGCAGTGCAGGCCAAAGCAGCGTCTTTCAGTGCTTTGACGTCCTGCTGGGCATCC..5'  880
                                                              Cys
 801  5'..CCTTCTGGGTTTCCTCAAACGTCCCCCGTCACGTCCGGTTTCGTCGCAGAAAGTCACGAAACTGCAGGACGACCCGTAGG..3'  880
                                    primer(2)-5'..TCGTCGCAGAAAGTTCGAAAACTGCAGGACGAC..3'
                                                              Ala
                                                    +HindIII

Cys322Ala
                                                  Ala
                                        primer(1)-3'..GCCTCATTAGAGTCAAATCCC..5'
 921  3'..GGACATGAGAAGATATATGCCACCAGCTCACAGGAACTTCCTGTGCTCATTAGAGTCAAATCCCTCAGTCCGTGAGTTTG..5' 1000
                                                  Cys
 921  5'..CCTGTACTCTTCTATATACGGTGGTCGAGTGTCCTTGAAGGACACGAGTAATCTCAGTTTAGGGAGTCAGGCACTCAAAC..3' 1000
                primer(2)-5'..GGTCGAGTGTCCTTGAAGGAC..3'

Cys349Ala          -HindIII
                                  Ala
     primer(1)-3'..GAAGCCTATGACGCCGCTGTGAAAGCTCTGGTC..5'
1021  3'..GGCCTGCGGGAAGCTTATGACGCCTGTGTGAAAGCTCTGGTCTCCCTGAGGAGCTACCATCTGCAAATCGTGACTAAGTA..5' 1100
                                  Cys
1021  5'..CCGGACGCCCTTCGAATACTGCGGACACACTTTCGAGACCAGAGGGACTCCTCGATGGTAGACGTTTAGCACTGATTCAT..3' 1100
     primer(2)-5'..CTTCGGATACTGCGGCGACACTTTCGAGACCAG..3'
                                  Ala
                -HindIII
```

The similar characteristics observed for the mutated and non-mutated rhIDO using CD studies, suggest that the change of the Cys to Ala at position Cys126, Cys286, Cys322 and Cys349 had subtle effects on the secondary structure of the rhIDO. It was also observed that the smallest difference in the CD spectra is between the mutant C286A and C322A, which is probably attributed to the fact that Cys286 is in spatial proximity to Cys322 in the rhIDO. Changes in the β-strand of C286A, C322A and C349A compared to that of C126A mutant may have been due to the location of Cys126, which is at the small domain and not at the large domain as the others in the rhIDO are. The CD studies suggested that there is subtle but significant effect of the cysteines and their localisation towards the overall secondary structure of rhIDO.

The results from the Soret region CD studies of the mutants and non-mutants suggested that changes from Cys to Ala in rhIDO give rise to environmental change in the heme pocket. The Soret region CD spectrum of C286A was almost identical to that of the non-mutated rhIDO, suggesting that Cys286 was not directly associated with the heme *b* co-factor binding. The other mutants C126A, C322A, and C349A showed shifts from the non-mutated rhIDO suggesting that they were associated with the heme *b* co-factor binding. The degree of the complexity and magnitude of the CD spectral change was in the order of C349A > C322A > C126A, suggesting that the site-directed mutagenesis of the Cys to Ala at positions Cys349 was directly associated with the heme *b* co-factor binding. From this study it is conceivable that the Cys to Ala site-directed mutagenesis of C349A, C322A and C126A of rhIDO induces subtle changes in the protein secondary structure, thereby facilitating the binding of the heme *b* co-factor, which was not the case

for C286A. Further studies to understand the significance of the cysteines towards the nature of the heme *b* binding in rhIDO and the effects toward the catalytic properties of rhIDO are recommended.

The result of the thermal melt experiments did not show any significant change in the thermal melt of the mutated rhIDO in comparison to the non-mutated rhIDO. UV-Vis spectroscopy studies did not show any significant changes upon mutation. All the mutants, C126A, C286A, C322A and C349A exhibited a decrease in specificity towards L-Trp with C322A showing the highest decrease (78% loss). However, with D-Trp, mutants C126A and C322A showed increased specificity, with C126A showing the highest increase (280%), while mutants C286A and C349A showed decreased activity with C349A having the greatest loss (67%). This study confirms that the cysteine moieties of rhIDO are involved in the normal catalytic function of the enzyme. It is highly likely that the change from Cys to Ala in the mutants changed the conformation of the enzyme, which was a determining factor to the accessibility of the specific substrates to the active site. This change in conformation resulted in the diverse kinetics observed.

Chapter 6

Conclusions and recommendations

Chapter 6

Conclusions and recommendations

Since the discovery by Hayaishi and co-workers, IDO has been intensively studied for the understanding, treatment, and preventing of various diseases.[172,181,183,186] IDO is involved in various aspects of biological systems and functions.[247,252,253] The ever expanding research on IDO has increased the demand for large quantities and better quality rhIDO, Reproducibility in the expression and purification of rhIDO is crucial in this respect. In our interest to further understand the nature and characteristics of IDO, this study investigated various aspects and approaches towards optimising the yields and quality of rhIDO expressed in *E. coli* EC538 (pQE-9-IDO, pREP4) and was aimed to i) optimise the expression of rhIDO in *E. coli* (pQE-9-IDO, pREP4) in order to obtain high quality enzyme, ii) evaluate the characteristics and stability of rhIDO in order to understand its behaviour as a support towards further studies, iii) study the re-incorporation of the heme *b* co-factor of rhIDO as an approach to optimising the availability of the enzyme for further studies and iv) evaluate the contribution of individual cysteines towards the overall catalytic properties and stability of rhIDO through mutagenesis studies.

Recombinant human indoleamine 2,3-dioxygenase (rhIDO) expressed in *E. coli* EC538 (pQE-9-IDO, pREP4) has a potential to offer a viable supply of IDO and in order to obtain substantial quantities of high quality rhIDO, the methods for the expression of rhIDO in *E. coli* EC538 (pQE-9-IDO, pREP4) by Littlejohn,[152] Austin[9.10] and their

co-workers were optimised. Specifically the lowering of the growth temperature of *E. coli* EC538 (pQE-9-IDO, pREP4) from 37 °C to 30 °C was shown to significantly reduce the formation of rhIDO as inclusion bodies and enhance the yield of soluble rhIDO. Better and reproducible yields of rhIDO were also obtained when the expression was carried out in the dark, without the additions of PMSF during growth and the addition of hemin prior to lysis of the cells. The Soret/protein ratio of rhIDO was observed to reach a maximum of 1.70:1.00 in this study and this value represents the quality of the rhIDO that is associated with rhIDO activity and purity. The incorporation of ALA and the optimal concentration of IPTG for induction for the expression of rhIDO were considered. Induction with high concentration of IPTG (100 μM or higher) was associated with the formation of rhIDO as inclusion bodies. High Soret/protein ratios and specific activity values that are characteristics of high quality rhIDO were achieved by inducing the expression of rhIDO in *E. coli* EC538 (pQE-9-IDO, pREP4) with 10 μM IPTG. Semi-anaerobic conditions did not have a significant effect on the yield and quality of the rhIDO.

In the 3D modelling and the docking experiments, the nature of IDO, its active site, its complex with L-Trp and its catalytic mechanism towards the reaction of L-Trp were studied. The ArgusDock docking engine was used to dock L-Trp into the active site of IDO. The docking experiments supported that the proximal side of the heme *b* co-factor is occupied only by side chains from the large domain Q (His346), S (Leu384, Phe387) and N (His287). The modelling and docking experiments were able to map IDO's active site and its complex with L-Trp.

In the characterisation of rhIDO, the mass spectrum from a direct injection ESI-MS of rhIDO was deconvoluted with Micromass MaxEnt1 processing giving a mass of 47,758 kDa for the rhIDO and due to adduct ion species of multiply charge rhIDO in the ESI-MS spectra, the value of 47,758 kDa for a direct injection ESI-MS of rhIDO is consistent with this mass. The SDS-PAGE of the rhIDO was consistent to the ESI-MS result. In this study, the Soret/protein ratio of rhIDO was observed to reach a maximum of 1.70:1.00. However, it was established that the ratios fluctuated from sample to sample depending upon the treatment of the samples.

Reduction of the rhIDO heme *b* co-factor iron from its ferric (Fe^{3+}) to its ferrous (Fe^{2+}) state with sodium dithionite was done. One minute after the initial reaction, the UV-Vis spectra showed an additional peak at 314 nm for dithionite and a shift of the peak at 406 nm to 421 nm. After ten minutes the peaks returned to their original position with a lower absorption at 406 nm. CD studies of the reduction suggested that one minute after the initial reaction, an increased α-helix but a lowered β-strand and random-coil conformations occurred. This result suggested that changes in conformations occurred to facilitate the reaction of rhIDO in its active site and perhaps it is important to take account this conformational changes in order to support the efficacy of IDO as a novel target in therapy and drug discovery.[113,119,126,163,169,192] Further studies on this are required. The findings on the reduction of the rhIDO heme *b* co-factor iron from its ferric (Fe^{3+}) to its ferrous (Fe^{2+}) state with sodium dithionite, suggested that, the reduction facilitates the reaction in the rhIDO active site, changing the conformations of rhIDO. This needs to be investigated further so as to support the rational design and development of potential IDO inhibitors in drug discovery.

Discrepancies between the previous findings[10,174] and the findings in this study were observed in the Soret/protein ratios, specific activities and CD spectral studies when rhIDO was incubated at a temperature range of 4 to 20 °C in a period of 2 to 6 hours. In this study it was found that under those conditions rhIDO was highly stable and retained its activity. In the study of the effect of cryoprotectants it was found that the use of 0.5 M sucrose as a cyroprotectant severely degraded rhIDO. The preservative effects of cyroprotectants in the freezing of rhIDO was in the order of 40% glycerol > 10% DMSO > absence of cryoprotectants > 0.5 M sucrose. From the study it could be seen that the process of freezing and thawing can result in severe damage to rhIDO. This is most probably due to the possibility of surface induced denaturation which occurs during freezing and thawing.[236] Upon fast freezing, it can be assumed that ice crystals and a large surface area of ice-liquid interface are formed and hence increasing the exposure of the rhIDO molecules to the ice-liquid interface.[237] Due to recrystallisation which exerts additional interfacial tension on entrapped rhIDO, further damage is probable during thawing. The patterns of the dependency on cryoprotectants showed that damage of rhIDO in aqueous solutions could be reduced by preserving rhIDO in 40% glycerol at -20°C as this resulted in only a small decrease in Soret/protein ratio (6%), specific activity (24%) and protein concentration (17%). The patterns of the dependency on cryoprotectants showed that damage of rhIDO in aqueous solutions could be reduced by preserving rhIDO in 40% glycerol at -20°C. This preservation, results only in a small decrease of the Soret/protein ratio (6%), specific activity (24%) and protein concentration (17%). It was found in this study that rhIDO is more stable in concentrated, rather than dilute solutions.

In the studies of rmIDO and rhIDO it was found that rhIDO utilises L-Trp more efficiently than rmIDO but the reverse is true for D-Trp. CD and thermal melt studies concluded that rhIDO is less helical (61% helix) than the rmIDO (71% helix) and that rhIDO has a lower melt temperature than rmIDO, indicating that rmIDO is more thermostable than rhIDO. Homology and database analysis of rhIDO and rmIDO showed some similarities in both physical and kinetic properties. Kinetic studies of rhIDO and rmIDO using L-Trp and D-Trp as substrates showed similar substrate preferences where the preference towards L-Trp (μM range) was greater than towards D-Trp (mM range). The relative catalytic efficiency of rhIDO towards L-Trp (3.73) was higher compared to rmIDO (1.40) whereas the relative catalytic efficiency of rhIDO towards D-Trp (0.02) was lower compared to rmIDO (0.03). From the study it could be concluded that rhIDO utilises L-Trp more efficiently than rmIDO but the reverse is true for D-Trp. CD and thermal melt studies established that rhIDO is less helical (61% helix) than rmIDO (71% helix). The studies also showed that rhIDO has a lower melt temperature (50 ºC) than rmIDO (65 ºC), indicating that rmIDO is more thermostable than rhIDO. From these observations, it could be concluded that there are significant differences between rhIDO and rmIDO despite their 60% similarities. These differences must be recognised and accounted for, before the interpretation of experimental findings from one system to another is applied, especially as murine models are commonly used to study human conditions relevant to the expression of IDO.

Heme release in rhIDO was observed during purification. This was consistent with fluctuations and decreases in the rhIDO Soret/protein ratio observed in previous studies

on rhIDO by Austin.[10] Studies of re-purification of rhIDO over ten cycles of consecutive re-freezing, re-thawing, re-dissolving and re-filtering with the Amicon Ultra-15 filter concluded that the degree of loss in Soret/protein ratio, protein content and enzyme activity could reach up to 71, 70 and 80% respectively. A desalting step using a PD-10 column prior to re-filtering with the Amicon Ultra-15 filter showed that the decrease in Soret/protein ratio, protein content and enzyme activity could reach 71, 82 and 62% respectively. This outcome concluded that elution through a PD-10 desalting column did not hinder the severe loss of heme during the re-purification with the Amicon Ultra-15 filter suggesting that the process of heme loss from rhIDO upon re-purifications is not salt dependent.

In this study, it was established that a gradual heme re-incorporation with hemin chloride showed a consistent gradual increase in Soret/protein ratio and enzyme activities. This increase was observed before and after the desalting process. Heme re-incorporation using low concentration of hemin chloride to rhIDO of low Soret/protein ratio, showed an increase in Soret/protein ratio and enzyme activity of 50% (from 1.1:1.0 to 1.7:1.0) and 71% (from 60.5 to 103.6 μmol/h/mg), respectively. Heme re-incorporation using a high concentration hemin chloride towards high Soret/protein ratio rhIDO showed an increase of Soret/protein ratio and enzyme activity of 28% (from 1.4:1.0 to 1.8:1.0) and 38% (from 76.1 to 105.0 μmol/h/mg), respectively. High initial Soret/protein ratio rhIDO showed a higher lowering of enzyme activity and Soret/protein ratio with increased hemin concentration after desalting than low initial Soret/protein ratio rhIDO. From this study, the observed lowering of rhIDO enzyme activity and Soret/protein ratio after desalting during the heme re-incorporation titration verified that burdening the

availability of heme occurred. It can be concluded that the loss of rhIDO activity is caused by the loss of the heme prosthetic group of the enzyme. The re-incorporation of the heme was considered to reverse the process. It was observed that the re-incorporation of heme to the apo-protein through heme re-incorporation was a possibility. However, supplementing hemin chloride prior to lysis of *E. coli* EC538 (pQE-9-IDO, pREP4) cells in the French Press was considered conducive in sustaining the availability of the heme. Investigations in this study also established that the stripping of the heme *b* co-factor of rhIDO through anion exchange chromatography resulted towards aggregated proteins. The matrices and elution conditions of the anion exchange chromatography used in this study did not result in the efficient stripping of the heme *b* co-factor from the rhIDO. However, this needs to be investigated further in light of the possibility of using anion exchange for the purification of rhIDO.

The site-directed mutagenesis-based study on Cys126 at helix E, Cys286 at helix M, Cys322 at helix O and Cys349 at helix Q completes the description of the structural/functional role of the cysteine residues in rhIDO. Site-directed mutagenesis of Cys126, Cys286, Cys322 and Cys347 to their corresponding alanines was done to investigate the influence of the selected cysteine residues on the overall characteristics and stability of rhIDO. The mutation of Cys126Ala, Cys286Ala and Cys349Ala utilised the QuikChange II Site-Directed Mutagenesis Kit (Stratagene) using the direct mutation of the double-stranded plasmid of pQE-9-IDO. The system could not be used for the mutation of Cys322Ala. Modifications in the oligonucleotide primers, procedures and conditions for the mutations, including steps in the PCR were unsuccessful. Mutation of

Cys322Ala was accomplished by using the TripleMaster PCR System (Eppendorf). The significant difference between the mutation of Cys126Ala, Cys286Ala and Cys349Ala and that of Cys322Ala is that whereas the mutation of Cys322Ala did not use the direct mutation of the double-stranded plasmid of pQE-9-IDO, the mutation of Cys322Ala used the 5'-phosphate ends of the oligonucleotide primers that were ligated at the final step.

The similar characteristics observed for the mutated and non-mutated rhIDO using CD studies, suggest that the change of the Cys to Ala at position Cys126, Cys286, Cys322 and Cys349 had subtle effects on the secondary structure of the rhIDO. It was also observed that the smallest difference in the CD spectra is between the mutant C286A and C322A, which is probably attributed to the fact that Cys286 is in spatial proximity to Cys322 in the rhIDO. Changes in the β-strand of C286A, C322A and C349A compared to that of C126A mutant may have been due to the location of Cys126, which is at the small domain and not at the large domain as the others in the rhIDO are. The CD studies suggested that there is subtle but significant effect of the cysteines and their localisation towards the overall secondary structure of rhIDO.

The results from the Soret region CD studies of the mutants and non-mutants suggested that changes from Cys to Ala in rhIDO give rise to environmental change in the heme pocket. The Soret region CD spectrum of C126A was almost identical to that of the non-mutated rhIDO, suggesting that Cys286 was not directly associated with the heme *b* co-factor binding. The other mutants C126A, C322A, and C349A showed shifts from the non-mutated rhIDO suggesting that they were associated with the heme *b* co-factor

binding. The degree of the complexity and magnitude of the CD spectral change was in the order of C349A > C322A > C126A, suggesting that the site-directed mutagenesis of the Cys to Ala at positions Cys349 was directly associated with the heme *b* co-factor binding. From this study it is conceivable that the Cys to Ala site-directed mutagenesis of C349A, C322A and C126A of rhIDO induces subtle changes in the protein secondary structure, thereby facilitating the binding of the heme *b* co-factor, which was not the case for C286A. Further studies to understand the significance of the cysteines towards the nature of the heme *b* binding in rhIDO and the effects toward the catalytic properties of rhIDO are recommended.

The result of the thermal melt experiments did not show any significant change in the thermal melt of the mutated rhIDO in comparison to the non-mutated rhIDO. UV-Vis spectroscopy studies did not show any significant changes upon mutation. All the mutants, C126A, C286A, C322A and C349A exhibited a decrease in specificity towards L-Trp with C322A showing the highest decrease (78% loss). However, with D-Trp, mutants C126A and C322A showed increased specificity, with C126A showing the highest increase (280%), while mutants C286A and C349A showed decreased specificity with C349A having the greatest loss (67%). This study confirms that the cysteine moieties of rhIDO are involved in the normal catalytic function of the enzyme. It is highly likely that the change from Cys to Ala in the mutants changed the conformation of the enzyme, which was a determining factor to the accessibility of the specific substrates to the active site. This change in conformation resulted in the diverse kinetics observed.

The study of IDO is crucial for the understanding of the process of immune escape,[99] which is a critical gateway to malignancy.[235] The emergence of this fundamental trait of cancer represents the defeat of immune surveillance,[104] a potent, multi-armed and essential mode of cancer suppression[235] that may influence the ultimate clinical impact of an early stage tumor. Immune escape was postulated to affect tumor dormancy versus progression, giving way to invasion and metastasis, thereby impacting therapeutic response.[4,20,325,346] Immune suppression and tumor escape are now central research themes, with IDO as one of the core. Clinical trials of several new IDO related therapeutic agents are already under way.[113,126,158] Indoleamine 2,3-dioxygenase (IDO) is implicated in suppressing T-cell immunity[156,310,329] in normal and pathological settings including cancer. New evidence suggests that during cancer progression, activation of IDO might act as a preferred pathway for immune escape.[191,235] The interconnections between signalling pathways[129] that control immune escape and those that control proliferation,[74,81,116] senescence,[230] apoptosis,[340] angiogenesis,[148,243] invasion and metastasis remain unexplored, giving vast opportunities for research.

Chapter 7

Experimental

Chapter 7

Experimental

7.1. Materials

Escherichia coli EC538 (pQE-9-IDO, pREP4) was provided by Tamantha S. Littlejohn, School of Biological Sciences, University of Wollongong, NSW, Australia. Imidazole and sodium hydroxide (NaOH) were from BDH. Ampicillin, DNase and kanamycin were from Bohringer Ingelheim. Bacteriological agar, tryptone and yeast extract were from Oxoid. EDTA-free protease cocktail inhibitor was from Roche. Acetic acid, agarose, δ-aminolevulinic acid (ALA), ammonium iron(III) citrate, ammonium persulphate [$(NH_4)_2S_2O_8$], boric acid [$B(OH)_3$], bromophenol blue, calcium chloride ($CaCl_2$), Coomassie Blue R-250, ethylenediaminetetraacetic acid (EDTA), ethylene glycol, glucose, glycerol, glycine, hemin chloride, isopropanol-β-D-thiogalactopyranoside (IPTG), lysozyme, magnesium chloride ($MgCl_2.6H_2O$), magnesium sulphate ($MgSO_4.7H_2O$), manganese chloride ($MnCl_2$), β-mercaptoethanol, phenylmethyl-sulphonylfluoride (PMSF), piperazine-1,4-bis(2-ethanesulfonic acid) (PIPES), potassium chloride (KCl), sodium chloride (NaCl), sodium dodecyl sulphate (SDS), *N,N,N′,N′*-tetra-methylethylenediamine (TEMED) and tris(hydroxymethyl)methylamine (Tris) were from Sigma Aldrich. Ethanol, hydrochloric acid (HCl), isopropanol, methanol, nitric acid (HNO_3), potassium dihydrogen phosphate (KH_2PO_4) and sodium hydrogen phosphate (Na_2HPO_4) were from May and Baker.

7.2. General procedures

All chemicals were of analytical grade unless otherwise specified. All buffers and reagents were made according to the procedures outlined in their respective sections. Protein concentration was determined with Bio-Rad dye reagent (1:5 dilutions with Milli-Q H_2O) using bovine serum albumin (0 - 1 mg/mL) as a standard. The coloured product was measured at 595 nm using a Shimadzu UV-Vis spectrophotometer. Circular dichroism (CD) spectra were recorded on a JASCO J-810 spectropolarimeter with 1 mm pathlength quartz cuvettes at a temperature of 20 °C. Sensitivity was 100 millidegrees and the scanning speed was 50 nm/minute for an accumulation of 4 scans. Far ultraviolet (UV) region CD data collected between 300 - 190 nm was performed on mutated and non-mutated rhIDO samples at a concentration of 1 mg/mL. Data collected in this region was further analysed using the K2D and K2D2 program (EMBL, Heidelberg, Germany) and CDPro Software consisting of three programs SELCON3, CDSSTR and CONTINLL for CD analysis (Colorado State University). Near UV and Soret region CD data collected between 250 - 450 nm was performed on mutated and non-mutated rhIDO samples at a concentration of 7 - 10 mg/mL. Thermal transition curves were measured by monitoring the CD at $\lambda_{222\ nm}$ as a function of the increasing temperature over the range 20 - 99 °C at 5 °C/minute on a JASCO J-810 spectropolarimeter. T_m values were determined by finding the first derivative of the thermal transition curve using peak processing of the JASCO J-810 spectropolarimeter. UV-Vis spectra of proteins were recorded with a Varian-CARY 1 Bio UV-Visible spectrophotometer, with a 1 cm pathlength cuvette, between wavelengths 200 - 600 nm. Controlled high pressure-temperature autoclave steam sterilisation and ultraviolet sterilised laminar flow cabinets were used to assure sterility in accordance to standard procedures.

7.3. Expression and purification of rhIDO

7.3.1. Expression of rhIDO

E. coli EC538 (pQE-9-IDO, pREP4) from a 10% glycerol stock culture stored at -80 °C was thawed in ice, inoculated on a Luria-Bertani (LB) agar plate **[7.1]** and grown overnight at 37 °C. A single colony from the overnight growth was re-inoculated on an LB plate and grown overnight. A single colony from the second overnight growth was inoculated into 100 mL LB media **[7.2]** and grown overnight at 37 °C (200 RPM). 40 mL of the overnight growth was added to 1 L of LB media **[7.2]** and grown to an optical density (OD) of 0.6 at 600 nm ($OD_{600\ nm}$). ALA, IPTG and PMSF were then added to a final concentration of 0.5 mM, 0.1 mM and 1 mM, respectively. The culture was further grown for 3 hours at 37 °C (250 RPM).

> **[7.1] LB agar plates**. 2% (w/v) Tryptone, 1.0% (w/v) yeast extract, 1.0% (w/v) NaCl and 1.5% (w/v) bacteriological agar in Milli-Q Water were mixed and autoclaved at 121 °C (20 minutes). After autoclaving, the media was cooled to 60 °C followed by the addition of filter-sterilised ampicillin and kanamycin to a final concentration of 100 μg/mL and 50 μg/mL, respectively, and gently mixed. The mixture was poured into sterile Petri-dish plates to set.
>
> **[7.2] LB media**. 2.0% (w/v) Tryptone, 1.0% (w/v) yeast extract and 1.0% (w/v) NaCl in Milli-Q Water were mixed and autoclaved at 121 °C (20 minutes). After autoclaving, the media was cooled to 60 °C followed by the addition of filter-sterilised ampicillin and kanamycin to a final concentration of 100 μg/mL and 50μg/mL, respectively, and gently mixed.

7.3.2. Harvesting of grown cells

The cells from the cultures (**Section 7.3.1**) were harvested by centrifugation (5,000 G, 20 minutes, 4 °C). The resulting cell pellet was resuspended in 20 mL ice-cold Dulbecco's phosphate-buffered saline (PBS) at pH 7.4 **[7.3]**, containing 1 mM PMSF (added freshly before use) and 1 mM EDTA and centrifuged at 5,000 G for 15 minutes at

4 °C. The pellet was stored at -80 °C for up to 1 month.

[7.3] PBS. 8.0% (w/v) NaCl, 0.2% (w/v) KCl, 1.1% (w/v) Na_2HPO_4 and 0.2% (w/v) KH_2PO_4 in Milli-Q H_2O were thoroughly mixed and the pH adjusted to pH 7.4 with concentrated HCl or NaOH. The 10 times stock solution was diluted 1:10 with Milli-Q H_2O before use.

7.3.3. Optimised expression of rhIDO

As given in **Section 7.3.1**, 10 mL of the overnight growth was added to 1 L of LB media **[7.2.]** and grown to an $OD_{600\ nm}$ of 0.6 at 30 °C. ALA and IPTG were then added to a final concentration of 0.5 mM and 0.01 mM, respectively and the *E. coli* was further grown for 6 hours at 30 °C (250 RPM) in the dark.

7.3.4. Purification of rhIDO

Pellets from 1 L of bacterial culture, obtained according to the method described in **Section 7.3.2**, were suspended in ice-cold re-suspension buffer **[7.4]**. The suspension was then centrifuged at 5,000 G for 20 minutes at 4 ºC and the supernatant discarded. The washed pellets were re-suspended in 20 mL of ice-cold buffer **[7.4]** with the addition of EDTA free-cocktail inhibitor tablets (2 tablets per 1 litre pellet) and DNase (1 mg). The suspension was lysed in the French Press twice (2 passes) at 16000 psi and then centrifuged at 5,000 G for 20 minutes, producing a clear supernatant and pellet. Pellets were preserved at -20 °C for studies on inclusion bodies. The clear supernatant (20 mL) was applied to a 1 mL Hi-Trap chelating column (Amersham Biosciences), charged with nickel ions according to the manufacturer's instructions and equilibrated with the basal buffer **[7.5]** containing 10 mM imidazole (30 mL). The protein was eluted on a stepwise gradient using imidazole concentrations of 30 mM, 40 mM, 50 mM, 65 mM, 80 mM and

190 mM in the basal buffer. The protein collected at the elution step was buffer-exchanged with 50 mM Tris-HCl pH 7.4 using a Sephadex G25 NAP-10 column (Pharmacia Biotech). The desalted fractions were pooled and concentrated to a volume of 125 µL using an Amicon Ultra-15 centrifugal device with a 30 kD molecular weight cut-off (Millipore). The concentrated fraction was applied to a Superdex 75 PC 3.2/30 (Pharmacia LKB Biotechnology) column, after equilibration with 50 mM Tris-HCl pH 7.4. All fractions were collected in 75 µL aliquots at a flow rate of 100 µL/minute over 3.5 mL.

[7.4] Re-suspension buffer. 25 mM Tris(hydroxymethyl)methylamine (Tris-HCl pH 7.4), containing 150 mM NaCl, 10 mM imidazole and 10 mM $MgCl_2$ in Milli-Q H_2O. PMSF was added to a final concentration of 1 mM before use.

[7.5] Basal buffer. 25 mM Tris-HCl pH 7.4 containing 150 mM NaCl in Milli-Q H_2O with PMSF added to a final concentration of 1 mM before use.

7.3.5. Optimised purification of rhIDO

Lysed cells and the clear supernatant (20 mL), as prepared in **Section 7.3.4**, was applied to a 5 mL Ni-NTA Hi-Trap chelating column (GE/Pharmacia) that had been equilibrated with the basal binding buffer **[7.5]**. The buffer contained 10 mM imidazole (25 mL) and 500 mM NaCl. The protein was eluted with the basal buffer (25 mL) containing imidazole concentrations of 10 mM, 30 mM and 60 mM, respectively. rhIDO was eluted with the basal buffer containing imidazole concentrations of 300 mM (25 mL). The resulting intense red fraction was collected. The protein collected from the elution was then buffer-exchanged with 50 mM Tris-HCl pH 7.4, using a Sephadex G25 column (GE NAP-10/Amersham PD-10 desalting column). The desalted fractions were pooled and concentrated to a volume of 250 µL using a 15 mL Amicon Ultra-15 centrifugal

device with a 30 kDa molecular weight cut-off (Millipore). After equilibration with 50 mM Tris-HCl pH 7.4, the concentrated fraction (50 µL) was applied to a Superdex 75 PC 3.2/30 (GE/Pharmacia). Separation and fraction collection were monitored at 280 and 406 nm on a fast protein liquid chromatography (FPLC) System (SMART-Pharmacia LKB Biotechnology) were collected in 100 µL aliquots at a flow rate of 100 µL/minute over 5.0 mL.

7.3.6. SDS-PAGE

Sodium dodecyl sulphate-polyacrylamide gel electrophoresis (SDS-PAGE) utilised a Bio-Rad Mini-Protean II system. For whole cell lysates, pelleted cells were resuspended in Milli-Q water and an equal volume of 2 times cracking buffer **[7.6]**. For soluble protein samples, an equal volume of 2 times cracking buffer was added to protein solutions. The samples were incubated at +90 ºC for 10 minutes and then centrifuged to remove any solids. Samples were separated through a 12% polyacrylamide gel, with a 4% stacking gel (Gradipore), immersed in SDS running buffer **[7.7]**. Protein samples were separated by electrophoresis for a period of 1.5 - 2 hours with a voltage of 120 V. Gels were sequentially immersed in gel fixing solution **[7.8]** for 1 minute, freed from the fixing buffer and stained with rapid Coomassie blue stain **[7.9]**. Gels were de-stained by overnight immersion in gel de-stain solution **[7.10]**. Stained gels were soaked in gel drying solution **[7.11]** and dried before being imaged using the ImageJ 1.41 imaging software from National Institutes of Health, USA.

> **[7.6] Cracking buffer**. 1% (w/v) SDS, 1% (v/v) β-mercaptoethanol, 10% (v/v) glycerol, 0.01% (w/v) bromophenol blue in 60 mM Tris-HCl adjusted to pH 6.8 with 6.0 M HCl.

[7.7] SDS running buffer. 1.5% (w/v) Tris base, 7.2% (w/v) glycine and 0.5% (w/v) SDS in Milli-Q H_2O. For final dilution, 5 times stock solution was diluted 1:5 with Milli-Q H_2O.

[7.8] Gel fixing solution. 50% (v/v) Ethanol and 10% (v/v) glacial acetic acid in Milli-Q H_2O.

[7.9] Gel staining solution. 40% (v/v) Methanol, 10% (v/v) glacial acetic acid and 0.00002% (w/v) Coomassie blue R-250 (20 mg in 1 litre) in Milli-Q H_2O.

[7.10] Gel de-stain solution. 10% (v/v) Glacial acetic acid and 4% (v/v) glycerol in Milli-Q H_2O

[7.11] Gel drying solution. 4% (v/v) Ethylene glycol and 35% (v/v) ethanol in Milli-Q H_2O

7.3.7. IPTG dependency on the expression of rhIDO

Individual bacterial cultures of *E. coli* EC538 (pQE-9-IDO, pREP4) were grown in LB media at 37 °C (**Section 7.3.1**). When the $OD_{600\ nm}$ reached 0.6, the cultures were supplemented with IPTG to a final concentration of 0, 1, 10, 100, 500, 1000 and 10000 μM. PMSF was also added to a final concentration of 1 mM. Cultures were incubated for a further 3 hours before centrifugation at 5000 G, after which they were lysed in the French Press at 16000 psi (2 passes), as given in **Section 7.3.4**. rhIDO activity was tested from lysed cellular supernatants with 200 μM L-Trp as the substrate (**Section 7.4.2**). Proteins were visualised by SDS-PAGE electrophoresis (**Section 7.3.6**).

7.3.8. Isolation of inclusion bodies

The pellet collected after lysis (**Section 7.3.4**) was resuspended twice in 1 mL Milli-Q water and centrifuged at 5,000 G for 10 minutes. The freshly washed pellets were resuspended in 1 mL of 1 mg/mL lysozyme and incubated for 10 minutes at room

temperature before centrifugation. The pellets were subsequently washed in 1 mL of 1% Triton X-100 and 1 mL of Milli-Q water before storage at -20 °C.

7.3.9. Peptide mass fingerprinting of inclusion bodies

Protein bands of interest were removed from SDS-PAGE gels (**Section 7.3.6**) by dissection with a clean pipette tip and digested with trypsin for 16 hour at 37 ºC. A 1 µL aliquot of the resulting tryptic digest was spotted onto a sample plate with 1 µL of matrix (8 mg/mL α-cyano-4-hydroxycinnamic acid, in 70% v/v acetonitrile, 1% v/v trifluoroacetic acid) and allowed to air dry. Matrix assisted laser desorption ionisation (MALDI) mass spectrometry was performed with an Applied Biosystems 4700 Proteomics Analyser with TOF/TOF optics in MS mode. An Nd:YAG laser (355 nm) was used to irradiate the sample. The spectra were acquired in reflectron mode in the mass range 800 to 3500 Th. Peptide mass fingerprinting was performed by the Australian Proteome Analysis Facility (APAF), Macquarie University.

7.3.10. Temperature and inclusion bodies formation

Individual bacterial cultures of *E. coli* EC538 (pQE-9-IDO, pREP4) were grown in LB media at 37 °C. When the $OD_{600\ nm}$ reached 0.6, the cultures were supplemented with IPTG and PMSF (**Section 7.3.1**). Cultures were incubated for a further 3 hours before centrifugation at 5000 G. The cells were lysed in the French Press at 16000 psi (2 passes). Isolated inclusion bodies (**Section 7.3.8**) were visualised by SDS-PAGE electrophoresis (**Section 7.3.6**) prior to densitometric analysis using ImageJ 1.41 imaging software developed at the National Institutes of Health, USA.

7.3.11. ALA supplementation

Individual bacterial cultures of *E. coli* EC538 (pQE-9-IDO, pREP4) were grown in LB media at 37 °C. When the $OD_{600\ nm}$ reached 0.6, the cultures were supplemented with IPTG and PMSF (**Section 7.3.1**). ALA was added to individual cultures to a final concentration of 0, 0.1, 0.5 and 1 mM. Cultures were incubated for a further 3 hours before centrifugation at 5000 G and lysis in a French Press at 16000 psi. Lysed cellular supernatants were tested for rhIDO activity with 200 μM L-Trp as the substrate (**Section 7.4.2**). Proteins were visualised by SDS-PAGE electrophoresis (**Section 7.3.6**).

7.4. Characterisation of rhIDO

7.4.1. Protein mass spectrometry

rhIDO from the expression in *E. coli* EC538 (pQE-9-IDO, pREP4) (**Section 7.3.5**) was identified by electrospray ionisation mass spectrometry (ESI-MS) with a probe source temperature maintained at 100 - 150°C, corona discharge at 3.50 kV and cone voltage set at 20 volts on a VG Quattro mass spectrometer (VG Biotech, Altrincham, UK). Samples were desalted with a mini-column of Sephadex G-50 equilibrated with Milli-Q water and injected at a concentration of 10 pmol/mL. The skimmer potential was set at 25 - 35 V. The mass was scanned at a rate of 1 second per 100 *m/z* and data from 10 - 20 scans were summed to obtain representative spectra. The raw mass spectra data from direct injection ESI-MS of 0.30 μg/μL rhIDO were deconvoluted with Micromass MaxEnt1 processing (Micromass Maximum Entropy algorithms for deconvolution of electrospray mass spectrometry data) to give the final mass spectra.

7.4.2. Specific activity of rhIDO

IDO activity was determined as described by Takikawa and co-workers[295] with minor modifications. In this procedure, the standard reaction mixture (200 µL) contained 50 mM potassium phosphate buffer (pH 6.5), 20 mM ascorbic acid (neutralised with NaOH), 200 µg/mL catalase, 10 µM methylene blue, 400 µM L-Trp and rhIDO. The reaction was carried out at 37 °C for 60 minutes and stopped by the addition of 40 µL of 30% (w/v) trichloroacetic acid. This was followed by heating at 65 °C for 15 minutes, after which the reaction mixtures were centrifuged at 12,000 G for 7 minutes. The supernatant (125 µL) was transferred into a 96-well micro-titre plate and mixed with 125 µL of 2% (w/v) *p*-dimethylaminobenzaldehyde (*p*-DMAB) in acetic acid. The yellow pigment derived from kynurenine was measured at 480 nm using a Fluostar micro-titre plate reader (BMG Lab Technologies). The reactions were conducted in triplicate. A standard curve of L-kynurenine was used, ranging in concentration from 0 – 500 µM. The protein concentration was determined using the Bradford protein assay[15] that utilises a standard curve of bovine serum albumin. In this study the curve was determined on a Varian-Cary double beam UV-Vis spectrophotometer (595 nm).

7.4.3. Kinetic characterisation of rhIDO

Kinetic evaluations utilised L-Trp and D-Trp as substrates and were conducted using the standard assay system described in **Section 7.4.2**. The concentrations of the substrates were 0, 10, 25, 50, 100, 200 µM for L-Trp and 0, 100, 250, 750, 1500, 3000 µM for D-Trp, with an incubation time of 20 minutes. The Michaelis-Menten constant (K_m), maximum reaction velocity (V_{max}) and catalytic efficiency (V_{max}/K_m) were determined. Kinetic evaluations were done towards non-mutated rhIDO, mutated rhIDO and

recombinant mouse IDO (rmIDO). The concentrations of the proteins were adjusted to give an initial velocity for each substrate for which the percentage of conversion of substrate to product at each concentration was less than 10% and the reactions were conducted in triplicate. The kinetic plots (Michaelis-Menten, Lineweaver-Burk, Eadie-Hofstee) and calculations of values utilised Prism 4 for Windows Version 4.02 from GraphPad Software Inc.

7.4.4. Modelling of IDO

Using the data from the findings of Sugimoto[284,285] and co workers and Research Collaboratory for Structural Bioinformatics (RCSB) Protein Data Bank™ database with ChemDraw™, ArgusLab™ and UCSF Chimera™ softwares, the heme environment and the active site of IDO was docked with L-Trp as a ligand and mapped to visualise the L-Trp-bound form in the active site of IDO.

7.4.5. Effect of cryoprotectants on rhIDO

rhIDO in 25 mM Tris-HCl pH 7.4 was freeze denaturated in the absence of cryoprotectants and with 40% glycerol, 0.5 M sucrose and 10% DMSO as protectants. For rhIDO stability evaluation, freezing with liquid nitrogen and storage at -80 ºC for 48 hours, followed by re-purification through the Ni-NTA and the NAP-10 columns, were done.

7.4.6. Effects of time and cryoprotectants on rhIDO

rhIDO in 25 mM Tris-HCl pH 7.4 was stored in the absence of protectants and with 40% glycerol and 10% DMSO as protectants at both room (20 ºC) and freezer (-20 ºC) temperature conditions for 0, 1, 2 and 3 months.

7.5. Re-incorporation of heme into rhIDO

7.5.1. Re-purification of rhIDO

rhIDO in 2.5 mL 25 mM Tris-HCl pH 7.4 were repeatedly (10x) filtered with a Millipore Amicon Ultra-15 30 kD cut-off filter. This was done with and without prior desalting through an Amersham Biosciences PD-10 (Sephadex G-25M) desalting column (desalting from 25 mM Tris-HCl pH 7.4) concentrating 2.5 mL to 250 µL of protein in a sequence of up to 10 consecutive pass. After each pass 80% glycerol (1:1 v/v) was added again to the rhIDO samples and kept in the freezer at -20 ºC for 2 hours prior to the next cycle of re-dissolving in 25 mM Tris-HCl pH 7.4 and re-purifying.

7.5.2. Re-incorporation of heme

Two sets of hemin chloride concentrations towards two sets of rhIDO with different Soret/protein ratio were used. Lower concentration increments of 0.0, 1.5, 3.0, 4.5, 6.0 and 7.5 µM of hemin chloride (in 20 mM NaOH) were used towards 600 µL rhIDO samples (1 mg/L in 25 mM Tris-HCl pH 7.4) of lower Soret/protein ratio (1.1:1.0). Higher concentration increments of 0.0, 1.7, 3.3, 5.0, 6.7 and 8.3 µM of hemin chloride were used towards 600 µL rhIDO samples (1 mg/L in 25 mM Tris-HCl pH 7.4) of higher

Soret/protein ratio (1.4:1.0). Hemin chloride solution was added slowly to the ice-cooled rhIDO solution to give a final volume of 750 µL. This was followed by gently shaking for 20 minutes and keeping the mixtures in ice as much as possible during the process.

7.5.3. Anion exchange of rhIDO

Ion exchange experiments using PI-20 (PEI Ligand/Binding capacity 35 mg/mL), QE-20 (QPEI Ligand/Binding capacity 40 mg/mL) and HQ-20 (QPEI Ligand/Binding capacity 60 mg/mL) POROS columns utilised NaCl, KCl and KCN (0 to 1 M, gradient, 2 mL/minute) in 50 mM Tris-HCl pH 7.4 and 8.0 on a fast protein liquid chromatography (FPLC) System (SMART-Pharmacia LKB Biotechnology), monitored at 280 and 406 nm. 2 mg/mL of purified rhIDO (**Section 7.3.5**) were applied to the 50 mM Tris-HCl pH 8 equilibrated POROS 20 PI, POROS 20 QE and POROS 20 HQ columns (Applied Biosystems). Elution was performed on a linear gradient from 50 mM Tris-HCl pH 8.0, 0 mM NaCl to 50 mM Tris-HCl pH 8.0, 500 mM NaCl over 40 minutes (Flow rate = 2 mL/minute). After elution, fractions were pooled, desalted (25 mM Tris-HCl pH 7.4) and concentrated before storage in 40% glycerol at -20 °C.

7.6. Site directed mutagenesis of rhIDO

7.6.1. Isolation of plasmid DNA

Plasmid DNA was isolated from a 5 mL LB media of *E. coli* EC538 (pQE-9-IDO, pREP4) cells harvested after overnight growth at 37 ºC using a GenElute Plasmid Miniprep Kit®, using pre-prepared solutions supplied in accordance to the manufacturer's instructions (Sigma). Pelleted *E. coli* EC538 (pQE-9-IDO, pREP4) cells

were resuspended in 200 µL of re-suspension solution containing RNase A. To the resuspended cells, 200 µL of lysis solution was added. The mixture was incubated at room temperature for ≤ 5 minutes before neutralisation through the addition of neutralisation/binding solution. This solution was then centrifuged in order to remove cellular debris produced during lysis. The clear lysate was loaded onto a pre-prepared GenElute Miniprep Binding column by centrifugation at 12,000 G for 1 minute. The column was then washed with wash solution in order to remove residual salt and contaminants by centrifugation at 12,000 G for 2 minutes. Purified plasmid DNA was then eluted from the column through application of elution solution. DNA purified by this method was then stored at -20 ºC for up to one month.

7.6.2. Mutant strand synthesis

Mutant strand synthesis was performed using the Quikchange® II site-directed mutagenesis kit (Stratagene) and TripleMaster PCR System. In the Quikchange® II site-directed mutagenesis, pre-prepared solutions supplied in accordance to the manufacturer's instructions, were used. Complimentary nucleotides (designated oligonucleotide primer #1 and #2) were resuspended as a stock solution in autoclaved TE buffer **[7.11]** to a concentration of 1000 ng/µL. 125 ng of oligonucleotide primers #1 and #2 were added to a reaction solution containing 20 ng template plasmid (pQE-9-IDO), as purified in **Section 7.6.1**. 10x-Reaction buffer (5 µL), 1 µL deoxyribonucleoside triphosphate (dNTP) and Milli-Q H_2O were made to a volume of 50 µL. In these reactions, plasmids (pWhitescript 4.5 kb) and primers (oligonucleotide control primers #1 and #2) were used as controls. Reaction mixtures were subjected to

thermal cycling after the addition of 1 µL PfuUltra HF DNA polymerase (2.5 U/µL). This was in accordance with the parameters outlined in **Chapter 5**, **Table 5.2**.

In the mutant strand synthesis using the TripleMaster PCR System (Eppendorf), pre-prepared solutions supplied in accordance to the manufacturer's instructions, were used. Complimentary nucleotides (designated oligonucleotide primer #1 and #2) were resuspended as a stock solution in autoclaved TE buffer **[7.12.]** to a concentration of 1000 ng/µL. 400 nM of oligonucleotide primers #1 and #2 were added to a reaction solution containing 1 - 2 ng template plasmids (pQE-9-IDO, as purified in **Section 7.6.1)** and molecular biology grade water to a volume of 20 µL (master mix-1). The master mix-1 was then mixed with 5 µL of 10x tuning buffer containing $MgCl_2$, dNTP mix (10mM) and molecular biology grade water to a volume of 30 µL (master mix-2). After mixing master mix-1 with master mix-2 the reaction mixtures were subjected to thermal cycling according to the parameters outlined in **Chapter 5**, **Table 5.5**.

> **[7.12] TE buffer**. 10 mM Tris and 1 mM EDTA was adjusted with 1 M HCl to pH 8.

After the thermo-cycling process, 1 µL DpnI restriction enzyme was added and mixed thoroughly. The mixture was then centrifuged and digested at 37ºC for 1 hour and ligated using T4 DNA Ligase overnight at 4ºC. 4 µL of the T4 DNA ligated DNA was added to a 50 µL competent cell, swirled and incubated on ice for 30 minutes.

7.6.3. Transformation of super-competent cells

1 µL of DpnI restriction enzyme (10 U/µL) was added to each amplification reaction. Addition of DpnI was followed by gentle mixing and incubation at 37 ºC for 1 hour. 5 µL of DpnI treated DNA was added to 100 µL of XL1-Blue super-competent cells containing 1.7 µL of β-mercaptoethanol. The reactions were incubated on ice for 30 minutes and then heat pulsed for 45 seconds at 42 ºC. Heat pulsing was followed by the addition of 0.9 mL Super Optimal broth with catabolite repression (SOC) media **[7.13]** and incubation at 37 ºC for one hour. 200 µL of the transformed competent cell mixture was plated on LB-ampicillin agar plates (**Section 7.3.1**) before an overnight incubation at 37 ºC. From an overnight growth in a 5 mL LB broth (containing ampicillin only to a final concentration of 100 µg/mL) at 37 ºC single colonies were selected and initially screened for mutations.

> **[7.13] SOC media**. 98% (v/v) SOB media (**Section 7.6.4**), 1% (v/v) 50:50 mixture of 1 M $MgCl_2.6H_2O$ and 1 M $MgSO_4.7H_2O$, 1% (v/v) 2 M glucose was dissolved in Milli-Q H_2O and autoclaved before use.

7.6.4. Preparation of chemically competent cells

A single colony of *E. coli* EC538 (pREP4) was inoculated into 10 mL LB media and grown overnight at 37 °C. The starter culture was used to inoculate Super Optimal Broth (SOB) media **[7.14]** that was incubated at 18 °C with shaking until an $OD_{600\ nm}$ of 0.6. The cells were then collected at low speed centrifugation (2500 G), before being washed in TB buffer **[7.15]**. The washed cells were again collected by centrifugation, before re-suspension in 7% (v/v) DMSO/TB buffer. They were stored at -80 °C for up to one month.

[7.14] SOB media. 2.0% (w/v) Tryptone, 0.5% (w/v) yeast extract, 1.0% (v/v) 1 M NaCl and 1.0% (v/v) 1 M KCl was dissolved in Milli-Q H_2O and autoclaved before use.

[7.15] TB buffer. PIPES, $CaCl_2$, KCl and $MnCl_2$ were dissolved in Milli-Q H_2O at concentrations of 10 mM, 15 mM, 250 mM, 55 mM, respectively. The pH was adjusted to 6.7 with 1 M HCl.

7.6.5. Transformation of chemically competent cells

Chemically competent *E. coli* EC538 (pREP4) cells (50 µL) (**Section 7.6.4**) were thawed slowly on ice. 5 µL of pQE-9-IDO mutant plasmid DNA was added to the competent cells. The reactions were incubated on ice for 30 minutes and then heat pulsed for 45 seconds at 42 ºC. Heat pulsing was followed by the addition of 0.5 mL Super Optimal broth with Catabolite repression (SOC) media (**Section 7.6.3**) and incubation at 37 ºC for one hour. 200 µL of the transformed competent cell mixture was plated on LB-ampicillin/kanamycin (100 µg/mL and 50 µg/mL, respectively) agar plates (**Section 7.3.1**) before an overnight incubation at 37 ºC, selecting for both the pQE-9-IDO mutant and pREP4.

7.6.6. Restriction enzyme digestion

Restriction enzyme digestions were set up using plasmid DNA isolated with a GenElute Plasmid Miniprep column (**Section 7.6.1**) to initially screen for the presence of mutations to the human IDO cDNA. To DNA (2 µL), restriction enzyme (0.5 µL), buffer (1 µL), BSA (1 µL) and sterile Milli-Q water (to 10 µL) were added. Reaction mixtures were incubated at 37 °C for 1 hour and 4 µL loaded onto a 1.2% agarose gel (**Section 7.6.7**).

7.6.7. Agarose electrophoresis

1.2% Agarose gels **[7.16]** were run in Tris-acetate-EDTA (TAE) buffer **[7.17]**. DNA, plasmid or restriction enzyme treated plasmid, was mixed in a 1:1 ratio with DNA loading dye **[7.18]** before application to the gel with the aid of a shark-tooth comb. 100 V was applied across gels in a Mini-Sub Cell (Bio-Rad). DNA was visualised by staining with ethidium bromide for 10 minutes, followed by illumination under UV light. Typically, lambda bacteriophage DNA digested with HindIII restriction enzyme was used as molecular weight marker, to determine the size of DNA fragments.

> **[7.16] Agarose gels**. 1.2% (w/v) Agarose was mixed in TAE buffer and heated in a microwave oven for 2 minutes on high (600 W). The hot solution of dissolved agarose was poured into a gel cast and allowed to set.
>
> **[7.17] TAE buffer**. 10x stock 4.8% (w/v) Tris base, 1.1% (v/v) glacial acetic acid, 2% (v/v) 0.5 M EDTA in Milli-Q H_2O. Solution was adjusted to pH 8 with 1 M NaOH. For final dilution, 10 times stock solution was diluted 1:10 with Milli-Q H_2O.
>
> **[7.18] DNA loading dye**. 0.25% (w/v) bromophenol blue and 10% (v/v) glycerol.

7.6.8. DNA sequence analysis

DNA sequencing analyses were run by Dr Paul Worden (Macquarie University) using an ABI Prism 377 DNA sequencer (Applied Biosciences). Sequencing reaction mixtures **[7.19]** were cycled with denaturing (96 °C for 30 seconds), annealing (60 °C for 15 seconds) and polymerisation (50 °C for 4 minutes), for a total of 35 cycles. The sequencing reaction mixture was precipitated by the addition of 3M sodium acetate (pH 4.6, 4 µL) and ethanol (100%, 58 µL) and was incubated at room temperature for 15 minutes. The sample was then centrifuged (13,000 G, 20 minutes) and the pellet was resuspended in ethanol (70%, 250 µL), re-centrifuged and the supernatant removed. The

pellet was then dried at 90 °C for 1 minute. The pellet was resuspended in formamide loading dye (6 µL) and the sample was heated (90 °C, 2 minutes) to promote denaturation and placed on ice prior to loading. A volume of 2 µL was loaded on to the DNA sequence gel **[7.20]** with the aid of a shark-tooth comb. The gel was then run for 10 hours on an ABI 377 DNA sequencer at a constant 37 W (~2350 V, 16 mA).

[7.19] Sequencing reaction mixtures. 2 µL of 1.6 pmol/µL primer (**Section 7.6.10**), 400 ng template DNA (**Section 7.6.2**), 8 µL Big Dye® ready reaction mix (Applied Biosciences) were mixed and sterile Milli-Q H_2O were added to make a final volume of 20 µL.

[7.20] DNA sequence gel. 4% (v/v) Acrylamide mix (19:1 acrylamide:bis-acrylamide), 10% (v/v) TBE **[7.21]**. For final dilution, 10 times stock solution was diluted 1:10 with Milli-Q H_2O, 0.0047% (v/v) of 10% (w/v) ammonium persulphate, 0.00065% (v/v) *N,N,N′,N′*-tetra-methylethylenediamine buffered with 34% (w/v) urea. This solution was injected into an ABI casting apparatus (Applied Biosciences) containing 48 cm glass plates. After a curing time of 2 hours, the gel was pre-run for 1 hour until the gel temperature was maintained at a constant 48 °C. Typical DNA sequence gel solution volume for 48 cm gels is 84.8 mL.

[7.21] TBE. 10x stock 1.62% (w/v) Tris base, 0.825% (v/v) boric acid, 0.12% (w/v) EDTA was dissolved in Milli-Q H_2O. The Solution was adjusted to pH 8.3 with 1 M NaOH.

7.6.9. Design of mutagenic primers

Primers were commercially synthesised by Sigma Genosys (Castle Hill, Australia). The mutagenic primers for mutagenesis using the Quikchange II site-directed mutagenesis kit (Stratagene) are given in **Table 7.1**. For each mutant, two complementary nucleotides were synthesised containing the desired mutation, flanked by an unmodified nucleotide sequence.

Table 7.1 Site-directed mutagenesis primers for Quikchange II.

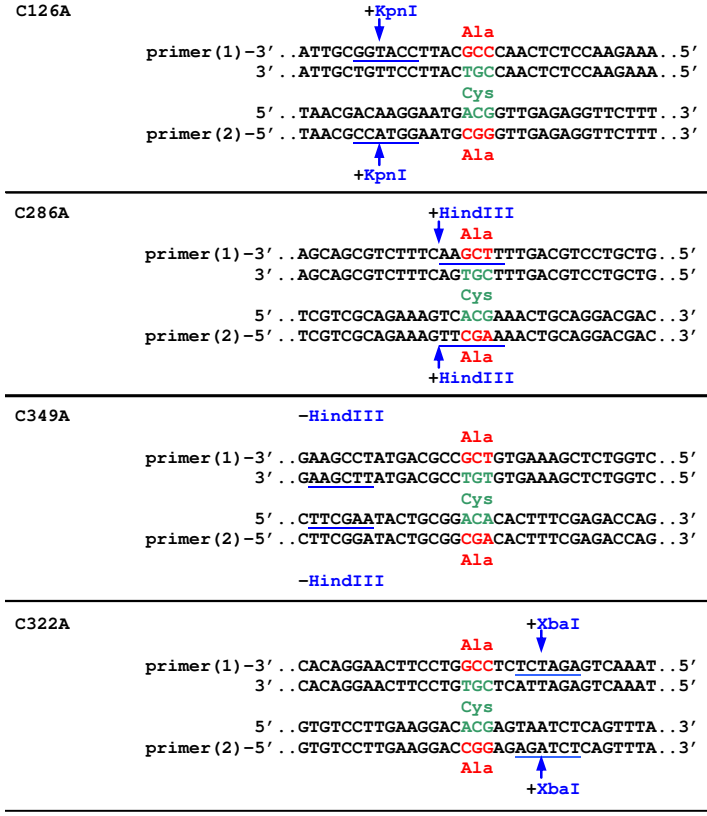

The mutagenic primers for mutagenesis using the TripleMaster PCR System are given in **Table 7.2.** The primers were purified by reversed phase cartridge chromatography at point of manufacture.

Table 7.2 Site-directed mutagenesis primers for TripleMaster PCR.

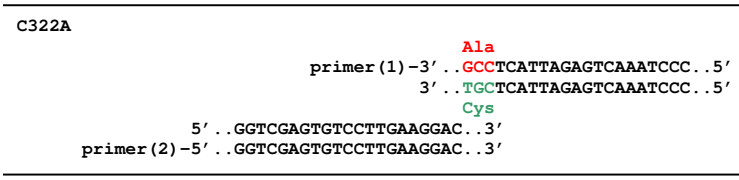

7.6.10. Design of sequencing primers

Primers for sequencing of pQE-9-IDO mutants, obtained from Sigma Genosys, are show in **Table 7.3**. Relative positions of primers on pQE-9-IDO are shown in **Figure 7.1**.

Table 7.3 Primers used for DNA sequence analysis for pQE-9-IDO mutants

Primer	Sequence
pQE-9 Promoter Region	CCCGAAAAGTGCCACCTG
pQE-9 Type III/IV	CGGATAACAATTTCACACAG
pQE-9 Reverse Sequencing	GTTCTGAGGTCATTACTGG

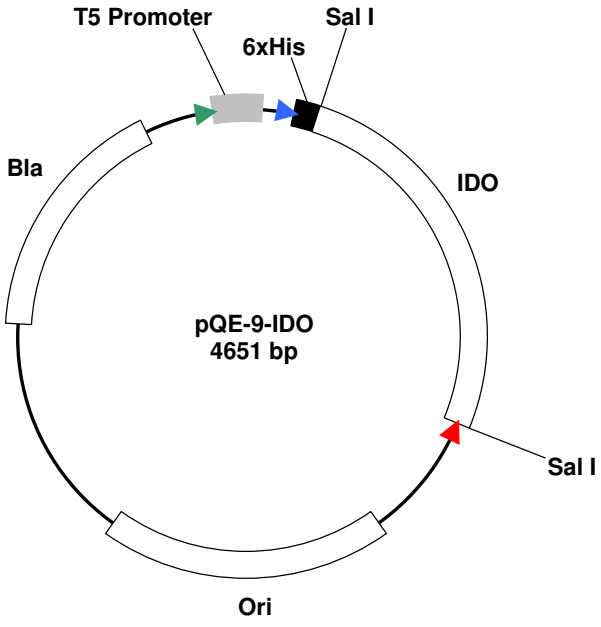

Figure 7.1 Diagrammatic representation of the expression plasmid pQE-9-IDO, which contains the human IDO cDNA inserted into the vector pQE-9, containing a hexahistidyl tag (black filled box), bacteriophage T5 promoter (grey filled box), β-lactamase gene (bla, open box) and *E. coli* origin of replication (ori, open box). Relative positions of DNA sequence primers are shown as coloured arrows, corresponding to the appropriate coloured text of **Table 7.3**. The plasmid is not drawn to scale and only Sal I restriction sites are shown.

References

1. Adam, R., D. Rüssing, O. Adams, A. Ailyati, K. Sik-Kim, H. Schroten, and W. Däubener, Role of human brain microvascular endothelial cells during central nervous system infection. Significance of indoleamine 2,3-dioxygenase in antimicrobial defence and immunoregulation. *Thrombosis and Haemostasis*, **2005**. *94*(2): p. 341-346.

2. Adams, O., K. Besken, C. Oberdorfer, C.R. MacKenzie, D. Russing, and W. Daubener, Inhibition of human herpes simplex virus type 2 by interferon gamma and tumor necrosis factor alpha is mediated by indoleamine 2,3-dioxygenase. *Microbes and Infection*, **2004**. *6*(9): p. 806-812.

3. Adams, O., K. Besken, C. Oberdörfer, C.R. MacKenzie, O. Takikawa, and W. Däubener, Role of indoleamine-2,3-dioxygenase in alpha/beta and gamma interferon-mediated antiviral effects against herpes simplex virus infections. *Journal of Virology*, **2004**. *78*(5): p. 2632-2636.

4. Adikari, S.B., H. Lian, H. Link, Y.M. Huang, and B.G. Xiao, Interferon-gamma-modified dendritic cells suppress B cell function and ameliorate the development of experimental autoimmune myasthenia gravis. *Clinical and Experimental Immunology*, **2004**. *138*(1): p. 230-23.

5. Aitken, J.B., S.E. Thomas, R. Stocker, S.R. Thomas, O. Takikawa, R.S. Armstrong, and P.A. Lay, Determination of the nature of the heme environment in nitrosyl indoleamine 2,3-dioxygenase using multiple-scattering analyses of x-ray absorption fine structure. *Biochemistry*, **2004**. *43*(17): p. 4892-4898.

6. Alberati-Giani, D., P. Malherbe, P. Ricciardi-Castagnoli, C. Köhler, S. Denis-Donini, and A.M. Cesura, Differential regulation of indoleamine 2,3-dioxygenase expression by nitric oxide and inflammatory mediators in IFN-gamma-activated murine macrophages and microglial cells. *Journal of Immunology*, **1997**. *159*(1): p. 419-426.

7. Alexander, A.M., M. Crawford, S. Bertera, W.A. Rudert, O. Takikawa, P.D. Robbins, and M. Trucco, Indoleamine 2,3-dioxygenase expression in transplanted NOD islets prolongs graft survival after adoptive transfer of diabetogenic splenocytes. *Diabetes*, **2002**. *51*(2): p. 356-365.

8. Astigiano, S., B. Morandi, R. Costa, L. Mastracci, A. D'Agostino, G.B. Ratto, G. Melioli, and G. Frumento, Eosinophil granulocytes account for indoleamine 2,3-dioxygenase-mediated immune escape in human non-small cell lung cancer. *Neoplasia*, **2005**. *7*(4): p. 390-396.

9. Austin, C.J.D., J. Mizdrak, A. Matin, N. Sirijovski, P. Kosim-Satyaputra, R.D. Willows, T.H. Roberts, R.J.W. Truscott, G. Polekhina, M.W. Parker, and J.F. Jamie, Optimised expression and purification of recombinant human indoleamine 2,3-dioxygenase. *Protein Expression and Purification*, **2004**. *37*(2): p. 392-398. (**Appendix 5**)

10. Austin, C.J.D, Structure and ligand-based investigations of indoleamine 2,3-dioxygenase, in *Chemistry and Biomolecular Sciences*. **2005**, Macquarie University: Sydney. pp. 207.

11. Austin, C.J.D, F. Astelbauer, P. Kosim-Satyaputra, H. Ball, R. Willows, J. Jamie, and N. Hunt, Mouse and human indoleamine 2,3-dioxygenase display some distinct biochemical and structural properties. *Amino Acids*, **2008**(February 15): p. 1-8. (**Appendix 6**)

12. Baban, B., P. Chandler, D. McCool, B. Marshall, D.H. Munn, and A.L. Mellor, Indoleamine 2,3-dioxygenase expression is restricted to fetal trophoblast giant cells during murine gestation and is maternal genome specific. *Journal of Reproductive Immunology*, **2004**. *61*(2): p. 67-77.

13. Baban, B., A.M. Hansen, P.R. Chandler, A. Manlapat, A. Bingaman, D.J. Kahler, D.H. Munn, and A.L. Mellor, A minor population of splenic dendritic cells expressing CD19 mediates IDO-dependent T cell suppression via type I IFN signaling following B7 ligation. *International Immunology*, **2005**. *17*(7): p. 909-919.

14. Baneyx, F. and M. Mujacic, Recombinant protein folding and misfolding in *Escherichia coli. Nature Biotechnology*, **2004**. *22*(11): p. 1399-1408.

15. Bradford, M.M, A rapid and sensitive method for the quantitation of microgram quantities of protein utilizing the principle of protein-dye binding, **1976**. *Analytical Biochemistry*. *72*(1): p. 248-254.

16. Barton, B.E., STAT3: a potential therapeutic target in dendritic cells for the induction of transplant tolerance. *Expert Opinion on Therapeutic Targets*, **2006**. *10*(3): p. 459-470.

17. Batabyal, D. and S.R. Yeh, Human tryptophan dioxygenase: a comparison to indoleamine 2,3-dioxygenase. *Journal of the American Chemical Society*, **2007**.

18. Bauer, T.M., L.P. Jiga, J.J. Chuang, M. Randazzo, G. Opelz, and P. Terness, Studying the immunosuppressive role of indoleamine 2,3-dioxygenase: tryptophan metabolites suppress rat allogeneic T-cell responses *in vitro* and *in vivo*. *Transplant International*, **2005**. *18*(1): p. 95-100.

19. Beutelspacher, S.C., R. Pillai, M.P. Watson, P.H. Tan, J. Tsang, M.O. McClure, A.J.T. George, and D.F.P. Larkin, Function of indoleamine 2,3-dioxygenase in corneal allograft rejection and prolongation of allograft survival by over-expression. *European Journal of Immunology*, **2006**. *36*(3): p. 690-700.

20. Beutelspacher, S.C., P.H. Tan, M.O. McClure, D.F.P. Larkin, R.I. Lechler, and A.J.T. George, Expression of indoleamine 2,3-dioxygenase (IDO) by endothelial cells: implications for the control of alloresponses. *American Journal of Transplantation*, **2006**. *6*(6): p. 1320-1330.

21. Boasso, A., J.P. Herbeuval, A.W. Hardy, C. Winkler, and G.M. Shearer, Regulation of indoleamine 2,3-dioxygenase and tryptophanyl-tRNA-synthetase by CTLA-4-Fc in human CD4+ T cells. *Blood*, **2005**. *105*(4): p. 1574-1581.

22. Bodaghi, B., O. Goureau, D. Zipeto, L. Laurent, J.L. Virelizier, and S. Michelson, Role of IFN-gamma-induced indoleamine 2,3-dioxygenase and inducible nitric oxide synthase in the replication of human cytomegalovirus in retinal pigment epithelial cells. *Journal of Immunology*, **1999**. *162*(2): p. 957-964.

23. Bonney, E.A. and P. Matzinger, Much IDO about pregnancy. *Nature Medicine*, **1998**. *4*: p. 1128 - 1129.

24. Bowden, G.A., A.M. Paredes, and G. Georgiou, Structure and morphology of protein inclusion bodies in *Escherichia coli*. *Nature Biotechnology*, **1991**. *9*(8): p. 725-730.

25. Brandacher, G., A. Perathoner, R. Ladurner, S. Schneeberger, P. Obrist, C. Winkler, E.R. Werner, G. Werner-Felmayer, H.G. Weiss, G. Göbel, R. Margreiter, A. Königsrainer, D. Fuchs, and A. Amberger, Prognostic value of indoleamine 2,3-dioxygenase expression in colorectal cancer: effect on tumor-infiltrating T cells. *Clinical Cancer Research*, **2006**. *12*(4): p. 1144-1151.

26. Braun, D., R.S. Longman, and M.L. Albert, A two-step induction of indoleamine 2,3-dioxygenase (IDO) activity during dendritic-cell maturation. *Blood*, **2005**. *106*(7): p. 2375-2381.

27. Britan, A., V. Maffre, S. Tone, and J.R. Drevet, Quantitative and spatial differences in the expression of tryptophan-metabolizing enzymes in mouse epididymis. *Cell and Tissue Research*, **2006**. *324*(2): p. 301-310.

28. Burke, F., R.G. Knowles, and F.R. Balkwill, The role of indoleamine 2,3-dioxygenase in the anti-tumour activity of human interferon-gamma *in vivo*. *International Journal of Cancer*, **1995**. *60*(1): p. 115-122

29. Burudi, E.M.E., M.C.G. Marcondes, D.D. Watry, M. Zandonatti, M.A. Taffe, and H.S. Fox, Regulation of indoleamine 2,3-dioxygenase expression in simian immunodeficiency virus-infected monkey brains. *Journal of Virology*, **2002**. *76*(23): p. 12233-12241.

30. Cady, S.G. and M. Sono, 1-Methyl-DL-tryptophan, beta-(3-benzofuranyl)-DL-alanine (the oxygen analog of tryptophan), and beta-[3-benzo(b)thienyl]-DL-alanine (the sulfur analog of tryptophan) are competitive inhibitors for indoleamine 2,3-dioxygenase. *Archives of Biochemistry and Biophysics*, **1991**. *291*(2): p. 326-333.

31. Cannon, M.J. and J.L. Pate, Indoleamine 2,3-dioxygenase participates in the interferon-gamma-induced cell death process in cultured bovine luteal cells. *Biology of Reproduction*, **2006**. *74*(3): p. 552-559.

32. Carlin, J.M., E.C. Borden, P.M. Sondel, and G.I. Byrne, Biologic-response-modifier-induced indoleamine 2,3-dioxygenase activity in human peripheral blood mononuclear cell cultures. *Journal of Immunology*, **1987**. *139*(7): p. 2414-2418.

33. Carlin, J.M., E.C. Borden, and G.I. Byrne, Interferon-induced indoleamine 2,3-dioxygenase activity inhibits *Chlamydia psittaci* replication in human macrophages. *Journal of Interferon Research*, **1989**. *9*(3): p. 329-337.

34. Carlin, J.M., E.C. Borden, and G.I. Byrne, Enhancement of indoleamine 2,3-dioxygenase activity in cancer patients receiving interferon-beta Ser. *Journal of Interferon Research*, **1989**. *9*(2): p. 167-173.

35. Carlin, J.M., E.C. Borden, P.M. Sondel, and G.I. Byrne, Interferon-induced indoleamine 2,3-dioxygenase activity in human mononuclear phagocytes. *Journal of Leukocyte Biology*, **1989**. *45*(1): p. 29-34.

36. Carlin, J.M., Y. Ozaki, G.I. Byrne, R.R. Brown, and E.C. Borden, Interferons and indoleamine 2,3-dioxygenase: role in antimicrobial and antitumor effects. *Experientia*, **1989**. *45*(6): p. 535-541.

37. Chaves, A.C., I.P. Cerávolo, J.A. Gomes, C.L. Zani, A.J. Romanha, and R.T. Gazzinelli, IL-4 and IL-13 regulate the induction of indoleamine 2,3-dioxygenase activity and the control of *Toxoplasma gondii* replication in human fibroblasts activated with IFN-gamma. *European Journal of Immunology*, **2001**. *31*(2): p. 333-344.

38. Chiarugi, A., P. Dello Sbarba, A. Paccagnini, S. Donnini, S. Filippi, and F. Moroni, Combined inhibition of indoleamine 2,3-dioxygenase and nitric oxide synthase modulates neurotoxin release by interferon-gamma-activated macrophages. *Journal of Leukocyte Biology*, **2000**. *68*(2): p. 260-266.

39. Choi, B.K., T. Asai, D.S. Vinay, Y.H. Kim, and B.S. Kwon, 4-1BB-mediated amelioration of experimental autoimmune uveoretinitis is caused by indoleamine 2,3-dioxygenase-dependent mechanisms. *Cytokine*, **2006**. *34*(5): p. 233-242.

40. Chon, S.Y., H.H. Hassanain, R. Pine, and S.L. Gupta, Involvement of two regulatory elements in interferon-gamma-regulated expression of human indoleamine 2,3-dioxygenase gene. *Journal of Interferon and Cytokine Research*, **1995**. *15*(6): p. 517-526.

41. Chon, S.Y., H.H. Hassanain, and S.L. Gupta, Cooperative role of interferon regulatory factor 1 and p91 (STAT1) response elements in interferon-gamma-inducible expression of human indoleamine 2,3-dioxygenase gene. *Journal of Biological Chemistry*, **1996**. *271*(29): p. 17247-17252.

42. Christen, S., E. Peterhans, and R. Stocker, Antioxidant activities of some tryptophan metabolites: possible implication for inflammatory diseases. *Proceedings of the National Academy of Sciences of the United States of America*, **1990**. *87*(7): p. 2506-2510.

43. Chung, L. W., X. Li, H. Sugimoto, Y. Shiro, K. Morokuma, Density functional theory study on a missing piece in understanding of heme chemistry: the reaction mechanism for indoleamine 2,3-dioxygenase and tryptophan 2,3-dioxygenase. *Journal of the American Chemical Society*, **2008**, *130(37)*: p. 12299-12309.

44. Connor, T.J., N. Starr, J.B. O'Sullivan, and A. Harkin, Induction of indolamine 2,3-dioxygenase and kynurenine 3-monooxygenase in rat brain following a systemic inflammatory challenge: a role for IFN-[gamma]? *Neuroscience Letters*, **2008**. *In Press, Corrected Proof* (June 7, 2008): p. 1-6.

45. Cook, J.S., C.I. Pogson, and S.A. Smith, Indoleamine 2,3-dioxygenase. A new, rapid, sensitive radiometric assay and its application to the study of the enzyme in rat tissues. *Biochemical Journal*, **1980**. *189*(3): p. 461-466.

46. Cozzi, A., A.L. Zignego, R. Carpendo, T. Biagiotti, A. Aldinucci, M. Monti, C. Giannini, M. Rosselli, G. Laffi, and F. Moroni, Low serum tryptophan levels, reduced macrophage IDO activity and high frequency of psychopathology in HCV patients. *Journal of Viral Hepatitis*, **2006**. *13*(6): p. 402-408.

47. Cupurdija, K., D. Azzola, U. Hainz, A. Gratchev, A. Heitger, O. Takikawa, S. Goerdt, R. Wintersteiger, G. Dohr, and P. Sedlmayr, Macrophages of human first trimester decidua express markers associated to alternative activation. *American Journal of Reproductive Immunology*, **2004**. *51*(2): p. 117-122.

48. Curreli, S., F. Romerio, P. Mirandola, P. Barion, K. Bemis, and D. Zella, Human primary CD4 + T cells activated in the presence of IFN-alpha 2b express functional indoleamine 2,3-dioxygenase. *Journal of Interferon and Cytokine Research*, **2001**. *21*(6): p. 431-437.

49. Dai, W. and S.L. Gupta, Regulation of indoleamine 2,3-dioxygenase gene expression in human fibroblasts by interferon-gamma. Upstream control region discriminates between interferon-gamma and interferon-alpha. *Journal of Biological Chemistry*, **1990**. *265*(32): p. 19871-19877.

50. Dai, W. and S.L. Gupta, Molecular cloning, sequencing and expression of human interferon-gamma-inducible indoleamine 2,3-dioxygenase cDNA. *Biochemical and Biophysical Research Communications*, **1990**. *168*(1): p. 1-8.

51. Dai, W., H. Pan, O. Kwok, and J.P. Dubey, Human indoleamine 2,3-dioxygenase inhibits *Toxoplasma gondii* growth in fibroblast cells. *Journal of Interferon Research*, **1994**. *14*(6): p. 313-317.

52. Daley-Yates, P.T., A.P. Powell, and L.L. Smith, Pulmonary indoleamine 2,3-dioxygenase activity and its significance in the response of rats, mice, and rabbits to oxidative stress. *Toxicology and Applied Pharmacology*, **1988**. *96*(2): p. 222-232.

53. Dang, Y., W.E. Dale, and O.R. Brown, Comparative effects of oxygen on indoleamine 2,3-dioxygenase and tryptophan 2,3-dioxygenase of the kynurenine pathway. *Free Radical Biology and Medicine*, **2000**. *28*(4): p. 615-624.

54. Däubener, W. and C.R. MacKenzie, IFN-gamma activated indoleamine 2,3-dioxygenase activity in human cells is an antiparasitic and an antibacterial effector mechanism. *Advances in Experimental Medicine and Biology*, **1999**. *467*(1): p. 517-524.

55. Däubener, W., B. Spors, C. Hucke, R. Adam, M. Stins, K.S. Kim, and H. Schroten, Restriction of *Toxoplasma gondii* growth in human brain microvascular endothelial cells by activation of indoleamine 2,3-dioxygenase. *Infection and Immunity*, **2001**. *69*(10): p. 6527-6531.

56. Depboylu, C., T.A. Reinhart, O. Takikawa, Y. Imai, H. Maeda, H. Mitsuya, D. Rausch, L.E. Eiden, and E. Weihe, Brain virus burden and indoleamine 2,3-dioxygenase expression during lentiviral infection of rhesus monkey are concomitantly lowered by 6-chloro-2',3'-dideoxyguanosine. *European Journal of Neuroscience*, **2004**. *19*(11): p. 2997-3005.

57. Du, M.X., W.D. Sotero-Esteva, and M.W. Taylor, Analysis of transcription factors regulating induction of indoleamine 2,3-dioxygenase by IFN-gamma. *Journal of Interferon and Cytokine Research*, **2000**. *20*(2): p. 133-142.

58. Edelstein, M.P., Y. Ozaki, and D.S. Duch, Synergistic effects of phorbol ester and INF-gamma on the induction of indoleamine 2,3-dioxygenase in THP-1 monocytic leukemia cells. *Journal of Immunology*, **1989**. *143*(9): p. 2969-2973.

59. Eguchi, N., Y. Watanabe, K. Kawanishi, Y. Hashimoto, and O. Hayaishi, Inhibition of indoleamine 2,3-dioxygenase and tryptophan 2,3-dioxygenase by beta-carboline and indole derivatives. *Archives of Biochemistry and Biophysics*, **1984**. *232*(2): p. 602-609.

60. Englander, S. W., D. B. Calhoun and J. J. Englander, Biochemistry without oxygen. *Analytical Biochemistry*, **1987**. *161*(2): p.300-306.

61. Espey, M.G. and M.A. Namboodiri, Selective metabolism of kynurenine in the spleen in the absence of indoleamine 2,3-dioxygenase induction. *Immunology Letters*, **2000**. *71*(1): p. 67-72.

62. Fallarino, F., C. Vacca, C. Orabona, M.L. Belladonna, R. Bianchi, B. Marshall, D.B. Keskin, A.L. Mellor, M.C. Fioretti, U. Grohmann, and P. Puccetti, Functional expression of indoleamine 2,3-dioxygenase by murine CD8 alpha(+) dendritic cells. *International Immunology*, **2002**. *14*(1): p. 65-68.

63. Fallarino, F., C. Orabona, C. Vacca, R. Bianchi, S. Gizzi, C. Asselin-Paturel, M.C. Fioretti, G. Trinchieri, U. Grohmann, and P. Puccetti, Ligand and cytokine dependence of the immunosuppressive pathway of tryptophan catabolism in plasmacytoid dendritic cells. *International Immunology*, **2005**. *17*(11): p. 1429-1438.

64. Feng, G.S. and M.W. Taylor, Interferon gamma-resistant mutants are defective in the induction of indoleamine 2,3-dioxygenase. *Proceedings of the National Academy of Sciences of the United States of America*, **1989**. *86*(18): p. 7144-7148.

65. Ferry, G., C. Ubeaud, P.H. Lambert, S. Bertin, F. Cogé, P. Chomarat, P. Delagrange, B. Serkiz, J.P. Bouchet, R.J.W. Truscott, and J.A. Boutin, Molecular evidence that melatonin is enzymatically oxidized in a different manner than tryptophan: investigations with both indoleamine 2,3-dioxygenase and myeloperoxidase. *Biochemical Journal*, **2005**. *388*(1): p. 205-215.

66. Friberg, M., R. Jennings, M. Alsarraj, S. Dessureault, A. Cantor, M. Extermann, A.L. Mellor, D.H. Munn, and S.J. Antonia, Indoleamine 2,3-dioxygenase contributes to tumor cell evasion of T cell-mediated rejection. *International Journal of Cancer*, **2002**. *101*(2): p. 151-155.

67. Fruk, L., J. Kuhlmann, and C.M. Niemeyer, Analysis of heme-reconstitution of apoenzymes by means of surface plasmon resonance. *Chemical communications*, **2009**. *2*(1): p. 230-232.

68. Fujigaki, S., K. Saito, K. Sekikawa, S. Tone, O. Takikawa, H. Fujii, H. Wada, A. Noma, and M. Seishima, Lipopolysaccharide induction of indoleamine 2,3-dioxygenase is mediated dominantly by an IFN-gamma-independent mechanism. *European Journal of Immunology*, **2001**. *31*(8): p. 2313-2318.

69. Fujigaki, S., K. Saito, M. Takemura, N. Maekawa, Y. Yamada, H. Wada, and M. Seishima, L-Tryptophan-L-kynurenine pathway metabolism accelerated by *Toxoplasma gondii* infection is abolished in gamma interferon-gene-deficient mice: cross-regulation between inducible nitric oxide synthase and indoleamine 2,3-dioxygenase. *Infection and Immunity*, **2002**. *70*(2): p. 779-786.

70. Fujigaki, S., M. Takemura, H. Hamakawa, M. Seishima, and K. Saito, The mechanism of interferon-gamma induced anti *Toxoplasma gondii* by indoleamine 2,3-dioxygenase and/or inducible nitric oxide synthase vary among tissues. *Advances in Experimental Medicine and Biology*, **2003**. *527*(1): p. 97-103.

71. Fujigaki, H., K. Saito, S. Fujigaki, M. Takemura, K. Sudo, H. Ishiguro, and M. Seishima, The signal transducer and activator of transcription 1alpha and interferon regulatory factor 1 are not essential for the induction of indoleamine 2,3-dioxygenase by lipopolysaccharide: involvement of p38 mitogen-activated protein kinase and nuclear factor-kappaB pathways, and synergistic effect of several proinflammatory cytokines. *Journal of Biochemistry*, **2006**. *139*(4): p. 655-662.

72. Fujiwara, M., M. Shibata, Y. Watanabe, T. Nukiwa, F. Hirata, N. Mizuno, and O. Hayaishi, Indoleamine 2,3-dioxygenase. Formation of L-kynurenine from L-tryptophan in cultured rabbit fineal gland. *Journal of Biological Chemistry*, **1978**. *253*(17): p. 6081-6085.

73. Fujiwara, M., M. Shibata, Y. Nomiyama, T. Sugimoto, F. Hirata, T. Tokuyama, S. Senoh, and O. Hayaishi, Formation of 5-hydroxykynurenine and 5-hydroxykynurenamine from 5-hydroxytryptophan in rabbit small intestine. *Proceedings of the National Academy of Sciences of the United States of America*, **1979**. *76*(3): p. 1145-1149.

74. Funeshima, N., M. Fujino, Y. Kitazawa, Y. Hara, Y. Hara, K. Hayakawa, T. Okuyama, H. Kimura, and X.K. Li, Inhibition of allogeneic T-cell responses by dendritic cells expressing transduced indoleamine 2,3-dioxygenase. *Journal of Gene Medicine*, **2005**. *7*(5): p. 565-575.

75. Furset, G., Y. Floisand, and M. Sioud, Impaired expression of indoleamine 2,3-dioxygenase in monocyte-derived dendritic cells in response to Toll-like receptor-7/8 ligands. *Immunology*, **2007** (August 28): p. 1-9.

76. Gajewski, T.F., Overcoming immune resistance in the tumor microenvironment by blockade of indoleamine 2,3-dioxygenase and programmed death ligand 1. *Current Opinion in Investigational Drugs*, **2004**. *5*(12): p. 1279-1283.

77. Gaspari, P., T. Banerjee, W.P. Malachowski, A.J. Muller, G.C. Prendergast, J. DuHadaway, S. Bennett, and A.M. Donovan, Structure-activity study of brassinin derivatives as indoleamine 2,3-dioxygenase inhibitors. *Journal of Medicinal Chemistry*, **2006**. *49*(2): p. 684-692.

78. Ghahary, A., Y. Li, E.E. Tredget, R.T. Kilani, T. Iwashina, A. Karami, and X. Lin, Expression of indoleamine 2,3-dioxygenase in dermal fibroblasts functions as a local immunosuppressive factor. *Journal of Investigative Dermatology*, **2004**. *122*(4): p. 953-964.

79. Gillet-Hladky, S., C.M. de Carvalho, J. Bernaud, C. Bendahou, C. Bloy, and D. Rigal, Rabbit antithymocyte globulin inhibits monocyte-derived dendritic cells maturation in vitro and polarizes monocyte-derived dendritic cells towards tolerogenic dendritic cells expressing indoleamine 2,3-dioxygenase. *Transplantation*, **2006**. *82*(7): p. 965-974.

80. González, Á., N. Varo, E. Alegre, A. Díaz, I. Melero, and S.M. Gregory, Immunosuppression routed via the kynurenine pathway: a biochemical and pathophysiologic approach, in *Advances in Clinical Chemistry*. **2008**, Elsevier. p. 155-197.

81. González-Hernandez, A., J. LeMaoult, A. Lopez, E. Alegre, J. Caumartin, S. Le Rond, M. Daouya, P. Moreau, and E.D. Carosella, Linking two immuno-suppressive molecules: indoleamine 2,3-dioxygenase can modify HLA-G cell-surface expression. *Biology of Reproduction*, **2005**. *73*(3): p. 571-578.

82. Grant, R.S., H. Naif, S.J. Thuruthyil, N. Nasr, T. Littlejohn, O. Takikawa, and V. Kapoor, Induction of indoleamine 2,3-dioxygenase in primary human macrophages by HIV-1. *Redox Report*, **2000**. *5*(2): p. 105-107.

83. Grant, R. and V. Kapoor, Inhibition of indoleamine 2,3-dioxygenase activity in IFN-gamma stimulated astroglioma cells decreases intracellular NAD levels. *Biochemical Pharmacology*, **2003**. *66*(6): p. 1033-1036.

84. Grohmann, U., F. Fallarino, R. Bianchi, M.L. Belladonna, C. Vacca, C. Orabona, C. Uyttenhove, M.C. Fioretti, and P. Puccetti, IL-6 inhibits the tolerogenic function of CD8alpha+ dendritic cells expressing indoleamine 2,3-dioxygenase. *Journal of Immunology*, **2001**. *167*(1): p. 708-714.

85. Grossmann, M.K., The use of phenylmethylsulfonyl fluoride in the study of catabolite inactivation and repression in intact cells of *Saccharomyces cerevesiae*. *Archives of Microbiology*, **1980**. *124*(2): p293-295.

86. Guillemin, G.J., B.J. Brew, C.E. Noonan, O. Takikawa, and K.M. Cullen, Indoleamine 2,3-dioxygenase and quinolinic acid immunoreactivity in Alzheimer's disease hippocampus. *Neuropathology and Aplied Neurobiology*, **2005**. *31*(4): p. 395-404.

87. Guillemin, G.J., G. Smythe, O. Takikawa, and B.J. Brew, Expression of indoleamine 2,3-dioxygenase and production of quinolinic acid by human microglia, astrocytes, and neurons. *Glia*, **2005**. *49*(1): p. 15-23.

88. Gupta, S.L., J.M. Carlin, P. Pyati, W. Dai, E.R. Pfefferkorn, and M.J. Murphy, Antiparasitic and antiproliferative effects of indoleamine 2,3-dioxygenase enzyme expression in human fibroblasts. *Infection and Immunity*, **1994**. *62*(6): p. 2277-2284.

89. Gurtner, G.J., R.D. Newberry, S.R. Schloemann, K.G. McDonald, and W.F. Stenson, Inhibition of indoleamine 2,3-dioxygenase augments trinitrobenzene sulfonic acid colitis in mice. *Gastroenterology*, **2003**. *125*(6): p. 1762-1773.

90. Gutierrez, G., J.S. Fitzgerald, T. Pohlmann, and I. Hoppe, Comparative effects of L-tryptophan and 1-methyl-tryptophan on immunoregulation induced by sperm, human pre-implantation embryo and trophoblast supernatants. *American Journal of Reproductive Immunology*, **2003**. *50*(4): p. 309-315.

91. Habara-Ohkubo, A., O. Takikawa, and R. Yoshida, Cloning and expression of a cDNA encoding mouse indoleamine 2,3-dioxygenase. *Gene*, **1991**. *105*(2): p. 221-227.

92. Habara-Ohkubo, A., T. Shirahata, O. Takikawa, and R. Yoshida, Establishment of an antitoxoplasma state by stable expression of mouse indoleamine 2,3-dioxygenase. *Infection and Immunity*, **1993**. *61*(5): p. 1810-1813.

93. Hansen, A.M., C. Driussi, V. Turner, O. Takikawa, and N.H. Hunt, Tissue distribution of indoleamine 2,3-dioxygenase in normal and malaria-infected tissue. *Redox Report*, **2000**. *5*(2): p. 112-115.

94. Hansen, A.M., H.J. Ball, A.J. Mitchell, J. Miu, O. Takikawa, and N.H. Hunt, Increased expression of indoleamine 2,3-dioxygenase in murine malaria infection is predominantly localised to the vascular endothelium. *International Journal for Parasitology*, **2004**. *34*(12): p. 1309-1319.

95. Hassanain, H.H., S.Y. Chon, and S.L. Gupta, Differential regulation of human indoleamine 2,3-dioxygenase gene expression by interferons-gamma and -alpha. Analysis of the regulatory region of the gene and identification of an interferon-gamma-inducible DNA-binding factor. *Journal of Biological Chemistry*, **1993**. *268*(7): p. 5077-5084.

96. Hayaishi, O., Properties and function of indoleamine 2,3-dioxygenase. *Journal of Biochemistry*, **1976**. *79*(4): p. 13-21.

97. Hayaishi, O., F. Hirata, T. Ohnishi, J.P. Henry, I. Rosenthal, and A. Katoh, Indoleamine 2,3-dioxygenase: incorporation of $18O_2$- and $18O_2$ into the reaction products. *Journal of Biological Chemistry*, **1977**. *252*(10): p. 3548-3550.

98. Hayaishi, O., T. Osamu, and Y. Ryotaro, Indoleamine 2,3-dioxygenase: properties and functions of a superoxide utilizing enzyme, in *Progress in Inorganic Chemistry*, J.L. Stephen, Editor. **1990**. p. 75-95.

99. Hayakawa, S., No cancer in cancers: evolutionary trade-off between successful viviparity and tumor escape from the adaptive immune system. *Medical Hypotheses*, **2006**. *66*(5): p. 888-897.

100. Hayashi, T., S.P. Rao, K. Takabayashi, J.H. Van Uden, R.S. Kornbluth, S.M. Baird, M.W. Taylor, D.A. Carson, A. Catanzaro, and E. Raz, Enhancement of innate immunity against *Mycobacterium avium* infection by immunostimulatory DNA is mediated by indoleamine 2,3-dioxygenase. *Infection and Immunity*, **2001**. *69*(10): p. 6156-6164.

101. Hayashi, T., L. Beck, C. Rossetto, X. Gong, O. Takikawa, K. Takabayashi, D.H. Broide, D.A. Carson, and E. Raz, Inhibition of experimental asthma by indoleamine 2,3-dioxygenase. *Journal of Clinical Investigation*, **2004**. *114*(2): p. 270-279.

102. Heikkinen, J., M. Mottonen, J. Komi, A. Alanen, and O. Lassila, Phenotypic characterization of human decidual macrophages. *Clinical and Experimental Immunology*, **2003**. *131*(3): p. 498-505.

103. Heikkinen, J., M. Mottonen, A. Alanen, and O. Lassila, Phenotypic characterization of regulatory T cells in the human decidua. *Clinical and Experimental Immunology*, **2004**. *136*(2): p. 373-378.

104. Herber, D.L., S. Nagaraj, J.Y. Djeu, and D.I. Gabrilovich, Mechanism and therapeutic reversal of immune suppression in cancer. *Cancer Research*, **2007**. *67*(11): p. 5067-5069.

105. Heyes, M.P., K. Saito, D. Jacobowitz, S.P. Markey, O. Takikawa, and J.H. Vickers, Poliovirus induces indoleamine-2,3-dioxygenase and quinolinic acid synthesis in macaque brain. *Federation of American Societies for Experimental Biology Journal*, **1992**. *6*(11): p. 2977-2989.

106. Hill, M., V. Pereira, C. Chauveau, R. Zagani, S. Remy, L. Tesson, D. Mazal, L. Ubillos, R. Brion, K. Asghar, K. Ashgar, M.F. Mashreghi, K. Kotsch, J. Moffett, C. Doebis, M. Seifert, J. Boczkowski, E. Osinaga, and I. Anegon, Heme oxygenase-1 inhibits rat and human breast cancer cell proliferation: mutual cross inhibition with indoleamine 2,3-dioxygenase. *Federation of American Societies for Experimental Biology Journal*, **2005**. *19*(14): p. 1957-1968.

107. Hirata, F. and O. Hayaishi, Studies on indoleamine 2,3-dioxygenase. I. Superoxide anion as substrate. *Journal of Biological Chemistry*, **1975**. *250*(15): p. 5960-5966.

108. Hirata, F., T. Ohnishi, and O. Hayaishi, Indoleamine 2,3-dioxygenase. Characterization and properties of enzyme. O_2-complex. *Journal of Biological Chemistry*, **1977**. *252*(13): p. 4637-4642.

109. Hissong, B.D., G.I. Byrne, M.L. Padilla, and J.M. Carlin, Upregulation of interferon-induced indoleamine 2,3-dioxygenase in human macrophage cultures by lipopolysaccharide, muramyl tripeptide, and interleukin-1. *Cellular Immunology*, **1995**. *160*(2): p. 264-269.

110. Hissong, B.D. and J.M. Carlin, Potentiation of interferon-induced indoleamine 2,3-dioxygenase mRNA in human mononuclear phagocytes by lipopolysaccharide and interleukin-1. *Journal of Interferon and Cytokine Research*, **1997**. *17*(7): p. 387-393.

111. Honig, A., L. Rieger, J. Dietl, and U. Kämmerer, Mechanisms regulating the expression of indoleamine 2,3-dioxygenase during decidualization of human endometrium. *Human Reproduction*, **2004**. *19*(11): p. 2683-2684.

112. Honig, A., L. Rieger, M. Kapp, M. Sütterlin, J. Dietl, and U. Kämmerer, Indoleamine 2,3-dioxygenase (IDO) expression in invasive extravillous trophoblast supports role of the enzyme for materno-fetal tolerance. *Journal of Reproductive Immunology*, **2004**. *61*(2): p. 79-86.

113. Hou, D., A.J. Muller, M.D. Sharma, J. DuHadaway, T. Banerjee, M. Johnson, A.L. Mellor, G.C. Prendergast, and D.H. Munn, Inhibition of indoleamine 2,3-dioxygenase in dendritic cells by stereoisomers of 1-methyl-tryptophan correlates with antitumor responses. *Cancer Research*, **2007**. *67*(2): p. 792-801.

114. Hsu, M.C., R.W. Woody, The origin of the heme Cotton effects in myoglobin and hemoglobin. *Journal of the American Chemical Society*, **1971**. *93(14)*: p. 3515-3525.

115. Hucke, C., C.R. MacKenzie, K.D.Z. Adjogble, O. Takikawa, and W. Däubener, Nitric oxide-mediated regulation of gamma interferon-induced bacteriostasis: inhibition and degradation of human indoleamine 2,3-dioxygenase. *Infection and Immunity*, **2004**. *72*(5): p. 2723-2730.

116. Hwang, S.L., N.P.Y. Chung, J.K.Y. Chan, and C.L.S. Lin, Indoleamine 2,3-dioxygenase (IDO) is essential for dendritic cell activation and chemotactic responsiveness to chemokines. *Cell Research*, **2005**. *15*(3): p. 167-175.

117. Hwu, P., M.X. Du, R. Lapointe, M. Do, M.W. Taylor, and H.A. Young, Indoleamine 2,3-dioxygenase production by human dendritic cells results in the inhibition of T Cell proliferation. *Journal of Immunology*, **2000**. *164*(7): p. 3596-3599.

118. Ino, K., E. Yamamoto, K. Shibata, H. Kajiyama, N. Yoshida, M. Terauchi, A. Nawa, T. Nagasaka, O. Takikawa, and F. Kikkawa, Inverse correlation between tumoral indoleamine 2,3-dioxygenase expression and tumor-infiltrating lymphocytes in endometrial cancer: its association with disease progression and survival. *Clinical Cancer Research*, **2008**. *14*(8): p. 2310-2317.

119. Ishio, T., S. Goto, K. Tahara, S. Tone, K. Kawano, and S. Kitano, Immunoactivative role of indoleamine 2,3-dioxygenase in human hepatocellular carcinoma. *Journal of Gastroenterology and Hepatology*, **2004**. *19*(3): p. 319-326.

120. Iwamoto, Y. and R. Kido, Operative deliveries induce a significant activation of indoleamine 2,3-dioxygenase in human placenta: existence of a new mechanism for activating the enzyme. *Materia Medica Polona*, **1995**. *27*(3): p. 111-114.

121. Jung, Y., J. Kwak, and Y. Lee, High-level production of heme-containing holoproteins in *Escherichia coli. Applied Microbiology and Biotechnology*, **2001**. *55*(2): p. 187-191.

122. Kadoya, A., S. Tone, H. Maeda, Y. Minatogawa, and R. Kido, Gene structure of human indoleamine 2,3-dioxygenase. *Biochemical and Biophysical Research Communications*, **1992**. *189*(1): p. 530-536.

123. Kai, S., S. Goto, K. Tahara, A. Sasaki, K. Kawano, and S. Kitano, Inhibition of indoleamine 2,3-dioxygenase suppresses NK cell activity and accelerates tumor growth. *Journal of Experimental Therapeutics and Oncology*, **2003**. *3*(6): p. 336-345.

124. Kai, S., S. Goto, K. Tahara, A. Sasaki, S. Tone, and S. Kitano, Indoleamine 2,3-dioxygenase is necessary for cytolytic activity of natural killer cells. *Scandinavian Journal of Immunology*, **2004**. *59*(2): p. 177-182.

125. Kamimura, S., K. Eguchi, M. Yonezawa, and K. Sekiba, Localization and developmental change of indoleamine 2,3-dioxygenase activity in the human placenta. *Acta Medica Okayama*, **1991**. *45*(3): p. 135-139.

126. Katz, J.B., A.J. Muller, and G.C. Prendergast, Indoleamine 2,3-dioxygenase in T-cell tolerance and tumoral immune escape. *Immunological Reviews*, **2008**. *222*(1): p. 206-221.

127. King, N.J.C. and S.R. Thomas, Molecules in focus: indoleamine 2,3-dioxygenase. *The International Journal of Biochemistry and Cell Biology*, **2007**. *39*(12): p. 2167-2172.

128. Kobayashi, K., K. Hayashi, and M. Sono, Effects of tryptophan and pH on the kinetics of superoxide radical binding to indoleamine 2,3-dioxygenase studied by pulse radiolysis. *Journal of Biological Chemistry*, **1989**. *264*(26): p. 15280-15283.

129. Koide, Y. and A. Yoshida, The signal transduction mechanism responsible for gamma interferon-induced indoleamine 2,3-dioxygenase gene expression. *Infection and Immunity*, **1994**. *62*(3): p. 948-955.

130. Konan, K.V. and M.W. Taylor, Importance of the two interferon-stimulated response element (ISRE) sequences in the regulation of the human indoleamine 2,3-dioxygenase gene. *Journal of Biological Chemistry*, **1996**. *271*(32): p. 19140-19145.

131. Kudo, Y. and C.A. Boyd, Human placental indoleamine 2,3-dioxygenase: cellular localization and characterization of an enzyme preventing fetal rejection. *Biochimica et Biophysica Acta*, **2000**. *1500*(1): p. 119-124.

132. Kudo, Y., C.A. Boyd, I.L. Sargent, and C.W. Redman, Modulation of indoleamine 2,3-dioxygenase by interferon-gamma in human placental chorionic villi. *Molecular Human Reproduction*, **2000**. *6*(4): p. 369-374.

133. Kudo, Y. and C.A. Boyd, The role of L-tryptophan transport in L-tryptophan degradation by indoleamine 2,3-dioxygenase in human placental explants. *Journal of Physiology*, **2001**. *531*(2): p. 417-423.

134. Kudo, Y., C.A. Boyd, I.L. Sargent, and C.W. Redman, Tryptophan degradation by human placental indoleamine 2,3-dioxygenase regulates lymphocyte proliferation. *Journal of Physiology*, **2001**. *535*(1): p. 207-215.

135. Kudo, Y., C.A.R. Boyd, I.L. Sargent, and C.W.G. Redman, Decreased tryptophan catabolism by placental indoleamine 2,3-dioxygenase in preeclampsia. *American Journal of Obstetrics and Gynecology*, **2003**. *188*(3): p. 719-726.

136. Kudo, Y., C.A.R. Boyd, I. Spyropoulou, C.W.G. Redman, O. Takikawa, T. Katsuki, T. Hara, K. Ohama, and I.L. Sargent, Indoleamine 2,3-dioxygenase: distribution and function in the developing human placenta. *Journal of Reproductive Immunology*, **2004**. *61*(2): p. 87-98.

137. Kudo, Y., T. Hara, T. Katsuki, A. Toyofuku, Y. Katsura, O. Takikawa, T. Fujii, and K. Ohama, Mechanisms regulating the expression of indoleamine 2,3-dioxygenase during decidualization of human endometrium. *Human Reproduction*, **2004**. *19*(3): p. 1222-1230.

138. Kuipers, H. and B.N. Lambrecht, Modification of dendritic cell function as a tool to prevent and treat allergic asthma. *Vaccine*, **2005**. *23*(37): p. 4577-4588.

139. Kvirkvelia, N., I. Vojnovic, T.D. Warner, V. Athie-Morales, P. Free, N. Rayment, B.M. Chain, T.W. Rademacher, T. Lund, I.M. Roitt, and P.J. Delves, Placentally derived prostaglandin E2 acts via the EP4 receptor to inhibit IL-2-dependent proliferation of CTLL-2 T cells. *Clinical and Experimental Immunology*, **2002**. *127*(2): p. 263-269.

140. Kwidzinski, E. and I. Bechmann, IDO expression in the brain: a double-edged sword. *Journal of Molecular Medicine*, **2007**(June 27): p. 1-9.

141. Le, A.V. and D.H. Broide, Indoleamine 2,3-dioxygenase modulation of allergic immune responses. *Current Allergy and Asthma Reports*, **2006**. *6*(1): p. 27-31.

142. Le Rond, S., A. Gonzalez, A.S.L. Gonzalez, E.D. Carosella, and N. Rouas-Freiss, Indoleamine 2,3-dioxygenase and human leucocyte antigen-G inhibit the T-cell alloproliferative response through two independent pathways. *Immunology*, **2005**. *116*(3): p. 297-307.

143. Lee, G.K., H.J. Park, M. Macleod, P. Chandler, D.H. Munn, and A.L. Mellor, Tryptophan deprivation sensitizes activated T cells to apoptosis prior to cell division. *Immunology*, **2002**. *107*(4): p. 452-460.

144. Leen, A.M., C.M. Rooney, and A.E. Foster, Improving T cell therapy for cancer. *Annual Review of Immunology*, **2007**. *25*(1): p. 243-265.

145. Lestage, J., D. Verrier, K. Palin, and R. Dantzer, The enzyme indoleamine 2,3-dioxygenase is induced in the mouse brain in response to peripheral administration of lipopolysaccharide and superantigen. *Brain, Behavior, and Immunity*, **2002**. *16*(5): p. 596-601.

146. Leung, B.S., L.E. Stout, E.G. Shaskan, and R.M. Thompson, Differential induction of indoleamine 2,3-dioxygenase (IDO) by interferon-gamma in human gynecologic cancer cells. *Cancer Letters*, **1992**. *66*(1): p. 77-81.

147. Li, Y., E.E. Tredget, and A. Ghahary, Cell surface expression of MHC class I antigen is suppressed in indoleamine 2,3-dioxygenase genetically modified keratinocytes: implications in allogeneic skin substitute engraftment. *Human Immunology*, **2004**. *65*(2): p. 114-123.

148. Li, Y., E.E. Tredget, A. Ghaffari, X. Lin, R.T. Kilani, and A. Ghahary, Local expression of indoleamine 2,3-dioxygenase protects engraftment of xenogeneic skin substitute. *Journal of Investigative Dermatology*, **2006**. *126*(1): p. 128-136.

149. Liebau, C., A.W.A. Baltzer, S. Schmidt, C. Roesel, C. Karreman, J.B. Prisack, H. Bojar, and H. Merk, Interleukin-12 and interleukin-18 induce indoleamine 2,3-dioxygenase (IDO) activity in human osteosarcoma cell lines independently from interferon-gamma. *Anticancer Research*, **2002**. *22*(2): p. 931-936.

150. Ligam, P., U. Manuelpillai, E.M. Wallace, and D. Walker, Localisation of indoleamine 2,3-dioxygenase and kynurenine hydroxylase in the human placenta and decidua: implications for role of the kynurenine pathway in pregnancy. *Placenta*, **2005**. *26*(6): p. 498-504.

151. Liong, E.C., Y. Dou, E.E. Scott, J.S. Olson, and G.N.J. Phillips, Waterproofing the heme pocket. Role of proximal amino acid side chains in preventing hemin loss from myoglobin. *Journal of Biological Chemistry*, **2001**. *276*(12): p. 9093-9100.

152. Littlejohn, T.K., O. Takikawa, D. Skylas, J.F. Jamie, M.J. Walker, and R.J. Truscott, Expression and purification of recombinant human indoleamine 2,3-dioxygenase. *Protein Expression and Purification*, **2000**. *19*(1): p. 22-29.

153. Littlejohn, T.K., O. Takikawa, J.F. Jamie, M.J. Walker, and R.J.W. Truscott, Production of truncated enzymically active human indoleamine 2,3-dioxygenase using site-directed mutagenesis. *International Congress Series*, **2002**. *1233*(1): p. 157-160.

154. Littlejohn, T.K., O. Takikawa, R.J.W. Truscott, and M.J. Walker, Asp274 and His346 are essential for heme binding and catalytic function of human indoleamine 2,3-dioxygenase. *Journal of Biological Chemistry*, **2003**. *278*(32): p. 29525-29531.

155. Liu, H., L. Liu, B.S. Fletcher, and G.A. Visner, Sleeping beauty-based gene therapy with indoleamine 2,3-dioxygenase inhibits lung allograft fibrosis. *Federation of American Societies for Experimental Biology Journal*, **2006**. *20*(13): p. 2384-2386.

156. Liu, H., L. Liu, B.S. Fletcher, and G.A. Visner, Novel action of indoleamine 2,3-dioxygenase attenuating acute lung allograft injury. *American Journal of Respiratory and Critical Care Medicine*, **2006**. *173*(5): p. 566-572.

157. Löb, S. and A. Königsrainer, Is IDO a key enzyme bridging the gap between tumor escape and tolerance induction? *Langenbeck's Archives of Surgery*, **2007**(December 7): p. 1-9.

158. Löb, S., A. Königsrainer, D. Zieker, B. Brücher, H. Rammensee, G. Opelz, and P. Terness, IDO1 and IDO2 are expressed in human tumors: levo- but not dextro-1-methyl tryptophan inhibits tryptophan catabolism. *Cancer Immunology, Immunotherapy*, **2008**(April 17, 2008): p. 1-8.

159. Logan, G.J., C.M.F. Smyth, J.W. Earl, I. Zaikina, P.B. Rowe, J.A. Smythe, and I.E. Alexander, HeLa cells cocultured with peripheral blood lymphocytes acquire an immuno-inhibitory phenotype through up-regulation of indoleamine 2,3-dioxygenase activity. *Immunology*, **2002**. *105*(4): p. 478-487.

160. Lopez, A.S., E. Alegre, A. Díaz, C. Mugueta, and A. González, Bimodal effect of nitric oxide in the enzymatic activity of indoleamine 2,3-dioxygenase in human monocytic cells. *Immunology Letters*, **2006**. *106*(2): p. 163-171.

161. Lopez, A.S., E. Alegre, J. LeMaoult, E. Carosella, and A. Gonzalez, Regulatory role of tryptophan degradation pathway in HLA-G expression by human monocyte-derived dendritic cells. *Molecular Immunology*, **2006**. *43*(14): p. 2151-2160.

162. Macchiarulo, A., R. Nuti, D. Bellocchi, E. Camaioni, and R. Pellicciari, Molecular docking and spatial coarse graining simulations as tools to investigate substrate recognition, enhancer binding and conformational transitions in indoleamine 2,3-dioxygenase (IDO). *Biochimica et Biophysica Acta (BBA) - Proteins & Proteomics*, **2007**. *1774*(8): p. 1058-1068.

163. Macchiarulo, A., E. Camaioni, R. Nuti, and R. Pellicciari, Highlights at the gate of tryptophan catabolism: a review on the mechanisms of activation and regulation of indoleamine 2,3-dioxygenase (IDO), a novel target in cancer disease. *Amino Acids*, **2008**(July 09, 2008): p. 1-21.

164. MacKenzie, C.R., U. Hadding, and W. Däubener, Interferon-gamma-induced activation of indoleamine 2,3-dioxygenase in cord blood monocyte-derived macrophages inhibits the growth of group B *Streptococci. Journal of Infectious Diseases*, **1998**. *178*(3): p. 875-878.

165. MacKenzie, C.R., R. Langen, O. Takikawa, and W. Däubener, Inhibition of indoleamine 2,3-dioxygenase in human macrophages inhibits interferon-gamma-induced bacteriostasis but does not abrogate toxoplasmastasis. *European Journal of Immunology*, **1999**. *29*(10): p. 3254-3261.

166. Mackler, A.M., E.M. Barber, O. Takikawa, and J.W. Pollard, Indoleamine 2,3-dioxygenase is regulated by IFN-gamma in the mouse placenta during *Listeria monocytogenes* infection. *Journal of Immunology*, **2003**. *170*(2): p. 823-830.

167. Maghzal, G.J., S.R. Thomas, N.H. Hunt, and R. Stocker, Cytochrome b5, not superoxide anion radical, is a major reductant of indoleamine 2,3-dioxygenase in human cells. *Journal of Biological Chemistry*, **2008**. *283*(18): p. 12014-12025.

168. Makrides, S.C., Strategies for achieving high-level expression of genes in *Escherichia coli. Microbiological Review*, **1996**. *60*(3): p. 512-538.

169. Malachowski, W.P., R. Metz, G.C. Prendergasi, and A.J. Muller, A new cancer immunosuppression target: indoleamine 2,3-dioxygenase (IDO). A review of the IDO mechanism, inhibition and therapeutic applications. *Drugs of the Future*, **2005**. *30*(9): p. 897-909.

170. Malina, H.Z. and X.D. Martin, Indoleamine 2,3-dioxygenase activity in the aqueous humor, iris/ciliary body, and retina of the bovine eye. *Graefe's Archive for Clinical and Experimental Ophthalmology*, **1993**. *231*(8): p. 482-486.

171. Malina, H.Z. and X.D. Martin, Indoleamine 2,3-dioxygenase: antioxidant enzyme in the human eye. *Graefe's Archive for Clinical and Experimental Ophthalmology*, **1996**. *234*(7): p. 457-462.

172. Maloney, E.M., O. St Claire Morgan, B. Widner, E.R. Werner, and D. Fuchs, Central nervous system activation of the indoleamine 2,3-dioxygenase pathway in human T cell lymphotropic virus type I-associated myelopathy/tropical spastic paraparesis. *Journal of Infectious Diseases*, **2000**. *181*(6): p. 2037-2040.

173. Marteau, F., N.S. Gonzalez, D. Communi, M. Goldman, J.M. Boeynaems, and D. Communi, Thrombospondin-1 and indoleamine 2,3-dioxygenase are major targets of extracellular ATP in human dendritic cells. *Blood*, **2005**. *106*(12): p. 3860-3866.

174. Matin, A., I.M. Streete, I.M. Jamie, R.J.W. Truscott, and J.F. Jamie, A fluorescence-based assay for indoleamine 2,3-dioxygenase. *Analytical Biochemistry*, **2006**. *349*(1): p. 96-102.

175. Meisel, R., A. Zibert, M. Laryea, U. Göbel, W. Däubener, and D. Dilloo, Human bone marrow stromal cells inhibit allogeneic T-cell responses by indoleamine 2,3-dioxygenase-mediated tryptophan degradation. *Blood*, **2004**. *103*(12): p. 4619-4621.

176. Melchior, D., N. Mézière, B. Sève, and N. Le Floc'h, Is tryptophan catabolism increased under indoleamine 2,3-dioxygenase activity during chronic lung inflammation in pigs? *Reproduction, Nutrition, Development*, **2005**. *45*(2): p. 175-183.

177. Mellor, A.L., P. Chandler, G.K. Lee, T. Johnson, D.B. Keskin, J. Lee, and D.H. Munn, Indoleamine 2,3-dioxygenase, immunosuppression and pregnancy. *Journal of Reproductive Immunology*, **2002**. *57*(2): p. 143-150.

178. Mellor, A.L., D.B. Keskin, T. Johnson, P. Chandler, and D.H. Munn, Cells expressing indoleamine 2,3-dioxygenase inhibit T cell responses. *Journal of Immunology*, **2002**. *168*(8): p. 3771-3776.

179. Mellor, A.L., B. Baban, P. Chandler, B. Marshall, K.G. Jhaver, A.M. Hansen, P.A. Koni, M. Iwashima, and D.H. Munn, Cutting edge: induced indoleamine 2,3-dioxygenase expression in dendritic cell subsets suppresses T cell clonal expansion. *Journal of Immunology*, **2003**. *171*(4): p. 1652-1655.

180. Mellor, A.L., P. Chandler, B. Baban, A.M. Hansen, B. Marshall, J. Pihkala, H. Waldmann, S. Cobbold, E. Adams, and D.H. Munn, Specific subsets of murine dendritic cells acquire potent T cell regulatory functions following CTLA4-mediated induction of indoleamine 2,3-dioxygenase. *International Immunology*, **2004**. *16*(10): p. 1391-1401.

181. Mellor, A.L., Indoleamine 2,3-dioxygenase and regulation of T cell immunity. *Biochemical and Biophysical Research Communications*, **2005**. *338*(1): p. 20-24.

182. Mellor, A.L., B. Baban, P.R. Chandler, A. Manlapat, D.J. Kahler, and D.H. Munn, Cutting edge: CpG oligonucleotides induce splenic CD19+ dendritic cells to acquire potent indoleamine 2,3-dioxygenase-dependent T cell regulatory functions via IFN type 1 signaling. *Journal of Immunology*, **2005**. *175*(9): p. 5601-5605.

183. Metz, R., J.B. DuHadaway, U. Kamasani, L. Laury-Kleintop, A.J. Muller, and G.C. Prendergast, Novel tryptophan catabolic enzyme IDO2 is the preferred biochemical target of the antitumor indoleamine 2,3-dioxygenase inhibitory compound D-1-methyl-tryptophan. *Cancer Research*, **2007**. *67*(15): p. 7082-7087.

184. Miller, C.L., I.C. Llenos, M. Cwik, J. Walkup, and S. Weis, Alterations in kynurenine precursor and product levels in schizophrenia and bipolar disorder. *Neurochemistry International*, **2008**. *52*(6): p. 1297-1303.

185. Miwa, N., S. Hayakawa, S. Miyazaki, S. Myojo, Y. Sasaki, M. Sakai, O. Takikawa, and S. Saito, IDO expression on decidual and peripheral blood dendritic cells and monocytes/macrophages after treatment with CTLA-4 or interferon-gamma increase in normal pregnancy but decrease in spontaneous abortion. *Molecular Human Reproduction*, **2005**. *11*(12): p. 865-870.

186. Miyara, M. and S. Sakaguchi, Natural regulatory T cells: mechanisms of suppression. *Trends in Molecular Medicine*, **2007**. *13*(3): p. 108-116.

187. Mocellin, S., S. Mandruzzato, P. Zanovello, and V. Bronte, Cancer rejection by the immune system: forcing the check-points of tumor immune escape. *Drug Discovery Today: Disease Mechanisms*, **2005**. *2*(2): p. 191-197.

188. Moffett, J.R. and M.A.A. Namboodiri, Tryptophan and the immune response. *Immunology and Cell Biology*, **2003**. *81*(4): p. 247-265.

189. Mohib, K., Q. Guan, H. Diao, C. Du, and A.M. Jevnikar, Proapoptotic activity of indoleamine 2,3-dioxygenase expressed in renal tubular epithelial cells. *American Journal of Physiology-Renal Physiology*, **2007**. *293*(3): p. F801-812.

190. Moreau, M., J. Lestage, D. Verrier, C. Mormede, K.W. Kelley, R. Dantzer, and N. Castanon, Bacille Calmette-Guérin inoculation induces chronic activation of peripheral and brain indoleamine 2,3-dioxygenase in mice. *Journal of Infectious Diseases*, **2005**. *192*(3): p. 537-544.

191. Muller, A.J., J.B. DuHadaway, P.S. Donover, E. Sutanto-Ward, and G.C. Prendergast, Inhibition of indoleamine 2,3-dioxygenase, an immunoregulatory target of the cancer suppression gene Bin1, potentiates cancer chemotherapy. *Nature Medicine*, **2005**. *11*(3): p. 312-319.

192. Muller, A.J., W.P. Malachowski, and G.C. Prendergast, Indoleamine 2,3-dioxygenase in cancer: targeting pathological immune tolerance with small-molecule inhibitors. *Expert Opinion on Therapeutic Targets*, **2005**. *9*(4): p. 831-849.

193. Muller, A.J. and G.C. Prendergast, Marrying immunotherapy with chemotherapy: why say IDO? *Cancer Research*, **2005**. *65*(18): p. 8065-8068.

194. Muller, A.J., R. Metz, and G.C. Prendergast, Differential targeting of tryptophan catabolism in tumors and in tumor-draining lymph nodes by stereoisomers of the IDO inhibitor 1-methyl-tryptophan. *International Congress Series*, **2007**. *1304*: p. 250-261.

195. Muller, A.J. and G.C. Prendergast, Indoleamine 2,3-dioxygenase in immune suppression and cancer. *Current Cancer Drug Targets*, **2007**. *7*: p. 31-40.

196. Müller, N. and M. Schwarz, A psychoneuroimmunological perspective to Emil Kraepelins dichotomy. *European Archives of Psychiatry and Clinical Neuroscience*, **2008**. *258*(0): p. 97-106.

197. Munn, D.H., M.D. Sharma, J.R. Lee, K.G. Jhaver, T.S. Johnson, D.B. Keskin, B. Marshall, P. Chandler, S.J. Antonia, R. Burgess, C.L. Slingluff, and A.L. Mellor, Potential regulatory function of human dendritic cells expressing indoleamine 2,3-dioxygenase. *Science*, **2002**. *297*(5588): p. 1867-1870.

198. Munn, D.H., M.D. Sharma, D. Hou, B. Baban, J.R. Lee, S.J. Antonia, J.L. Messina, P. Chandler, P.A. Koni, and A.L. Mellor, Expression of indoleamine 2,3-dioxygenase by plasmacytoid dendritic cells in tumor-draining lymph nodes. *Journal of Clinical Investigation*, **2004**. *114*(2): p. 280-290.

199. Munn, D.H., M.D. Sharma, and A.L. Mellor, Ligation of B7-1/B7-2 by human CD4+ T cells triggers indoleamine 2,3-dioxygenase activity in dendritic cells. *Journal of Immunology*, **2004**. *172*(7): p. 4100-4110.

200. Munn, D.H., M.D. Sharma, B. Baban, H.P. Harding, Y. Zhang, D. Ron, and A.L. Mellor, GCN2 kinase in T cells mediates proliferative arrest and anergy induction in response to indoleamine 2,3-dioxygenase. *Immunity*, **2005**. *22*(5): p. 633-642.

201. Munn, D.H., Indoleamine 2,3-dioxygenase, tumor-induced tolerance and counter-regulation. *Current Opinion in Immunology*, **2006**. *18*(2): p. 220-225.

202. Munn, D.H. and A.L. Mellor, The tumor-draining lymph node as an immune-privileged site. *Immunological Reviews*, **2006**. *213*(1): p. 146-158.

203. Munn, D.H. and A.L. Mellor, Indoleamine 2,3-dioxygenase and tumor-induced tolerance. *Journal of Clinical Investigation*, **2007**. *117*(5): p. 1147-1154.

204. Musso, T., G.L. Gusella, A. Brooks, D.L. Longo, and L. Varesio, Interleukin-4 inhibits indoleamine 2,3-dioxygenase expression in human monocytes. *Blood*, **1994**. *83*(5): p. 1408-1411.

205. Nelson, D.E., D.P. Virok, H. Wood, C. Roshick, R.M. Johnson, W.M. Whitmire, D.D. Crane, O. Steele-Mortimer, L. Kari, G. McClarty, and H.D. Caldwell, Chlamydial IFN-gamma immune evasion is linked to host infection tropism. *Proceedings of the National Academy of Sciences of the United States of America*, **2005**. *102*(30): p. 10658-10663.

206. Noakes, R., L. Spelman, and R. Williamson, Is the L-tryptophan metabolite quinolinic acid responsible for eosinophilic fasciitis? *Clinical and Experimental Medicine*, **2006**. *6*(2): p. 60-64.

207. Obojes, K., O. Andres, K.S. Kim, W. Däubener, and J. Schneider-Schaulies, Indoleamine 2,3-dioxygenase mediates cell type-specific anti-measles virus activity of gamma interferon. *Journal of Virology*, **2005**. *79*(12): p. 7768-7776.

208. Oda, S.I., H. Sugimoto, T. Yoshida, and Y. Shiro, Crystallization and preliminary crystallographic studies of human indoleamine 2,3-dioxygenase. *Acta Crystallographica. Section F, Structural Biology and Crystallization Communications*, **2006**. *62*(3): p. 221-223.

209. Odemuyiwa, S.O., A. Ghahary, Y. Li, L. Puttagunta, J.E. Lee, S. Musat-Marcu, A. Ghahary, and R. Moqbel, Cutting edge: human eosinophils regulate T cell subset selection through indoleamine 2,3-dioxygenase. *Journal of Immunology*, **2004**. *173*(10): p. 5909-5913.

210. Oh, G.S., H.O. Pae, B.M. Choi, S.C. Chae, H.S. Lee, D.G. Ryu, and H.T. Chung, 3-Hydroxyanthranilic acid, one of metabolites of tryptophan via indoleamine 2,3-dioxygenase pathway, suppresses inducible nitric oxide synthase expression by enhancing heme oxygenase-1 expression. *Biochemical and Biophysical Research Communications*, **2004**. *320*(4): p. 1156-1162.

211. Ohnishi, T., F. Hirata, and O. Hayaish, Indoleamine 2,3-dioxygenase. Potassium superoxide as substrate. *Journal of Biological Chemistry*, **1977**. *252*(13): p. 4643-4647.

212. Okamoto, A., T. Nikaido, K. Ochiai, S. Takakura, M. Saito, Y. Aoki, N. Ishii, N. Yanaihara, K. Yamada, O. Takikawa, R. Kawaguchi, S. Isonishi, T. Tanaka, and M. Urashima, Indoleamine 2,3-dioxygenase serves as a marker of poor prognosis in gene expression profiles of serous ovarian cancer cells. *Clinical Cancer Research*, **2005**. *11*(16): p. 6030-6039.

213. Okuma, M., T. Tokuyama, S. Senoh, F. Hirata, and O. Hayaishi, Antagonism of 5-hydroxykynurenamine against serotonin action on platelet aggregation. *Proceedings of the National Academy of Sciences of the United States of America*, **1976**. *73*(2): p. 643-645.

214. Oliveira, L.J., J.M. Monteiro, S.C. Oloris, M.R. Rodrigues, S.S. Okada, F.V.T. Verechia, F.V. Meirelles, J.A. Visintin, A. Campa, and J.R. Kfoury, Immunolocalization of indoleamine 2,3-dioxygenase in placenta from bovine cloned conceptus pregnancy. *Reproduction Fertility and Development*, **2006**. *18*(2): p. 178-179.

215. Orabona, C., P. Puccetti, C. Vacca, S. Bicciato, A. Luchini, F. Fallarino, R. Bianchi, E. Velardi, K. Perruccio, A. Velardi, V. Bronte, M.C. Fioretti, and U. Grohmann, Toward the identification of a tolerogenic signature in IDO-competent dendritic cells. *Blood*, **2006**. *107*(7): p. 2846-2854.

216. Ozaki, Y., J.F. Reinhard, and C.A. Nichol, Cofactor activity of dihydroflavin mononucleotide and tetrahydrobiopterin for murine epididymal indoleamine 2,3-dioxygenase. *Biochemical and Biophysical Research Communications*, **1986**. *137*(3): p. 1106-1111.

217. Ozaki, Y., M.P. Edelstein, and D.S. Duch, The actions of interferon and antiinflammatory agents of induction of indoleamine 2,3-dioxygenase in human peripheral blood monocytes. *Biochemical and Biophysical Research Communications*, **1987**. *144*(3): p. 1147-1153.

218. Ozaki, Y., C.A. Nichol, and D.S. Duch, Utilization of dihydroflavin mononucleotide and superoxide anion for the decyclization of L-tryptophan by murine epididymal indoleamine 2,3-dioxygenase. *Archives of Biochemistry and Biophysics*, **1987**. *257*(1): p. 207-216.

219. Ozaki, Y., M.P. Edelstein, and D.S. Duch, Induction of indoleamine 2,3-dioxygenase: a mechanism of the antitumor activity of interferon gamma. *Proceedings of the National Academy of Sciences of the United States of America*, **1988**. *85*(4): p. 1242-1246.

220. Paguirigan, A.M., G.I. Byrne, S. Becht, and J.M. Carlin, Cytokine-mediated indoleamine 2,3-dioxygenase induction in response to *Chlamydia* infection in human macrophage cultures. *Infection and Immunity*, **1994**. *62*(4): p. 1131-1136.

221. Pan, T.L., C.L. Lin, C.L. Chen, Y.C. Lin, S. Gojo, T.H. Lee, Y.H. Wang, R. Lord, C.Y. Lai, L.W. Tsu, H.P. Tseng, M.L. Wu, Y. Iwashita, S. Kitano, K.C. Chiang, T. Hashimoto, A. Sugioka, and S. Goto, Identification of the indoleamine 2,3-dioxygenase nucleotide sequence in a rat liver transplant model. *Transplant Immunology*, **2000**. *8*(3): p. 189-194.

222. Pan, K., H. Wang, M. Chen, H. Zhang, D. Weng, J. Zhou, W. Huang, J. Li, H. Song, and J. Xia, Expression and prognosis role of indoleamine 2,3-dioxygenase in hepatocellular carcinoma. *Journal of Cancer Research and Clinical Oncology*, **2008**(April 26, 2008): p. 1-11.

223. Pantoja, L.G., R.D. Miller, J.A. Ramirez, R.E. Molestina, and J.T. Summersgill, Inhibition of *Chlamydia pneumoniae* replication in human aortic smooth muscle cells by gamma interferon-induced indoleamine 2,3-dioxygenase activity. *Infection and Immunity*, **2000**. *68*(11): p. 6478-6481.

224. Papadopoulou, N.D., M. Mewies, K.J. McLean, H.E. Seward, D.A. Svistunenko, A.W. Munro, and E.L. Raven, Redox and spectroscopic properties of human indoleamine 2,3-dioxygenase and a His303Ala variant: implications for catalysis. *Biochemistry*, **2005**. *44*(43): p. 14318-14328.

225. Pellegrin, K., G. Neurauter, B. Wirleitner, A.W. Fleming, V.M. Peterson, and D. Fuchs, Enhanced enzymatic degradation of tryptophan by indoleamine 2,3-dioxygenase contributes to the tryptophan-deficient state seen after major trauma. *Shock*, **2005**. *23*(3): p. 209-215.

226. Pereira, A., E. Vottero, M. Roberge, A.G. Mauk, and R.J. Andersen, Indoleamine 2,3-dioxygenase inhibitors from the Northeastern Pacific Marine Hydroid *Garveia annulata. Journal of Natural Products*, **2006**. *69*(10): p. 1496-1499.

227. Persidsky, Y. and L. Poluektova, Immune privilege and HIV-1 persistence in the CNS. *Immunological Reviews*, **2006**. *213*(1): p. 180-194.

228. Pertovaara, M., A. Raitala, H. Uusitalo, J. Pukander, H. Helin, S.S. Oja, and M. Hurme, Mechanisms dependent on tryptophan catabolism regulate immune responses in primary Sjogren's syndrome. *Clinical and Experimental Immunology*, **2005**. *142*(1): p. 155-161.

229. Pertovaara, M., M. Heliövaara, A. Raitala, S.S. Oja, P. Knekt, and M. Hurme, The activity of the immunoregulatory enzyme indoleamine 2,3-dioxygenase is decreased in smokers. *Clinical and Experimental Immunology*, **2006**. *145*(3): p. 469-473.

230. Pertovaara, M., A. Raitala, T. Lehtimäki, P.J. Karhunen, S.S. Oja, M. Jylhä, A. Hervonen, and M. Hurme, Indoleamine 2,3-dioxygenase activity in nonagenarians is markedly increased and predicts mortality. *Mechanisms of Ageing and Development*, **2006**. *127*(5): p. 497-499.

231. Petroff, M.G., Immune interactions at the maternal-fetal interface. *Journal of Reproductive Immunology*, **2005**. *68*(1): p. 1-13.

232. Pfefferkorn, E.R., S. Rebhun, and M. Eckel, Characterization of an indoleamine 2,3-dioxygenase induced by gamma-interferon in cultured human fibroblasts. *Journal of Interferon Research*, **1986**. *6*(3): p. 267-279.

233. Poljak, A., R. Grant, C.J.D. Austin, J.F. Jamie, R.D. Willows, O. Takikawa, T.K. Littlejohn, R.J.W. Truscott, M.J. Walker, P. Sachdev, and G.A. Smythe, Inhibition of indoleamine 2,3-dioxygenase activity by H_2O_2. *Archives of Biochemistry and Biophysics*, **2006**. *450*(1): p. 9-19.

234. Potula, R., L. Poluektova, B. Knipe, J. Chrastil, D. Heilman, H. Dou, O. Takikawa, D.H. Munn, H.E. Gendelman, and Y. Persidsky, Inhibition of indoleamine 2,3-dioxygenase (IDO) enhances elimination of virus-infected macrophages in an animal model of HIV-1 encephalitis. *Blood*, **2005**. *106*(7): p. 2382-2390.

235. Prendergast, G.C., Immune escape as a fundamental trait of cancer: focus on IDO. *Oncogene*, **2008**(March 3, 2008): p. 1-12.

236. Qiagen, The QIAexpressionist™. A handbook for high-level expression and purification of 6xHis-tagged proteins. 5th ed. **2003**, Valencia, California: Qiagen. 126pp.

237. Qiagen, The Qiagen bench guide. **2001**, Valencia, California: Qiagen. 105pp.

238. Raitala, A., M. Pertovaara, J. Karjalainen, S.S. Oja, and M. Hurme, Association of interferon-gamma +874(TA) single nucleotide polymorphism with the rate of tryptophan catabolism in healthy individuals. *Scandinavian Journal of Immunology*, **2005**. *61*(4): p. 387-390.

239. Raitala, A., J. Karjalainen, S.S. Oja, T.U. Kosunen, and M. Hurme, Indoleamine 2,3-dioxygenase (IDO) activity is lower in atopic than in non-atopic individuals and is enhanced by environmental factors protecting from atopy. *Molecular Immunology*, **2006**. *43*(7): p. 1054-1056.

240. Raso S.W., P.L. Clark, C. Haase-Pettingell, J. King, G.J.Jr. Thomas, Distinct cysteine sulfhydryl environments detected by analysis of Raman S-H markers of Cys→Ser mutant proteins. *Journal of Molecular Biology*, **2001**. *307*(3): p.899-911.

241. Reddy, P., Y. Sun, T. Toubai, R. Duran-Struuck, S.G. Clouthier, E. Weisiger, Y. Maeda, I. Tawara, O. Krijanovski, E. Gatza, C. Liu, C. Malter, P. Mascagni, C.A. Dinarello, and J.L.M. Ferrara, Histone deacetylase inhibition modulates indoleamine 2,3-dioxygenase–dependent DC functions and regulates experimental graft-versus-host disease in mice. *Journal of Clinical Investigation*, **2008**. *118*(7): p. 2562–2573.

242. Riesenberg, R., C. Weiler, O. Spring, M. Eder, A. Buchner, T. Popp, M. Castro, R. Kammerer, O. Takikawa, R.A. Hatz, C.G. Stief, A. Hofstetter, and W. Zimmermann, Expression of indoleamine 2,3-dioxygenase in tumor endothelial cells correlates with long-term survival of patients with renal cell carcinoma. *Clinical Cancer Research*, **2007**. *13*(23): p. 6993-7002.

243. Ritter, M.R., S.K. Moreno, M.I. Dorrell, J. Rubens, J. Ney, D.F. Friedlander, J. Bergman, B.B. Cunningham, L. Eichenfield, J. Reinisch, S. Cohen, T. Veccione, R. Holmes, S.F. Friedlander, and M. Friedlander, Identifying potential regulators of infantile hemangioma progression through large-scale expression analysis: a possible role for the immune system and indoleamine 2,3-dioxygenase (IDO) during involution. *Lymphatic Research and Biology*, **2003**. *1*(4): p. 291-299.

244. Robinson, C.M., P.T. Hale, and J.M. Carlin, NF-kappaB activation contributes to indoleamine dioxygenase transcriptional synergy induced by IFN-gamma and tumor necrosis factor-alpha. *Cytokine*, **2006**. *35*(2): p. 53-61.

245. Rödel, J., A. Groh, M. Hartmann, K.H. Schmidt, M. Lehmann, W. Lungershausen, and E. Straube, Expression of interferon regulatory factors and indoleamine 2,3-dioxygenase in *Chlamydia trachomatis*-infected synovial fibroblasts. *Medical Microbiology and Immunology*, **1999**. *187*(4): p. 205-212.

246. Rodrigues, M.R., D. Rodriguez, L. Henrique Catalani, M. Russo, and A. Campa, Interferon-gamma independent oxidation of melatonin by macrophages. *Journal of Pineal Research*, **2003**. *34*(1): p. 69-74.

247. Romani, L., F. Bistoni, K. Perruccio, C. Montagnoli, R. Gaziano, S. Bozza, P. Bonifazi, G. Bistoni, G. Rasi, A. Velardi, F. Fallarino, E. Garaci, and P. Puccetti, Thymosin alpha1 activates dendritic cell tryptophan catabolism and establishes a regulatory environment for balance of inflammation and tolerance. *Blood*, **2006**. *108*(7): p. 2265-2274.

248. Rossi-Fanelli, A. and E. Antonini, Dissociation of hematin from hemoproteins at neutral pH. *Journal of Biological Chemistry*, **1960**. *234*(2): p. 4-5.

249. Roy, E.J., O. Takikawa, D.M. Kranz, A.R. Brown, and D.L. Thomas, Neuronal localization of indoleamine 2,3-dioxygenase in mice. *Neuroscience Letters*, **2005**. *387*(2): p. 95-99.

250. Rubin, B.Y., S.L. Anderson, G.R. Hellermann, N.K. Richardson, R.M. Lunn, and J.E. Valinsky, The development of antibody to the interferon-induced indoleamine 2,3-dioxygenase and the study of the regulation of its synthesis. *Journal of Interferon Research*, **1988**. *8*(5): p. 691-702.

251. Saito, K., A. Lackner, S.P. Markey, and M.P. Heyes, Cerebral cortex and lung indoleamine-2,3-dioxygenase activity is increased in type-D retrovirus infected macaques. *Brain Research*, **1991**. *540*(1): p. 353-356.

252. Sakash, J.B., G.I. Byrne, A. Lichtman, and P. Libby, Cytokines induce indoleamine 2,3-dioxygenase expression in human atheroma-asociated cells: implications for persistent *Chlamydophila pneumoniae* infection. *Infection and Immunity*, **2002**. *70*(7): p. 3959-3961.

253. Sakuma, M., Y. Mizuno, H. Nakamura, and M. Urashima, Activation of indoleamine 2,3-dioxygenase in children with acute febrile diseases. *Japan Medical Association Journal*, **2005**. *48*(6): p. 277-282.

254. Sakurai, K., J.P. Zou, J.R. Tschetter, J.M. Ward, and G.M. Shearer, Effect of indoleamine 2,3-dioxygenase on induction of experimental autoimmune encephalomyelitis. *Journal of Neuroimmunology*, **2002**. *129*(2): p. 186-196.

255. Saluta, M. and P.A. Bell, Troubleshooting GST fusion protein expression in *E. coli*. *Life Science News (Amersham Pharmacia Biotech)*, **1998**. *1*: p. 1-3.

256. Samelson-Jones, B.J. and S.R. Yeh, Interactions between nitric oxide and indoleamine 2,3-dioxygenase. *Biochemistry*, **2006**. *45*(28): p. 8527-8538.

257. San, K.Y., G.N. Bennett, A.A. Aristidou, and C.H. Chou, Strategies in high-level expression of recombinant protein in *Escherichia coli*. *Annals of the New York Academy of Sciences*, **1994**. *721*(1): p. 257-267.

258. Santoso, D.I.S., P. Rogers, E.M. Wallace, U. Manuelpillai, D. Walker, and S.B. Subakir, Localization of indoleamine 2,3-dioxygenase and 4-hydroxynonenal in normal and pre-eclamptic placentae. *Placenta*, **2002**. *23*(5): p. 373-379.

259. Sardar, A.M. and G.P. Reynolds, Frontal cortex indoleamine-2,3-dioxygenase activity is increased in HIV-1-associated dementia. *Neuroscience Letters*, **1995**. *187*(1): p. 9-12.

260. Sarkhosh, K., E.E. Tredget, A. Karami, H. Uludag, T. Iwashina, R.T. Kilani, and A. Ghahary, Immune cell proliferation is suppressed by the interferon-gamma-induced indoleamine 2,3-dioxygenase expression of fibroblasts populated in collagen gel (FPCG). *Journal of Cellular Biochemistry*, **2003**. *90*(1): p. 206-217.

261. Sarkhosh, K., E.E. Tredget, Y. Li, R.T. Kilani, H. Uludag, and A. Ghahary, Proliferation of peripheral blood mononuclear cells is suppressed by the indoleamine 2,3-dioxygenase expression of interferon-gamma-treated skin cells in a co-culture system. *Wound Repair and Regeneration*, **2003**. *11*(5): p. 337-345.

262. Sayama, S., R. Yoshida, T. Oku, J. Imanishi, T. Kishida, and O. Hayaishi, Inhibition of interferon-mediated induction of indoleamine 2,3-dioxygenase in mouse lung by inhibitors of prostaglandin biosynthesis. *Proceedings of the National Academy of Sciences of the United States of America*, **1981**. *78*(12): p. 7327-7330.

263. Schein, C.H. and M.H.M. Noteborn, Formation of soluble recombinant proteins in *Escherichia coli* is favored by lower growth temperature. *Nature Biotechnology*, **1988**. *6*(3): p. 291-294.

264. Schein, C.H., Production of soluble recombinant proteins in bacteria. *Nature Biotechnology*, **1989**. *7*(11): p. 1141-1149.

265. Schein, C.H., Solubility as a function of protein structure and solvent components. *Nature Biotechnology*, **1990**. *8*(4): p. 308-317.

266. Schomburg, D., EC 1.13.11.52 - indoleamine 2,3-dioxygenase. *BRENDA The Comprehensive Enzyme Information System*. 2004-2009. Institut fuer Biochemie und Bioinformatik, Technische Universität Braunschweig, Langer Kamp, Braunschweig: from www.brenda-enzymes.org.

267. Schroten, H., B. Spors, C. Hucke, M. Stins, K.S. Kim, R. Adam, and W. Däubener, Potential role of human brain microvascular endothelial cells in the pathogenesis of brain abscess: inhibition of *Staphylococcus aureus* by activation of indoleamine 2,3-dioxygenase. *Neuropediatrics*, **2001**. *32*(4): p. 206-210.

268. Sedlmayr, P., A. Blaschitz, R. Wintersteiger, M. Semlitsch, A. Hammer, C.R. MacKenzie, W. Walcher, O. Reich, O. Takikawa, and G. Dohr, Localization of indoleamine 2,3-dioxygenase in human female reproductive organs and the placenta. *Molecular Human Reproduction*, **2002**. *8*(4): p. 385-391.

269. Sedlmayr, P., M. Semlitsch, G. Gebru, E. Karpf, O. Reich, T. Tang, R. Wintersteiger, O. Takikawa, and G. Dohr, Expression of indoleamine 2,3-dioxygenase in carcinoma of human endometrium and uterine cervix. *Advances in Experimental Medicine and Biology*, **2003**. *527*(1): p. 91-95.

270. Serbecic, N. and S.C. Beutelspacher, Indoleamine 2,3-dioxygenase protects corneal endothelial cells from UV mediated damage. *Experimental Eye Research*, **2006**. *82*(3): p. 416-426.

271. Shimizu, T., S. Nomiyama, F. Hirata, and O. Hayaishi, Indoleamine 2,3-dioxygenase. Purification and some properties. *Journal of Biological Chemistry*, **1978**. *253*(13): p. 4700-4706.

272. Silva, N.M., C.V. Rodrigues, M.M. Santoro, L.F.L. Reis, J.I. Alvarez-Leite, and R.T. Gazzinelli, Expression of indoleamine 2,3-dioxygenase, tryptophan degradation, and kynurenine formation during in vivo infection with *Toxoplasma gondii*: induction by endogenous gamma interferon and requirement of interferon regulatory factor 1. *Infection and Immunity*, **2002**. *70*(2): p. 859-868.

273. Smith, M.L., J. Paul, P.I. Ohlsson, K. Hjortsberg, and K.G. Paul, Heme-protein fission under nondenaturing conditions. *Proceedings of the National Academy of Sciences of the United States of America*, **1991**. *88*(3): p. 882–886.

274. Sono, M., T. Taniguchi, Y. Watanabe, and O. Hayaishi, Indoleamine 2,3-dioxygenase. Equilibrium studies of the tryptophan binding to the ferric, ferrous, and CO-bound enzymes. *Journal of Biological Chemistry*, **1980**. *255*(4): p. 1339-1345.

275. Sono, M. and J.H. Dawson, Extensive studies of the heme coordination structure of indoleamine 2,3-dioxygenase and of tryptophan binding with magnetic and natural circular dichroism and electron paramagnetic resonance spectroscopy. *Biochimica et Biophysica Acta*, **1984**. *789*(2): p. 170-187.

276. Sono, M., Spectroscopic and equilibrium properties of the indoleamine 2,3-dioxygenase-tryptophan-O_2 ternary complex and of analogous enzyme derivatives. Tryptophan binding to ferrous enzyme adducts with dioxygen, nitric oxide, and carbon monoxide. *Biochemistry*, **1986**. *25*(20): p. 6089-6097.

277. Sono, M., The roles of superoxide anion and methylene blue in the reductive activation of indoleamine 2,3-dioxygenase by ascorbic acid or by xanthine oxidase-hypoxanthine. *Journal of Biological Chemistry*, **1989**. *264*(3): p. 1616-1622.

278. Sono, M., Enzyme kinetic and spectroscopic studies of inhibitor and effector interactions with indoleamine 2,3-dioxygenase. 2. Evidence for the existence of another binding site in the enzyme for indole derivative effectors. *Biochemistry*, **1989**. *28*(13): p. 5400-5407.

279. Sono, M. and S.G. Cady, Enzyme kinetic and spectroscopic studies of inhibitor and effector interactions with indoleamine 2,3-dioxygenase. 1. Norharman and 4-phenylimidazole binding to the enzyme as inhibitors and heme ligands. *Biochemistry*, **1989**. *28*(13): p. 5392-5399.

280. Sono, M., M.P. Roach, E.D. Coulter, and J.H. Dawson, Heme-containing oxygenases. *Chemical Reviews*, **1996**. *96*(7): p. 2841-2888.

281. Sotero-Esteva, W.D., D. Wolfe, M. Ferris, and M.W. Taylor, An indoleamine 2,3-dioxygenase-negative mutant is defective in stat1 DNA binding: differential response to IFN-gamma and IFN-alpha. *Journal of Interferon and Cytokine Research*, **2000**. *20*(7): p. 623-632.

282. Steckel, N.K., U. Kuhn, D.W. Beelen, and A.H. Elmaagacli, Indoleamine 2,3-dioxygenase expression in patients with acute graft-versus-host disease after allogeneic stem cell transplantation and in pregnant women: association with the induction of allogeneic immune tolerance? *Scandinavian Journal of Immunology*, **2003**. *57*(2): p. 185-191.

283. Stratagene, QuikChange® II site-directed mutagenesis kit. **2006**, La Jolla, California: Stratagene. 18pp.

284. Sugimoto, H., S.I. Oda, T. Otsuki, T. Hino, T. Yoshida, and Y. Shiro, Crystal structure of human indoleamine 2,3-dioxygenase: catalytic mechanism of O_2 incorporation by a heme-containing dioxygenase. *Proceedings of the National Academy of Sciences of the United States of America*, **2006**. *103*(8): p. 2611-2616.

285. Sugimoto, H., S. Oda, T. Otsuki, K. Yotsuya, T. Hino, T. Yoshida, and Y. Shiro, X-ray structure and reaction mechanism of human indoleamine 2,3-dioxygenase. *International Congress Series*, **2007**. *1304*: p. 85-97.

286. Sun, Y., Indoleamine 2,3-dioxygenase: a new antioxidant enzyme. *Materia Medica Polona*, **1989**. *21*(3): p. 244-250.

287. Suzuki, T. and T. Takagi, A myoglobin evolved from indoleamine 2,3-dioxygenase. *Journal of Molecular Biology*, **1992**. *228*(2): p. 698-700.

288. Suzuki, T., H. Kawamichi, and K. Imai, A myoglobin evolved from indoleamine 2,3-dioxygenase, a tryptophan-degrading enzyme. *Comparative Biochemistry and Physiology. Part B, Biochemistry and Molecular Biology*, **1998**. *121*(2): p. 117-128.

289. Suzuki, S., S. Toné, O. Takikawa, T. Kubo, I. Kohno, and Y. Minatogawa, Expression of indoleamine 2,3-dioxygenase and tryptophan 2,3-dioxygenase in early concepti. *Biochemical Journal*, **2001**. *355*(2): p. 425-429.

290. Swanson, K.A., Y. Zheng, K.M. Heidler, T. Mizobuchi, and D.S. Wilkes, CDllc+ cells modulate pulmonary immune responses by production of indoleamine 2,3-dioxygenase. *American Journal of Respiratory Cell and Molecular Biology*, **2004**. *30*(3): p. 311-318.

291. Sweeten, T.L., M. Ferris, C.J. McDougle, P. Kwo, and M.W. Taylor, Induction of indoleamine 2,3-dioxygenase *in vivo* by IFN-con1. *Journal of Interferon and Cytokine Research*, **2001**. *21*(8): p. 631-633.

292. Szanto, S., T. Koreny, K. Mikecz, T. Glant, Z. Szekanecz, and J. Varga, Inhibition of indoleamine 2,3-dioxygenase-mediated tryptophan catabolism accelerates collagen-induced arthritis in mice. *Arthritis Research and Therapy*, **2007**. *9*(3): p. R50.

293. Takikawa, O., R. Yoshida, and O. Hayaishi, Monooxygenase activities of dioxygenases. Benzphetamine demethylation and aniline hydroxylation reactions catalyzed by indoleamine 2,3-dioxygenase. *Journal of Biological Chemistry*, **1983**. *258*(11): p. 6808-6815.

294. Takikawa, O., R. Yoshida, R. Kido, and O. Hayaishi, Tryptophan degradation in mice initiated by indoleamine 2,3-dioxygenase. *Journal of Biological Chemistry*, **1986**. *261*(8): p. 3648-3653.

295. Takikawa, O., T. Kuroiwa, F. Yamazaki, and R. Kido, Mechanism of interferon-gamma action. Characterization of indoleamine 2,3-dioxygenase in cultured human cells induced by interferon-gamma and evaluation of the enzyme-mediated tryptophan degradation in its anticellular activity. *Journal of Biological Chemistry*, **1988**. *263*(4): p. 2041-2048.

296. Takikawa, O., A. Habara-Ohkubo, and R. Yoshida, IFN-gamma is the inducer of indoleamine 2,3-dioxygenase in allografted tumor cells undergoing rejection. *Journal of Immunology*, **1990**. *145*(4): p. 1246-1250.

297. Takikawa, O., A. Habara-Ohkubo, and R. Yoshida, Induction of indoleamine 2,3-dioxygenase in tumor cells transplanted into allogeneic mouse: interferon-gamma is the inducer. *Advances in Experimental Medicine and Biology*, **1991**. *294*(1): p. 437-444.

298. Takikawa, O., T. Littlejohn, J.F. Jamie, M.J. Walker, and R.J. Truscott, Regulation of indoleamine 2,3-dioxygenase, the first enzyme in UV filter biosynthesis in the human lens. Relevance for senile nuclear cataract. *Advances in Experimental Medicine and Biology*, **1999**. *467*(1): p. 241-245.

299. Takikawa, O., Y. Tagawa, Y. Iwakura, R. Yoshida, and R.J. Truscott, Interferon-gamma-dependent/independent expression of indoleamine 2,3-dioxygenase. Studies with interferon-gamma-knockout mice. *Advances in Experimental Medicine and Biology*, **1999**. *467*(1): p. 553-557.

300. Takikawa, O., T.K. Littlejohn, and R.J. Truscott, Indoleamine 2,3-dioxygenase in the human lens, the first enzyme in the synthesis of UV filters. *Experimental Eye Research*, **2001**. *72*(3): p. 271-277.

301. Takikawa, O., R.J.W. Truscott, M. Fukao, and S. Miwa, Age-related nuclear cataract and indoleamine 2,3-dioxygenase-initiated tryptophan metabolism in the human lens. *Advances in Experimental Medicine and Biology*, **2003**. *527*(1): p. 277-285.

302. Takikawa, O., Biochemical and medical aspects of the indoleamine 2,3-dioxygenase-initiated L-tryptophan metabolism. *Biochemical and Biophysical Research Communications*, **2005**. *338*(1): p. 12-19.

303. Takikawa, O., Clinical aspects of indoleamine 2,3-dioxygenase (IDO)-initiated tryptophan metabolism: IDO is a target of drug discovery for various diseases. *International Congress Series*, **2007**. *1304*: p. 290-297.

304. Taniguchi, T., F. Hirata, and O. Hayaishi, Intracellular utilization of superoxide anion by indoleamine 2,3-dioxygenase of rabbit enterocytes. *Journal of Biological Chemistry*, **1977**. *252*(8): p. 2774-2776.

305. Taniguchi, T., M. Sono, F. Hirata, O. Hayaishi, M. Tamura, K. Hayashi, T. Iizuka, and Y. Ishimura, Indoleamine 2,3-dioxygenase. Kinetic studies on the binding of superoxide anion and molecular oxygen to enzyme. *Journal of Biological Chemistry*, **1979**. *254*(9): p. 3288-3294.

306. Taylor, M.W. and G.S. Feng, Relationship between interferon-gamma, indoleamine 2,3-dioxygenase, and tryptophan catabolism. *Federation of American Societies for Experimental Biology Journal*, **1991**. *5*(11): p. 2516-2522.

307. Terajima, M. and A.M. Leporati, Role of Indoleamine 2,3-dioxygenase in antiviral activity of interferon-gamma against *Vaccinia* virus. *Viral Immunology*, **2005**. *18*(4): p. 722-729.

308. Terentis, A.C., S.R. Thomas, O. Takikawa, T.K. Littlejohn, R.J.W. Truscott, R.S. Armstrong, S.R. Yeh, and R. Stocker, The heme environment of recombinant human indoleamine 2,3-dioxygenase. Structural properties and substrate-ligand interactions. *Journal of Biological Chemistry*, **2002**. *277*(18): p. 15788-15794.

309. Terness, P., T.M. Bauer, L. Röse, C. Dufter, A. Watzlik, H. Simon, and G. Opelz, Inhibition of allogeneic T cell proliferation by indoleamine 2,3-dioxygenase-expressing dendritic cells: mediation of suppression by tryptophan metabolites. *Journal of Experimental Medicine*, **2002**. *196*(4): p. 447-457.

310. Terness, P., J.J. Chuang, T. Bauer, L. Jiga, and G. Opelz, Regulation of human auto- and alloreactive T cells by indoleamine 2,3-dioxygenase (IDO)-producing dendritic cells: too much ado about IDO? *Blood*, **2005**. *105*(6): p. 2480-2486.

311. Terness, P., J.J. Chuang, and G. Opelz, The immunoregulatory role of IDO-producing human dendritic cells revisited. *Trends in Immunology*, **2006**. *27*(2): p. 68-73.

312. Tissue, B. M., Size exclusion chromatography (SEC). *Analytical Chemistry and Instrumentation*, **1996**. Hypermedia for Science Education (Science Hypermedia): from www.scimedia.com.

313. Thomas, S.R., D. Mohr, and R. Stocker, Nitric oxide inhibits indoleamine 2,3-dioxygenase activity in interferon-gamma primed mononuclear phagocytes. *Journal of Biological Chemistry*, **1994**. *269*(20): p. 14457-14464.

314. Thomas, S.R. and R. Stocker, Redox reactions related to indoleamine 2,3-dioxygenase and tryptophan metabolism along the kynurenine pathway. *Redox Report*, **1999**. *4*(5): p. 199-220.

315. Thomas, S.R., H. Salahifar, R. Mashima, N.H. Hunt, D.R. Richardson, and R. Stocker, Antioxidants inhibit indoleamine 2,3-dioxygenase in IFN-gamma-activated human macrophages: posttranslational regulation by pyrrolidine dithiocarbamate. *Journal of Immunology*, **2001**. *166*(10): p. 6332-6340.

316. Tolia, N.H. and L. Joshua-Tor, Strategies for protein coexpression in *Escherichia coli*. *Nature Methods*, **2006**. *3*(1): p. 55-64.

317. Tone, S., A. Kadoya, H. Maeda, Y. Minatogawa, and R. Kido, Assignment of the human indoleamine 2,3-dioxygenase gene to chromosome 8 using the polymerase chain reaction. *Human Genetics*, **1994**. *93*(2): p. 201-203.

318. Tone, S., O. Takikawa, A. Habara-Ohkubo, A. Kadoya, R. Yoshida, and R. Kido, Primary structure of human indoleamine 2,3-dioxygenase deduced from the nucleotide sequence of its cDNA. *Nucleic Acids Research*, **1990**. *18*(12): p. 367.

319. Travers, M.T., I.F. Gow, M.C. Barber, J. Thomson, and D.B. Shennan, Indoleamine 2,3-dioxygenase activity and L-tryptophan transport in human breast cancer cells. *Biochimica et Biophysica Acta*, **2004**. *1661*(1): p. 106-112.

320. Tsukada, J., A. Ozaki, T. Hanada, T. Chinen, R. Abe, A. Yoshimura, and M. Kubo, The role of suppressor of cytokine signaling 1 as a negative regulator for aberrant expansion of CD8alpha+ dendritic cell subset. *International Immunology*, **2005**. *17*(9): p. 1167-1178.

321. Tu, H., P. Rady, T. Juelich, E. Smith, S. Tyring, and T. Hughes, Cytokine regulation of tryptophan metabolism in the hypothalamic-pituitary-adrenal (HPA) axis: implications for protective and toxic consequences in neuroendocrine regulation. *Cellular and Molecular Neurobiology*, **2005**. *25*(3): p. 673-680.

322. Uchida, K., T. Shimizu, R. Makino, K. Sakaguchi, T. Iizuka, Y. Ishimura, T. Nozawa, and M. Hatano, Magnetic and natural circular dichroism of L-tryptophan 2,3-dioxygenases and indoleamine 2,3-dioxygenase. I. Spectra of ferric and ferrous high spin forms. *Journal of Biological Chemistry*, **1983**. *258*(4): p. 2519-2525.

323. Uchida, K., H. Bandow, R. Makino, K. Sakaguchi, T. Iizuka, and Y. Ishimura, Infrared spectra of carbon monoxide complexes of indoleamine 2,3-dioxygenase and L-tryptophan 2,3-dioxygenases. Effects of substrates on the CO-stretching frequencies. *Journal of Biological Chemistry*, **1985**. *260*(3): p. 1400-1406.

324. Urade, Y., R. Yoshida, H. Kitamura, and O. Hayaishi, Induction of indoleamine 2,3-dioxygenase in alveolar interstitial cells of mouse lung by bacterial lipopolysaccharide. *Journal of Biological Chemistry*, **1983**. *258*(10): p. 6621-6627.

325. Uyttenhove, C., L. Pilotte, I. Théate, V. Stroobant, D. Colau, N. Parmentier, T. Boon, and B.J. Van den Eynde, Evidence for a tumoral immune resistance mechanism based on tryptophan degradation by indoleamine 2,3-dioxygenase. *Nature Medicine*, **2003**. *9*(10): p. 1269-1274.

326. van der Sluijs, K.F., M. Nijhuis, J.H.M. Levels, S. Florquin, A.L. Mellor, H.M. Jansen, T. van der Poll, and R. Lutter, Influenza-induced expression of indoleamine 2,3-dioxygenase enhances interleukin-10 production and bacterial outgrowth during secondary pneumococcal pneumonia. *Journal of Infectious Diseases*, **2006**. *193*(2): p. 214-222.

327. van Wissen, M., M. Snoek, B. Smids, H.M. Jansen, and R. Lutter, IFN-gamma amplifies IL-6 and IL-8 responses by airway epithelial-like cells via indoleamine 2,3-dioxygenase. *Journal of Immunology*, **2002**. *169*(12): p. 7039-7044.

328. Varadkar, S. and R. Surtees, Glutaric aciduria type I and kynurenine pathway metabolites: a modified hypothesis. *Journal of Inherited Metabolic Disease*, **2004**. *27*(6): p. 835-842.

329. von Bergwelt-Baildon, M.S., A. Popov, T. Saric, J. Chemnitz, S. Classen, M.S. Stoffel, F. Fiore, U. Roth, M. Beyer, S. Debey, C. Wickenhauser, F.G. Hanisch, and J.L. Schultze, CD25 and indoleamine 2,3-dioxygenase are up-regulated by prostaglandin E2 and expressed by tumor-associated dendritic cells *in vivo*: additional mechanisms of T-cell inhibition. *Blood*. Vol. 108. **2006**. 228-237.

330. von Bubnoff, D., G. Bezold, H. Matz, D. Hanau, H. De La Salle, and T. Bieber, Quantification of indoleamine 2,3-dioxygenase gene induction in atopic and non-atopic monocytes after ligation of the high-affinity receptor for IgE, Fc(epsilon)RI and interferon-gamma stimulation. *Clinical and Experimental Immunology*, **2003**. *132*(2): p. 247-253.

331. von Bubnoff, D., D. Hanau, J. Wenzel, O. Takikawa, B. Hall, S. Koch, and T. Bieber, Indoleamine 2,3-dioxygenase-expressing antigen-presenting cells and peripheral T-cell tolerance: another piece to the atopic puzzle? *Journal of Allergy and Clinical Immunology*, **2003**. *112*(5): p. 854-860.

332. von Bubnoff, D., H. Bausinger, H. Matz, S. Koch, G. Häcker, O. Takikawa, T. Bieber, D. Hanau, and H. de la Salle, Human epidermal langerhans cells express the immunoregulatory enzyme indoleamine 2,3-dioxygenase. *Journal of Investigative Dermatology*, **2004**. *123*(2): p. 298-304.

333. von Bubnoff, D., R. Fimmers, M. Bogdanow, H. Matz, S. Koch, and T. Bieber, Asymptomatic atopy is associated with increased indoleamine 2,3-dioxygenase activity and interleukin-10 production during seasonal allergen exposure. *Clinical and Experimental Allergy*, **2004**. *34*(7): p. 1056-1063.

334. Vottero, E., A. Balgi, K. Woods, S. Tugendreich, T. Melese, R.J. Andersen, A.G. Mauk, and M. Roberge, Inhibitors of human indoleamine 2,3-dioxygenase identified with a target-based screen in yeast. *Biotechnology Journal*, **2006**. *1*(3): p. 282-288.

335. Wagner, G.C., Perez, M., Toscano, W.A., Jr., and Gunsalus, I.C., Apoprotein formation and heme reconstitution of cytochrome P-450cam, *Journal of Biological Chemistry*, **1981**. *256*(12): p. 6262-6265.

336. Watanabe, Y., R. Yoshida, M. Sono, and O. Hayaishi, Immunohistochemical localization of indoleamine 2,3-dioxygenase in the argyrophilic cells of rabbit duodenum and thyroid gland. *Journal of Histochemistry and Cytochemistry*, **1981**. *29*(5): p. 623-632.

337. Webster, N.L., J. Wee, S.J. Uren, W. Boyle, and M.S. Sandrin, Production and purification of human indoleamine 2,3-dioxygenase (HuIDO) protein in a baculovirus expression system and production and characterization of egg yolk antibody against the purified HuIDO. *Immunology and Cell Biology*, **2005**. *83*(5): p. 542-548.

338. Werner, E.R., G. Werner-Felmayer, D. Fuchs, A. Hausen, G. Reibnegger, and H. Wachter, Influence of interferon-gamma and extracellular tryptophan on indoleamine 2,3-dioxygenase activity in T24 cells as determined by a non-radiometric assay. *Biochemical Journal*, **1988**. *256*(2): p. 537-541.

339. Werner, E.R., G. Werner-Felmayer, D. Fuchs, A. Hausen, G. Reibnegger, and H. Wachter, Parallel induction of tetrahydrobiopterin biosynthesis and indoleamine 2,3-dioxygenase activity in human cells and cell lines by interferon-gamma. *Biochemical Journal*, **1989**. *262*(3): p. 861-866.

340. Wichers, M.C. and M. Maes, The role of indoleamine 2,3-dioxygenase (IDO) in the pathophysiology of interferon-alpha-induced depression. *Journal of Psychiatry and Neuroscience*, **2004**. *29*(1): p. 11-17.

341. Wichers, M.C., G.H. Koek, G. Robaeys, R. Verkerk, S. Scharpé, and M. Maes, IDO and interferon-alpha-induced depressive symptoms: a shift in hypothesis from tryptophan depletion to neurotoxicity. *Molecular Psychiatry*, **2005**. *10*(6): p. 538-544.

342. Wirleitner, B., G. Neurauter, K. Schrocksnadel, B. Frick, and D. Fuchs, Interferon-gamma-induced conversion of tryptophan: immunologic and neuropsychiatric aspects. *Current Medicinal Chemistry*, **2003**. *10*(16): p. 1581-1591.

343. Wolf, A.M., D. Wolf, H. Rumpold, A.R. Moschen, A. Kaser, P. Obrist, D. Fuchs, G. Brandacher, C. Winkler, K. Geboes, P. Rutgeerts, and H. Tilg, Overexpression of indoleamine 2,3-dioxygenase in human inflammatory bowel disease. *Clinical Immunology*, **2004**. *113*(1): p. 47-55.

344. Wood, H., C. Fehlner-Gardner, J. Berry, E. Fischer, B. Graham, T. Hackstadt, C. Roshick, and G. McClarty, Regulation of tryptophan synthase gene expression in *Chlamydia trachomatis*. *Molecular Microbiology*, **2003**. *49*(5): p. 1347-1359.

345. Xiao, B.G., X. Liu, and H. Link, Antigen-specific T cell functions are suppressed over the estrogen-dendritic cell-indoleamine 2,3-dioxygenase axis. *Steroids*, **2004**. *69*(10): p. 653-659.

346. Xiao, B.G., X.C. Wu, J.S. Yang, L.Y. Xu, X. Liu, Y.M. Huang, B. Bjelke, and H. Link, Therapeutic potential of IFN-gamma-modified dendritic cells in acute and chronic experimental allergic encephalomyelitis. *International Immunology*, **2004**. *16*(1): p. 13-22.

347. Yamamoto, S. and O. Hayaishi, Tryptophan pyrrolase of rabbit intestine. D-and L-tryptophan-cleaving enzyme or enzymes. *Journal of Biological Chemistry*, **1967**. *242*(22): p. 5260-5266.

348. Yasui, H., K. Takai, R. Yoshida, and O. Hayaishi, Interferon enhances tryptophan metabolism by inducing pulmonary indoleamine 2,3-dioxygenase: its possible occurrence in cancer patients. *Proceedings of the National Academy of Sciences of the United States of America*, **1986**. *83*(17): p. 6622-6626.

349. Yoshida, R. and O. Hayaishi, Induction of pulmonary indoleamine 2,3-dioxygenase by intraperitoneal injection of bacterial lipopolysaccharide. *Proceedings of the National Academy of Sciences of the United States of America*, **1978**. *75*(8): p. 3998-4000.

350. Yoshida, R., Y. Urade, M. Tokuda, and O. Hayaishi, Induction of indoleamine 2,3-dioxygenase in mouse lung during virus infection. *Proceedings of the National Academy of Sciences of the United States of America*, **1979**. *76*(8): p. 4084-4086.

351. Yoshida, R., J. Imanishi, T. Oku, T. Kishida, and O. Hayaishi, Induction of pulmonary indoleamine 2,3-dioxygenase by interferon. *Proceedings of the National Academy of Sciences of the United States of America*, **1981**. *78*(1): p. 129-132.

352. Yoshida, Z., Oxygen binding and activation with hemoproteins: model approach using iron-porphyrin complexes. *Pure and Applied Chemistry*, **1981**. *53*: p. 293-304.

353. Yoshida, R., T. Oku, J. Imanishi, T. Kishida, and O. Hayaishi, Interferon: a mediator of indoleamine 2,3-dioxygenase induction by lipopolysaccharide, poly(I) X poly(C), and pokeweed mitogen in mouse lung. *Archives of Biochemistry and Biophysics*, **1986**. *249*(2): p. 596-604.

354. Yuan, W., A. Collado-Hidalgo, T. Yufit, M. Taylor, and J. Varga, Modulation of cellular tryptophan metabolism in human fibroblasts by transforming growth factor-beta: selective inhibition of indoleamine 2,3-dioxygenase and tryptophanyl-tRNA synthetase gene expression. *Journal of Cellular Physiology*, **1998**. *177*(1): p. 174-186.

355. Yuasa, H.J. and T. Suzuki, Do molluscs possess indoleamine 2,3-dioxygenase? *Comparative Biochemistry and Physiology. Part B, Biochemistry and Molecular Biology*, **2005**. *140*(3): p. 445-454.

356. Zamanakou, M., A.E. Germenis, and V. Karanikas, Tumor immune escape mediated by indoleamine 2,3-dioxygenase. *Immunology Letters*, **2007**. *111*(2): p. 69-75.

Appendices

Appendix 1 *Ab initio* calculations and comparative models of protein domains of indoleamine 2,3-dioxygenase done by the Robetta Server gave the following homology results (Human IDO is given as 100% identity).

Species	Alignments	Identity	Length	Description
Homo sapiens	6.67%	100	403	indoleamine-pyrrole 2,3 dioxygenase [*Homo sapiens*]
Rattus norvegicus	6.67%	64	395	indoleamine 2,3-dioxygenase [*Rattus norvegicus*]
Mus musculus	6.67%	63	395	indoleamine-pyrrole 2,3 dioxygenase [*Mus musculus*]
Gibberella zeae PH-1	13.33%	31	429	hypothetical protein FG02657.1 [*Gibberella zeae* PH-1]
Candida albicans SC5314	6.67%	32	409	hypothetical protein CaO19.8215 [*Candida albicans* SC5314]
Aspergillus nidulans FGSC A4	6.67%	30	422	hypothetical protein AN2509.2 [*Aspergillus nidulans* FGSC A4]
Neurospora crassa	10.00%	31	441	hypothetical protein [*Neurospora crassa*]
Eremothecium gossypii	3.33%	30	427	ACR188Cp [*Eremothecium gossypii*]
Nordotis madaka	3.33%	33	389	indoleamine dioxygenase-like myoglobin [*Nordotis madaka*]
Sulculus diversicolor	3.33%	34	388	IDO-like myoglobin [*Sulculus diversicolor*]
Saccharomyces cerevisiae	3.33%	31	426	tryptophan 2,3-dioxygenase Bna2p [*Saccharomyces cerevisiae*]
Omphalius pfeifferi	3.33%	27	373	indoleamine dioxygenase like-myoglobin [*Omphalius pfeifferi*]
Batillus cornutus	3.33%	28	374	indoleamine dioxygenase like-myoglobin [*Batillus cornutus*]
Magnaporthe grisea 70-15	6.67%	19	441	hypothetical protein MG00755.4 [*Magnaporthe grisea* 70-15]
Ustilago maydis 521	3.33%	22	438	hypothetical protein UM03728.1 [*Ustilago maydis* 521]
Marmota monax	3.33%	67	161	indoleamine 2,3-dioxygenase [*Marmota monax*]
IMS101	6.67%	21	164	hypothetical protein [*Trichodesmium erythraeum* IMS101]
Macaca mulatta	3.33%	87	54	indoleamine 2,3-dioxygenase [*Macaca mulatta*]

Appendix 2 Compilation of data from various databases on human IDO (Brenda EC 1.13.11.52)

SUBSTRATE	PRODUCT	ORGANISM	COMMENTARY
5-hydroxytryptamine + O2	-	Homo sapiens	-
D-Trp + O2	*N*-formyl-D-kynurenine	Homo sapiens	-
L-5-hydroxytryptophan + O2	-	Homo sapiens	-
L-Trp + O2	L-formylkynurenine	Homo sapiens	-
tryptamine + O2	-	Homo sapiens	-

NATURAL SUBSTRATE	NATURAL PRODUCT	ORGANISM	COMMENTARY
L-Trp + O2	L-formylkynurenine	Homo sapiens	initial enzyme of tryptophan degradation pathway; lipopolysaccharide and muramyl tripeptide upregulate enzyme induction through a mechanism independent of interleukin 1alpha; first enzyme in the biosynthetic pathway of UV filters from Trp; Trp degradation by the enzyme regulates lymphocyte proliferation; interleukin-4 inhibits expression of the enzyme in monocytes; activity is increased in important biological processes, such as protection of the fetus from rejection during pregnancy and possibly T cell death in HIV-infected patients
L-Trp + O2	L-formylkynurenine	Homo sapiens	rate-limiting enzyme in the catabolism of tryptophan

Appendix 2 Compilation of data from various databases on human IDO (Continued)

COFACTOR	ORGANISM	COMMENTARY
heme	Homo sapiens	enzyme contains heme; the already active reduced holoenzyme does not require haematin for activity, the heme-free predominant apoenzyme does; characterization of the heme environment, strong proximal Fe-His bond and strong H-bonding and/or steric interactions between L-Trp and dioxygen in the distal pocket are likely crucial for the enzymatic activity of the recombinant enzyme

INHIBITORS	ORGANISM	COMMENTARY
1-methyltryptophan	Homo sapiens	competitive; 2 mM, 70% inhibition
NO	Homo sapiens	-
norharman	Homo sapiens	2 mM, 98% inhibition, uncompetitive

ACTIVATING COMPOUND	ORGANISM	COMMENTARY
methylene blue	Homo sapiens	native and recombinant enzyme require methylene blue and ascorbic acid for activity

KM VALUE [mM]	KM VALUE [mM] Maximum	SUBSTRATE	ORGANISM	COMMENTARY
0.44	-	5-hydroxy-L-tryptophan	Homo sapiens	recombinant enzyme
5	-	D-Trp	Homo sapiens	recombinant enzyme
0.02	-	L-Trp	Homo sapiens	recombinant enzyme
0.02	-	L-Trp	Homo sapiens	-

Ki VALUE [mM]	Ki VALUE [mM] Maximum	INHIBITOR	ORGANISM	COMMENTARY
0.06	-	1-methyltryptophan	Homo sapiens	-
0.17	-	Norharman	Homo sapiens	-

TURNOVER NUMBER	TURNOVER Maximum	SUBSTRATE	ORGANISM	COMMENTARY
124	-	D-Trp	Homo sapiens	-
93	-	L-Trp	Homo sapiens	-
3.9	-	5-hydroxy-L-tryptophan	Homo sapiens	-

SPECIFIC ACTIVITY [µM/min/mg]	SPECIFIC ACTIVITY Maximum	ORGANISM	COMMENTARY
2.58	-	Homo sapiens	-

pH OPTIMUM	pH MAXIMUM	ORGANISM	COMMENTARY
6.5	-	Homo sapiens	-

Appendix 3 Austin, C.J.D., J. Mizdrak, A. Matin, N. Sirijovski, P. Kosim-Satyaputra, R.D. Willows, T.H. Roberts, R.J.W. Truscott, G. Polekhina, M.W. Parker, and J.F. Jamie, Optimised expression and purification of recombinant human indoleamine 2,3-dioxygenase. *Protein Expression and Purification*, 2004. *37*(2): p. 392-398.

Available online at www.sciencedirect.com
SCIENCE DIRECT®
Protein Expression and Purification 37 (2004) 392–398
Protein Expression & Purification
www.elsevier.com/locate/yprep

Optimised expression and purification of recombinant human indoleamine 2,3-dioxygenase

Christopher J.D. Austin[a], Jasminka Mizdrak[a], Azadeh Matin[a], Nicholche Sirijovski[b], Priambudi Kosim-Satyaputra[a], Robert D. Willows[b], Thomas H. Roberts[b], Roger J.W. Truscott[c], Galina Polekhina[d], Michael W. Parker[d], Joanne F. Jamie[a,*]

[a] *Department of Chemistry, Macquarie University, Sydney, Australia*
[b] *Department of Biological Sciences, Macquarie University, Sydney, Australia*
[c] *Australian Cataract Research Foundation, University of Wollongong, Wollongong, Australia*
[d] *St. Vincent's Institute of Medical Research, Melbourne, Australia*

Received 8 April 2004, and in revised form 18 June 2004
Available online 6 August 2004

Abstract

The hemoprotein indoleamine 2,3-dioxygenase (IDO) is the first and rate-limiting enzyme in mammalian tryptophan metabolism. It has received considerable attention in recent years, particularly due to its role in the pathogenesis of many diseases. Here, we report attempts to improve soluble expression and purification of hexahistidyl-tagged recombinant human IDO from *Escherichia coli* (EC538, pREP4, and pQE9-IDO). Significant formation of inclusion bodies was noted at the growth temperature of 37 °C, with reduced formation at 30 °C. The addition of the natural biosynthetic precursor of protoporphrin IX, δ-aminolevulinic acid (ALA), coupled with optimisation of IPTG induction levels during expression at 30 °C and purification by nickel–agarose and size exclusion chromatography, resulted in protein with 1 mol of heme/mol of protein and a specific activity of 160 μmol of kynurenine/h/mg of protein (both identical to native human IDO). The protein was homogeneous in terms of electrophoretic analysis. Yields of soluble protein (3–5 mg/L of bacterial culture) and heme content are greater than previously reported.

The kynurenine pathway is responsible for 90% of human tryptophan catabolism [1]. The first and rate-limiting step of the kynurenine pathway is the oxidative cleavage of the 2,3-double bond of the indole ring of tryptophan, via the incorporation of molecular oxygen or superoxide anion [1–3]. Indoleamine 2,3-dioxygenase (IDO) [EC 1.13.11.17] is a cytosolic, monomeric hemoprotein and is the major enzyme capable of catalysing this oxidation reaction in mammals. Native human IDO is 403 amino acids long, with a molecular weight of 45,326 Da and a p*I* of 7.1 [4,5].

In healthy humans, IDO activation remains low, with kynurenine pathway metabolites existing in sub-nanomolar concentrations and apparently exerting little or no physiological effects [6]. As an immune response to a variety of pathological conditions, such as viral [7–10], bacterial [11,12], and protozoan infection [13–15], and tumour regression [16], IDO is over-expressed and tryptophan depletion ensues [17,18]. Rejection of the allogeneic foetus from the placenta is believed to be prevented during pregnancy by a similar mechanism [19–21]. Induction of IDO within the central nervous system leads to increased concentrations of kynurenine pathway metabolites, most notably, two neurotoxic compounds, 3-hydroxykynurenine and quinolinic acid. Increased levels of quinolinic acid are implicated in neurological disorders, such as AIDS dementia complex

* Corresponding author. Fax: +61-2-9850-8313.
E-mail address: joanne.jamie@mq.edu.au (J.F. Jamie).

1046-5928/$ - see front matter © 2004 Elsevier Inc. All rights reserved.
doi:10.1016/j.pep.2004.06.025

[22–24], cerebral malaria [25], and ischemic brain injury [26,27]. The metabolite 3-hydroxykynurenine is a potent neurotoxin and may be a contributing factor in some neurological diseases, such as Huntington's disease [28,29]. This metabolite has also been shown to react with lens proteins (crystallins), producing a tanned/yellow product resembling nuclear cataractous materials [30], suggesting a relationship between 3-hydroxykynurenine and age-related nuclear cataract formation, a major cause of blindness.

With the importance of IDO in human physiology and disease becoming increasingly recognised it would be highly advantageous to have access to large quantities of pure human IDO to allow studies on its structure and mechanism of action. The reported isolation and purification protocol of native human IDO from the human placenta [31,32] incorporated cation exchange chromatography, hydroxyapatite chromatography, gel filtration, and isoelectric focusing. A 10,000-fold purification was achieved with a yield of 0.9% and a specific activity of 157 μmol kynurenine/h/mg of protein. Littlejohn et al. [33] have previously reported expression of recombinant human IDO (6His-IDO) in *E. coli* at 37 °C with 7 μM hemin supplementation in the media, and subsequent purification using a combination of phosphocellulose and nickel–agarose affinity chromatography. The resultant protein had a specific activity of 149 μmol kynurenine/h/mg of protein and was produced with 0.8 mol heme/mol of IDO in a yield of 1.4 mg/L of bacterial culture. Here, we report an expression and purification protocol for 6His-IDO that shows improved yield, specific activity and heme to protein ratio.

Experimental procedures

Materials

δ-Aminolevulinic acid (ALA), ampicillin, ascorbic acid, catalase (bovine), imidazole, isopropyl-β-D-thiogalactopyranoside (IPTG), L-kynurenine, kanamycin, lysozyme, *p*-dimethylaminobenzaldehyde (*p*-DMAB), phenylmethylsulfonyl fluoride (PMSF), and L-tryptophan were obtained from Sigma–Aldrich. Bovine serum albumin (BSA) (Fraction V) was obtained from Amersham. Coomassie Blue R250 was purchased from Bio-Rad. DNase and EDTA-free cocktail inhibitor tablets were products of Roche. All other chemicals were of analytical grade unless otherwise specified.

Bacterial strains and plasmids

The *E. coli* strain used (EC538, pREP4, and pQE9–IDO) was the same as outlined in Littlejohn et al. [33].

General methods

Expression of 6His-IDO

Escherichia coli was routinely grown at 37 °C in Luria–Bertani (LB) medium containing 100 μg/mL ampicillin and 50 μg/mL kanamycin. A single colony of *E. coli* (EC538) cells containing plasmids pQE9-IDO and pREP4 was inoculated in 100 mL LB medium and cultured overnight. The 100 mL culture was added to 900 mL of the same medium and incubated at 30 °C to a density of 0.6 OD at 600 nm. IPTG (100 mM), ALA (500 mM), and PMSF (1 M) were then added at final concentrations of 0.1, 0.5, and 1 mM, respectively. Each culture was incubated for a further 3 h. Cells were collected as a pellet by centrifugation at 5000*g* for 20 min at 4 °C. The pellet was suspended in 20 mL ice-cold (Dulbecco's) phosphate-buffered saline (PBS) containing 1 mM PMSF and 1 mM ethylenediaminetetraacetic acid (EDTA) and centrifuged at 15,000*g* for 15 min at 4 °C. The pellet was stored at −80 °C for up to 1 month.

Purification of 6His-IDO

One litre pellets of bacterial culture, obtained according to the method described above, were suspended in 25 mM Tris(hydroxymethyl)methylamine (Tris) buffer at pH 7.4, containing 150 mM NaCl, 10 mM imidazole, 10 mM $MgCl_2$, and 1 mM PMSF. The suspension was then centrifuged at 5000*g* for 20 min at 4 °C and the supernatant was discarded. This process removed the EDTA, which was used for storage. EDTA can act as a metal chelator, which will interfere with proper binding of the protein to the charged Ni–NTA agarose.

The newly washed pellets were resuspended in 20 mL ice-cold buffer as outlined above, with the addition of EDTA free-cocktail inhibitor tablets (2×) and DNase (<1 mg). The suspension was French pressed three times at 10,000 psi and centrifuged at 5000*g* for 20 min to obtain a clear supernatant and pellet. The clear supernatant (20 mL) was then applied to a 1 mL Hi-Trap chelating column (Amersham Biosciences) charged with nickel ions; equilibrated with the basal buffer (Tris 25 mM, pH 7.4; 150 mM NaCl; and 1 mM PMSF) containing 10 mM imidazole. After washing with 18 mL of this buffer, 6His-IDO was eluted on a stepwise gradient incorporating washings at imidazole concentrations of 30; 40; 50; 65; 80; and elution at 190 mM.

The protein collected at the elution step was then buffer-exchanged into 50 mM Tris, pH 7.4, using a Sephadex G25 column (NAP 10—Pharmacia Biotech). The desalted fractions were pooled and concentrated to a volume of 50 μL using an Amicon Ultra (Millipore) 4 mL centrifugal device with a 30,000 Da molecular weight cut-off. The concentrated fraction was then applied to a Superdex 75 PC 3.2/30 (Pharmacia LKB Biotechnology) column according to the manufacturer's instructions, after equilibration with 50 mM Tris, pH

7.4. Fractions were collected in 75 μL aliquots at a flow rate of 60 μL/min over 3.5 mL.

Isolation of inclusion bodies

Each pellet, collected after French pressing, was resuspended twice in 1 mL MilliQ water and centrifuged at 5000*g* for 10 min. The freshly washed pellets were then resuspended in 1 mL of 1 mg/mL lysozyme and incubated for 10 min at room temperature before centrifugation. The pellets were then washed in 1 mL of 1% Triton X-100 and 1 mL MilliQ water before storage at −20 °C.

IDO assay

IDO activity was determined as described by Takikawa et al. [32] with minor modifications. In brief, the standard reaction mixture (200 μL) contained 50 mM potassium phosphate buffer (pH 6.5), 20 mM ascorbic acid (neutralised with NaOH), 200 μg/mL catalase, 10 μM methylene blue, 400 μM L-tryptophan, and IDO (either crude or purified). The reaction was carried out at 37 °C for 60 min and stopped by the addition of 40 μL of 30% (w/v) trichloroacetic acid. After heating at 65 °C for 15 min, the reaction mixtures were centrifuged at 11,500*g* for 7 min. The supernatant (125 μL) was transferred into a well of a 96-well microtitre plate and mixed with 125 μL of 2% (w/v) *p*-DMAB in acetic acid. The yellow pigment derived from kynurenine was measured at 480 nm using a Fluostar microtitre plate reader (BMG Lab Technologies). A standard curve of L-kynurenine was used, ranging in concentration from 0 to 500 μM. Protein concentration was determined using the Bradford protein assay [34] and a standard curve of bovine serum albumin, ranging in concentration from 0 to 1 mg/mL.

Optimisation of IPTG, ALA, and iron source levels

EC538 (pREP4, pQE9-IDO) was grown according to the general method outlined above. Concentrations of IPTG were varied at the induction stage, using the final concentrations: 0, 1, 10, 100, 500, and 1000 μM. Concentrations of ALA were varied at the induction stage, using the final concentrations: 0, 100, 500, and 1000 μM at 100 μM IPTG. Ten micromolar of ammonium iron(III) citrate was added to ALA trials at 100, 500, and 1000 μM ALA. Growth trials were performed in 100 mL LB broth at both 37 and 30 °C. Specific activity was determined via the IDO assay procedure outlined above.

Molecular techniques

SDS PAGE was performed according to the method of Laemmli [35] using a Bio-Rad Mini-Protean II system. Protein bands removed from SDS PAGE gels for peptide mass fingerprinting underwent a 16 h tryptic digest at 37 °C. A 1 μL aliquot was spotted onto a sample plate with 1 μL matrix (α-cyano-4-hydroxycinnamic acid, 8 mg/mL in 70% v/v acetonitrile, and 1% v/v trifluoroacetic acid) and allowed to air-dry. Matrix assisted laser desorption ionisation (MALDI) mass spectrometry was performed with an Applied Biosystems 4700 Proteomics Analyser with TOF/TOF optics in MS mode. A Nd:YAG laser (355 nm) was used to irradiate the sample. The spectra were acquired in reflectron mode in the mass range 800–3500 Th.

UV and visible spectra of proteins were recorded with a Shimadzu UV spectrophotometer. Gel densitometry was performed using ImageJ imaging software, a freeware program available from http://rsb.info.nih.gov/ij. Protein mass spectra were obtained using an API QSTAR Pulsar I (Applied Biosystems MDS SCIEX) Mass spectrometer.

Results and discussion

Qiagen, the manufacturer of the expression vector used in these studies, recommends 1 mM IPTG for induction [36]. Littlejohn et al. [33], however, performed a number of trials to determine an optimum IPTG level of 10 μM for the expression of soluble active IDO at 37 °C.

Expression of genetically engineered proteins in bacteria, especially *E. coli*, often results in the accumulation of insoluble protein aggregates, known as inclusion bodies [37]. Growths at 37 °C utilising 10 μM IPTG may not be optimised for total IDO production. Lowering the growth temperature is a common method for shifting protein production from inclusion bodies to a soluble, active form [38,39]. *E. coli* (EC538, pREP4, and pQE9-IDO) growths were therefore conducted at 37 and 30 °C to examine the formation of inclusion bodies. To ensure the removal of soluble protein, cell pellets were incubated with lysozyme after initial lysing. Inclusion bodies were observed via SDS–PAGE. Fig. 1 shows gels of inclusion bodies at 37 and 30 °C. Peptide sequencing indicated that the inclusion bodies produced were of IDO, as well as some *E. coli* specific proteins.

Reduced inclusion body formation was noted at 30 °C compared to 37 °C at corresponding IPTG levels. Densitometric analysis revealed relative levels of inclusion bodies. Ten micromolar and 100 μM IPTG at 37 °C showed significantly higher inclusion body formation than other IPTG concentrations, and their 30 °C counterparts (Fig. 2). Inclusion body formation showed no obvious trend with IPTG levels at 30 °C.

As less IDO was being expressed as inclusion bodies at a reduced growth temperature, the optimal concentration of IPTG required for soluble, active 6His-IDO expression in EC538 cells at 30 °C was determined. As shown in Fig. 3, IDO specific activity was dependent on the concentration of IPTG and max-

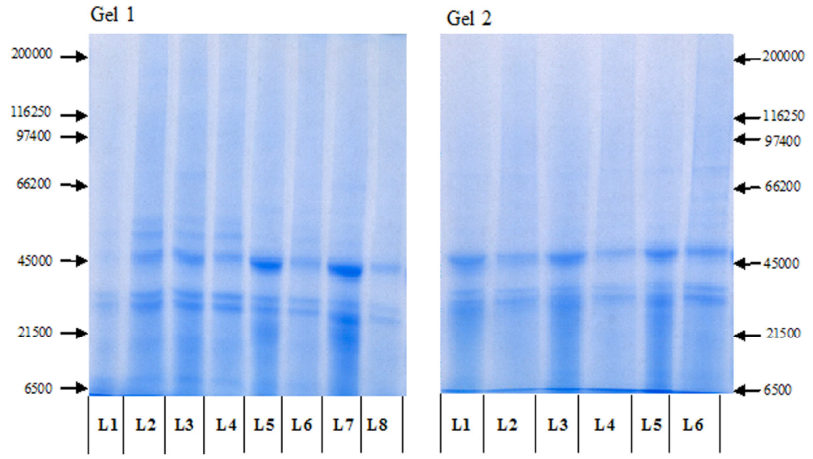

Fig. 1. SDS–PAGE analysis of the inclusion bodies formed by *E. coli* EC538 (pREP4, pQE9-IDO) at growth temperatures of 37 and 30 °C and with different levels of IPTG levels. Gel 1: Lane 1 (L1)—37 °C, 0 μM IPTG; Gel 1: L2—30 °C, 0 μM IPTG; Gel 1: L3—37 °C, 1 μM IPTG; Gel 1: L4—30 °C, 1 μM IPTG; Gel 1: L5—37 °C, 10 μM IPTG; Gel 1: L6—30 °C, 10 μM IPTG; Gel 1: L7—37 °C, 100 μM IPTG; and Gel 1: L8—30 °C, 100 μM IPTG; Gel 2: L1—37 °C, 500 μM IPTG; Gel 2: L2—30 °C, 500 μM IPTG; Gel 2: L3—37 °C, 1000 μM IPTG; Gel 2: L4—30 °C, 1000 μM IPTG; Gel 2: L5—37 °C, 10,000 μM IPTG; and Gel 2: L6—30 °C, 10,000 μM IPTG. The numbers on the left and right indicate molecular mass of markers in Da.

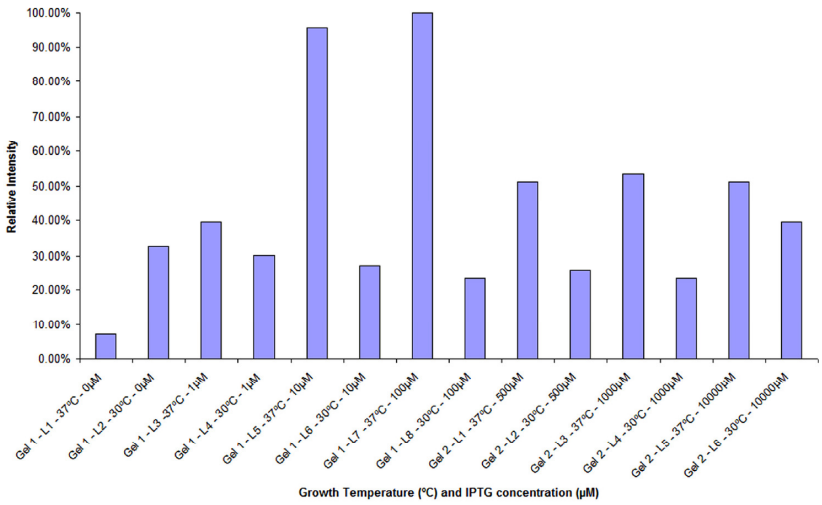

Fig. 2. Relative levels of inclusion bodies formed by *E. coli* EC538 (pREP4, PQE9-IDO) at growth temperatures of 37 and 30 °C and with different IPTG concentrations. All inclusion body levels were determined via gel densitometry and are expressed as a relative percentage of the maximum density observed—Gel 1: L7—37 °C, 100 μM IPTG.

imum protein specific activity was observed at approximately 100 μM. Gel densitometry revealed a plateau of IDO expression, at approximately 16% of total (soluble and insoluble) protein production, above 10 μM IPTG.

In preliminary purification trials performed by Littlejohn et al. [33], the heme (protoporphyrin IX) content of near homogeneous 6His IDO, as seen on SDS PAGE, was low, approximately 0.4 mol/mol of enzyme. This indicated that 60% of the 6His IDO preparation was free from heme (i.e., an apoenzyme). Heme content was increased to 0.8 mol/mol of enzyme by supplementation of the culture medium with 7 μM hemin in the induction phase.

To increase the heme content further, ALA was trialled as an alternative to hemin supplementation. ALA, the natural biosynthetic precursor to heme, has been used for increasing heme content of other hemoproteins [40]. ALA is more soluble than hemin and is

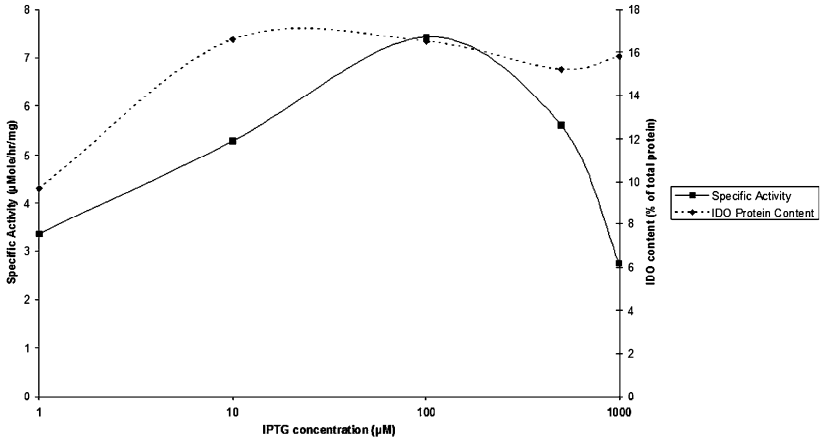

Fig. 3. IPTG dependency of expression of 6His-IDO in *E. coli* EC538 (pREP4, pQE9-IDO) cells grown at 30 °C. Bacteria were grown for 3 h with the indicated concentrations of IPTG in 100 mL cultures. IDO specific activity was determined on each bacterial crude extract after lysing cells via French press at 10,000 psi. IDO protein content was determined via gel densitometry as the proportion of IDO expressed as a percentage of total protein (soluble and insoluble).

less toxic to bacteria [41]. It was therefore hypothesised that uptake from *E. coli* may be improved and the heme to protein molar ratio (holoenzyme levels) may also be increased. To ensure that enough free iron was present during heme synthesis, the culture medium was supplemented with ammonium iron(III) citrate during ALA trials. Fig. 4 shows a comparison of the IDO activities of bacterial crude extracts obtained from growths with 100 μM IPTG and different levels of ALA and/or supplemented with 10 μM ammonium iron(III) citrate.

The supplementation of ammonium iron(III) citrate was found to have a deleterious effect on specific activity at 1 mM ALA. Due to the response of EC538 bacteria to the addition of an extraneous iron source, it was concluded that 1 mM ALA may be at the upper limit of the bacterial tolerance, and as a result, all large scale growths were performed at the lower ALA concentration of 0.5 mM. Owing to the large drop in specific activity caused by the addition of ammonium iron(III) citrate at 1 mM ALA, during large scale growths, no extraneous iron source was added.

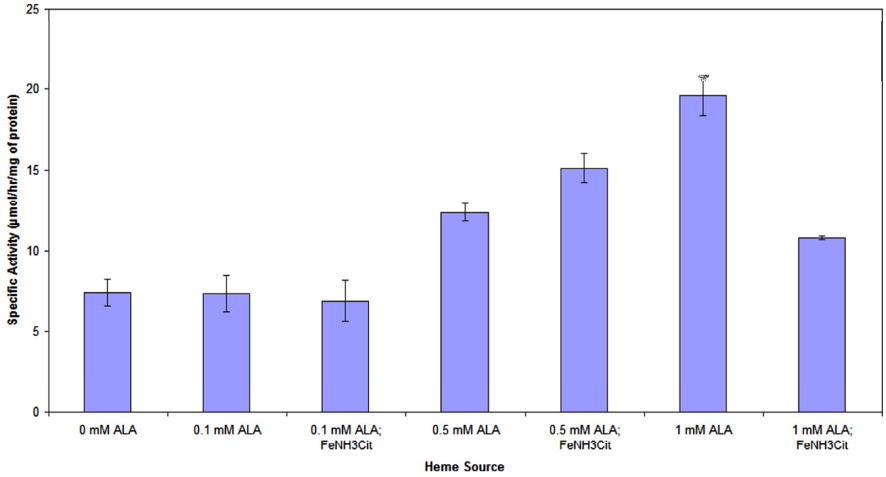

Fig. 4. Specific activity comparison of ALA and iron source addition to culture medium grown in the presence of 100 μM IPTG. ALA and ammonium iron(III) citrate (FeNH3Cit) were added to 100 mL cultures upon induction. Specific activity of IDO was determined on bacterial crude extract after lysing cells via a French press at 10,000 psi.

Table 1
Purification of 6His-IDO from *E. coli* EC538 (pREP4, pQE9-IDO)[a]

Step	Volume (mL)	Total protein (mg)	Total activity[b] (μmol/h)	Specific activity of IDO (μmol/h/mg)	Yield (%)	Purification
Crude extract	20.0	340	4216	12.4	100	1
Ni–NTA agarose	3.50	10.6	1480	140	35	11.3
Superdex 75–size exclusion	0.25	3.5	560	160	13	13.0

[a] Purification was achieved from the cells of a 1 L culture of *E. coli* EC538 (pREP4, pQE9-IDO).
[b] The enzyme activity was determined with L-tryptophan as the substrate.

As with the native enzyme purified from the human placenta, 6His-IDO is a ferric (Fe^{3+}) type hemoprotein, exhibiting a characteristic spectrum with peaks in the Soret (406 nm) and visible regions. The ratio of absorbance at 280 to 406 nm for fractions purified by Hi-Trap Ni–NTA, followed by Superdex 75, was 2.2, the same as the native enzyme [32], indicating full heme incorporation of the protein in purified samples.

Table 1 shows a summary of purification of 6His-IDO from the bacterial pellets of 1 L of culture. The enzyme was purified approximately 13-fold from the crude extract through two chromatography steps using metal affinity chromatography (Ni NTA agarose) and size exclusion chromatography (Superdex 75). The final sample gave a single band on SDS–PAGE. Recovery was 13% from the crude extract and the yield was 3.5 mg/L of LB broth.

Mass spectrometric analysis confirmed that IDO purified according to the protocol outlined in this communication had a mass consistent with the theoretical molecular weight of 46,976 Da [31].

Conclusion

Here, we report an improved expression and purification protocol for recombinant human IDO. Inclusion body formation by EC538 of 6His-IDO was significantly lowered through reduction in growth temperature from 37 to 30 °C. The use of ALA, the biosynthetic precursor of protoporphrin IX, coupled with metal-affinity chromatography and size exclusion chromatography, produced 6His-IDO with a protein to heme ratio of 1:2.2, the same as the native enzyme—better than heme levels previously reported for recombinant human IDO—and a specific activity of 160 μmol kynurenine/h/mg of protein.

Acknowledgments

This work was supported in part by the Australian Postgraduate Award Scheme for a Ph.D. scholarship (Christopher J.D. Austin) and the Australian National Health and Medical Research Council. We are grateful to Dr. Tamantha K. Littlejohn for technical support and assistance. This research has been facilitated by access to the Australian Proteome Analysis Facility established under the Australian Government's Major National Research Facilities program.

References

[1] O. Takikawa, R. Yoshida, R. Kido, O. Hayaishi, Tryptophan degradation in mice initiated by indoleamine 2,3-dioxygenase, J. Biol. Chem. 261 (1986) 3648–3653.
[2] T.R. Shane, R. Stocker, Redox reactions related to indoleamine 2,3-dioxygenase and tryptophan metabolism along the kynurenine pathway, Redox Rep. 4 (1999) 199–220.
[3] F. Moroni, Tryptophan metabolism and brain function: focus on kynurenine and other indole metabolites, Eur. J. Pharmacol. 375 (1999) 87–100.
[4] T.W. Stone, Inhibitors of the kynurenine pathway, Eur. J. Med. Chem. 35 (2000) 179–186.
[5] O. Hayaishi, O. Takikawa, R. Yoshida, Indoleamine 2,3-dioxygenase: properties and functions of a superoxide utilizing enzyme, Prog. Inorg. Chem.: Bioinorg. Chem. 38 (1990) 75–95.
[6] T.W. Stone, L.G. Darlington, Endogenous kynurenines as targets for drug discovery and development [Review], Nat. Rev. Drug Discov. 1 (2002) 609–620.
[7] R. Yoshida, Y. Urade, M. Takuda, O. Hayaishi, Induction of indoleamine 2,3-dioxygenase in mouse lung during virus infection, Proc. Natl. Acad. Sci. 76 (1979) 4084–4086.
[8] K. Saito, A. Lankner, S.P. Markey, M.P. Heyes, Cerebral cortex and lung indoleamine 2,3-dioxygenase activity is increased in type-D retrovirus infected macaques, Brain Res. 540 (1991) 353–356.
[9] M.P. Heyes, K. Saito, K. Jacobowitz, S.P. Markey, O. Takikawa, J.H. Vickers, Poliovirus induces indoleamine 2,3-dioxygenase and quinolinic acid synthesis in macaque brain, FASEB J. 6 (1992) 2977–2989.
[10] J.F. Reinhard Jr., Altered tryptophan metabolism in mice with herpes simplex virus encephalitis: increases in spinal cord quinolinic acid, Neurochem. Res. 23 (1998) 661–665.
[11] H. Schroten, B. Spors, C. Hucke, M. Stins, K.S. Kim, R. Adam, W. Daubener, Potential role of human brain microvascular endothelial cells in the pathogenesis of brain abscess: inhibition of *Staphylococcus aureus* by activation of indoleamine 2,3-dioxygenase, Neuropediatrics 32 (2001) 206–210.
[12] J.L. Perfettini, T. Darville, A. Dautry-Varsat, R.G. Rank, D.M Ojcius, Inhibition of apoptosis by gamma interferon in cells and mice infected with *Chlamydia muridarum* (the mouse pneumonitis strain of *Chlamydia trachomatis*), Infect. Immun. 70 (2002) 2559–2565.
[13] W. Daubener, B. Spors, C. Hucke, R. Adam, M. Stins, K.S. Kim, H. Schroten, Restriction of *Toxoplasma gondii* growth in human brain microvascular endothelial cells by activation of indoleamine 2,3-dioxygenase, Infect. Immun. 69 (2001) 6527–6531.

[14] N.M. Silva, C.V. Rodrigues, M.M. Santoro, L.F.L. Reis, J.I. Alvarez-Leite, R.T. Gazzinelli, Expression of indoleamine 2,3-dioxygenase, tryptophan degradation, and kynurenine formation during in vivo infection with *Toxoplasma gondii*: induction by endogenous gamma interferon and requirement of interferon regulatory factor 1, Infect. Immun. 70 (2002) 859–868.

[15] S. Fujigaki, K. Saito, M. Takemura, N. Maekawa, Y. Yamada, H. Wada, M. Seishima, L-Tryptophan-L-kynurenine pathway metabolism accelerated by *Toxoplasma gondii* infection is abolished in gamma interferon-gene-deficient mice: cross-regulation between inducible nitric oxide synthase and indoleamine-2,3-dioxygenase, Infect. Immun. 70 (2002) 779–786.

[16] C. Uyttenhove, L. Pilotte, I. Theate, V. Stroobant, D. Colau, N. Parmentier, T. Boon, B.J. Van den Eynde, Evidence for a tumoral immune resistance mechanism based on tryptophan degradation by indoleamine 2,3-dioxygenase, Nat. Med. 9 (2003) 1269–1274.

[17] N. Sepp, B. Widner, E. Kowald, U. Ortner, B. Wirleitne, P. Fritsch, G. Baier-Bitterlich, D. Fuchs, Enhanced tryptophan degradation in systemic lupus erythematosus, Immunobiology 201 (2000) 621–630.

[18] A. Habara-Ohkubo, T. Shirahata, O. Takikawa, R. Yoshida, Establishment of an antitoxoplasma state by stable expression of mouse indoleamine 2,3-dioxygenase, Infect. Immun. 61 (1993) 1810–1813.

[19] A.L. Mellor, D.H. Munn, Extinguishing maternal immune responses during pregnancy: implications for immunosuppression [Review], Semin. Immunol. 13 (2001) 213–218.

[20] Y. Kudo, C.A.R. Boyd, The physiology of immune evasion during pregnancy: the critical role of placental tryptophan metabolism and transport, Pflugers Arch. 442 (2001) 639–641.

[21] A.L. Mellor, D.H. Munn, Tryptophan catabolism prevents maternal T cells from activating lethal anti-fetal immune responses, J. Reprod. Immunol. 52 (2001) 5–13.

[22] S.J. Kerr, P.J. Armati, L.A. Pemberton, G. Smythe, B. Tattam, B.J. Brew, Kynurenine pathway inhibition reduced neurotoxicity of HIV-1-infected macrophages, Neurology 49 (1997) 1671–1681.

[23] M.P. Heyes, K. Saito, A. Lackner, C.A. Wiley, C.L. Achim, S.P. Markey, Sources of the neurotoxin quinolinic acid in the brain of HIV-1-infected patients and retrovirus-infected macaques, FASEB J. 12 (1998) 881–896.

[24] E.M.E. Burudi, M.C.G. Marcondes, D.D. Watry, M. Zandonatti, M.A. Taffe, H.S. Fox, Regulation of indoleamine 2,3-dioxygenase expression in simian immunodeficiency virus-infected monkey brains, J. Virol. 76 (2002) 12233–12241.

[25] L.A. Sanni, B.N. Tattam, D.E. Moore, G. Chaudhri, R. Stocker, N.H. Hunt, Dramatic changes in oxidative tryptophan metabolism along the kynurenine pathway in experimental cerebral and noncerebral malaria, J. Virol. 76 (1998) 12233–12241.

[26] M.P. Heyes, K. Saito, C.Y. Chen, M.G. Proescholdt, T.S.J. Nowak, J. Li, K.E. Beagles, M.A. Proescholdt, M.A. Zito, K. Kawai, S.P. Markey, Species heterogeneity between gerbils and rats: quinolinate production by microglia and astrocytes and accumulations in response to ischemic brain injury and systemic immune activation, J. Neurochem. 69 (1997) 1519–1529.

[27] K. Saito, T.S. Nowak Jr., S.P. Markey, M.P. Heyes, Mechanism of delayed increases in kynurenine pathway metabolism in damaged brain regions following transient cerebral ischemia, J. Neurochem. 60 (1993) 180–192.

[28] S.J. Pearson, G.P. Reynolds, Increased brain concentrations of a neurotoxin, 3-hydroxykynurenine, in Huntington's disease, Neurosci. Lett. 144 (1992) 199–201.

[29] P. Guidetti, R.P. Hemachandra, D.A. Tagle, R. Schwarcz, Early kynurenergic impairment in huntington's disease and in transgenic animal model, Neurosci. Lett. 283 (2000) 233–235.

[30] J.A. Aquilina, J.A. Carver, R.J.W. Truscott, Oxidation products of 3-hydroxykynurenine bind to lens proteins: relevance for nuclear cataract, Exp. Eye Res. 64 (1997) 727–735.

[31] O. Hayaishi, O. Takikawa, R. Yoshida, Indoleamine 2,3-dioxygenase: properties and functions of a superoxide utilizing enzyme, Prog. Inorg. chem.: Bioinorg. Chem. 38 (1990) 75–95.

[32] O. Takikawa, T. Kuroiwa, F. Yamazaki, R. Kido, Mechanism of interferon-γ action: characterisation of indoleamine 2,3-dioxygenase in cultured human cells induced by interferon-γ and evaluations of the enzyme-mediated tryptophan degradation in its anticellular activity, J. Biol. Chem. 263 (1988) 2041–2048.

[33] T.K. Littlejohn, O. Takikawa, D. Skylas, J.F. Jamie, M.F. Walker, R.J.W. Truscott, Expression and purification of recombinant human indoleamine 2,3-dioxygenase, Protein Expr. Purif. 19 (2000) 22–29.

[34] M. Bradford, A rapid and sensitive for the quantitation of microgram quantities of protein utilizing the principle of protein-dye binding, Anal. Biochem. 72 (1976) 248–254.

[35] U.K. Laemmli, Cleavage of structural proteins during the assembly of the head of bacteriophage T4, Nature 227 (1970) 680–685.

[36] The QIAexpressionist, Qiagen, 2003.

[37] A. Villaverde, M. Mar Carrio, Protein aggregation in recombinant bacteria: biological role of inclusion bodies, Biotechnol. Lett. 25 (2003) 1385–1395.

[38] J.J. Chalmers, E. Kim, J.N. Telford, E.Y. Wong, W.C. Tacon, M.L. Shuler, D.B. Wilson, Effects of temperature on *Escherichia coli* overproducing β-lactamase or human epidermal growth factor, Appl. Environ. Microbiol. 56 (1990) 104–111.

[39] C.H. Schein, M.H.M. Noteborn, Formation of soluble recombinant proteins in *Escherichia coli* is favored by lower growth temperature, Bio/technology 6 (1988) 291–294.

[40] J. Delcarte, M. Fauconnier, P. Jacques, K. Matsui, P. Thonart, M. Marlier, Optimization of expression and immobilized metal ion affinity chromatographic purification of recombinant (His)6-tagged cytochrome P450 hydroperoxide lyase in *Escherichia coli*, J. Chromatogr. B Analyt. Technol. Biomed. Life Sci. 786 (2003) 229–236.

[41] I. Stojiljkovic, B.D. Evavold, V. Kumar, Antimicrobial properties of porphyrins, Expert Opin. Investig. Drugs 10 (2001) 309–320.

Pages 215-222 of this thesis have been removed as they contain published material under copyright. Removed contents published as:

Austin, C.J.D., Astelbauer, F., Kosim-Satyaputra, P. et al. (2009) Mouse and human indoleamine 2,3-dioxygenase display some distinct biochemical and structural properties. *Amino Acids*, vol. 36, no. 1, pp. 99–106. https://doi.org/10.1007/s00726-008-0037-6

Recombinant human indoleamine 2,3-dioxygenase

Priambudi Kosim-Satyaputra
Chemistry and Biomolecular Sciences-Macquarie University

Abstract

Indoleamine 2,3-dioxygenase (IDO) is a heme-containing dioxygenase that catalyses the first and rate-limiting step in the kynurenine (Kyn) pathway of L-tryptophan (L-Trp) catabolism. Attention has been focused on IDO because the Kyn metabolic pathway is involved in a variety of physiological functions and diseases. In this study the expression and purification of recombinant human indoleamine 2,3-dioxygenase (rhIDO) in *E. coli* (pQE-9-IDO, pREP4) was investigated in order to obtain high quality enzyme in high yields. This study concluded that optimisation could still be achieved by lowering the growth temperature from 37 °C to 30 °C and reduction of IPTG induction from 100 μM to 10 μM. Better yields of rhIDO were obtained when the expression was carried out under dark conditions without the addition of PMSF, addition of hemin prior to lysis of the cells, increasing the NaCl concentration from 150 mM to 500 mM and lowering the imidazole variation from 10, 30, 40, 65, 80, 90, 190 to 10, 30, 60, 300 mM in the purification through Ni-NTA.

Evaluation of the characteristics and stability of rhIDO in order to understand its behaviour as a support towards further studies showed that rhIDO activity and yield under certain conditions of purification were significantly decreased. Further studies concluded that the loss of rhIDO activity was most probably due to the loss of the heme prosthetic group of the enzyme or the non effectiveness of the heme-protein complex. A study with hemin to examine the possibility of re-incorporation of heme showed moderate re-incorporation. It was concluded, however, that keeping the heme intact through the supplementation of hemin prior to lysis is a much better alternative for preserving the activity of the enzyme. Comparison studies between rhIDO and rmIDO showed that the relative catalytic efficiency of rhIDO towards L-Trp (3.73) was higher compared to rmIDO (1.40) whereas the relative catalytic efficiency of rhIDO towards D-Trp (0.02) was lower compared to rmIDO (0.03). CD and thermal melt studies established that rhIDO is less helical (61% helix) than rmIDO (71% helix). The studies also showed that rhIDO has a lower melt temperature (50 ºC) than rmIDO (65 ºC) indicating that rmIDO is more thermostable than rhIDO.

The contribution of individual cysteines towards the overall catalytic properties and stability of the rhIDO was evaluated through mutagenesis studies. This was done by comparing the resulting outcomes from the C126A, C286A, C322A and C349A rhIDO mutations towards that of the non-mutated rhIDO. All the mutants exhibited a decrease in specificity towards L-Trp with C322A showing the highest decrease of 78% loss. However, with D-Trp, mutants C126A and C322A showed increased specificity where C126A showing the highest increase (280%). Mutants C286A and C349A showed decreased activity with C349A having the most (67% loss). This study confirms that the Cys to Ala site-directed mutagenesis contributes to the changes in the kinetics of the mutated rhIDO, and that the cysteine moieties of rhIDO are involved in the normal catalytic function of the enzyme. It is highly likely that the change from Cys to Ala in the mutants changed the conformation of the enzyme, which was a determining factor to the accessibility of the specific substrates to the active site. This change in conformation resulted in diverse kinetics observed.

Kosim-Satyaputra, P., Recombinant human indoleamine 2,3-dioxygenase, in *Chemistry and Biomolecular Sciences*. **2009**, Macquarie University: Sydney. pp. i-xxiv, 1-222.